Screw Pyrolysis of Biogenic Feedstock with Integrated Hot Gas Filtration

A thesis accepted by the Faculty of Energy-, Process- and Bio-Engineering
of the University of Stuttgart to fulfill the requirements
for the degree of Doctor of Engineering Sciences (Dr.-Ing.)

Submitted by

Marco Tomasi Morgano

from Como (Italy)

Main referee:	Prof. Dr.-Ing. Helmut Seifert
Co-referee:	Prof. Dr. techn. Günter Scheffknecht
Day of the oral Exam:	12.03.2019

Institute of Combustion and Power Plant Technology (IFK) of the University of Stuttgart

2019

ACKNOWLEDGEMENTS

The submitted work was completed between July 2013 and March 2019 at the Institute for Technical Chemistry (ITC) at the Karlsruhe Institute of Technology (KIT).

First of all, I would like to thank my Doktorvater Prof. Dr.-Ing. Helmut Seifert for the scientific supervision and engagement during the revision time. He gave me complete freedom in the organization of project and believed in me during these years at the institute.

Many thanks to Prof. Dr. techn. Günter Scheffknecht (IFK, University of Stuttgart) for taking over the co-supervision of this work. For their precious contributions thanks to Univ.-Prof. Dr. Andreas Kronenburg and Apl. Prof. Dr.-Ing. Uwe Schnell.

Special thanks goes to Mr. Hans Leibold at the Dept. of Pyrolysis and Gas Treatment for allowing me to work on this challenging topic. We share the belief on the potential of our technology. Time proved us right. I greatly appreciate the discussions and the idea that we can sometime disagree on the details but agreeing on targets is what matters at the end of the day.

Another special thank goes to my buddy and "Lebensretter" Mr. Frank Richter. He built whatever I had in mind much better than I could even imagine. His critical point of view kept my feet on the ground and always remind me that the team makes the difference. The discussions we had helped me growing as a researcher and as a man.

Many thanks go to my colleagues at the Dept. of Pyrolysis and Gas Treatment for the relaxed atmosphere and the constant willingness to help. I also want to thank all the colleagues at ITC for the continuous support, the many analyses carried out for me and for always being kind and friendly. I greatly appreciated being part of this enlarged family.

Thanks to my students. You all made major contributions to the success of this work. Thank you to Leon, Philip and Chiara for the interesting and challenging scientific collaborations and for the productive discussion on the future of biomass, bioenergy and biofuels.

Thank you to my family and to all the friends here in Karlsruhe and in Italy. The time spent together brought always new energy to continue with this work.

Finally, the most important thank you goes to my wife Nina and to my son Claudio. Without your presence and support I would have never completed this PhD. You take care for me every day. I am grateful for having you on my side.

Marco Tomasi Morgano

Karlsruhe, March 2019

TABLE OF CONTENT

LIST OF SYMBOLS

Symbol	Unit	Significate
Latin		
A (context)	-	Absorption Coefficient
A (context)	1/s	Pre-exponential factor
C	-	Constant
c	kJ/(kg K)	Specific heat capacity
d (context)	-	Differential
D, d (context)	m	Diameter
E	-	Residence time distribution
E_a	kJ/mol	Activation energy
f	-	Function
F	-	Cumulative residence time distribution
Fr	-	Froude number
g	m/s^2	Gravitational acceleration
h	kJ/kg	Specific enthalpy
$\dot{H}$	kW	Enthalpy flow
H, h	m	Filling height
k (context)	mol/s; kg/s	Reactions rate
k (context)	m^2	Permeability
L, l	m	Length
m	kg	Mass
$\dot{m}$	kg/h; kg/s	Mass flow rate
Mm	kg/kmol	Molar mass
N	-	Number
n (context)	1/min	Rotational speed
n (context)	-	Number of moles
$\dot{n}$	mol/s	Molar flow
p	Pa; mbar	Pressure, Partial pressure
Ph	-	Phase Change number
Py	-	Pyrolysis number
$\dot{Q}$	kW	Heat flow
R (context)	J/(kmol K)	Universal gas constant
R, r (context)	m	Radius
S (context)	m^2	Surface
T	°C; K	Temperature
t (context)	s; min; h	Time
t (context)	m	Thickness
V	m^3	Volume
$\dot{V}$	m^3/h; m^3/s	Volume flow
$\dot{W}$	kW	Electric power
X	-	Moisture of solids

x	mol/mol	Volumetric concentration
y	kg/kg	Mass concentration

Greek

α (context)	W/(m^2 K)	Heat transfer coefficient
α (context)	-	Conversion degree
α (context)	-	Angle of repose
β	m/s	Mass transfer coefficient
δ	m	Particle roughness
Δ	-	Difference
ε	-	Emissivity
κ	m^2/s	Diffusivity
γ	-	Accommodation coefficient
γ	-	angle of the shaft covered by solids
μ	kg/(m s)	Dynamic viscosity
λ (context)	W/(m K)	Conductivity
λ (context)	-	Stoichiometric number
π	-	Archimede's constant
ρ	kg/m^3	Density, Bulk density
ξ	-	Dimensionless front
τ	s; min; h	Residence time
σ	W/(m^2 K^4)	Stefan-Boltzmann constant
ϑ	-	non-dimensional time
ϑ	-	angle of the screw covered by solids
ϕ	-	Porosity

Subscript

0	Starting/initial condition
a	Activation
AIR	Leakage air
AQUEOUS	Aqueous Condensate
AR	As received basis
ASH	Ash
bed	bulk solid bed
BIO-OIL	Oil-phase
BULK	Bulk solid
C	Carbon
CAKE	Filter Cake
CELL	Cellulose
CHAR	Char
CM	Cooling medium
COND	Condensation
COND-C1	Condensate from Condenser 1
CONDENSATE	Condensate = Liquid from pyrolysis
COND-ESP	Condensate from Electrostatic Precipitator
DAF	Dry and Ash free basis
DRY; dry	Dry basis
eff	Effective
ESP	Electrostatic Precipitator
EXT-SURFACE	External surface of the oven

f(SOLIDS)	function of the solids
FAST	Fast reaction
FB	Freeboard
FC	Fixed Carbon
FEED	Feedstock
FILTER	Filter candle
G	Gas
GAS	Gas
GEOM	Geometric
$H_2O(g)$	Water steam
HEMI	Hemicellulose
i	i-th component
IN	Input
LAT	Latent
LIGN	Lignin
LOSS	Loss
LV	Liquid-Vapor
MEAN	Mean residence time
MIX	Mixing
MOISTURE	Water content
N.	Normal conditions (pressure, temperature)
N_2	Nitrogen gas
O_2	Oxygen gas
OUT	Output
p	Constant Pressure
PG	Permanent gas from pyrolysis
pyro	Pyrolysis
R	Stagnant period
rad	radiative
react	reaction
S	Solid
SAMPLING	Sampling
SAT	Saturation condition
SCREW	Screw
sec	Secondary Reactions
SG	Solid-to-Gas
Sh	Shaft
SHAFT	Shaft
ShS	Shaft-to-Solid
ShΔm	Shaft-to-Vertical Gas
SLOW	Slow reaction
SOLIDS	Solids
ST	Space time
SURROUNDINGS	Surroundings area
SΔm	Solid-to-Vertical Gas
VAPORS	Pyrolysis vapors

W		Wall
WG		Wall-to-Gas
WS		Wall-to-Solid
WΔm		Wall-to-Vertical Gas
α		Convective
Δm		Vertical gas
ΔmG		Vertical Gas-to-Gas
ε		Radiative

Abbreviations

BET		Brunauer-Emmett-Teller
CCR		Conradson Carbon Residue
CER		Chemical Energy Recovery
CHO		Carbon Hydrogen Oxygen
CFD		Computational Fluid Dynamics
CGE		Cold Gasification Efficiency
CPE		Cold Pyrolysis Efficiency
DAEM		Distributed Activation Energy Model
DoF	-	Degree of Filling
DTA		Differential Thermal Analysis
DTG		Differential Thermogravimetric
ESP		Electrostatic Precipitator
FID		Flame Ionization Detector
FT-IR		Fourier-Transform Infrared Spectrograph
GC		Gas Chromatograph
HDO		Hydrodeoxygenation
HHV		Higher Heating Value
HTC		Hydrothermal Carbonization
LFR		Laminar Flow Reactor
LHV		Lower Heating Value
MS		Mass Spectrometer
MSW		Municipal Solid waste
N-CSTR		N-series of Continuously Stirred Tank Reactors
NMR		Nuclear Magnetic Resonance
PFR		Plug Flow Reactor
Py		Pyrolysis
RTD	-	Residence time distribution
S (context)	-	Segment
SEM		Scanning Electron Microscope
TGA		Thermogravimetric Analysis
XRD		X-Ray Diffraction

ABSTRACT

The Institute for Technical Chemistry of the Karlsruhe Institute of Technology developed an innovative screw pyrolysis reactor (STYX) with integrated hot gas filtration, which enables the production of particle-free vapors, and respective condensate and gas. To support the development of the technology, experimental and theoretical work aiming at understanding and controlling the thermal and chemical processes taking place during pyrolysis of biogenic residues at the STYX is necessary. The absence of solids in the vapors minimizes the typical issues of pyrolysis, i.e. clogging and blocking in the hot pipelines and in the condensation unit, and it is of immense advantage for the following direct applications such as combustion of the vapors for heat and power conversion and for upgrading of the liquids into fuels and chemicals. Moreover, a solid hygienized and carbonized product, the pyrolysis char, is always produced during pyrolysis. It finds applications in the energy industry as fuel and in agricultural industry as soil enhancer and fertilizer, depending on the initial content of nutrients of the feedstock. Robustness and flexibility are the keys of the economic feasibility of the STYX technology.

The effects of the pyrolysis process parameters on the products yields and properties of beech wood as a reference biogenic material were investigated experimentally at STYX. The feedstock was characterized in details with focus on the chemical composition. The temperature of the reactor was adopted as fundamental parameter since it influences the thermodynamic equilibrium and ultimately defines the yields of the products. Mass, elemental and energy balances were carried out at the reactor for selected conditions globally and regarding local situations. The pyrolysis chars and oils were investigated for further utilization as fuels. Moreover, the pyrolysis oils were characterized for further upgrading applications. The aqueous condensate, is often considered the by-product of pyrolysis processes. In this work, it was identified as feedstock for the production of valuable chemicals. The permanent gas, or non-condensable gas, was characterized as fuel as well.

Successively, the pyrolysis of different biogenic feedstock with high inert and inorganic contents was investigated in the STYX reactor at well-defined process conditions. Low-grade biogenic feedstock, such as solid manure and dried sewage sludge, have a distinctive behavior from typical lignocellulosic biomass. The inert content is responsible for higher yields of pyrolysis solids compared to the reference feedstock. The yields of the pyrolysis oils are comparable or higher than those of lignocellulosic feedstock, whereas the yields of the aqueous condensate and of the permanent gas are considerably reduced. Furthermore, the presence of

nitrogen, sulfur and chlorine as well as of minerals and metals implies the necessity for removal concepts or feasible recovery of potential pollutants.

Transport mechanisms of granular solids and the hydrodynamics of the gas in screw reactor were evaluated experimentally in the STYX reactor and adopted as basis for the development of a thermochemical model of screw reactors. Consequently the reactor was modelled as a cascade of perfectly mixed reactors for both the solid and the gas/vapor phases. The processes taking place in the reactor were described on the basis of available models obtained from literature. The mechanical behavior of the solids was modelled in terms of mixing quality. The heat exchange between the reactor and the vapors was described taking into account forced convection and radiative heat transfer mechanisms. The heat exchange between the reactor and the granular solid was described by the penetration model, regarding the granular solid with interstitial gas as a continuous system. Pyrolysis mechanism was described by the chemical kinetics for the decomposition of model compounds present in wood biomass. On the basis of the reactor model, an extensive sensitivity analysis was carried out assessing the most important parameters.

Finally, the thermochemical model was validated experimentally at the STYX reactor. Experiments were carried out to describe the heat transfer of an inert dry granular solid. The temperature of the solids was measured online adopting temperature-sensitive dyes, thus the real temperature of the solid surface was measured. The drying mechanisms of an inert porous granular solid were investigated experimentally and compared with the numerical results. The pyrolysis mechanism was studied extensively validating the decomposition of beech wood and the secondary gas phase reactions along the reactor as well as the overall yields distributions and the compositions as a function of the process parameters. The thermochemical model developed in this work could be shown a validated and flexible tool for the scale-up of pyrolysis reactor based on the STYX technology.

Because filtration plays a decisive role for the quality of the vapors and of the condensate, the fundamental mechanisms involved during filtration need to be investigated thoroughly. For future implementation in the thermochemical model of the reactor filtration should be modelled as well. The pyrolysis mechanisms of non-lignocellulosic model compounds should be integrated into the numerical tool in order to extend its capabilities to more attractive feedstock for pyrolysis applications at decentral scale.

KURZFASSUNG

Das Institut für Technische Chemie des Karlsruher Instituts für Technologie entwickelte einen innovativen Pyrolyseschneckenreaktor mit integrierter Heißgasfiltration (STYX), der die Erzeugung partikelfreier Dämpfe bzw. Kondensate und Gase ermöglicht. Zur Unterstützung der Technologieentwicklung sind experimentelle und theoretische Arbeiten notwendig, die dem Verständnis und der Beeinflussung der thermischen und chemischen Prozesse bei der Pyrolyse biogener Reststoffe dienen. Dadurch, dass die Dämpfe frei von organischen und mineralischen Partikeln sind, werden typische Probleme der Pyrolyse wie das Zusetzen und Verstopfen von Rohrleitungen und Kondensatoren minimiert. Die Partikelfreiheit ist auch von großem Vorteil für nachgelagerte Anwendungen wie die Verbrennung der Dämpfe zur Wärme- und Stromerzeugung sowie für die Aufarbeitung der Kondensate in Kraftstoffe oder Chemikalien. Im Pyrolyseprozess wird immer auch ein fester, hygienisierter Pyrolysekoks erzeugt. Er kann als Brennstoff zur Energienutzung eingesetzt werden und je nach Nährstoffgehalt der Einsatzstoffe auch als Bodenverbesserer oder Dünger in der Landwirtschaft. Besondere Kennzeichen der STYX Technologie sind Unempfindlichkeit und Flexibilität bei den Einsatzstoffen.

Für Buchenholz als Referenzmaterial wurde am STYX Reaktor experimentell der Einfluss der Prozessparameter auf die Produktverteilung und die Eigenschaften der Pyrolyseprodukte untersucht. Der Einsatzstoff wurde detailliert in Bezug auf die chemische Zusammensetzung charakterisiert. Die Reaktortemperatur wurde als wesentlicher Parameter identifiziert, da sie das thermodynamische Gleichgewicht beeinflusst und letztlich die Produktverteilung bestimmt. Für ausgewählte Bedingungen wurden am Pyrolysereaktor globale und lokale Massen-, Elementar- und Energiebilanzen erstellt. Pyrolysekokse und –öle wurden hinsichtlich des Einsatzes als Brennstoffe untersucht. Außerdem wurden die resultierenden Produkte bei der Aufarbeitung der Pyrolyseöle ermittelt. Das wässrige Kondensat wird bei Pyrolyseprozessen vielfach als Abfallprodukt angesehen. In dieser Arbeit konnte seine Eignung als Ausgangsstoff zur Erzeugung wertvoller Chemikalien gezeigt werden. Das Permanentgas oder nicht-kondensierbare Gas wurde ebenfalls als Brennstoff charakterisiert.

In der Folge wurden am STYX Reaktor bei definierten Prozessbedingungen verschiedene biogene Einsatzstoffe mit hohem Inert- bzw. Mineralanteil untersucht. Die Pyrolyse minderwertiger biogener Einsatzstoffe wie Geflügelkot und getrockneter Klärschlamm unterscheidet sich von der typischer lignozelluloser Biomasse. Der Inertanteil ist verantwortlich für den höheren Anteil fester Pyrolyseprodukte im Vergleich zum Referenz-Einsatzstoff. Der

Anteil an Pyrolyseöl ist vergleichbar oder höher als bei lignozellulosem Einsatzstoff, wogegen die Anteile an wässrigem Kondensat und beim Permanentgas deutlich geringer sind. Weiterhin erfordern die Stickstoff-, Schwefel- und Chlorkonzentrationen ebenso wie der Mineral- und der Metallanteil Konzepte zur Abtrennung oder Rückgewinnung möglicher Schadstoffe.

Die Transportmechanismen für rieselfähige Feststoffe und die Hydrodynamik des Gases im Schneckenreaktor wurden am STYX Reaktor experimentell untersucht und als Basis für die Entwicklung eines thermochemischen Modells des Schneckenreaktors verwendet. Darauf aufbauend wurde der Reaktor als Kaskade von perfekt gemischten Rührkesseln für den Feststoff und die Gas-Dampfphase modelliert. Die im Reaktor ablaufenden Einzelprozesse wurden auf der Grundlage von verfügbaren Literaturmodellen beschrieben. Das mechanische Verhalten der Feststoffe wurde über die Mischungsqualität des Schüttgutes beschrieben. Zur Beschreibung des Wärmeaustausches zwischen Reaktor und Dampfphase wurden erzwungene Konvektion und Wärmestrahlung berücksichtigt. Der Wärmeaustausch zwischen Reaktor und Schüttgut wurde mit dem Penetrationsmodell beschrieben, das Partikel und Gaszwischenvolumen als Kontinuum betrachtet. Der Pyrolyseprozess des Referenzmaterials Buchenholz wurde anhand der Kinetik für die Zersetzung von Modellkomponenten beschrieben. Für das Reaktormodell wurde außerdem eine umfangreiche Sensitivitätsanalyse zum Einfluss der wichtigsten Parameter durchgeführt.

Abschließend wurde das thermochemische Reaktormodell experimentell am STYX Reaktor validiert. Dazu wurden Experimente zur Wärmeübertragung eines trockenen Schüttgutes durchgeführt. Die Temperatur des Feststoffes wurde dabei mit temperaturempfindlichen Farbstoffen bestimmt, sodass die wirkliche Oberflächentemperatur der Feststoffpartikel gemessen werden konnte. Der Trocknungsprozess eines inerten porösen Schüttgutes wurde gemessen und mit den numerischen Ergebnissen verglichen. Der Pyrolyseprozess wurde ausführlich untersucht. Die Validierung umfasste die Umsetzung von Buchenholz und sekundärer Gasphase entlang des Reaktors, die Gesamtverteilung und Zusammensetzung der Produkte jeweils als Funktion der Prozessparameter. Es konnte gezeigt werden, dass das thermochemische Modell, das in dieser Arbeit entwickelt wurde, als validiertes und flexibles Werkzeug für das Scale-up des Pyrolysereaktors auf Basis der STYX Technologie eingesetzt werden kann.

Da die Heißgasfiltration eine entscheidende Rolle für die Qualität von Dämpfen und Kondensaten spielt, sollten zukünftig die Vorgänge während des Filtrationsprozesses intensiv untersucht werden. Außerdem sollte die Filtration für die Implementierung in das

Reaktormodell ebenfalls modelliert werden. Weiterhin sollten die Pyrolysemechanismen für Modellkomponenten von nicht lignozellulosehaltigen Biomassen in das numerische Modell integriert werden, um die Anwendbarkeit für attraktive Einsatzstoffe dezentraler Pyrolyseprozesse zu erweitern.

1. INTRODUCTION

Pyrolysis of biomass for the production of liquids is a relatively new technology even if pyrolysis for the production of biochar is a well-known process since ancient times. The pioneering research goes back to the first crude oil crisis during the early seventies, when the importance of developing technologies for substituted liquid fuels from renewable resources became clear. However, pyrolysis for liquid production is a known technology since World War II, when Germany developed technologies to convert local coal into liquids for transportation. In the metallurgical industry, BTEX (Benzene, Toluene, Ethylbenzene, Xylene) are obtained from the pyrolysis of coal for the production of coke. The main advantages of pyrolysis for liquids or fast pyrolysis may be summarized in technical and economic ones. The main advantage is probably the possibility of decoupling the production from the utilization in scale, time and location. In fact, the pyrolysis reactor may be operated 24/7 reducing the specific costs, while the utilization of the pyrolysis oil in a combustion engine or turbine for power generation may take place during the daily peak in another location and utilizing the oil at a different, higher, nominal capacity. Based on the aforementioned example, the second great advantage of pyrolysis is the production of renewable fuels, the bio-oil and the biochar, which are much more flexible than the source feedstock. Biochar may be used in co-firing very large-scale facilities or used locally, while the bio-oil may be applied in a wide range of applications, such as oil boilers, engines and turbines as well as a gasification feedstock. Another important advantage, which enables different utilization of the pyrolysis products, is the mineral separation. In fact, during pyrolysis, the minerals are normally retained completely in the char, which may be used for soil applications closing the main nutrients cycles, while providing some sort of carbon sequestration. More advanced utilizations are related to the biomass-based refinery or biorefinery concept. In such facilities, secondary upgrading of the bio-oil into transportation fuels, special chemicals and additives as well as primary separation of the cellulose and lignin-derived fractions are pursued. In fast pyrolysis, bio-oil has other economical superior properties compared to its original feedstock. The costs of storage and transportation are greatly reduced because of the volume reduction. The handling efforts are reduced, too.

1.1 Legal framework

The European Union committed itself to tackle the aspiring target of the Kyoto Protocol and the Doha Amendment of reducing the emissions of greenhouse gases [118]. Specifically, the EU approved the Directive 2009/28/EC, which focused on the development of energy markets based on renewable resources [69]. It set targets for the member states in terms of share of renewable sources (20%),

energy efficiency (20%) and share of biofuels for transportation (10%) till 2020. The generation of electricity may be achieved by a wide spectrum of technologies and sources, such as solar, wind and hydropower. On the other hand the production of biofuels is limited to those sources which contain carbon. The Article 2 of the aforementioned Directive distinguishes between biomass "*biodegradable fraction of products, waste and residues from biological origin from agriculture (including vegetal and animal substances), forestry and related industries including fisheries and aquaculture, as well as the biodegradable fraction of industrial and municipal waste"*, landfill gas, sewage treatment plant gas and biogases. Sewage sludge is not mentioned as renewable energy source in the Directive 2009/28/EC because of its historical relevance. It has its own Directive 86/278/EEC since 1986, which has been updated in the following years to its actual version from 2009 [51]. The directive imposes a treatment of the sewage sludge before being adopted for agricultural scopes.

At a national level, Germany regulates the utilization of renewable sources through the Renewable Energy Sources Act (Erneuerbare-Energien-Gesetz – EEG 2014), which follows the EU guidelines [75]. The utilization of biomass in the energy sector is further regulated by the Biomass Regulation (Biomasse Verordnung - BiomasseV), which explicitly does not recognize sewage and other sludge, landfill and sewer gases as biomass [23]. In opposition to the Directive 2009/28/EC, which relates to and allows the utilization of *"biodegradable fraction of industrial and municipal waste"*, the BiomasseV excludes mixed municipal waste from private households and similar waste from other origins areas including mixed waste from leached biomass fractions.

The new German Sewage Sludge Regulation (AbfKlärV) foresees the recovery of phosphorus from sewage sludge for large wastewater treatment facilities and from sewage sludge ashes from thermal plants as well as more stringent limitations for soil applications [222, 70].

In relation to thermochemical processes, the difference between biodegradable, biogenic and biomass fraction is of minor relevance. However, it plays a relevant role for the authorization of the facility, essentially related to the emissions limits [35]. Biomass from lignocellulosic materials are covered by the TA Luft [37, 36], which defines the emission limits from the combustion of non-waste materials [194].

1.2 Motivation

The conversion of lignocellulosic biomass through pyrolysis aims at the production of intermediate liquids, which will require further upgrading to transportation fuels or to chemicals [48]. In order to maximize the yield of the liquids, small particles sizes and low ash content are required for very fast heating rates, no secondary intra-particles reactions, followed by an extremely rapid quenching. Vapors residence times in the high temperature zone below 2 seconds are expected to match the

requirements. Therefore, fluidized bed reactors with high flow rates of inert purging gas suit at best the purpose. Twin-screw reactors with solid carrier medium, pre-heated sand or metal granulates, are also suitable for the purpose [84]. Liquid production using fast pyrolysis technologies, however, makes sense for lignocellulosic feedstock with low ash content. As already mentioned, minerals act as catalyst favoring the formation of coke against that of organic vapors. The mechanism can be very well related to the deactivation of catalysts in processes involving the conversion of hydrocarbons [11]. Therefore, low-grade biogenic feedstock (heterogeneous and with high inorganic content) are more suitable for the production of char, while the organic vapors may be used to ensure the self-sustainable operation of the pyrolysis plant. Under these circumstances the requirements of fast pyrolysis in terms of operational parameters (fast heating rates) and physical features of the feedstock (small particle sizes) are not necessary. More robust reactors can be designed for the purpose. Not to forget is that low-grade biogenic feedstock is widely distributed in relatively low amounts; thus small-scale and simple design is beneficial. Single screw reactors belong to this category and appear to suit particularly well the requirements of robustness, design and scale. Moreover, screw reactors may provide an interesting option for decentral generation of liquid intermediates, which will be then transported to centralized large facilities for further upgrading. The characterization of the pyrolysis process and of the products of low-grade feedstock in screw reactors is fundamental for the development of successful concepts.

1.3 Targets

The STYX reactor was developed as an intermediate pyrolysis reactor with integrated hot gas filtration with the aim of producing particles and ash free pyrolysis condensates from the thermal decomposition of biomass as well as the pyrolysis char, which can be used as alternative solid fuel or for agricultural applications.

With the aim of balancing the reactor and of generating sufficient pyrolysis products for an exhaustive characterization in terms of liquid and solid fuels, a large number of experimental investigations were carried out. The pyrolysis products shall be characterized in relation to the chemical and physical properties as a function of the process parameters. The effect of the reactor temperature is the most important one having a major impact on the yields and on the properties; thus its effect was investigated adopting a reference feedstock with well-known and defined properties. Moreover, the characterization of the pyrolysis products from real low-grade feedstock was of fundamental relevance to assess the potential of the future implementation of the STYX technology. Finally, the development and the experimental validation of a thermo-chemical model of the reactor is mandatory

to understand the fundamental mechanisms involved during the pyrolysis of a biogenic feedstock as well as required for scale-up of the technology.

1.4 Dissertation flow

This dissertation deals with the pyrolysis process in a well-defined reactor with well-defined feedstock. The feedstock were characterized by means of fuel properties. The reactor was characterized by means of hydrodynamics of the gas, of transport of the solids and of indirect heat exchange through the vessel. The feedstock and the STYX reactor influences the pyrolysis process, which is evaluated and assessed taking into account the process conditions defined by the reactor technology as well as the properties of the adopted feedstock.

The knowledge gained was used to develop a thermo-chemical model of the reactor. Finally, the model is validated experimentally at the bench-scale reactor for the pyrolysis of a selected feedstock.

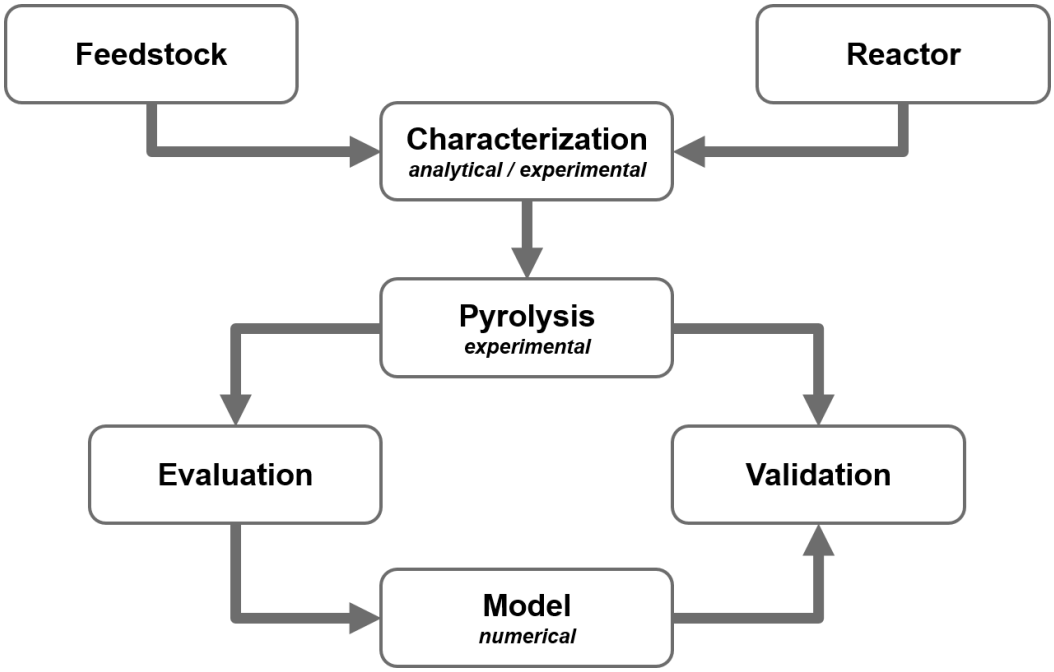

Figure 1. Dissertation scheme

The dissertation is structured as follows. **Chapter 2** is devoted to an extensive review of the pyrolysis process, from the fundamentals to the main reactor technologies. **Chapter 3** describes the experimental facilities as well as the methods adopted to critically evaluate the results of the experimental investigations. **Chapter 4** reports the results of the experimental campaigns carried out to evaluate the most important process parameters and feedstock characteristics. Moreover, it provides the experimental data for the development of the thermo-chemical model. **Chapter 5** describes the thermo-chemical model. After the discussion of the main feature of the model, an

extended sensitivity analysis is carried out. Following the model is validated with experiments carried out at the experimental facilities. Finally, **Chapter 6** summarizes the overall achievements of this work and provides the backbone for further research.

2. STATE-OF-THE-ART

The following chapter aims at reviewing the actual state of the art related to the chemical treatments adopted nowadays to modify the physico-chemical properties of biogenic feedstock with specific attention to the thermochemical processes. The targets of each treatment process may be different in a wide spectrum ranging from solving handling issues to producing intermediates for chemical specialties. Afterwards, a review related to the more advanced thermo-chemical processes is reported with the aim of highlighting pros and cons of each pathway and related technologies. Finally, the research field of pyrolysis is described spacing from the fundamentals to the technological advancements.

2.1 Fundamentals

2.1.1 Biogenic feedstock classifications

Classifying biogenic feedstock is a complex exercise, which starts from the meaning of *biogenic*. If the Greek origin of the term is adopted, then biogenic defines all the resources of biological origin (*genesis*). In such a way fossil fuels, such as coal and crude oil, may be included in the category of biogenic feedstock. Therefore, the first classification is on the age of the biogenic feedstock, thus a distinction between fossil biogenic feedstock and renewable biogenic feedstock is mandatory, where the latter are renewable in the human timescale. Crude oil, peat, lignite and coal are fossil biogenic feedstock and therefore excluded from further classification. A potential organization of the renewable biogenic feedstock is given based on the German Biomass Regulation [23] and on the overview offered by Vassilev et al. [218]. A resume is depicted graphically in Figure 2.

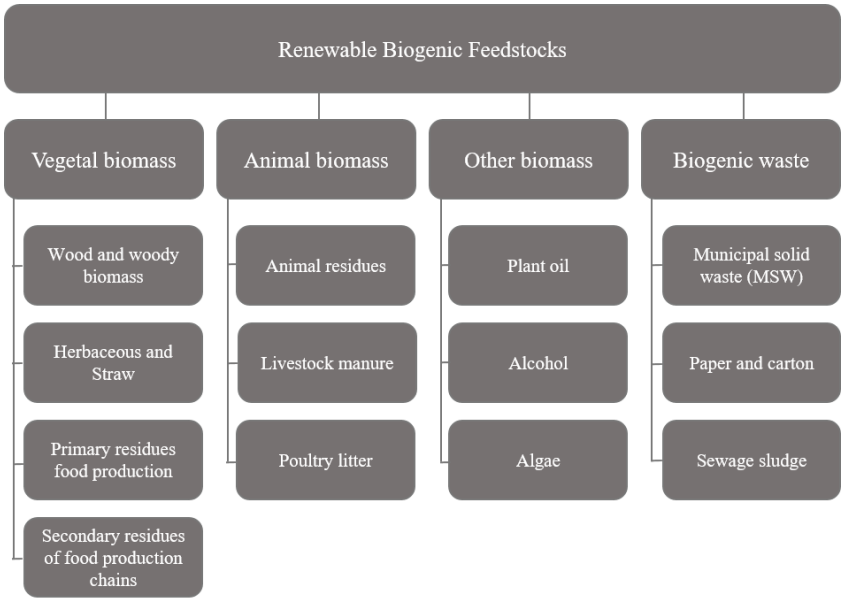

Figure 2. Classification of Renewable Biogenic Feedstock (RBF). Own elaboration based on [23, 218].

Although biogenic feedstock can also be liquid and gaseous, the main focus of this work relies on solid feedstock, which is suitable for thermo-chemical conversion using pyrolysis technology. Biogenic feedstock may be distinguished between biomass and non-biomass feedstock (see Figure 2). The first group is further classified into vegetal, animal and other biomass, such as plant oils and algae. Vegetal biomass have four sub-classes. The first includes wood, such as beech, pine and poplar, as well as a spectrum of woody materials like bark and sawdust; herbaceous feedstock include mainly grass as switchgrass and miscanthus or straw from rice or wheat. Residues from the production of food may also be distinguished between primary residues and secondary ones, which are generated along the production chain. Examples of primary residues are coconuts shells, bagasse and olive stones; secondary residues are the by-products from the production of coffee, such as husks, silverskin, defective beans and spent grounds. Excluding some feedstock from the production of food, vegetal biomass is characterized by nitrogen and sulfur contents below 1.0 wt.% of the feedstock (daf) basis. Most of vegetal biomass can be classified as lignocellulosic materials, which are a combination of the three main components of wood, i.e. cellulose, hemicellulose and lignin [219]. The chemical composition of the feedstock is of fundamental relevance for the pyrolysis process and its products [3].

In the class of animal biomass, animal residues such as meat and bone meals are to be named, whereas manures and poultry litter are the products of livestock husbandry. Manures consist essentially of feces and can be solid (farmyard) or liquid (farm slurry). Litter, on the other hand, is a mixture of excreta and bedding materials, which may include straw or other woody feedstock as well as other dry low-cost materials. These biogenic feedstock is characterized by a high nitrogen content mainly from proteins. Animal biomass is interesting for the recycling of phosphorus [42, 94]. The German Biomass Regulation recognizes a further range of biomass, which includes liquid feedstock, such as alcohol and plant oils. In Figure 2, algae is included in this category. Although algae is an important feedstock for the production of biofuels, it is of marginal interest for the purpose of this work, which is dedicated to solid biogenic feedstock on the one hand as well as due to the individual physical characteristics of algae, i.e. a suspension requiring energy and cost intensive pretreatments.

The last category of renewable biogenic feedstock includes biogenic wastes, which are not recognized as biomass by the German Biomass Regulation and are defined as *semi-biomass* in the classification of Vassilev et al. [218]. Municipal solid waste, i.e. its organic fraction, and sewage sludge have experienced wide interest from the research community because of the withstanding recycling potential in the framework of the European Circular Economy [153]. Biogenic wastes are characterized by heterogeneous composition and by the presence of contaminants and pollutants.

Another classification of biogenic feedstock is based on the water content, distinguishing between *wet* (above 50% of water content) and *dry* (below 50% of water) feedstock. Such distinction is mainly based on the most suitable or economic technology to convert the raw material and not on the origin of it. For instance, sewage sludge is a wet feedstock with a water content of about 90% but, in many cases, it is pre-treated through dewatering and drying of water content before being converted [214].

2.1.2 Composition of biogenic feedstock

Biogenic feedstock is made of complex macromolecules, which include carbohydrates in crystalline and amorphous form (cellulose and hemicellulose), lignin, fats and extractives, as well as proteins and a wide spectrum of minerals. A detailed description of each molecule goes far beyond the scope of this work; however, in the field of biomass thermochemical processing it is widely accepted to describe the feedstock as the weighted sum of its main components. Therefore, a brief description is reported here.

Cellulose

Cellulose is the main component of the cell walls, being responsible for the strength of the wood. It is a linear crystalline polysaccharide with the elementary formula $(C_6H_{10}O_5)_n$. The structural formula is depicted in Figure 3. Cellulose is composed of β-D glucopyranose units connected to each other by (1→4) glycosidic bonds. The structure of cellulose is characterized by the degree of polymerization, which can be above 10000 in unaltered wood.

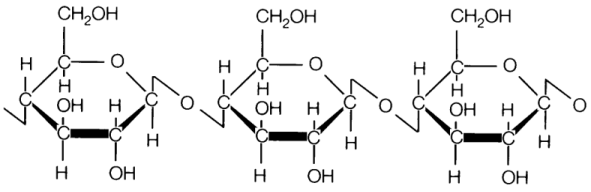

Figure 3. Structural formula of Cellulose.

The aggregation of cellulose is formed of completely linear chains of molecules within microfibriles, which provide the highly crystalline structure. Cellulose is not soluble in most of the solvents. The crystalline structure of cellulose ensures high resistance against thermal degradation and enzymatic hydrolysis [90]. It may undergo gelatinization, as starch does, but requires severe conditions in the range of 300°C and pressure of 25 MPa to become amorphous in water [56]. Thermal degradation of cellulose takes place in a narrow range of temperatures between 250°C and 350°C. The process of pyrolysis is almost complete at 360°C.

Hemicellulose

Hemicellulose is related to all non-cellulosic polysaccharides and related substances. It is the second most abundant component of wood, up to 40wt. % depending on wood type (hardwood or softwood). Surrounding and connecting the linear chains of cellulose, hemicellulose acts as supporting material in the cell walls of wood. Two main classes of sugar polymers compose the fundamental building blocks of hemicellulose: six-carbon sugars such as mannose, galactose, glucose and 4-O-methyl-D-glucuronic acid as well as five-carbon sugars like xylose and arabinose. The structure of hemicellulose presents branched configuration and somewhat shorter polymers than cellulose of about 50 to 200 monomer units and therefore it is susceptible to chemical degradation and more soluble (see Figure 4). Its decomposition covers a wider range of temperatures from 200°C to 300°C with a pyrolysis peak at about 260°C. Because of its amorphous shape hemicellulose produces more solid residues and gases than cellulose at the expense of tar [193].

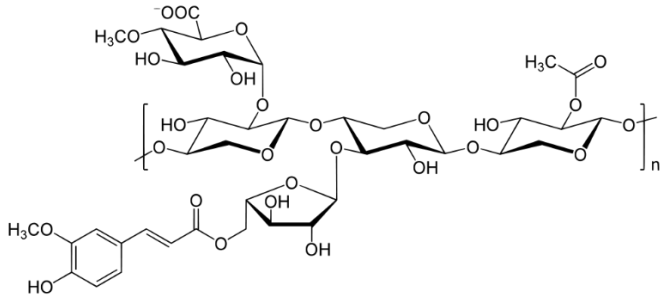

Figure 4. Potental structure of Xylan (Hemicellulose). Elaboration from [71]

Lignin

Lignin is the third main component in wood. The content depends on the wood type, i.e. 23-33wt. % for softwood and 16-25wt. % for hardwood. Lignin is the resin responsible for the rigidity of the cell wall and works as binder of the cellulosic structure. Made of polyphenol and phenylpropane units, lignin is an extremely complex three dimensional polymer, which shields the fibers against fungi and bacteria. Lignin may be isolated from wood only through chemical alteration of its composition by breaking the bonds to the cellulosic fibers. The resultant lignin, often named according to the extracting process, has lower molar weight, different chemical structures and different traces of organic species [38]. Therefore, the studies related to the thermal decomposition of technical lignin and of non-pretreated biomass may produce discording results [50]. The decomposition of lignin proceeds slowly in a wide range of temperatures from 100°C to 900°C because of its complexity in terms of chemical bonds. The pyrolysis of lignin produces methoxyphenols such as guaiacol and

syringol as primary condensable products. However, the aromatic structure of lignin leads to conspicuous solid residue compared to those of cellulose and hemicellulose.

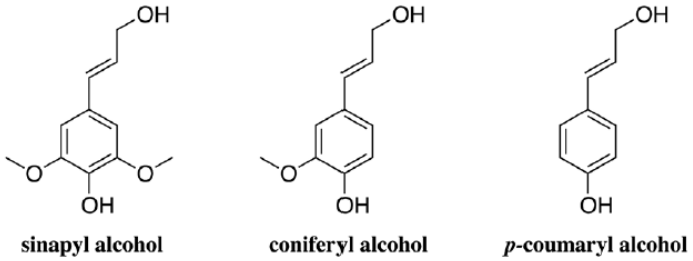

Figure 5. The three main monomers buildings block of lignin [201]

Extractives and Fats

Organic extractives of biogenic feedstock, and in particular of wood, include aliphatic, aromatic and alicyclic compounds, hydrocarbons, alcohols, ketones and various acids, ester, phenolic compounds, resins and others substances, which are not integral part of the plant structure. The role of these substances is to act against microbes and insects as well as intermediaries of the plant metabolism. Wood extractives are useful for chemical and material industries, accounting for less than 5% in wood and easily extractable using organic solvents (toluene, hexane and alcohol) or water [90]. Among the extractives, fat is one of the three main macronutrients, also known as triglycerides. The fundamental structure of fats is made of three fatty acid chains and the alcohol glycerol (Figure 6).

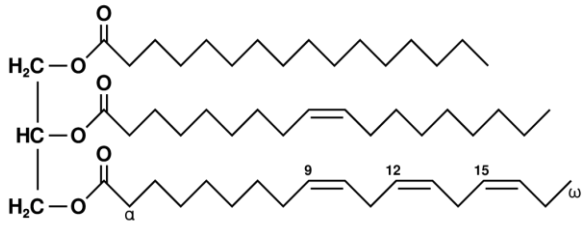

Figure 6. Fat triglyceride as typical extractive from wood. Elaboration from [125]

Like other lipids, fats are generally hydrophobic esters, insoluble in water, but soluble in organic solvents. Fats share all the same chemical structure, although a wide spectrum of different variation is available. Most fats are glycerides, particularly triglycerides, i.e. triesters of glycerol. One chain of fatty acid is bonded to each of the three -OH groups of the glycerol by the reaction of the carboxyl end of the fatty acid (-COOH) with the alcohol. In the process of esterification, water is eliminated and the carbons are linked by an -O- bond through dehydration synthesis [105]. Carboxylic acids, such as oleic acid, as well as hydrocarbons are the main products of fats pyrolysis [133].

Proteins

Proteins are large macromolecules built on one or more long chains of amino acid residues. Proteins are very important for the life of an organism, since they carry out a large number of activities within it, such as catalyzing metabolic reactions and transporting molecules from one location to another. Most proteins are linear polymers built from series of up to 20 different L-α-amino acids. Amino acids precursors of proteins possess common structural features, where an amino group, a carboxyl group, and a variable side chain are bonded to an α-carbon (see Figure 7). The sequence of amino acids distinguishes one protein from another. The sequence of the genes defines the specific three-dimensional structure of each protein and determines its activity. A polypeptide is a linear chain of amino acid residues. At least one long polypeptide is contained in every protein. Polypeptides with chains shorter than 20–30 residues are seldom considered to be proteins and are commonly called peptides. Many proteins are enzymes that catalyze biochemical reactions and play a vital role to metabolism [91]. Proteins are found in animal biomass and residues, as well as in sewage sludge and are responsible for the high contents of nitrogen and of sulfur [124].

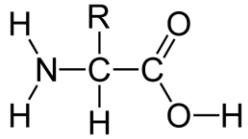

Figure 7. Fundamental structure of proteins (amino acid)

Minerals

The inorganic matter of biogenic feedstock includes mainly minerals, poorly crystallized mineraloids and amorphous inorganic phases [219]. Mineral composition depends on several factors, such as the biomass type, the soil and the fertilizer, when related to vegetal biomass as well as impurities and contaminants in the case of biogenic residues, manure or sewage sludge for instance. Minerals are found in biogenic feedstock in many different forms. Inorganic constituents are alkali metals like sodium (Na) and potassium (K), alkaline earth metals such as calcium (Ca) and magnesium (Mg) as well as other elements such as silicon (Si) and phosphorus (P), which form complexes like silicates, carbonates, phosphate and others [219]. The reactions of alkali metals with silica (SiO_2) produce a sticky and mobile liquid phase, the slag, which leads to the blockage of airways in furnaces and boiler plants [138]. Besides the aforementioned elements, other metals (Fe, Zn, Al, etc.) but also contaminants such as heavy metals as copper (Cu) and cadmium (Cd) [58] are present in variable content. Chromium (Cr), lead (Pb) and nickel (Ni) are also frequently reported [167]. These are found in the form of oxides, chlorides and sulfates; they may act as catalyst during the process of pyrolysis [192].

2.1.3 Overview of conversion processes for biogenic feedstock

Conversion of biogenic feedstock may follow two primary pathways, i.e. **thermochemical** and **biochemical** processing, depending on several factors related both on technical considerations as well as on economic and environmental assessments. Demirbaş, in his review [57], considers mechanical extraction or *agrochemical process* of vegetable oil as separated conversion pathways, which consist essentially in crushing seed crops and use directly the extracted oil in diesel motors.

Some authors distinguish the processing of biogenic feedstock between *pre-treatments* and *conversion processes*. However, a clear distinction is difficult to achieve, since some processes may be adopted as condition step of a further treatment, as it is the case of bioliq® [54] for pyrolysis (pre-treatment or conditioning step) followed by gasification (conversion process) and synthesis (refining), or they are used as stand-alone processes for the production of heat and power where, nevertheless, a combustion step is still necessary. Biogenic feedstock may be converted into three categories of products, i.e. heat and power, fuels and chemicals. Usually, the desired main product is the first factor in determining which chemical route will be embraced, followed by the feedstock type and quality [138].

Biochemical processes are usually considered to be a new approach for converting biogenic fuels in valuable products; however, fermentation is used since ancient times and scientific reports go back to the early twentieth century [96]. Biochemical processes uses enzymes and microorganisms to break down biomass and other biogenic feedstock and produce sugars as building blocks of biofuels. Biochemical processes are **anaerobic digestion** and **alcoholic fermentation**, which differentiate one from another by the absence or presence of oxygen in the atmosphere [202]. The main advantage of biochemical processes is the high selectivity to the desired products, while drawbacks are the relatively low throughput as well as the discontinuity of the process, i.e. batch operation.

Anaerobic digestion is the fermentation of organic materials in anaerobic conditions, i.e. in the absence of oxygen, to produce biogas. Anaerobic digestion has been applied to a wide range of biogenic waste such as sewage sludge and animal manures even in combination with pyrolysis process to valorize the solid residues, too [44, 147]. Digestion is nowadays recognized as one of the most mature technologies to produce heat and power from renewable sources. Anaerobic digestion produces a biogas, which is a mixture of methane and carbon dioxide with variable concentrations in the range of 60% and 40% of the volume respectively. Moreover, traces of H_2S (hydrogen sulfide) are released and usually removed in a dry sorption unit before further utilization. Biogas is converted into heat and power in a CHP motor (Combined Heat and Power) or further upgraded into biomethane and introduced into the methane pipelines to improve the profitability of the process [185, 200].

Alcoholic fermentation is a well-established technology for the production of ethanol from sugars and, after a hydrolysis pre-treatment, from lignocellulosic materials. Most of bioethanol is obtained from sugar cane. USA and Brazil are leading the market in terms of volume produced. Ethanol is produced from hexoses (C_6 sugars) and pentoses (C_5 sugars) thanks to microorganisms under aerobic conditions. Several countries have supported the introduction of bioethanol as alternative fuels, mixed with gasoline [202].

Thermochemical processes rely on the temperature, and somewhere on the pressure, in order to convert biogenic feedstock into heat and power, syngas and liquid (intermediate) fuels or chemicals. They include combustion, gasification, pyrolysis and hydrothermal upgrading (carbonization and liquefaction). Thermochemical processes, and particularly combustion, have been used since ancient times and have dominated the energy sector since the beginning of the industrial age and underwent centuries of optimization adopting fossil fuels. Therefore, one of the main advantages of thermochemical processes is the wide experience with solid feedstock. The process and the design of the reactor just have to be adapted to the new biogenic feedstock. Moreover, thermochemical processes are characterized by the high throughput and capacity, up to 140 MW of thermal input for the biomass wood gasifier in Vaskiluodon Voima in Finland [143, 24]. Despite the high throughput and favorable economy of scale, thermochemical conversion routes are not free of drawbacks, in particular the low selectivity to a defined product.

Thermo-chemical processes are classified as function of the air-to-fuel ratio or stoichiometric ratio. It is an operational definition, related to the process, since it is not possible to control the presence of oxygen from 0 to >1 because biogenic feedstock contain up to 50 wt.-% of oxygen. Pyrolysis, for instance, may be defined as the thermochemical decomposition of an organic material in *"absence of a gasification medium",* and not in *"absence of oxygen"* as often reported in the scientific literature. The classification as function of the stoichiometric ratio is depicted graphically in Figure 8.

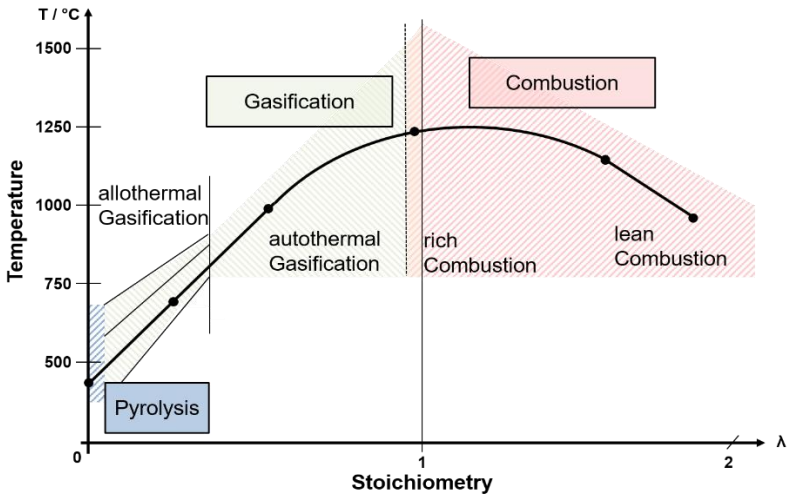

Figure 8. Classification of the thermo-chemical processes as function of the stoichiometric ratio [189].

Direct combustion is still the most important thermochemical process, even if much of the research focused on the production of liquid biofuels for transportation. It has been argued that producing heat and power in centralized large biomass combustion facilities and, then loading the batteries of electric cars and vehicles is more environmentally friendly than producing green biofuels [30]. Combustion is broadly defined as the burning of solid fossil and biogenic feedstock; it is a very complex process involving drying, devolatilization and oxidation of volatiles, as well as heterogeneous combustion of char. Hot flue gases are produced and eventually converted into pressurized steam for process heat or further expanded for power generation. Combustion is the most widely implemented process for heat and power production from biogenic feedstock, which can rely on the advanced infrastructure already available. On the other hand, combustion of biogenic feedstock is affected by some technical drawbacks such as fouling and slagging as well as logistic issues like the difficulties of supply enough feedstock to the power plants [110, 30, 202].

Gasification is defined as the thermal conversion of organic materials into burnable gases under reducing conditions with a stoichiometric ratio below one [30]. The obtained gases are normally named differently depending on several factors. Bain and Broer assign the name *producer gas* to the low heating value gas mixture from air gasification, while the name *syngas* is given to the high heating value gas mixture of CO and H_2 from oxygen and steam gasification of carbonaceous materials followed by gas cleaning and CO_2 separation. Kan and Strezov do not distinguish between air and oxygen/steam gasification but only between the raw mixture including tar impurities and the clean one, after cleaning, water and CO_2 separation [30, 202]. Although gasification has less problems in terms of slagging and other ash-related issues, the strict syngas quality control and cleaning requirements have limited the commercial spread of gasifiers based on biogenic feedstock [227].

Pyrolysis is the thermal decomposition of organic matter in the absence of additional oxygen [28]. The products of pyrolysis are a solid residue, the char, and a mixture of organic condensable vapors, water vapor and non-condensable or permanent gases in different distributions depending on the feedstock, on the process conditions and on the reactor technology, among others [29]. If the desired product is the liquid, high heating rates and fast quenching should be pursued; on the other hand, if the solid biochar is the wanted product, slow heating rates and relatively mild temperatures, i.e. 400°C, are the target process parameters. Despite the great flexibility of the pyrolysis process, few units are currently in operation at demonstration scale. Technical issues on the one hand but mainly economic constraints are behind lack of references. The research related to pyrolysis mostly focused on the yield of the condensate for decades, while the production of a qualitatively sound liquid fuel became a major target only in the last ten to fifteen years due to the rise of catalytic pyrolysis. However, the strategies adopted are not yet mature for a large scale implementation (see chapter 2.2) [65].

If pyrolysis is carried out under subcritical liquid water, it adopts the name of **hydrothermal carbonization or HTC**, where the main aim is to obtain a solid product, the so-called biochar or hydrochar or carbonized solid. The process is meant to suit to wet biogenic feedstock without drying and to gain access to ionic reactions under liquid water conditions [202]. As well as pyrolysis, hydrothermal carbonization is a complex system of parallel reactions, which include hydrolysis and dehydration, which defines the exothermicity of the process, along decarboxylation, condensation, polymerization and aromatization [82]. The severity, i.e. temperature, water pressure and residence time, influences strongly the properties of the hydrothermal carbonized solid. HTC for the generation of liquids and of syngas takes the name of liquefaction and hydrothermal gasification at the lower and higher limits of severity, respectively. Although HTC is a recent technology, it already found its way to commercial demonstration [18].

2.2 Pyrolysis

Pyrolysis is the thermal decomposition of organic matter under inert environment at high temperatures. It is the first chemical step in gasification and combustion of solids, but it may also be used as stand-alone process for the upgrading of biogenic feedstock for the production of more valuable products. During pyrolysis, three main products are obtained, i.e. a solid residue (char), non-condensable gases and a condensate (the bio-oil or pyrolysis oil). The distribution of the products yields depends on different factors. The composition and the structure of the feedstock on the one hand delimits mainly the range of products yields and compositions; the process parameters on the other hand determine the optimal output for the desired application. While the process temperature is the most relevant operational parameter, the pyrolysis process is often defined by the heating rate, i.e. the time required by the feedstock particle to reach the process temperature. As a first approach, pyrolysis processes may be distinguished between conventional (slow) and fast pyrolysis, where the main product is a carbonized solid and an intermediate condensate, the so-called pyrolysis oil, respectively [146]. Several authors have attempted to organize a more detailed classification based on the heating rate and on the process temperature [59, 28]. Distinctions are made between fast and flash pyrolysis, or between carbonization, slow and intermediate pyrolysis, as well as between torrefaction and carbonization. However, there is a strict correlation between the particle size and the effective heating rate [61]. Hence, the mentioned classification can be associated directly to the reactor technology, which is adopted to perform pyrolysis. Some authors even include variations of the typical pyrolysis definition, which could be defined as reactive pyrolysis. In such cases, the inert environment, made of an inert purging gas, is replaced by a reactive one using hydrogen, steam or methanol (allothermal gasification in Figure 8). A classification, based on the one proposed by Bridgwater [28], is reported in Table 1. Typical temperatures and residence times of the vapors are reported, together with the products yields distributions.

Table 1. Classification of pyrolysis types, including the main feature and products yields of wood pyrolysis (on dry basis) [28].

Mode	Temperature	Residence Time	Liquid	Char	Gas
Fast	~ 500°C	Gas ~ 1 s; Solids < 1 min	75%	12%	13%
Intermediate	~ 500°C	Gas < 30 s; Solids ~ 10 min	50%	25%	25%
Carbonization (slow)	~ 400°C	Solids ~ days	30%	35%	35%
Torrefaction (slow)	< 290°C	Solids ~60 min	< 5%	80%	20%
Gasification	< 900°C	< 1 s	5%	10%	85%

While most of the research focused on the production of liquids from relatively high quality feedstock, such as bark-free wood, pyrolysis of waste and of other residual streams has been always seen as an alternative disposal of technology compared to incineration. This view is arguable since the products of pyrolysis still require refining steps before further utilization. If disposal of the residues is planned,

there is no real advantage. For instance, the pyrolysis plant in Burgau in South Germany, which generated electricity from the post-combustion of the pyrolysis vapors from household waste must sustain the requirements of the German regulation 17. BImSchV, i.e. the one in force for waste and sewage sludge combustion plants. Moreover, the carbonized solid is disposed of occupying more landfill volume per unit of waste than the respective incinerated ash. Ultimately, the MSW pyrolysis facility in Burgau is not allowed anymore to operate as disposal plant.

In conclusion, also pyrolysis of waste and residual streams should be intended to be either a pre-treatment step for the production of liquid fuels or a stand-alone process for the generation of heat and power from the post-combustion of the pyrolysis vapors and of a useful carbonized solid.

The scientific effort during the few last decades on pyrolysis-related research and development followed four main lines:

- Understanding the fundamentals of pyrolysis, mainly related to kinetics and particle modeling;
- Design of novel reactor technologies;
- Characterization of the pyrolysis products from different feedstock. The focus was mainly on the chemical characterization of the bio-oil and of the biochar, while the application-related characterizations are gaining importance in the last years;
- Development of process chains based on pyrolysis, mainly in relation to biorefinery concepts.

In the following section, the scientific work related to pyrolysis will be discussed in terms of fundamentals, products characterizations and reactor design with focus on the works related to screw/auger reactors.

2.2.1 Fundamentals of pyrolysis

Pyrolysis of organic matter, and more specifically of biomass, is a complex mechanism that involves the heat transfer from the surroundings to the surface of a particle and following heat penetration into the particle by conduction. Depending on the particle size and on the reaction rate, primary decomposition reactions or secondary cracking/charring reactions will dominate and influence the yields and composition of the pyrolysis products.

The study of pyrolysis fundamentals consists essentially in combining different time and length scales, with the aim of describing chemical and thermal processes using first principles [6]. The chemical reaction kinetics are studied at molecular level, where activation energies and reaction rates are the results of mainly micro thermogravimetric analysis (TGA); at particle level, the equation of

the mass, momentum and energy conservation are solved normally approaching the problem adopting dimensionless numbers on the footsteps of the Thiele modulus from coke combustion [170].
As very first approach, pyrolysis of a solid particle consists of the following steps:

- Heating and drying, where the free water content is removed together with some loosely bound water;
- Devolatilization is the main stage, in which the most of the volatile matter is released;
- Secondary reactions, such as tar cracking, if the temperature is high enough (normally above 300°C), where the main organic compounds are further decomposed into non-condensable gases and lighter organics accompanied by the formation of aromatics or polymerization and condensation reactions at lower temperatures;
- Charring, is the structural modification of the solid particle with a consistent increase of the porosity due to the release of the volatile matter.

The choice of a pyrolysis model for the conversion of biogenic feedstock depends on the target of its utilization. Several models with increasing degree of complexity are available in the scientific literature. For instance, for the basic design of a reactor it may be sufficient to adopt continuous global models, which neglect heat and mass transfer within the core of the particle and provide a composition of the products for the bulk solid. For the investigation of the relative importance of primary and secondary reactions in the pores of the particle, the combined effects of mass and energy transport may be required. Moreover, if the main target is the evaluation of the individual reactions at molecular level, the utilization of quantum mechanics could also be employed to determine the activation energy.
The following paragraphs will provide an overview of the mechanisms involved during pyrolysis with the aim of motivating the assumptions made for the development of the model used in this work.

Reaction mechanisms and kinetics

Pyrolysis scientific literature is packed with possible reaction mechanisms taking place during the thermal decomposition of a wide range of biogenic feedstock.
Pyrolysis involves a convoluted network of chemical reactions. In the first step, under inert conditions and supply of energy in the form of heat, the organic matter is decomposed into a solid residue and organic vapors, a complex mixture of CO, CO_2, non-condensable hydrocarbons, moisture and reaction water as well as organic oxygenated condensable vapors. The formation mechanism of the primary products has been widely investigated experimentally and models have been developed on that basis. Whether char and vapors are formed by competitive reactions with different kinetic rates

(Figure 9 left), by the thermodynamic equilibrium (Figure 9 right) or by secondary (charring) reactions in the particle is still a matter of discussion in the pyrolysis community. Cellulose, for instance, does not produce any char if vapor-solid interactions are minimized. Therefore, char is essentially a product of secondary intra-particle reactions of cellulose pyrolysis [8]. As pointed out by Antal and Varhegyi [8], the utilization of parallel reactions (Figure 9 right) for the production of the two products is not necessarily correct from the point of view of analytical chemistry because the selectivity should be addressed in that case; however, it allows accounting for the constant increase of the yields of condensable organics and gases at the expenses of the char [61]. Hence, the two competitive reactions mechanism appears to be a suitable way to address this issue from the point of view of apparent kinetics, which are normally used in the modelling of chemical reactors, if modeling considerations on the single solid particle are avoided.

On the other hand, char is a primary product of lignin pyrolysis. Due to its complex aromatic structure, pyrolysis takes place on a wide range of temperatures where the side chains are removed leaving the inter-bonding aromatic units unaltered, which form the backbone of char [117].

Figure 9. Schematic mechanism of one-step reaction (left) and two competitive reactions (right)

In the successive phase, the vapors undergo a wide number of secondary reactions, taking place both homogeneously, e.g. tar cracking, and heterogeneously on the solid surface. The severity of the conditions, essentially a combination of the reactor temperature, pressure and conversion, as well as the extent of the secondary reactions define the composition and yields of the pyrolysis products. At low temperature, in the range of 300°C, repolymerization and condensation reactions are favored. At higher temperatures, above 500°C, further cracking of the condensable organics dominates the mechanism and leads to higher yields for non-condensable gases. Diebold [66] described at first the importance of the gas phase reactions of biomass pyrolysis, reporting high yields of ethylene and other olefins from flash pyrolysis of wood. Following this study, Antal [7] discussed the effect of reactor's kinetic severity on the yield and composition of the non-condensable gases evidencing the more relevant influence of temperature compared to that of the time. In the same work, using the competition for carbon atoms, a model similar to that of Figure 9 (right) was deduced, where two first-order reactions were used to describe (1) cracking of the reactive volatile matter to smaller and less reactive species and (2) the production of more stable condensable organics yielding tar or "some

combination of water-soluble organic compounds". On this basis, Boroson et al. [26] proceeded with a further simplification of the reaction mechanism, lumping the reaction scheme with either a single reaction with a first-order rate constant or using a distributed activation energy model (DAEM) fitting the kinetic parameters using their own experimental data. Both Antal and Boroson et al. highlighted that CO_2 is a primary product from wood pyrolysis, while the main product of secondary reaction was CO followed by CH_4 (methane) and C_2H_4 (ethylene). Morf et al. [148] extended the previous works deeply investigating the secondary reactions of tar. The main focus was on condensable organics, with specific attention to phenols, mono- and polyaromatic hydrocarbons such as benzene and naphthalene as well as to soot formation. It was stated that soot was one of the major products of biomass secondary reactions. The provided model adopted a straight-forward series of three consecutive first-order reactions as depicted in Figure 10, where gravimetric tar has probably the same significance of refractory condensable organics adopted by Antal in [7] and k_{N1}, k_{N2} and k_{N3} are the kinetics rate constants of the reactions.

Figure 10. Secondary and following gas phase reactions of gravimetric tar. Adapted from [148]

Probably the most complete and clear description of the complex network of biomass pyrolysis was offered by Diebold and depicted in Figure 11. Biomass undergoes pyrolysis at relatively low temperatures, where the produced primary tar is still in liquid form but vaporizes immediately under rapid heating rates at temperatures above 500°C and low pressures or is converted in secondary liquid tar and carbonizes releasing water under slow heating rates, low temperatures and high partial pressures. The vaporized primary tars are fragmented at high temperatures to produce a wide range of oxygenated compounds. From this point, depending on the process operational conditions, an extreme large spectrum of products may be derived, i.e. from gravimetric tars to secondary vapors such as phenols, from light hydrocarbons and olefins to carbon black. Despite the tremendous effort undertaken in the last thirty years, the detailed chemical mechanisms involved in the secondary gas phase reactions of biomass are still undisclosed.

Attempts were made to describe the detailed mechanisms of biomass pyrolysis by considering the linear combination of its main components, i.e. cellulose, hemicellulose and lignin. Most of the scientific work was reviewed by Di Blasi [62] and more recently by Anca-Cuoce [6]. Reaction mechanisms were derived from that of cellulose, firstly described in the seventies by Shafizadeh and further developed by Broido and co-workers [8].

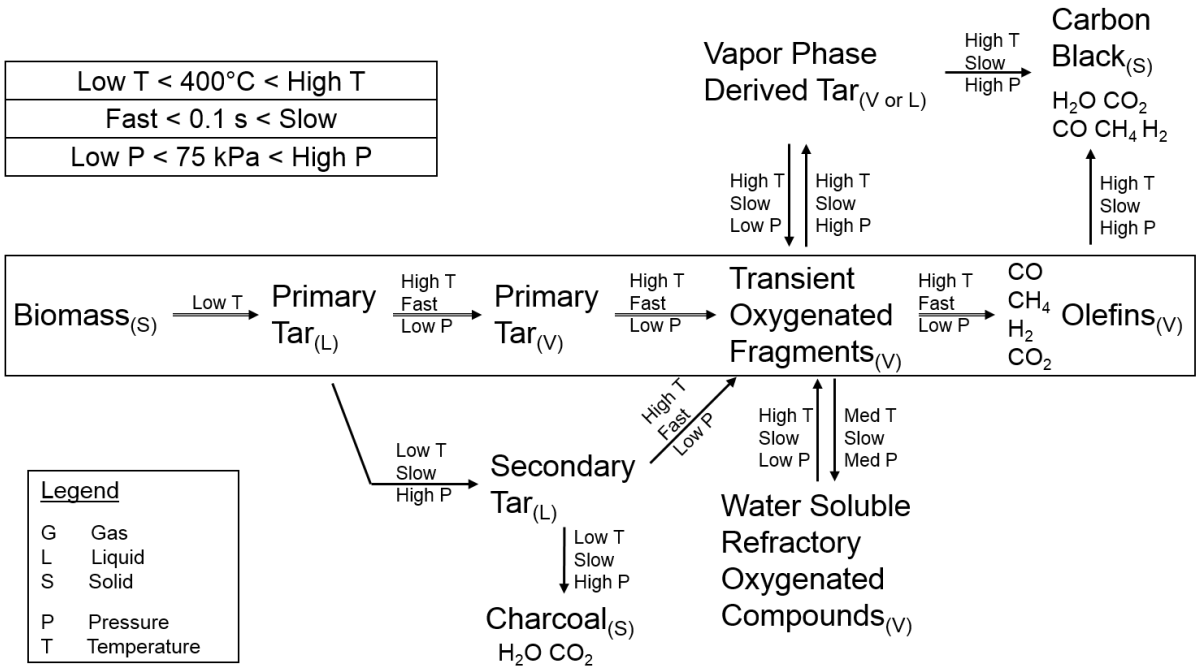

Figure 11. Mechanism of biomass pyrolysis. Source: [66]

The model is nowadays known as Shafizadeh-Broido model, where cellulose undergoes a first activation step with decrease in the degree of polymerization and without mass loss, followed by two competitive reactions to form condensable organics (tars) on the one hand; char and non-condensable gases on the other side. Further investigations by Piskorz [171] placed the formation of char and water pathway in competition to the activation step of cellulose for slow heating rates and low temperatures. On the other hand, after the activation step, the decomposition of cellulose was due to two competitive reactions, i.e. fragmentation with high yields of hydroxyacetaldehyde and other low molecular weight organics and transglycosylation to form levoglucosan in liquid phase, which was finally recognized by Banyasz to be the precursor of secondary char during its vaporization [20]. Other works highlighted the importance of minerals and the intra-particle secondary reactions to form more char and gases and less condensable organics as well as the interactions with hemicellulose and lignin during wood pyrolysis [176, 104, 228].

Decomposition of hemicellulose follows the same schemes as cellulose. However, its branched structure makes the description of the single pathways and reaction products more complex than for cellulose and favors the production of char. Hemicellulose has been described by single decomposition mechanisms as well as by a complex network of reactions leading to the production of acetic acid, furfural (for hardwoods) or 5-methyl-furfural (for softwoods) and other gases, such as CO, CO_2 and H_2O [229, 193, 62].

The decomposition mechanism of lignin, as third most important model compound of wood has been also studied by several groups. The reaction takes place on a wide range of temperatures, because of the complex tridimensional structure made of different side chains, which leads to the formation of a large spectrum of intermediate products in condensed phase followed by the production of the so-called pyrolytic lignin, char and light gases and condensable organics [38]. Lignin has been modeled as single pseudo-compound and as a combination of three components by Favarelli and co-workers [78], rich in carbon, hydrogen and oxygen, respectively in order to describe the differences between softwood and hardwood lignins.

Most of the reaction mechanisms for single or multi component pyrolysis are limited by the fact that they are not able to predict the composition of the three pseudo-products, i.e. the char, condensable organics and non-condensable gases, and therefore it is not possible to close the elemental balances. Only in recent years, attempts were taken to overcome this issue. The work of Ranzi and his group tried to describe the chemical kinetic mechanism of wood by characterizing the biomass as a weighted mixture of three main components with respective CHO composition, describing the release of the volatile matter by a complex lumping procedure to obtain a mixture of real species and finally modeling the chemical evolution, i.e. the secondary reactions, of the gas phase [175]. The model has undergone some upgrading, in particular by the contribution of Anca-Couce to take into account the charring reactions, which lead to a much lower levoglucosan yield and high char yield [5].

The superposition of the three main components allows the prediction of the degradation curves of different kinds of lignocellulosic biomass [145]. However, most of the untreated biomass and other biogenic feedstock as well contain a variable amount and composition of minerals and metals, whose effect is extremely strong and relatively complex to characterize [176, 177]. Demineralization as well as minerals and metals enrichment of the biomass were investigated to gain knowledge on the effect of ash on yields and product compositions. A general negative correlation between the ash content and yield of the condensable organics as well as an increase of the gas yields was observed. Potassium (K) and Sodium (Na) ions appear to have the most important effects [156]. Moreover, ash reduces the pyrolysis temperature, independently from being of acid or alkaline nature [231].

As already stated, pyrolysis is a kinetic process, which depends on the applied heating rate and on the presence of contaminants, such as metals and minerals [231, 176]. The determination of the kinetic parameters plays a fundamental role for the description of the process and for the following design and optimization of the selected reactor. The most used techniques to determine the kinetic parameters are thermogravimetric analysis (TGA) under single or multiple heating rates, differential thermal analysis (DTA) and pyrolysis gas-chromatography/mass-spectrometry (Py-GC/MS) [33]. TGA is a non-isothermal method applied to determine the temperature dependence of the decomposition,

plotting the mass loss against the actual temperature [30]. The obtained curves are normally fitted using the Arrhenius equation (Equation 1), where E_a is the activation energy, A_0 is the frequency or pre-exponential factor; R is the universal gas constant and T is the corresponding temperature of reaction.

$$k_0 = A_0 \exp\left(-\frac{E_a}{RT}\right) \qquad \text{Equation 1}$$

The kinetic parameters for several different biogenic feedstock have been vastly investigated adopting TGA analysis, by fitting the obtained curves, usually more than one at different heating rates, to the Arrhenius equation. Values are provided for single polymers, such as plastics or cellulose, as well as for heterogeneous and complex materials, like municipal solid waste or sewage sludge [195, 188]. The pyrolysis kinetics of lignocellulosic biomass are often described by the superposition of the single kinetics of its main components. Other biogenic, non-lignocellulosic feedstock is described by one-component kinetic parameters. The application of thermogravimetric analysis for the experimental determination of reaction kinetics relies on the assumption that heat and mass transfer are negligible. Therefore, very small samples are required even at low heating rates posing the issue of sample homogeneity and representativeness. The kinetic parameters determined by TGA should be referred as “apparent” or “global”, since the reported values can deviate from the “intrinsic” kinetics of each individual step. However, global kinetics may well represent multi-step processes with a single rate-limiting step. Even for relatively homogeneous materials such as cellulose, different authors provide completely different values. The differences are associated to different experimental set-ups, different mathematical approaches, etc. [6, 62, 145]. Another important limitation of TGA is that the applied heating rates are far below the ones reached in technical systems. To overcome this issue, other approaches may be employed to evaluate the kinetics at high heating rates. A typical approach consists on the adoption of drop tubes, which enables heating rates in the range of 10^4 to 10^5 K/s and therefore is able to decouple the kinetics from the mass and heat transfer. The evaluation of the kinetics at high temperatures in a drop tube closely simulates industrial conditions [121]. However, for complex bio-polymers such as biomass, the kinetics of the single components overlap, reducing the prediction capabilities of the approach for materials with different chemical and structural compositions. Because of the structural changes of the solid and of the synergistic mechanisms between the model compounds of the feedstock, i.e. cellulose, hemicellulose and lignin, a different approach was proposed and mainly adopted for TGA experiments. The so-called distributed activation energy model (DAEM) assumes an infinite number of first-order parallel reactions with different activation energies and same frequency factor occurring simultaneously [198, 39]. The

DAEM models assume that the activation energy of each model compound changes at different conversions; thus, they try to account for solid-state rearrangement of the pores structure. However, also the models based on the DAEM approach should be considered formal or global kinetics, since they do not explicitly consider the mechanism taking place in the pores. Model-free methods were also proposed to derive the kinetic parameters [224, 4]. This approach estimates first the activation energy and the frequency factor and secondly, in a separate step, defines the conversion function [190]. One issue of all the discussed models is that they are not able to predict the decrease of the solid yield at the thermodynamic equilibrium under increasing offset temperature. A popular approach in reaction kinetics is to adopt two competitive reactions, the first leading to solid and gas and the second leading to condensable compounds. The first reaction is faster at low temperatures, thus the solid residue decreases with increasing offset temperature or heating rate. This simplification may avoid modeling the heat and mass transfer taking place in the single particle, thus reducing the computational effort in basic reactor design. However, the prediction capabilities are limited to a narrow range of process conditions and feedstock [145].

In conclusion, the choice of kinetic parameters is necessary in every pyrolysis process; however, depending on the purpose of the analysis, considerations related to the mass and heat transfer within the single particle may also be taken into account. The following paragraph will discuss the issues related to the combined effects of reactions kinetics and thermal mechanisms.

Heat and Mass Transfer (Single particle)

Heat and mass transfer becomes of fundamental relevance during pyrolysis of a biomass particle. In fact, besides chemical reactions, transport of energy, mass and momentum influence greatly the composition and yields, acting on the residence time and local temperature, therefore influencing the reaction rates of primary and secondary (thermal cracking/charring) pyrolysis mechanisms.

The impact of heat and mass transfer has been studied widely in the scientific literature on pyrolysis of biomass. One way to approach the problem is using non dimensional numbers, i.e. the Biot number (Bi in Equation 2) and the Pyrolysis numbers Py (Equation 3), referring to internal heat penetration, and Py' (Equation 4) to external heat transport to the particle [172]. The Biot number is widely used in heat transfer analysis indicating the ratio between the heat transfer resistances in the core and on the surface of the solid particle. For Biot numbers < 0.1, the conductive heat transfer inside the particle is sufficiently fast to assume negligible temperature gradient in the body. The Biot number decreases with decreasing particle size and increasing thermal conductivity of the solid. The Pyrolysis numbers Py and Py' describe the ratio between the heat transfer and the reaction rate. Small pyrolysis numbers

indicate heat transfer control, i.e. the reactions proceed fast and the process is limited by heat transfer. Again, a larger particle size implies small Py and Py', thus the process is thermally limited.

$$Bi = \frac{\alpha L}{\lambda} \quad \text{Equation 2} \qquad Py = \frac{\lambda}{k_0 c_p L^2} \quad \text{Equation 3} \qquad Py' = \frac{\alpha}{k_0 c_p L} \quad \text{Equation 4}$$

By using the mentioned approach, four regions of relevance are defined and depicted in Figure 12, as reported by Anca-Couce [6]:

- Regime I: pure kinetic regime at low Biot numbers and high reactions rates, i.e. below 0.1 and at low temperatures, respectively, the pyrolysis process is controlled by the kinetics at constant temperature. This is the typical situation obtained during micro TGA experiments, where the set heating rate is relatively low, i.e. in the range of 10 K/min;
- Regime II: thermally thin regime is obtained at low Biot numbers, where no internal temperature gradients are present and at relatively high temperatures. This is the typical fast pyrolysis situation, where high heating rates are applied to small particles. In such situation, the temperature may be only estimated; thus the determination of the kinetic parameters in this pyrolysis regime is particularly challenging, since thermal decomposition at low temperatures will probably take place even in the very short transitory phase to the final temperature;
- Regime III: thermally thick regime applies for larger particles at low temperatures, where the internal conduction is much slower than the external heat transfer. Thermal gradients will be present within the particle, leading to a complex reaction mechanism where secondary reactions, such as tar cracking and charring may become dominant;
- Regime IV: thermal wave regime is found at high Biot numbers and high temperatures. It is mainly applied to shrinking core models, where pyrolysis takes place on an infinitely thin layer, which separates the reacted char from the virgin biomass [32].

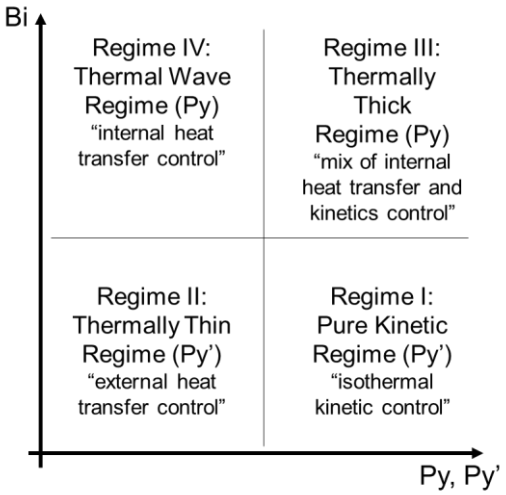

Figure 12. Pyrolysis regimes based on non-dimensional numbers. Elaboration from [6].

Considerations related to the pyrolysis regime are of fundamental relevance during the modeling of a pyrolysis reactor, where the processes at particle level are normally neglected, and the granular bed is treated as a continuum with the interstitial gas and it is defined by effective properties. In the case of thermally controlled processes, the effective reaction rate will require an "adjustment" to take into account the thermal delay occurring within the particles. The choice of the correct formal or apparent kinetic parameters is a crucial factor in reactor modeling and scale-up for known feedstock, even if it does not have prediction function for other materials or for the same material with particle sizes outside a defined range. In this sense, a more accurate description of the mechanisms should prefer the coupling of structural model of the particle with the conservation of energy and momentum and use intrinsic kinetics [187]. An interesting approach is offered by Schinkel [183]. In his work, he proposed a model, which included the mechanism of chemisorption equilibrium to describe the reaction complex. Such degree of complexity may be excessive for the basic design of a pyrolysis reactor and require demanding computational time. Another important issue related to heat and mass transfer is given by the bulk of solid material. Conventional heating proceeds from the exterior of the bulk to the core; temperature gradients are present and may influence the local reaction rate [120].

2.2.2 Pyrolysis reactors

As already mentioned, the mode of pyrolysis is essentially defined by the reactor technology, which is chosen in order to achieve a desired target in terms of products yields. Most of the technological effort of the last 40 years dealt with the development of fast pyrolysis reactors for liquid production from biomass, and particularly from wood. The main specification to address is the critically elevated heating rate, which typically requires a fine milled material. Several reactors were investigated at

different scale and, nowadays, only four systems have been applied at commercial level. A very detailed review is reported by Meier and Faix [140] and by Bridgwater [28].

- Bubbling Fluidized Bed (BFB) Reactors (fast pyrolysis): also referred as fluidized bed to distinguish it from the circulating bed reactor; this is a well-understood technology. Because of the high solid density inside the reactor, temperature control and heat transfer are very well warranted. Sand is usually used as solid phase, with a volume ratio of sand to biomass around 20. Liquids are of good quality and a high yield is typically achieved. Char is not accumulated inside the bed, but quickly ejected and then separated in a cyclone. The residence time of the solid residue is higher than that of the vapor phase, which is instead controlled by the flow rate of the fluidizing gas. At pyrolysis temperatures, the char acts as a catalyst for vapor cracking reactions. Finally, a careful design of the hydrodynamics of fluidized solids is important;
- Circulating Fluidized Bed (CFB) Reactors (fast pyrolysis): the design is characterized by higher circulating flow and by larger reactor diameters than that of the BFB. The main difference is the residence time of the solids, which is reduced and, in this case, equal to that of the vapors because of the higher speed of the fluidizing gas. As a consequence, the probability of finding solid residues inside the condensate increases unless extensive implementation of char removal equipment. Moreover, the heat transfer is reduced, compared with bubbling bed reactors, because of the increased importance of convective heat transfer with respect to conductive heat transfer. Therefore, in comparison to BFB reactors, particles of a smaller size are employed to facilitate the conversion. Often, a second vessel is employed: the char mixed with sand, which is recovered in the cyclones, goes in this second vessel where it is burnt in order to re-heat the solid medium. Burning the solid residues leads to an increased ash content in the sand, which aggravates the influence of catalyzed cracking reactions, thus reducing the oil yield. However, the possibility of CFB to operate with very high throughputs makes this technology competitive;
- Rotating cone (fast pyrolysis): it is a more recent development of the University of Twente and implemented by BTG at large scale. The technology operated as a transported bed using centrifugal forces instead of fluidizing gas. It is a rather complex technology with three main components, i.e. the rotating cone, the riser for sand recycling and the BFB char combustor. Less gas is required and the liquid yields are slightly lower compared to the other fluidized bed technologies;

- Ablative Pyrolysis Reactors (fast pyrolysis): the concept of ablative pyrolysis reactors is completely different from those of the other categories, in which the heat transfer through the particles is the limiting factor of the process. For his reason, these latter processes are not compatible with large biomass particles. In the ablative pyrolysis, heating is achieved by pressing down and moving the feedstock over a hot wall surface. The pressurized process enhances the rate of melting. Pyrolysis proceeds unidirectionally through the biomass particle; the solid is mechanically removed while the residual oil provides lubrication for the following particles and evaporates quickly. Thus, it can be removed and then condensed in the common way also used by other configurations. The reactions are strongly influenced by pressure, relative motion between the biomass and the hot wall, shear forces, which reduce particles size and increase surface area, and the reactor surface temperature. The inherent complexity is the main disadvantage of this configuration;
- Rotary Kiln Reactors (intermediate and slow pyrolysis): the reactor is a cylindrical vessel, inclined slightly to the horizontal direction, which is rotated slowly around its axis. The material gradually moves forward undergoing stirring and mixing. The heat required is provided by hot gases, which are produced in an external furnace. The pyrolysis vapors flow along the reactor in co-current flow with the solid material; the residence time of vapors is controlled by a blower. The vapors are cleaned in cyclones and usually burnt in a combustion chamber to provide hot gas, which is used to supply the required heat to the process and to generate steam.
- Screw or Auger Reactors (intermediate and slow pyrolysis): in this configuration, a screw is used to move the feedstock through an oxygen-free, heated tube. During the passage, the feedstock is heated-up to the process temperature causing pyrolysis. The configuration allows continuous processing, in which char is produced. Vapors are collected as condensate and permanent gas. The residence time of vapors can be modified by controlling the length of the heated zone. In some cases, the process does not require a carrier gas. Screw reactors can be adopted for fast pyrolysis, if a solid heating medium is employed to enhance the heat transfer within the bulk, as well as for intermediate or slow pyrolysis. In this situation, no heating medium is used and the overall heat transfer coefficient is an order of magnitude lower compared to that of fast pyrolysis conditions. The compact design of this configuration is pursued in order to reduce the energy costs. Screw reactors are suitable for decentralized plants due to the issues related to the heat transfer (see also Chapter 2.2.3).

- Fixed Bed Reactors (slow pyrolysis): this technology is well known for the production of char. The heat transfer is rather slow and the residence time of the vapors is higher reducing the conversion of the feedstock to liquid products.
- Vacuum Pyrolysis Reactors (fast pyrolysis): this category of reactors is characterized by a much lower heating rate, thus it does not fall within the spectrum of fast pyrolysis reactors due to the much lower overall heat transfer coefficient. Pyrolysis products evolve from the solid phase over a longer time scale, nevertheless the residence time of vapors is comparable to that of fast pyrolysis reactors. Thermal decomposition takes place under reduced pressure; the fragmented products are vaporized and withdrawn from the reactor by vacuum. They are recovered by condensation as oils with a high boiling point and may undergo further decomposition if vacuum is not applied. The extremely fast vaporization and removal reduce the effect of secondary reactions. The process is usually carried out at 450°C and a total pressure of 15 kPa; residence times of vapors and char are decoupled. Poor heat and mass transfer are still unsolved problems which affect the desirability of the configuration;

Excluding few but fundamental technologies like grate systems, entrained flow and shaft reactors, most of the reactor systems are essentially the same for combustion, gasification and pyrolysis. In fact, the main driver is the trade-off between technical challenges of the process and economics of the reactor technologies.

2.2.3 Brief review of pyrolysis using screw reactors

Screw or auger reactors have been used since centuries for a wide spectrum of applications. Also known as Archimedes' screw, auger reactors are characterized by robustness and found their main application as transport device, able to move bulk solids, liquids and slurries. The following is an incomplete list of applications for screw reactors:

- Transport (feeding or moving);
- Compaction (reduction of the volume of waste);
- Processing (several application in food and chemical industries);
- Extrusion;
- Cooling;
- Heating;
- Drying;
- Torrefaction;
- Pyrolysis.

The robustness, associated with the low costs and an unmatched transport efficiency, makes screw reactors one of the favorite technology in most of the aforementioned applications. Single screw augers are suitable for processes such as indirect heating and cooling. However, in applications where high heat transfer rates are required, twin-screw reactors are preferred because of the better mixing quality [179]. For drying, torrefaction and slow pyrolysis of biomass, high heating rates are not required; therefore single screw reactors are often adopted. On the other hand, for fast pyrolysis applications, twin-screw reactors and a direct heat transfer through a co-fed solid medium is preferred [95]. However, with the raising interest to the in-situ catalytic pyrolysis, solid media with catalytic effect were also co-fed in single screw reactors [223, 236].

The history of auger reactors for pyrolysis purposes goes back to 1960, when Lakshmanan reported on the production of levoglucosan in a screw pyrolyzer [119]. In 1990, Camp discussed the pyrolysis of brown coal in a screw conveyor, mainly to highlight the drawbacks of the technology and scale-up as well as the problematic of low throughput and formation of sticky tar on the unheated shaft of the screw [41].

The scientific work published in the last ten years related to the pyrolysis process in screw reactors is essentially dedicated to the distribution and characterization of the products as function of the process conditions, i.e. the reactor temperature, feedstock composition as well as in combination with secondary processes directly coupled with the pyrolysis unit, such as in-situ or ex-situ catalysis. Most of the research work was carried out adopting second generation biomass, i.e. lignocellulosic feedstock, for the production of liquid fuel intermediates [223, 236]. However, few studies were devoted to the production of bio-char and of gas.

Table 2 gives a list of references, where screw reactors were adopted for pyrolysis. The feedstock, the process parameters and yields of the products are reported. The yield of the char ranges between 35 wt.-% and 20 wt.-% depending mainly on the reactor temperature and on the ash content. The yield of the total condensate reached almost 60 wt.-% in one case, but the majority of the experiments shows a yield of 45 wt.-% to 50 wt.-%. In the case of biogenic residues, such as digestate, lower yields are obtained (about 35 wt.-%).

As already mentioned, most of the work had the focus on the characterization of the liquids. For example, Thangalazhy-Gupakumar et al. studied the effect of the reactor temperature on the physical and chemical properties of bio-oil derived from pine wood pyrolysis [206]. Ingram et al. focused their work on the characterization of bio-oil produced by the pyrolysis of different wood and bark. In their analysis, the authors compared the bio-oils with data from other fast pyrolysis technologies. Even if some doubts still remained because of the higher char yield, the main conclusion was that bio-oil from auger reactors are very similar to those produced at much higher heating rates [107]. Several

other studies focusing on the bio-oil properties are reported in the scientific literature. The main conclusion is that the bio-oil yield and properties are essentially a function of the native feedstock composition [127, 136, 93, 114].

Despite most of the works were devoted to the maximization and characterization of the bio-oil, there is a number of studies focusing on the improvement of the properties of the non-condensable gases. It is recognized that low-grade biogenic feedstock, i.e. biomass with relatively high ash contents, are not suitable for the exploitation of the derived bio-oil, mainly because of its instability. First of all, the bio-oil separates into an aqueous and into an organic phase. This second one is liquid but not homogenous; it tends to accumulate high viscous compounds, to polymerize and to eventually produce solid tar at room temperature. With the mentioned background, few studies implemented a number of technics in order to reduce the condensable organics favoring the production of high quality gas, which may be used in decentralized combined heat and power plants [72]. Among them, it is worth to mention the works of Hornung et al. and of Mahmood et al., which implemented catalytic low temperature steam reforming units downstream the pyrolysis reactor [103, 134, 100, 99]. From the experimental results, the heating value as well as the hydrogen concentration increased depending on the severity of the reforming and on the addition of steam. In a more recent paper, Neumann et al. introduced a thermo-catalytic reforming process, which adopted a screw reactor to convert digestate into pyrolysis products, followed by a second reactor, in which the pyrolysis vapors were “reformed”, passing through a solid bed of pyrolysis char. The increase of the reforming temperature from 500°C to 750°C led to an increase of the permanent gases, a slight decrease of the water-like phase and to a consistent decrease of the bio-oil phase and of the char [154]. Zhao et al., as well as Veses et al., approached the upgrading of the pyrolysis gas in a different fashion. Adopting calcium-based materials, pyrolysis experiments were carried out in screw reactors, where the catalysts were fed together with the biomass in order to produce high quality fuel gas and to improve the properties of the bio-oil, respectively. Although the targets were different, a shared conclusion was that the adoption of inexpensive in-situ catalyst/sorbent reduces the heat of reactions and improves the quality of the volatile products [223, 238].

In conclusion, pyrolysis of biomass and other biogenic feedstock in screw reactor was extensively investigated experimentally by a number of scientific groups. A wide spectrum of biomass, ranging from high quality second generation lignocellulosic feedstock to low-rank agricultural residues, were characterized in term of yields and products properties. Several integration concepts were developed to upgrade the products from the pyrolysis of biomass in a screw reactor, using both in-situ and ex-situ catalytic media.

From the commercial side, few companies were established in the last few years. In Germany, PYREG, Regenis and Susteen Technologies GmbH developed pyrolysis technologies based on screw reactors for bio-char and for heat and power applications, respectively. In France, Biogreen from the ETIA Group offers pyrolysis plants based on screw pyrolysis technology for biofuels as well as for soil applications [173, 178, 204, 22].

Table 2. Selected publications related to the pyrolysis of biogenic feedstock in screw reactors. Yields of the products in wt.% of the feedstock. Diff means difference to 100%.

Study	Feedstock	Temperature	Feedstock Residence Time	Mass Flow Rate	Char	Bio-Oil	Aqueous Condensate	Total Liquid (H_2O)	Permanent Gases
Garcia-Perez [88]	Pine	500°C	6 min	1.5 kg/h	30	19.6	38.3	57.9 (30.9)	12.2
A. Hornung [101]	Wheat Straw	325°C	4 min	1.4 kg/h	73	-	-	18	9
	Wheat Straw	350°C	4 min	1.4 kg/h	48	-	-	34	18
	Wheat Straw	375°C	4 min	1.4 kg/h	38.2	-	-	37.7	24.1
	Wheat Straw	400°C	4 min	1.4 kg/h	33.5	-	-	34.6	31.9
U. Hornung[103]	Wheat Straw	450°C	10 min	2.4 kg/h	28	13.9	35.6	49.5	22.5
Ingram [107]	Pine	450°C	50 sec	1 kg/h	17.9 – 19.8	-	-	48.7 – 55.2 (16.0)	diff
	Pine Bark	450°C	50 sec	1 kg/h	9.7- 23.2	-	-	42.8 – 44.2 (19.8)	diff
	Oak	450°C	50 sec	1 kg/h	17.5 – 19.9	-	-	49.6 – 56.3 (22.5)	diff
	Oak Bark	450°C	50 sec	1 kg/h	21.3 – 27.8	-	-	43.8 – 49.8 (22.0)	diff
Kim [115]	Pine	500°C	72 sec	10 kg/h	22.6	-	-	59.5	17.6
	Pine	525°C	72 sec	10 kg/h	23.2	-	-	55.2	21.5
	Pine	550°C	72 sec	10 kg/h	17.5	-	-	53.6	28.9
Liaw [127]	Douglas Fir	500°C (pre 380°C)	30 sec	720 g/h	20	-	-	50 (14.0)	28
Mahmood [134]	Brewer Spent Grain	450°C	1 - 4 min	-	29	-	-	52 (41.1)	19

Study	Feedstock	Temperature	Feedstock Residence Time	Mass Flow Rate	Char	Bio-Oil	Aqueous Condensate	Total Liquid (H_2O)	Permanent Gases
Mura [151]	Wood	400°C	15 min	12.3 kg/h	33	-	-	-	diff
	Wood	500°C	20 min	11 kg/h	29	-	-	-	diff
	Wood	600°C	40 min	9 kg/h	20	-	-	-	diff
Mura [151]	Sewage Sludge	400°C	20 min	39 kg/h	70	-	-	-	diff
	Sewage Sludge	500°C	35 min	23 kg/h	30	-	-	-	diff
	Sewage Sludge	600°C	40 min	16 kg/h	22	-	-	-	diff
Neumann [154]	Digestate	400°C (ref 500°C)	5 min	1.6 kg/h	36	11	26	37	27
	Digestate	400°C (ref 600°C)	5 min	1.6 kg/h	33	9	24	33	34
	Digestate	400°C (ref 750°C)	5 min	1.6 kg/h	29	6	21	27	44
Ouadi [164]	De-Inking Sludge	450°C	-	15 kgh	75	9	1	10	15
Thangalazhy-Gopakumar [206]	Pine	425°C	Batch	500 g	35	-	-	45	20
	Pine	450°C	Batch	500 g	27	-	-	50	23
	Pine	475°C	Batch	500 g	22.5	-	-	45	32.5
	Pine	500°C	Batch	500 g	20	-	-	37.5	42.5
Veses [223]	Pine (+ Sand)	450°C	7 min	2 kg/h (+ 6 kg/h)	25	-	-	48 (21.0)	27
	Pine (+Sand+1/1 CaO)	450°C	7 min	2 kg/h (+ 6 kg/h)	27	-	-	50 (16.0)	23
	Pine (Sand+1/1CaOMgO)	450°C	7 min	2 kg/h (+ 6 kg/h)	26	-	-	50 (19.0)	24

2.2.4 Products properties

Every pyrolysis process generates typically four main products: the pyrolysis char, the pyrolysis- or bio-oil, an aqueous condensate by spontaneous separation from the bio-oil and a non-condensable gas. Pyrolysis may be adjusted to favor one specific product yield. Fast pyrolysis, for instance, focuses all its effort in producing the largest yield of bio-oil and converting the residual char, and the non-condensable gases, to heat for internal utilization within the process. On the other hand, slow pyrolysis or carbonization aim at producing char and minimize bio-oil.

The yields and the properties of the pyrolysis products can be influenced by the process conditions, which differ from one feedstock to another. The most important parameter is the temperature of the reactor, which defines the chemical equilibrium. An increase of the temperature leads to a steady decrease of the yield of the solid residues and to an increase of the non-condensable gases. The yield of the pyrolysis oil increases with increasing temperature up to a maximum value of about 75 wt.% for wood at 500°C. With further increase of the temperature, it decreases due to secondary cracking reactions. The carbon yields and distribution follow a similar trend with increasing temperature. Horne and Williams reported a decrease of the carbon yield from 35.8 wt.% at 400°C to 26.6 wt.% at 550°C for the flash pyrolysis of wood in a fluidized bed rector [98]. Other authors investigated the elemental distribution of carbon at various temperatures reporting similar trends [166, 19, 42]. The carbon distribution among the volatile products shifts from the condensate to the non-condensable gases with prolonged time under reaction conditions. At fixed temperature, the relative ratio between the yields of condensate and gases decreases with increasing residence time. The effect is more enhanced with increasing temperature [97]. The energy yields of the pyrolysis products may also be related to the process conditions. The mass and energy yields follow close trends as function of the pyrolysis temperature.

In the following section, the properties of the pyrolysis products will be briefly discussed in relation to their applications.

Bio-char

Pyrolysis char, bio-char or charcoal, is the carbonized solid residue of pyrolysis processes. It is the most important and valuable product of slow pyrolysis and carbonization processes. Charcoal is probably the oldest manufactured product in human history [9], having a production of 53 million tons in 2014 [77] and still being the favorite fuel for house cooking.

In their review, Antal and Grønli describe the thermodynamics of charcoal formation under variable temperature and pressure conditions, highlighting the exothermic nature of the reaction in contrast to the production of bio-oil under fast pyrolysis conditions [9].

Bio-char may be described at first by its proximate composition, made of water, volatile matter, ash and fixed carbon contents. With increasing temperature and decreasing pressure, though to a lesser extent, the fixed carbon content increases at the expenses of the volatile matter, which is removed from the carbonized matrix as organic vapors and condensed to produce bio-oil, pyrolysis oil or "tar". The total char yield includes the mineral content of the feedstock, i.e. the ash, which quantitatively remains in the carbonized matrix at typical carbonization and pyrolysis conditions below 550°C. The second most important analysis is the elemental composition. Bio-char from wood is rich in elemental carbon, poor in hydrogen and oxygen. Other components, mainly nitrogen, from non-woody origin of the feedstock, remain in relatively constant concentrations. The heating values are also of fundamental relevance for combustion applications. Depending on the ash content, wood-derived biochar has LHV up to about 30 MJ/kg. It increases with increasing temperature of the reactor, due to the release of the volatile matter, which leads to a decrease of the contents of hydrogen and of oxygen. The release of the volatile matter from the solid matrix increases the surface area and pore volume of the bio-char. Values between 1 m^2/g and 100 m^2/g are reported. Several authors investigated how the surface area may be enhanced for adsorbent or even activated carbon applications. An extended study by Brown et al. evidenced that the surface area is maximized at relatively high temperatures (750°C) and lower heating rates [31]. FT-IR (Fourier Transform InfraRed) spectrometry is widely used to describe the organic bonds in bio-chars. It is recognized that increasing the pyrolysis temperature leads to an aromatization of the carbonaceous matrix, whereas at 950°C the charcoal has the same structure as graphite [203, 92, 111]. X-Ray Diffraction (XRD) was employed to assess the carbon structure as well as the mineralogical composition of the pyrolysis char. Studying wheat straw chars, Hasan Khan Tushar et al. reported that low pyrolysis temperatures and short residence times are preferred for both energy and soil applications [92].

Bio-char applications cover energy and non-energy markets. Because of their low ash content and of enhanced grindability woody bio-chars may be used for co-firing applications in large coal power plants to reduce the carbon footprint of the coal industry. Moreover, char may be used as gasification fuel to generate syngas and chemicals through following synthesis processes. For such application, the combustion and gasification reactivity is an important property [63, 83]. However, because of the low costs of energy and power generation, combustion and gasification applications are not economically feasible. For metallurgical applications, pyrolysis char needs to have seen higher temperatures in order to achieve the required fixed carbon content [2, 1].

The most interesting applications of bio-char are soil-related. Biochar or charcoal may be applied as soil enhancer and carbon sequestration sink. Since the discovery of the Terra Preta of Amazonia, soil applications have been investigated by a large number of scientific groups. The European Union provided the legal background for the institution of a European Biochar Certificate for soil applications of biochar [76]. Biochar may also be produced from agricultural residues and animal manures, which contains large amount of nutrients. In particular, phosphorus recycling may become a critical issue in the short future; therefore, pyrolysis-derived biochar with high phosphorus and carbon contents combines fertilizer and soil enhancer properties [174, 52, 86].
Pyrolysis char may be applied in gas treatment, as adsorbent or activated carbon. Sewage sludge char, because of the high zinc content, is particularly suitable for such applications [186, 196]. However, since the activation step introduces costs into the process chain, such market is still relatively limited.

Bio-Oil

Table 3. Comparison of pyrolysis oil, upgraded oils after hydrodeoxygenation (HDO) and conventional oils.

Feedstock		**Wood**	**Wood**	**Wood**	**HDO-oil from wood**	**Heavy fuel oil**
Pyrolysis Temperature		**450°C**	**450°C**	**500°C**	**500°C**	**-**
Pyrolysis Technology		**STYX Auger**	**Auger**	**Fluidized bed fast pyrolysis**	**Fluidized bed fast pyrolysis**	**-**
Reference		own data	[107]	[216]	[216]	[53]
Moisture	wt.%	12.4	16.0	25.4	6.7	0.1
Ash	wt.%	0.0	0.2	0.016	0.017	0.1
C	wt.%	55.4	61.0	45.5	67.6	85
H	wt.%	7.1	7.0	5.8	8.1	11
N	wt.%	< 0.03	-	<0.1	<0.1	0.3
O	wt.%	37.5	32.0	48.8	24.2	1.0
pH	-	2.84	3.1	2.9	3.1	-
Specific gravity	-	1.18	1.20	1.17	1.11	0.94
HHV	MJ/kg	26.6	21.9	16-23	27	40
Dynamic Viscosity	cPa s	45 @ 40°C	53 @ 50°C	13 @ 40°C	149 @ 40°C	180 @ 50°C
Solids	wt.%	0.0	0.19	0.04	-	1
Distillation Residue	wt.%	7.6	-	-	-	1

Pyrolysis oil or bio-oil is a free-flowing liquid made of a complex mixture of oxygenated organics with a dark brown to black color and a smoky odor [131]. Physical and chemical properties of the bio-oil differ much from those of crude-derived oils (see Table 3). A wide amount of scientific literature has been published in the last decades in relation to the characterization and standardization of characterization methodologies. VTT scientists led the development of standardized techniques [158],[159, 160].

Bio-oils from lignocellulosic feedstock show similar composition and properties. Pyrolysis oil presents low volatility, which hinders the utilization of conventional methods such as GC/MS for exhaustive chemical characterization. Techniques based on solvent fractionation were developed for the characterization of the whole pyrolysis liquid. Classes of components are extracted with a sequential method, which is able to separate the pyrolysis oil into: volatile acids, aldehydes and ketones, sugars, low and high molecular weight lignin and others [159, 161, 87]. However, GC/MS was also widely used to characterize the chemical composition of bio-oils. Combined with solvent fractionations, it allows a detailed insight into the composition of pyrolysis oil [132, 181, 107]. A typical example of the chemical composition is given in Oasmaa and Peacoke for pine-derived pyrolysis oil [159]. Pyrolysis oils from lignocellulosic feedstock, such as wood or straw are therefore characterized by a pH of 2 to 3 and a TAN (total acid number) of 60 to 100 mg_{KOH}/g. Their acidic nature reflect the chemical composition of the oil and it can be well correlated to the acids content, mainly acetic and formic acids [162]. The stability of pyrolysis oils is affected by the presence of large amounts of reactive oxygen-containing, low-boiling compounds. The aging process leads to an increase of the water content (dehydration reactions), an increase of the viscosity (thickening from repolymerization reactions) and phase separation during storage even at room temperature [158],[67, 73]. Oils from animal residues and sewage sludge have a neutral to alkaline nature, because of the high nitrogen content [80]. Bio-oils are partially soluble in water, which is one of the main products of wood pyrolysis. If the total water content is below 30 wt.%, the pyrolysis condensate will be a single-phase liquid, otherwise it will separate into an organics-rich phase (the bio-oil) and into an aqueous phase (Figure 13).

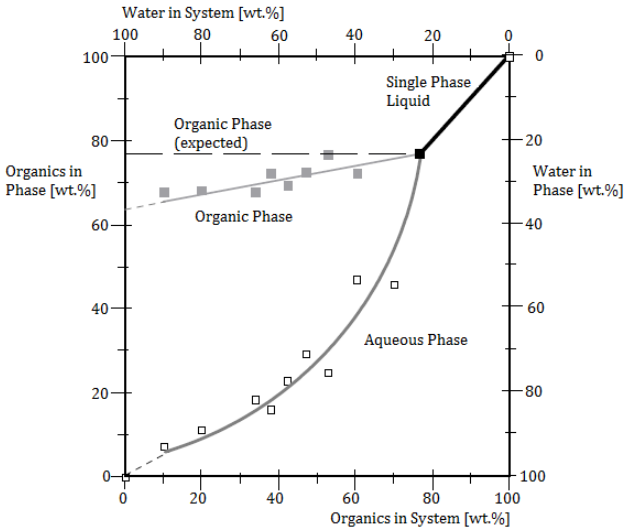

Figure 13. Phase separation diagram of pyrolysis liquid - water. Source [159].

Depending on the pyrolysis technology, the pyrolysis oil may include solid particles and ash, which have negative effects on the combustion properties and on its stability as well. Solid particles have been recognized as one of the important sources of aging of the pyrolysis oil. Viscosity is another important physical property of bio-oil ranging from 10 to 1000 mPa s. Bio-oils usually reflect Newtonian behavior, i.e. viscosity does not depend on the shear rate [157]. However, pyrolysis oils contaminated with char particles (bio-slurry) may present non-Newtonian behavior at low shear rate [210]. The calorific value of fast pyrolysis oils from wood is about half of conventional liquid fuels, i.e. 17-20 MJ/kg [28].

The physical and chemical properties of the bio-oil define the potential applications. A wide overview is given by Czernik and Bridgwater [53]. There are mainly two lines of applications for pyrolysis oil. On the one hand, it can be applied as a whole for energy applications, i.e. liquid fuel, or for chemical applications, such as wood preservative; on the other hand, it can be used for specific chemical purposes after fractionation, extraction or other upgrading technologies.

Most of the attention was given to energy applications. Pyrolysis oil is used as a substitute of heavy fuels in boilers, where it performs quite well without extensive design modification of the burner. In boilers, bio-oil produces more CO, less NO_X and SO_X emissions compared to heavy oil. Combustion in boilers is nowadays the only successful application of pyrolysis oil at commercial scale (Fortum pyrolysis plant in Finland and Empyro based on BTG technology in the Netherlands) [142, 74]. Diesel engines and gas turbine power generation applications have more stringent requisites compared to boiler applications, which make the utilization of pyrolysis oil more expensive because of the required modifications by the burner and atomizer. Several tests were carried out in the last years. Pyrolysis oil was successfully combusted in short-term tests but failed on long runs because of corrosion of the

burner [40, 47, 123]. The direct utilization of pyrolysis oil as transportation fuel is excluded; therefore, several upgrading processes were used to enable the utilization of bio-oil as drop-in fuel. Because of the high oxygen content, bio-oil is not miscible with conventional fuel, nor suitable for fossil fuel-based refineries. The reduction of the oxygen content remains a major topic. Online catalytic pyrolysis (in-situ or ex-situ) or hydrodeoxygenation (HDO) are the two most investigated pathways for upgrading. The topic goes beyond the purposes of this work. Suggested further readings are [85, 81, 34, 149, 237].

Aqueous Condensate

The aqueous condensate is essentially the by-product of pyrolysis applications. It retains most of the moisture and reaction water as well as most of the water-soluble species produced during the reactions. Since it was mainly considered a by-product, its characterization was somehow overlooked. However, the organic content and the dry CHO composition, which is about 20 to 30 wt.%, reflect that of organic acids, mainly acetic acid. The calorific value is very low or even negative; the pH of wood-derived aqueous phase is about 2 to 2.5. On the other hand, aqueous phases from food industry residues, animal manures and sewage sludge are alkaline, with a nitrogen content up to 10 wt.% in the form of ammonia. That makes the aqueous condensate suitable for fertilizer applications.
Speaking of lignocellulosic aqueous condensates, few applications were investigated. Some authors investigated the steam reforming process for the generation of hydrogen and syngas from the aqueous phase of pyrolysis condensate [163, 139]. Effort was devoted to the development of catalysts and process conditions optimization. Another application for the aqueous condensate may be fermentation for the production of biogas [106].

Permanent Gas

Permanent or non-condensable gases are a by-product of pyrolysis. The composition of the permanent gas is investigated adopting standard gas chromatography. Main components are carbon oxides and light hydrocarbons up to C_4. Carbon dioxide is the second major single product after water and it is mainly released during the primary devolatilization; on the other hand, CO is the major product of secondary gas phase reactions. Methane and CO contents enable the combustion of the non-condensable gases for process heating. The heating value of the permanent gases increases with increasing temperature from 4 MJ/kg to about 10-14 MJ/kg at 500°C, in the typical range of biogas. The increase is correlated with the secondary reactions of the pyrolysis vapors, which produce CO and light hydrocarbons from the thermal cracking. Pyrolysis of agricultural residues and other

biogenic residues produces traces of sulfur and nitrogen gases, such as H_2S and HCN [230, 43, 180, 130].

As already mentioned, the primary application of the permanent gases is the production of process heat for the autothermal operation of the pyrolysis reactor. However, upgrading to syngas was investigated by means of pyrolysis followed by catalytic steam reforming of the vapors to minimize the water content of the condensate and to enhance the production of hydrogen [103, 72, 12].

3. MATERIALS, FACILITIES AND EXPERIMENTAL METHODS

The development and validation of a thermochemical model for the pyrolysis of biogenic feedstock in the screw reactor STYX requires the knowledge of chemical and physical parameters of the selected material as well as the geometrical features of the described reactor. Moreover, a range of analytical methods are required for the experimental validation. This section is devoted to the description of the overall experimental approach adopted for the experimental validation of the developed numerical model, which will be discussed in Chapter 5.

3.1 Feedstock characterization

3.1.1 Chemical and physical properties

The characterization of the feedstock used in this work aims at giving insight on the physical and chemical properties, both of relevance in thermochemical processing. The adopted feedstock is enlisted in Table 4.

Table 4. Summary of the selected biogenic feedstock.

Feedstock	Typology	Particle Size	Structure
Beech Wood KL1-4	Lignocellulosic - reference	1 to 4 mm	Grain
Beech Wood HB500-1000	Lignocellulosic	0,5 to 1 mm	Powder
Beech Wood KL2-16	Lignocellulosic	2 to 16 mm	Grain
Wheat Straw	Lignocellulosic – high ash	0,5 to 1 mm	Grain
Chicken Manure pellets	Animal residues – high proteins	10 x 40 mm	Pellets
Sewage Sludge	Biogenic waste	2 to 4 mm	Grain

Most of the work was carried out adopting beech wood with a particle size of 1 to 4 mm as the reference feedstock. The selected beech wood is an ash and bark-free lignocellulosic feedstock, which ensures reproducibility and reliable comparison with scientific literature. Moreover, in order to evaluate the importance of the particle size, the same beech wood was also purchased in powder form (0.5 to 1 mm) and in a larger particle size range (2 to 16 mm), which keeps the grain structure. Besides the reference feedstock, a number of biogenic feedstock was selected in order to cover a wide spectrum of parameters, including non-organic content and compositions as well as nitrogen, sulfur and chlorine. First, wheat straw was adopted as a second lignocellulosic feedstock with a higher ash content and a low bulk density. Second, chicken manure, in pelletized form, was investigated to cover the second class of feedstock as reported in Figure 2. Animal residues are characterized by high contents of minerals and proteins, potentially important players for nutrients recovery. Finally, sewage sludge was implemented as representative biogenic waste, being one of the largest single waste streams around the world [113].

All the feedstock were characterized by means of chemical analysis for solid fuels after the respective German DIN Standards. The chemical properties are reported in Figure 14 and in Table 5.
The main analyses are briefly enlisted:

- Elemental composition: CHNS and O by difference, in weight % of the feedstock on dry basis
- Halogens contents Cl and F, in weight % of the feedstock
- Moisture content: in weight % of the feedstock on as received basis
- Proximate analysis: ash, volatile matter and fixed carbon by difference, in weight % of the feedstock on dry basis
- Calorific properties: higher and lower heating values, in MJ/kg on dry basis
- Metals contents: in mg/kg of the feedstock on dry basis
- Minerals contents: in mg/kg of the feedstock on dry basis.

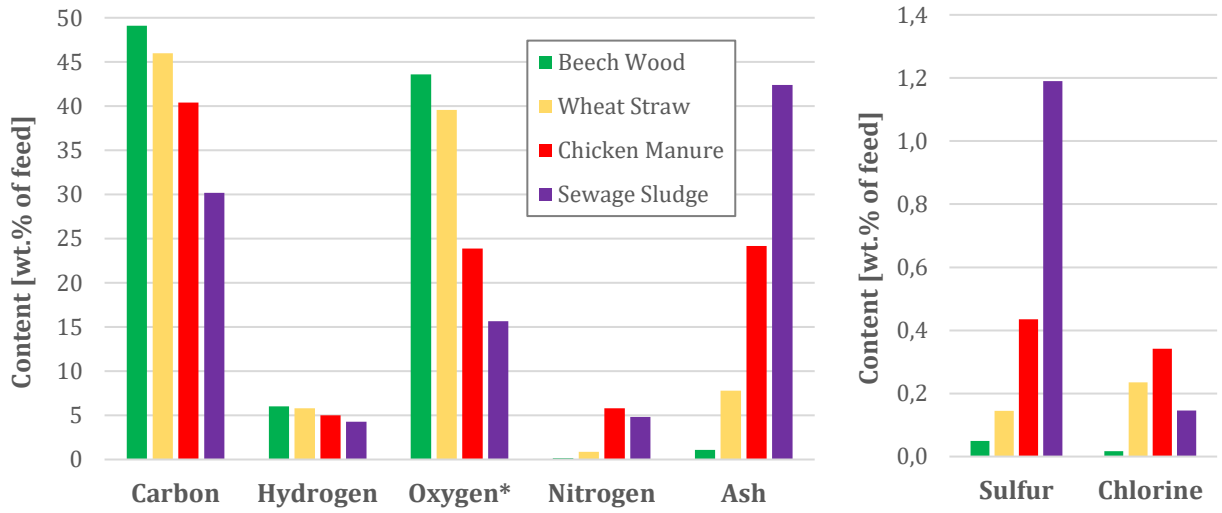

* calculated by difference

Figure 14. Elemental composition and ash content of the low-biogenic feedstock on dry basis.

In comparison to beech wood and in general to woody biomass low-grade feedstock is characterized by lower carbon and oxygen contents. On the other hand the hydrogen content is almost constant, thus the ratio H/C is higher for non-lignocellulosic feedstock. The nitrogen content is low for woody and plant biomass, i.e. below 1 wt.%; on the other hand, chicken manure and sewage sludge present contents of 5.8 wt.% and 4.8 wt.%, respectively. Nitrogen is a primary nutrient and a main component of proteins, which are expelled through excretion and found in manures and wastewater [124]. Sulfur represents a trace element in plant biomass, while it becomes of relevance and concern in animal residues and sewage sludge. Sulfur may be found both in organic form and in the ash. Of greater importance for thermochemical processes is chlorine because of corrosion and slagging issues, which

is found in the bark and shells of plant biomass as well as in animal manures and sewage sludge (0.15 wt.%). In wastewater systems, for instance, chlorine is used for disinfection; it is then recovered in the sewage sludge [215].

Table 5. Analysis of the selected feedstock. Water content on wt.% of the feed as received. Proximate analysis and hologens contents are reported in wt.% of the feed (dry). Metals and mineral elements reported as mg/kg of the feedstock (dry).

		Beech Wood	Wheat Straw	Chicken Manure	Sewage Sludge
Water *(wt.%)*		10.0	8.7	10.0	10.0
Proximate Analysis *(wt.% dry)*					
Ash		1.1	7.8	24.2	42.4
Volatile matter		84.2	74.1	67.1	54.2
Fixed carbon		14.7	18.1	8.8	3.4
Halogens *(wt.% dry)*					
Chlorine (total)		0.017	0.235	0.342	0.146
Chlorine (inorganic)		-	-	-	0.120
Fluorine		< 0.001	< 0.001	< 0.001	0.029
Calorific properties *(dry)*					
HHV	MJ/kg	19.7	18.5	14.4	13.4
LHV	MJ/kg	18.4	17.2	13.3	12.5
Minerals in ash *(mg/kg dry feed)*					
Silicon	Si	70	18160	7450	57580
Aluminum	Al	20	950	1920	21770
Calcium	Ca	2695	6350	63270	38460
Magnesium	Mg	460	1320	7300	4860
Phosphorus	P	95	1290	14050	29620
Sodium	Na	40	115	2690	1260
Potassium	K	1350	10485	24100	4570
Sulfur	S	120	1060	3580	6275
Metals in ash *(mg/kg dry feed)*					
Antimony	Sb	< 1	< 1	< 1	8
Arsenic	As	< 0.8	< 0.8	< 0.8	6.3
Lead	Pb	< 2	< 2	< 2	59
Cadmium	Cd	< 0.2	< 0.2	< 0.2	59
Chromium	Cr	< 1	11	5	260
Cobalt	Co	< 1	< 1	< 1	9
Copper	Cu	1	5	77	420
Iron	Fe	-	-	1310	48600
Manganese	Mn	73	61	530	840
Nickel	Ni	< 1	6	7	110
Mercury	Hg	< 0.07	< 0.07	< 0.07	0.49
Thallium	Tl	< 0.2	< 0.2	< 0.2	< 0.2
Tin	Sn	< 3	< 3	< 3	25
Vanadium	V	< 1	2	5	36
Zinc	Zn	-	-	-	1400

Finally, the ash content of low-grade biogenic feedstock is higher. The origins are very different. For example, wheat straw has a high content of silica, which is a non-essential nutrient but affects plant growth and quality in field crops [144]. Chicken manure is rich in calcium, and specifically in calcium carbonate and dolomite, which are used as drying medium. Sewage sludge is rich is silica from sand in wastewater treatment, phosphorus and calcium from detergents and other industrial processes as well as iron and zinc, which are used to enhance the flocculation process in wastewater [122].

Mercury and heavy metals are also present in relevant contents in sewage sludge. Mercury is of particular concern due to its high volatility at pyrolysis conditions, which imposes specific measures for emission control [205, 116]. The ash content and the respective composition is well known in the scientific literature to have one of the most predominant impacts on the pyrolysis process and on the properties of the products. Investigating the effects of the ash content on the pyrolysis process is not a main task for this work; however, the impact cannot be neglected and will be referenced during the discussion of the experimental results.

The lignocellulosic feedstock were characterized in terms of cellulose, hemicellulose and lignin contents following the methods developed by Kürschner and Klason, respectively (see Table 6). The knowledge of the contents of the main chemical components is expected to provide the input data for the pyrolysis model.

Table 6. Chemical composition of the lignocellulosic feedstock beech wood and of wheat straw.
Moisture content on wt.% as received; ash on wt.% dry; chemical composition on wt.% on dry ash free basis.

		Beech Wood	Wheat Straw
Moisture	wt.% ar	10.0	8.7
Ash	wt.% dry	1.0	7.8
Cellulose	wt.% daf	43.1	46.0
Hemicellulose	wt.% daf	35.7	30.0
Lignin	wt.% daf	21.2	21.0
Others	wt.% daf	-	3.0

Alongside chemical data the reactor model foresees the input of some physical properties, which are required for the simulation of the transport and of the heat transfer mechanisms.

The bulk density is a property of powder and granular solids. It defines the mass of the particles of the material divided by the total occupied volume, which includes the particles, the inter-particle and pore void volumes. The bulk density was measured using a graduate cylinder following the ASTM D7481-09 Standard [14] and a cube of 0.3x0.3x0.2 m. The angle of repose was measured adopting two methods. First, the Carr index (static angle of repose) was measured following the Standard ASTM D6393-14 [15]. Secondly, the dynamic angle of repose was measured by means of a rotating drum. The static angle of repose defines the slope instability and it is useful for design and selection of feeding hoppers. The dynamic angle of repose is observed during the continuous movement of a bulk solid, which is relevant for the transport in a screw reactor. The results of the measurements are reported in Table 7.

Table 7. Bulk density and angles of repose for beech wood.

	Unit	Beech Wood KL1-4
Bulk density (Cylinder)	kg/m^3	263.3 (± 7.6)
Bulk density (Cube)	kg/m^3	266.1 (± 7.7)
Static angle of repose	-	40° 24’ (± 2° 00’)
Dynamic angle of repose	-	41° 36’ (± 4° 48’)

3.1.2 Thermogravimetric analysis of beech wood

The thermal degradation of the reference feedstock was investigated adopting thermogravimetric analysis. The feedstock was milled and dried for 24 h at 105°C. About 10 mg of milled beech wood were introduced in the crucible and flushed with nitrogen to provide an inert atmosphere. The furnace was heated up to 900°C at constant heating rate. Duplicates were made with heating rates between 5 K/min and 50 K/min in order to cover the wide range of heating rates, which are expected to take place under the conditions of the bench-scale reactor. As an example, the results for heating rates of 5 K/min and 25 K/min are reported in Figure 15. The blue and purple lines represent the solid yield as weight percent of the dried feedstock; the red and the green lines in Figure 15 describe the DTG (differential TGA) in mg/min. From the DTG, the typical decomposition behavior of lignocellulosic biomass can be well established. The main peak area describes the combined decomposition of cellulose and hemicellulose, with a maximum conversion rate at 348°C for heating rate of 5 K/min. The shoulder on the left side describes the degradation of hemicellulose, whose decomposition starts at lower temperatures. The slow decomposition on the right side of the main peak of cellulose represents the residual degradation of lignin, which covers a wide range of temperatures up the final temperature of 900°C. The final yield of the solid is 16.5 wt.%, which is slightly higher than the results from the proximate analysis indicating that the decomposition is not completed at 900°C.

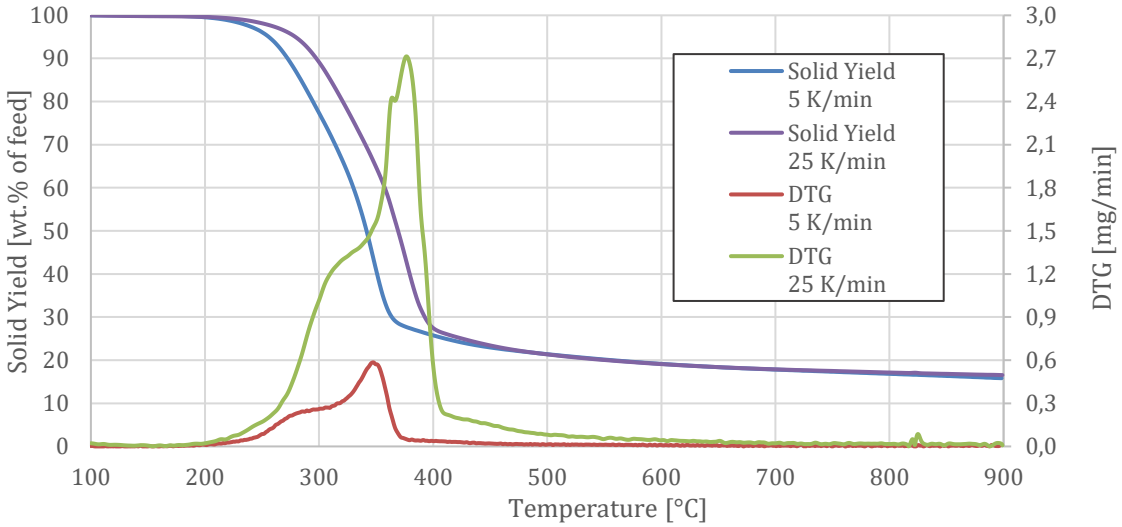

Figure 15. Solid yields and DTG from the TGA of beech wood at heating rates of 5 K/min and 25 K/min.

The solid yield and the DTG for a heating rate of 25 K/min is adopted for a direct comparison between different heating rates in Figure 15. Both the solid yield and the DTG show a shift of the decomposition to higher temperatures. The peak of cellulose decomposition is at a temperature of 380°C, i.e. about 30°C higher than that at 5 K/min. This significant variation is the result of the delay in the conversion process due to a thermal lag. Even if the thermocouple is placed just on the bottom

and in contact with the crucible, the effective temperature of the biomass may be lower than the measured one. According to the scientific literature [46], the thermal lag leads to a decrease of the activation energy and to an increase of the pre-exponential factor with increasing heating rate.

3.2 Experimental facility – STYX

The experimental validation of the thermochemical model as well as the characterization of the pyrolysis process for the selected reference and biogenic feedstock were carried out at the bench scale screw pyrolysis reactor with integrated hot gas filtration STYX. The patented reactor was developed at the Institute for Technical Chemistry (ITC) of the Karlsruhe Institute of Technology (KIT) starting from 2011. The STYX served for the most of the experimental validation and was thoroughly optimized during the time span of this work. A schematic representation of the main units of the facility is depicted in Figure 16.

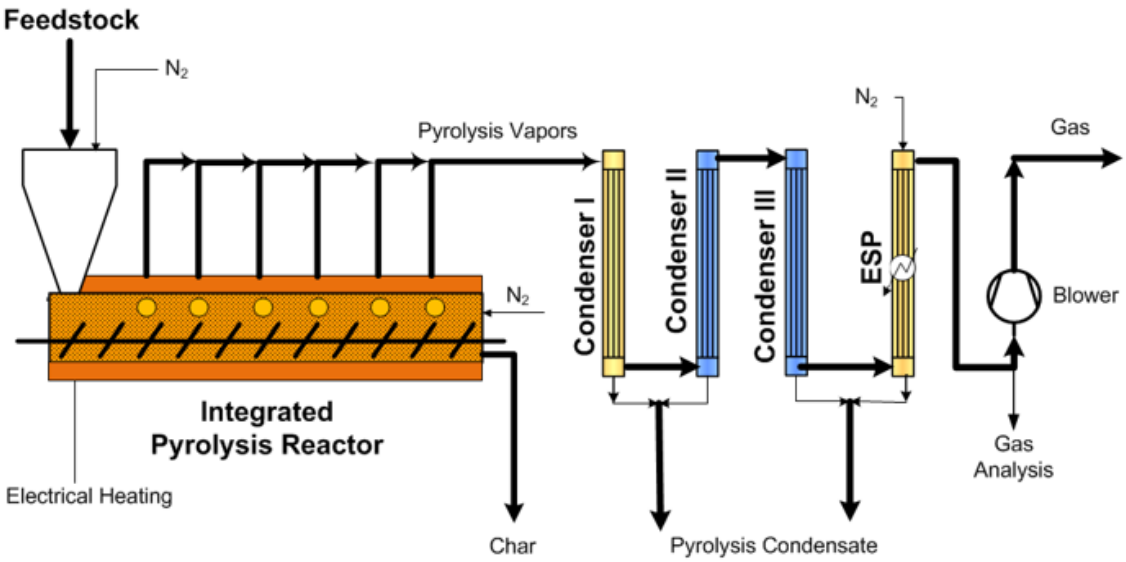

Figure 16. Schematic representation of the main units of the experimental facility STYX.

The STYX facility is composed of three main units. The reactor with the integrated hot gas filtration, which includes the feeding system, the char recovery hopper and the sampling ports for the extraction of the local solids and vapors; the condensation unit for the recovery of the pyrolysis condensates and the gas induced draft with the online gas analytics. Moreover, the facility is equipped with extensive instrumentation.

3.2.1 Reactor with integrated hot gas filtration

The reactor with integrated hot gas filtration is the core of the experimental facility. Figure 17 reports a 3D insight of the reactor, showing its main components.

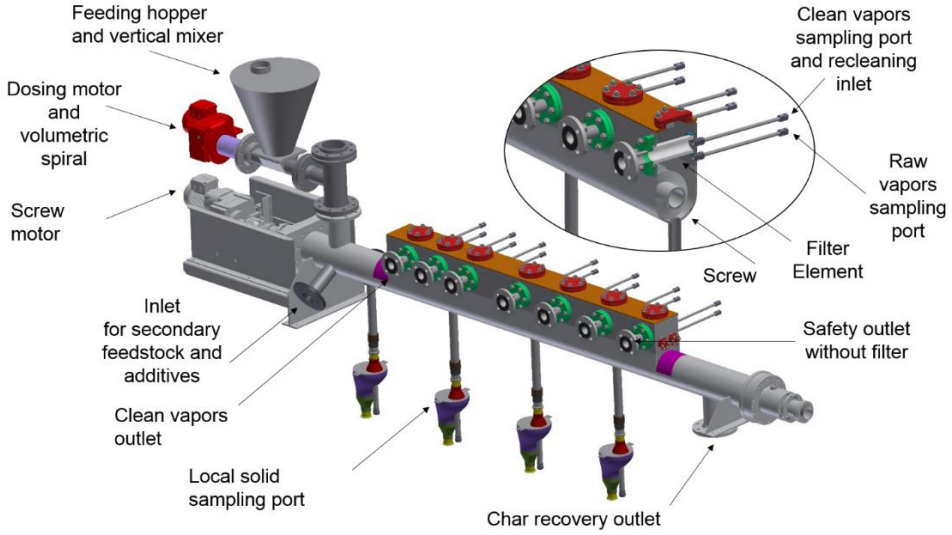

Figure 17. 3D detail of the bench-scale pyrolysis reactor STYX.

The feeding system is composed of a gas-tight container (feeding hopper), a vertical mixer (not shown in Figure 17) to avoid blockages caused by bridge-building feedstock and a dosing motor and volumetric spiral, which allows the accurate control of the mass flow rate. Moreover, an inlet for a secondary feedstock or for other additives is displaced below the main inlet. The main nominal parameters of the reactor are reported in Table 8. Figure 18 depicts the side view of the reactor. The heated length is 2 m, for a total length from inlet to outlet of 2.5 meters.

Table 8. Design parameters of the integrated pyrolysis reactor with hot gas filtration.

Reactor data		
Number of heaters	8	-
Nominal heating capacity	40	kW_E
Max reactor temperature	600	°C
Max pyrolysis temperature	550	°C
Max throughput	10	kg/h
Residence time	2.5 – 40	min
Filtration data		
Number of filters/sampling points	6/7	-
Filter support material	coarse silicon carbide	SiC
Filter membrane	Aluminosilicate	Al_2SiO_5
Filter length	150	mm
Filter diameter	60/40	mm
Filter porosity	38	%
Filter permeability	55 x 10^{-13}	m^2

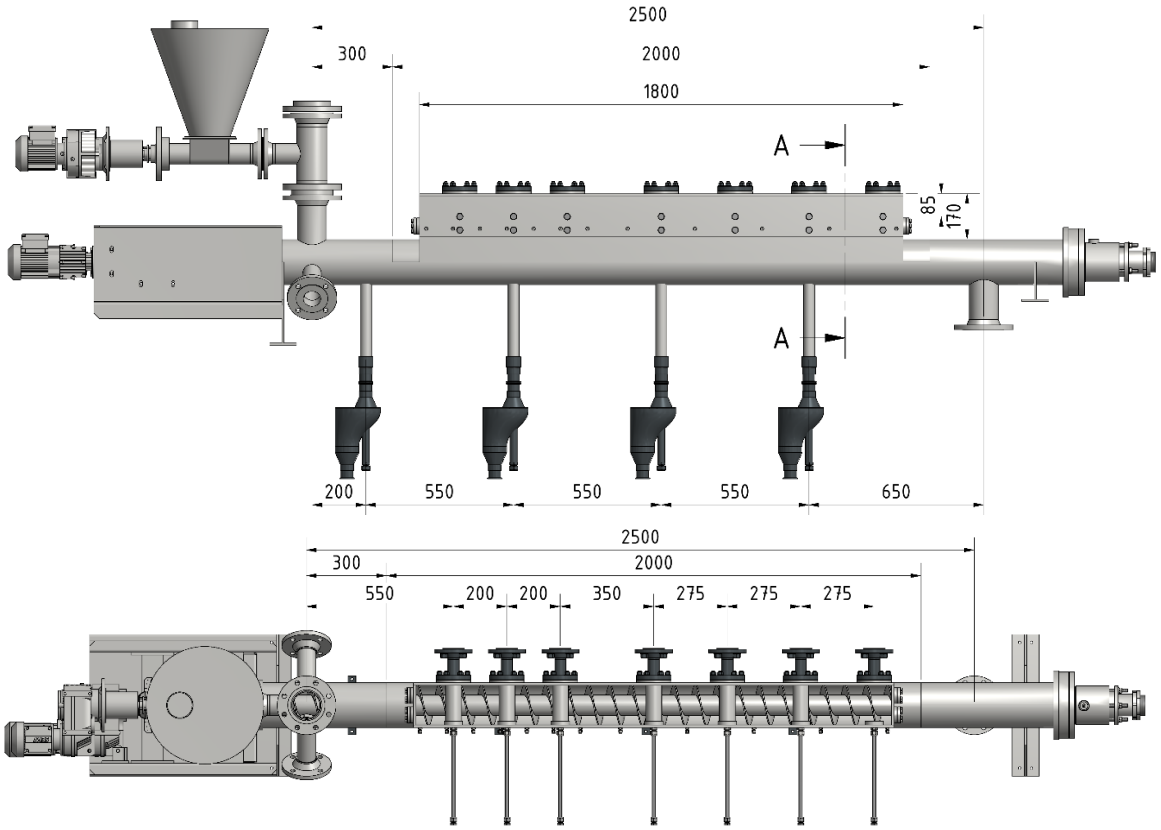

Figure 18. Side (above) und top (bottom) views of the reactor.

The solid residues are recovered in a gas-tight container at the tail of the reactor (char recovery outlet). The feeding system as well as the char recovery hopper are flushed with nitrogen gas to displace the reactive pyrolysis vapors. The inlet and the outlet of the reactor are allocated outside the heated zone, which limits are marked in violet in Figure 17.

The temperature of the reactor can be regulated up to 600°C by 8 independent electric heaters for a total nominal output of 40 kW_E. However, the maximum pyrolysis temperature of 550°C may be adjusted due to restrictions of the vessel material. The temperature of the reactor can be adjusted to maintain isothermal conditions along the screw; however, ramp temperature profiles may also be provided. The screw is allocated on the bottom side of the reactor. The diameter of the flights, i.e. of the screw is 150 mm, the diameter of the shaft is 76 mm, the pitch is 80 mm and the flight thickness is 4 mm (Figure 19).

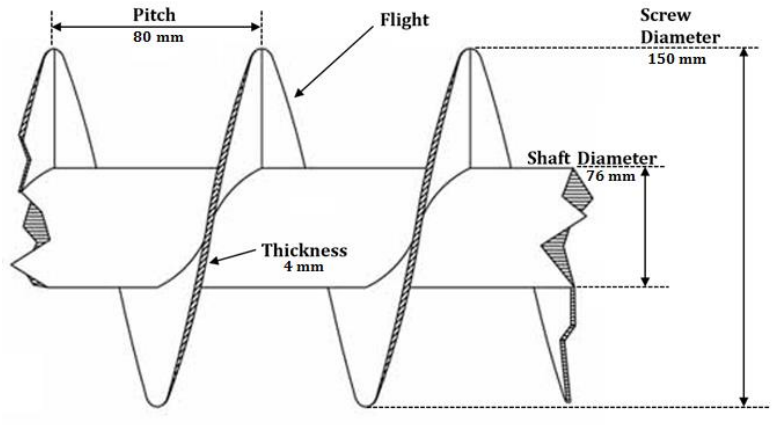

Figure 19. Main components of the screw conveyor.

The main tasks of the screw are to transport the feedstock along the hot zone and to define the residence time of granulate or pellets ensuring a homogeneous heat transfer within the solids. The residence time in the heated zone can be regulated from 2.5 minutes to 40 minutes, adjusting the speed of rotation of the screw (screw motor). The trough screw design allows the displacement of the filters directly inside the vessel. Above the screw, and perpendicularly to it, six filter elements are arranged along the axis (see Figure 20). The candles are Schumalith elements, with a coarse-grained support made of silicon carbide (SiC) associated with a fine aluminosilicate filter membrane. The length of the filter is 0.15 m with diameters of 60/40 mm. The porosity of the filters is 38% and with specific permeability of 55 x 10^{-13} m^2. The candles have openings on both sides for the suction of the vapors and for the online recleaning of the filters, respectively. The recleaning of the hot gas filters is based on the CPP (Coupled Pressure Pulse) technology, developed at the institute [135]. Heated and pressurized (up to 4 bar) nitrogen is used for the recleaning. The overpressure detaches the filter cake from the surface, which falls back to the bottom of the reactor and it is conveyed to the char recovery hopper. The filters are operable simultaneously or independently one from another. As depicted in Figure 20, the filters are displaced along the axis of the reactor, which enables the selective extraction and filtration of the pyrolysis vapors.

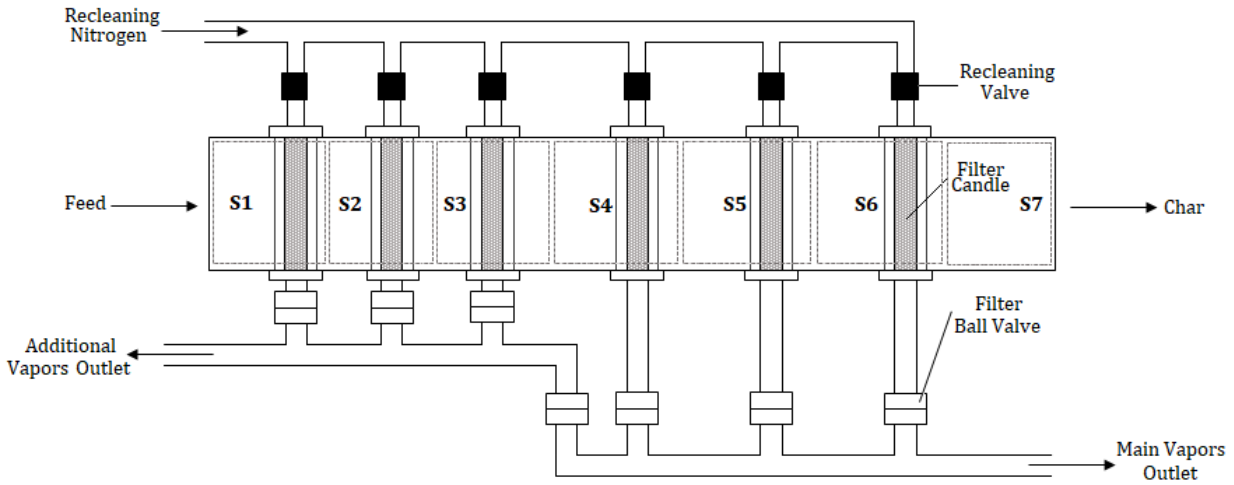

Figure 20. Top view of the reactor with highlight of the filtration unit.

The trough design of the reactor allows the locally released vapors to flow vertically from the bottom of the screw to the freeboard, where it can be directly extracted without being mixed. In normal operation, the vapors are collected after the filtration and sent to the condensation unit. However, each vapor stream can also be condensed independently in order to concentrate the desired compounds in a selected stream. For instance, during the pyrolysis of lignocellulosic feedstock, water vapor from the moisture content as well as reaction water and CO_2 from the early thermal decomposition, can be removed in the early part of the reactor. As direct consequence, the vapors released in successive stages of pyrolysis can be concentrated into a more valuable organic phase. The details of the sequential extraction and filtration have been discussed in details [207, 208]. The experimental investigations related to the sequential extraction and filtration of the pyrolysis vapors revealed that, using online measurements of the CO to CO_2 ratio, the calorific value of the main organic vapors stream can be increased by 67%. The overall stream of vapors had a calorific value of 10 MJ/kg, whereas the separated fraction had about 8 MJ/kg in the early section of the screw and 16 MJ/kg at the tail.

3.2.2 Condensation unit

After the hot gas filtration, the clean vapors are forwarded to the condensation unit, as depicted in Figure 16. The train is made of a series of three concentric double tubes and an electrostatic precipitator (ESP). The condensers are cooled adopting a mixture of water and glycol (2 to 1 ratio), which allows the supercooling of water below 0°C. The cooling medium flows through the condensers in counter flow to minimize the final temperature of the gases. The vapors from the reactor at the pyrolysis temperature are cooled down to about 15°C and collected in two steps. Most of the water and the heavy organics are recovered at the bottom of the first condenser, where the temperature

of the vapors is about 80°C in steady-state operation. In the second condenser, the remaining vapors flow upwards and are further cooled to 20°C at the top. The condensed liquid flows back to the first collecting bottle. The residual organic vapors are cooled to about 15°C in the third condenser and recovered in the second collecting bottle. Finally, the fine air-borne organic aerosols are condensed in the electrostatic precipitator (ESP), which was developed in the framework of this promotion and consists of a glass and metal pipe and a metal tube with pins along its axis. The electric field is generated at high voltage up to 18 kV. The head of the ESP is purged with nitrogen gas avoiding condensation and liquid drops formation, which may lead to flashover.

3.2.3 Induced draft and online gas analytics

The pyrolysis vapors are extracted from the reactor using a suction fan, displaced after the condensation unit. Although the pyrolysis process takes place at slight overpressure, the filtration unit provides a considerable pressure resistance; therefore an active removal of the vapors is required. The suction fan is regulated to maintain a desired pressure inside the main reactor. In addition to the induced draft, i.e. the suction fan, online gas analytics is present at the tail for overall process control. A water-filled volumetric gas flow meter is positioned upstream the suction fan. Downstream of the main fan, a continuous sample flow of non-condensable gases is removed from the main stream, dried at 5°C and forwarded to the online gas detectors. The gas-analysis unit consists of a number of devices displaced in parallel, which enable a complete characterization of the gas composition and calorific content. Finally, a gas sampling port is attached for offline analytics of the gases.

3.2.4 Instrumentation

The STYX facility is equipped with extensive instrumentation for process control, sampling and data recording. The volumetric flow rate of the nitrogen gas is regulated and recorded using an independent mass flow controller for each inlet. The heating system of the reactor is regulated by thermocouples, one per independent heater, which are connected to the main power unit and provide the feedback for temperature control. In addition, eight thermocouples are displaced along the axis of the reactor, on the bottom and on the freeboard, for data recording. Each filter element is equipped with an additional thermocouple and an outlet for pressure measurement. The pressure difference among each filter can be measured independently with a pressure gauge. The filter for the pressure measurement can be selected manually acting on the manifold. In such a way, it is possible to evaluate the dust loading at each filter separately. Moreover, an additional pressure gauge measures the relative pressure inside the reactor and controls the induced draft. Finally, excessive overpressure in the reactor during the recleaning is avoided with a safety valve. The electrical requirement of the heating system is recorded

automatically using a mobile device with an integrated software. The condensation unit is also equipped with online instrumentation for data recording. A thermocouple is displaced at the inlet and at the outlet of each condenser, on both process and cooling side. The mass flow rate of the cooling medium is measured with a cone flow meter and it is recorded manually. The online gas-analytics is composed by several detectors, which measure and record the most important parameters. Two parallel ABB Advance Optima units measure CO, CO_2, CH_4 and O_2 using infra-red photometers and paramagnetic analyzer, respectively. The total carbon content is measured in a SIEMENS FID unit. The lower heating value (LHV) of the gases is measured in a CWD200 combustion calorimeter using the specific density cell and the Wobbe index.

3.2.5 Sampling equipment

Solids sampling

In order to evaluate the progression of the pyrolysis process along the axis of the reactor, the bottom of the vessel was equipped with four ports, equally spaced (see Figure 21). The first port (S-0) is placed outside the oven, with the aim of evaluating the actual inlet conditions of the feedstock into the heated part of the reactor. The other three ports, i.e. S-2, S-4 and S-6, are positioned at 0.55 m, 1.10 m and 1.65 m from the oven insulation. The openings of the vessel are connected with a steel tube to the outside of the oven. On the bottom of each tube, a small pot (or container) is attached and connected with a gas-tight flask, which is purged with nitrogen to avoid reactions with oxygen, to displace the pyrolysis vapors and to cool down the recovered sample (left side of Figure 21). During regular operation, the openings at the bottom of the reactor are closed. The blocking element is pulled down to the pot for sampling operations. The sample falls down to the pot and finally to the recovery flask. The design ensures gas-tight sampling, which is fundamental to avoid the immediate oxidation of the solid samples. After the completion of the sampling, the flasks are immediately removed and placed in a cold water bad, in order to reduce rapidly the temperature and avoid further organic release.

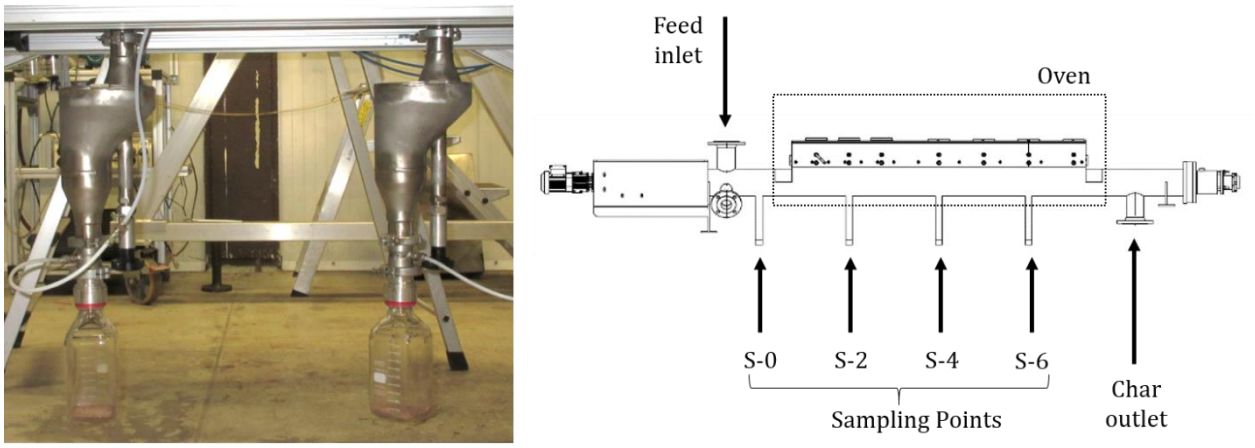

Figure 21. Picture (left) and scheme (right) of the solids sampling equipment.

Vapors sampling unit

A sampling unit was specifically developed for the extraction of the pyrolysis vapors from the local sampling ports. The unit consists of a condenser and an ESP based on the same principle of the main condensation unit of the plant. The sampling unit is showed in Figure 22 (left side) and graphically depicted in Figure 22 (right side). The vapors flow from the top of the condenser to the bottom, where the flask is connected. The remaining aerosols flow upward in the ESP, where they are completely condensed. Since the temperature on the ESP side is lower, there is a reduced risk of re-evaporation. That adjustment improved greatly the sampling capacity of the unit.

After the ESP, the sampling unit is equipped with a thermocouple and a pressure gauge. The vapors are extracted by a pump, whose flow rate may be adjusted by a regulation valve. Finally, after the volumetric flow meter, the non-condensable gases may be collected in a glass tube for offline GC analysis as well as forwarded to the online gas analyzers.

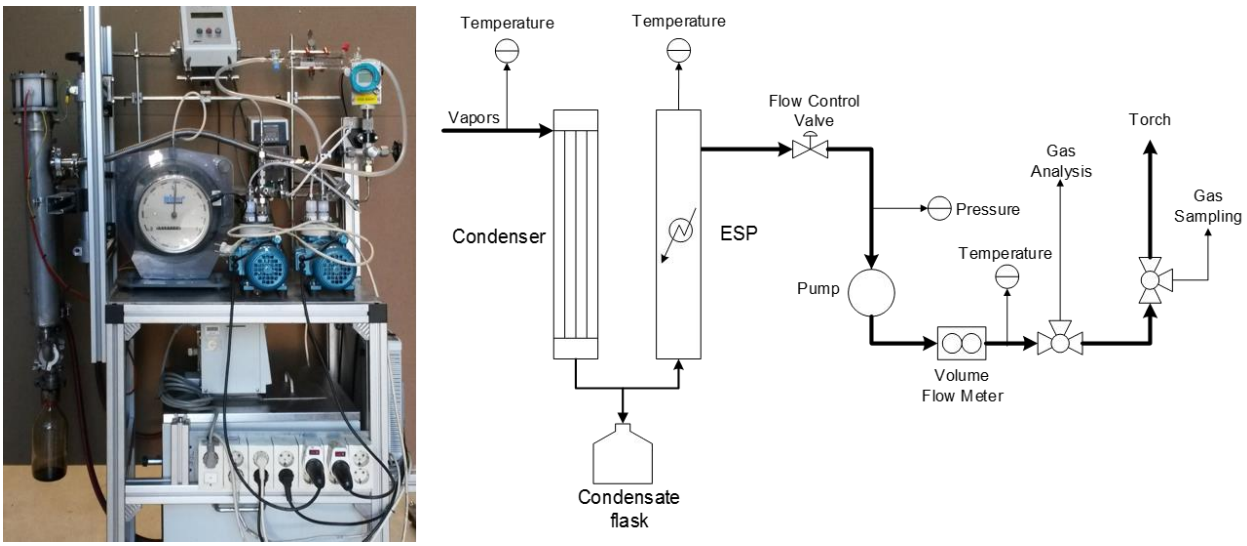

Figure 22. Picture (left) and scheme (right) of the vapors sampling unit.

3.2.6 Cold transport reactor

The mechanisms of transport of the solid granulate in a screw conveyor were investigated experimentally in the cold transport reactor, which was designed and constructed to mimic the STYX reactor and to gain a deeper understanding of the parameters influencing the transport mechanisms of granular solids in a screw. It consisted of a trough vessel, open on the top, and a screw with the identical geometric characteristics of the pyrolysis reactor (see Figure 23). The total length of the screw was 1.68 m, whereas the open trough was 1 m. The geometry of the screw reproduces that of the pyrolysis reactor (see Figure 19). The rotational speed of the electric motor can be adjusted to control the rotational speed of the screw up to 10 rpm corresponding to a residence time of the solids of 1.25 minutes in the transport reactor and of 2.5 minutes in the heated zone of the STYX reactor.

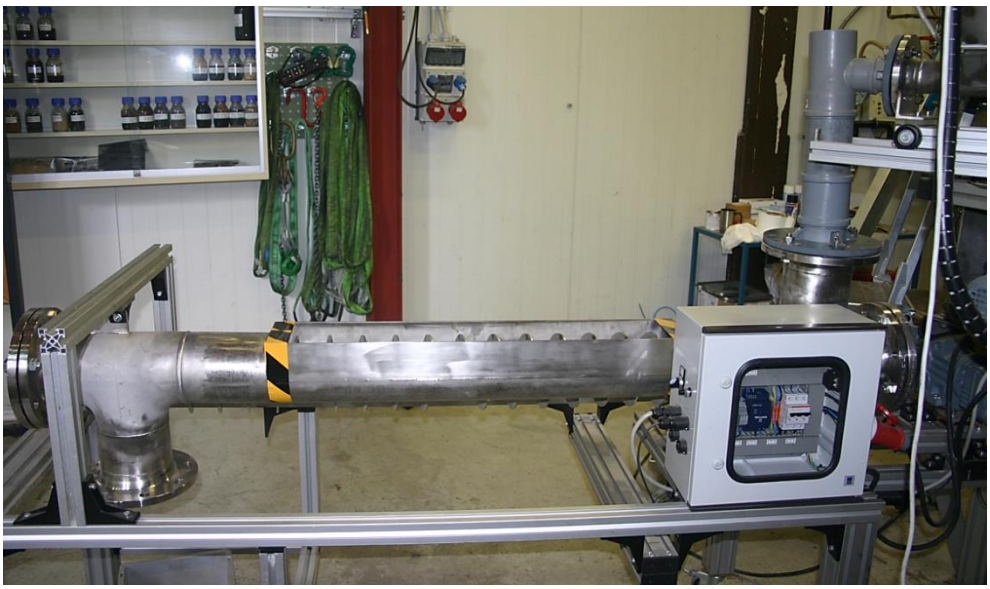

Figure 23. Picture of the cold transport reactor.

3.2.7 Experimental execution

The experimental execution of a pyrolysis trial at the STYX reactor is composed of the following phases:

1. Dosing protocol
2. Preparation and set-up of the pyrolysis process parameters
3. Start-up and initial transitory phase
4. Steady-state central phase
5. Shut-down and final transitory phase
6. Control of the end status of the filters
7. Removal of the products

Dosing protocol

The first phase before a pyrolysis experiment with a new feedstock consists in the compilation of the *dosing protocol*. This procedure is carried out for each new feedstock as well as repeated once in a time for known materials. A repetition before each experiment with known material is not required. The feeding hopper is detached from the main reactor and it is filled with the material. The rotational speed of the dosing motor is adjusted to the desired value. The material is dosed in an empty container, which is positioned on a balance. The weight of the extracted material is recorded manually every 4 minutes for 20 minutes. The procedure is repeated at least three times adjusting the rotational speed of the dosing motor to the desired value. A linear correlation is finally developed, which allows to evaluate the mass flow rate as a function of the rotational speed of the motor.

Preparation and set-up of the pyrolysis process parameters

In the *preparation* of an experiment, the desired temperature of the reactor is adjusted at the main power unit. A temperature ramp of 50 °C/h is automatically set. However, the off-set temperature of the reactor can be adjusted and reached overnight; therefore, the preparation of the experiment can avoid this step once the desired temperature is achieved and stabilized overnight.

Following, the feeding hopper is filled with a known amount of the selected feedstock and sealed. The cooling system is initiated and brought to steady-state conditions, i.e. inlet temperature in the first condenser of 10°C. Empty recovery bottles for the pyrolysis condensates as well as the char recovery hopper are weighted and displaced at the recovery positions. The nitrogen gas is increased to the desired volumetric flow rate, in order to remove the oxygen from the bulk of the feedstock as well as to render inert the reactor and the char hopper. Afterwards, the induced draft is started-up and set to the automatic regulation, which controls the draft in order to have slight overpressure in the reactor for safety purposes. The ESP is switched on to high voltage. The voltage is usually set at 12 kV; however, it can be adjusted to the optimal value during the experiment. The system remains in idle until the online gas measurement reaches an oxygen content below 0.5 vol.%.

The initial status of the filters can be evaluated as a whole unit or individually. In the first case, the filters are all open. The average pressure drop of the filtration unit is measured online and recorded. In the second situation, only one filter is set to open, while the other ones are closed. In this condition, the purge gas can flow only through the open filter. The overpressure in the reactor increases rapidly when only one filter is in operation. However, the induced fan is able to regulate the pressure and recover the desired condition of defined overpressure inside the reactor. Once stable conditions are reached, the pressure drop of the open filter can be measured adjusting the selection valve at the

manifold. The procedure is repeated for each filter, in order to obtain an overview of the status of the filtration unit.

During the *set-up of pyrolysis process parameters*, the residence time of the solids is adjusted to the selected value by acting on the front panel of the respective Labview program. The rotational speed of the screw motor is regulated automatically. The mass flow of the feedstock is adjusted manually with the help of the dosing protocol selecting the rotational speed of the dosing motor.

Start-up and initial transitory

Before the *start-up* of the experiment, a round check is performed following the checklist. First, experiment protocol is compiled with the selected initial parameters; secondly, the temperature of the reactor, the residence time of the solids as well as the volumetric flow of nitrogen gas and the oxygen content can be evaluated directly on the front panel of the Labview program. Finally, the configuration of the filtration unit is checked. The experiment starts with the release of the dosing motor, which reaches quickly the desired rotational speed. Minor adjustments can be done manually, if necessary. In the *initial transitory* the first material falls from the dosing spiral into the main screw and it is transported to the heated zone. The feedstock starts to react and the first vapors are released. The pressure drop over the filtration unit increases rapidly due to the increase of the volumetric flow rate of the vapors. The induced draft is adjusted to provide a slight overpressure of 0.5 to 1 mbar in the reactor and to avoid uncontrolled suction of secondary air. The solids flow along the reactor and reach the char recovery hopper. From the point of view of the solids, the steady-state is reached. The increase of the content of CO_2 is the second signal that pyrolysis is taking place. When the initially introduced material reaches two third of the reactor, the first pyrolysis vapors start to condense and are recovered in the flasks. The increase of the contents of CO, CH_4 and of the total carbon is slightly delayed in comparison to that of CO_2. The temperature of the vapors in the reactor and along the condensation unit reaches equilibrium conditions after approx. twofold residence time of the solids. The equilibrium conditions depend on the mass flow rate and on the water steam content of the vapors. The temperature of the vapors at the first two measuring positions in the reactor is considerably below the off-set temperature, i.e. up to 100°C in difference. The equilibrium temperature at the bottom of the first condenser is in the range of 60°C to 80°C; 20°C to 25°C at the top of the second one and between 15°C and 20°C at the bottom of the third condenser, before the second recovery flask.

Steady-state central phase

The *steady-state central phase* is the main part of the experimental execution, where pyrolysis takes place under controlled conditions. Depending on the residence time of the solids, the central phase

may last at least 2 hours. In such a way, the central phase contributes to 75% of the total duration of the experiment. The concentrations of the main gases and the respective heating value are used to monitor the stability of the operations. The oxygen content is maintained under strict monitoring. Its increase is an indication of secondary air flowing into the facility. The internal protocol foresees a maximal oxygen content of 4 vol.%. Above this limit, the experiment is aborted. Moreover, the pressure drop among the filtration unit continuously increases; thus, it is constantly monitored. During operations with all opened filters, the pressure drop is equalized among the filters. The distribution of the vapors depends on the resistance generated by the filter cake, which can be different from one filter to another. After a desired operation time, the recleaning system is activated to reduce the pressure drop. Each filter is regenerated automatically. The regeneration strategy can be adjusted manually, depending on the actual conditions of the filtration unit. The bottles for the condensate recovery are also monitored during the operations. The substitution of full bottles with empty ones is carried out manually. The new bottle is purged shortly with nitrogen gas to provide inert conditions. After weighting and recording, the new bottles replace the full one. The condensate release valve is closed and reopened after the substitution. The full bottle must be immediately sealed to avoid the release of aerosols and cooled down. Afterwards, the weight is recorded in the experiment protocol. These operations are repeated as required.

The composition of the non-condensable gases as well as the other values generated by the online gas analytics are recorded manually on the experiment protocol every 20 to 30 minutes. At least two gas samples are recovered during the experiment and immediately injected in the GC of the nearby laboratory.

In the case more feedstock is required for the experiment, a container is filled, weighted and shortly purged with nitrogen gas. Afterwards, the sealing of the hopper is opened, filled and immediately reclosed. The proper handling of the described operation avoids the introduction of oxygen in the system. The replacement of the char recovery hopper is not required for the duration of the experiment.

Shut-down and final transitory phase

The *shut-down and final transitory phase* consists firstly in the locking of the dosing motor. No more feedstock is delivered to the main reactor. The time between the release and the locking of the dosing motor defines the total mass of implemented feedstock. Within the duration of an additional residence time, the char is completely recovered in the respective hopper. Once the pyrolysis of the last material is completed, the pressure drop at the filtration unit decreases rapidly due to the reduced volumetric flow. The content of CO_2 in the non-condensable gases decreases. Again, the decrease of the other

gases is slightly delayed. The system is held in idle operation until the non-condensable gases are completely removed. The phase has duration equivalent to four residence times of the solids.

The main phases of the experiment execution are depicted graphically in Figure 24, where the evolution of the concentration of CO_2 is used to distinguish among the phases. Moreover, the development of the pressure drop over the filters is reported, including an online re-cleaning step. In this phase, the pressure drop decreases drastically to a residual pressure drop, then the build-up of the pressure drop restarts with unchanged rate.

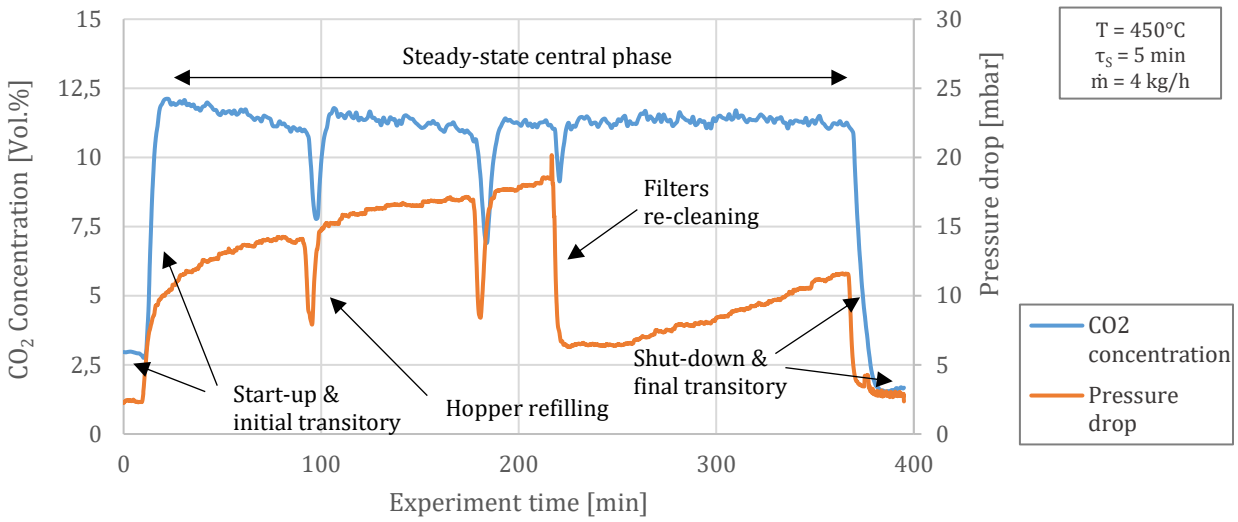

Figure 24. Diagram of the typical experimental phases.

Control of the end status of the filters

In the following step of the experimental execution, i.e. *control of the end status of the filters*, the reactor is held in idle operation with constant volumetric flow rate of nitrogen gas. The induced fan is manually adjusted to generate no overpressure in the reactor. The residual pressure drop among the filters is investigated following the corresponding procedure, as described for the initial status of the filters. At the end of the monitoring operations, the volumetric flow rate of the nitrogen gas can be reduced to the minimum. The reactor is retained in inert condition.

Removal of the products

The *removal of the products* takes place the next day for an exhaustive recovery of the condensates. The flasks as well as the char recovery hopper are removed and weighted. To complete the experiment, the two-phase condensate from the first condensation stage is weighted and separated mechanically in a decanter (see separation procedure in section 3.4.1). The homogeneous bio-oil and the aqueous condensate are weighted. The sampling procedure is reproduced for the pyrolysis char. Finally, the samples are analyzed in the adjacent laboratory or used otherwise.

3.3 Balance of the reactor

The evaluation of the mass and energy balance of the reactor plays a fundamental role in the determination of the effects of the main pyrolysis process parameters on the yields, material and energy distributions. The balances at STYX can be carried out in terms of integral yields, i.e. considering the final products of the overall facility, as well as local yields. Figure 25 reports a schematic representation of the control volumes used for the local and global balances of the facility. In the schema, the segments indicate the positions of the sampling point along the reactor. Segment 2 accounts for the first sampling point of the solids as well as for the filters 1 and 2. Segment 4 considers the second sampling point of the solids and filters 3 and 4. Segment 6 is for the third solid sampling position and filters 5 and 6 (see also Figure 20).

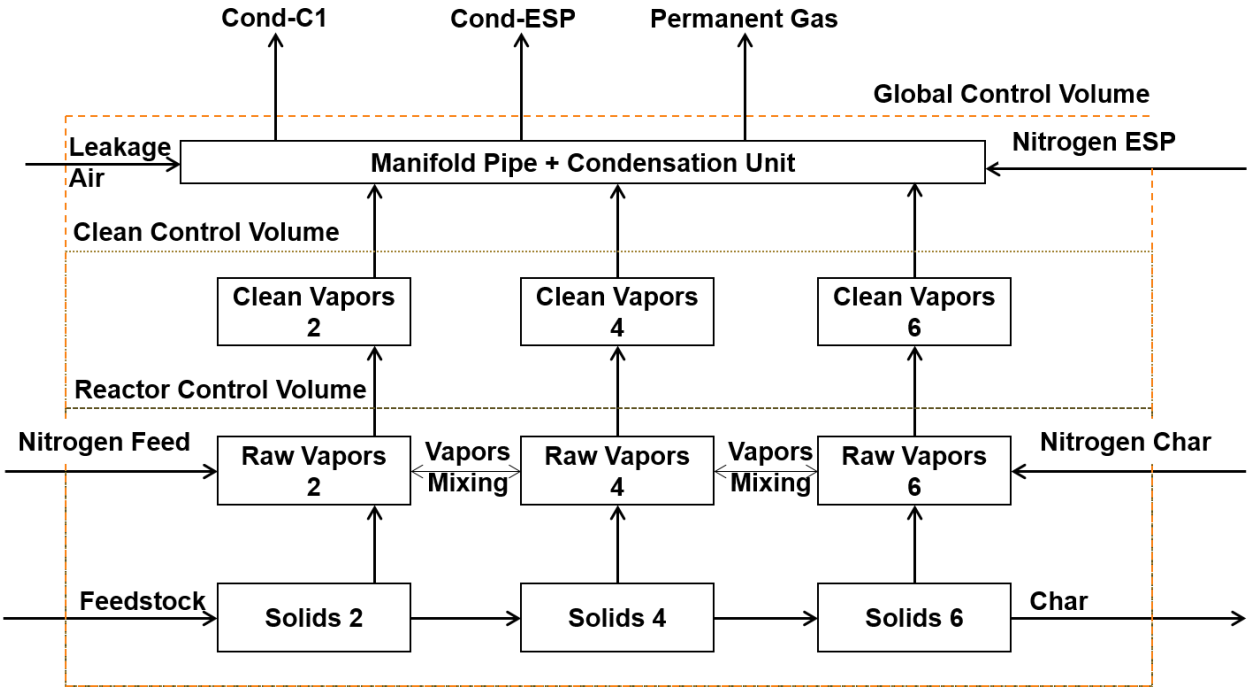

Figure 25. Schematic representation of the control volumes for mass and energy balances at the STYX reactor.

Three control volumes are provided. From the bottom to the top of Figure 25, the reactor and the clean gas control volumes are meant for the local balances within the oven of the reactor, upstream and downstream the filtration unit. The global control volume takes into account the condensation unit. Therefore, it is the reference for comparison with the literature of the overall yields distribution among the pyrolysis products.

3.3.1 Local mass balance

The local mass balance is carried out for both the reactor and the clean gas control volumes. The local mass flow of the solids is evaluated considering the following procedure. Once the steady-state

operation is reached, the sampling of the solids and of the vapors is performed as described in section 3.2.5. The samples are characterized by means of elemental and proximate analysis. Assuming that the mass of ash (*ASH*) is constant (Equation 5), i.e. no minerals are released to the vapor phase, the local mass flow of the solids is calculated from the initial and actual content of ash (Equation 6). Moreover, to evaluate the local mass flow of the solids, the mass flow of fixed carbon (Equation 7) and the mass flow of the sum of fixed carbon and ash (Equation 8) were assumed to be constant, respectively. On the basis of the contents of fixed carbon and ash, the mass flow of the solids was calculated. In such a way, it was possible to validate the fluctuation of the measurements.

By difference from two consecutive mass flow rates of the solids, the locally released mass flow of the vapors is also calculated and described by the subscript *VAPORS* in Equation 9. In the reported equations, *i* (i =2,4,6) is the sampling position of the solids with increasing value from the feeding to char recovery hopper.

$$\dot{m}_{ASH,i-2} - \dot{m}_{ASH,i} = 0 \qquad \text{Equation 5}$$

$$y_{ASH,i-2}\,\dot{m}_{SOLIDS,i-2} - y_{ASH,i}\,\dot{m}_{SOLIDS,i} = 0 \qquad \text{Equation 6}$$

$$\dot{m}_{FC,i-2} - \dot{m}_{FC,i} = 0$$

$$y_{FC,i-2}\,\dot{m}_{SOLIDS,i-2} - y_{FC,i}\,\dot{m}_{SOLIDS,i} = 0 \qquad \text{Equation 7}$$

$$\dot{m}_{(FC+ASH),i-2} - \dot{m}_{(FC+ASH),i} = 0$$

$$\left(y_{FC,i-2} + y_{ASH,i-2}\right)\dot{m}_{SOLIDS,i-2} - \left(y_{FC,i} + y_{ASH,i}\right)\dot{m}_{SOLIDS,i} = 0 \qquad \text{Equation 8}$$

$$\dot{m}_{VAPORS,f(SOLIDS),i} = \dot{m}_{SOLIDS,i-2} - \dot{m}_{SOLIDS,i} \qquad \text{Equation 9}$$

The mass flow rate of the sampled stream of vapors can be adjusted, while those flushing through the other outlets are equalized. Therefore, the flow rate of the sampled stream is adjusted by acting on the regulation valve of the vapors sampling unit to reproduce the equivalent conditions of the normal operation.

The local mass flow rate of the permanent gas (PG) from the pyrolysis process in Equation 11 is calculated by subtracting the content of nitrogen gas from the total of the extracted stream of non-condensable gases (GAS), as described in Equation 10. Finally, the mass flow rate of the vapors is obtained by adding the mass flow of the condensate, which is evaluated through the recovered mass and the duration of the sampling, to the mass flow rate of the permanent gas (Equation 12). The mixing of the vapors within the reactor can be estimated from comparing the vapors released from

the solids and the vapors recovered at the sampling positions. In the reported equations, *i* (i =2,4,6) is the sampling position of the vapors.

$$\dot{m}_{N_2,i} = \rho_{N_2} x_{N_2,i} \dot{V}_{GAS,i} \quad \text{Equation 10}$$

$$\dot{m}_{PG,i} = \rho_{GAS,i} \dot{V}_{GAS,i} - \dot{m}_{N_2,i} \quad \text{Equation 11}$$

$$\dot{m}_{VAPORS,f(VAPORS),i} = \dot{m}_{PG,i} + \frac{m_{CONDENSATE,i}}{t_{SAMPLING,i}} \quad \text{Equation 12}$$

3.3.2 Global mass balance

The global mass balance of a pyrolysis experiment is evaluated on the basis of the global control volume depicted in Figure 25, taking into account the condensation unit. The first expression describing the mass balance is reported in Equation 13

$$\dot{m}_{FEED} + \dot{m}_{N_2} = \dot{m}_{CHAR} + \dot{m}_{COND-C1} + \dot{m}_{COND-ESP} + \dot{m}_{GAS} \quad \text{Equation 13}$$

The mass flow rate of the feedstock and of the nitrogen gas are set as reported in section 3.2.7. The mass flow rates of the char and of the condensates, i.e. *COND-C1* (condensate at the bottom of the first condenser) and *COND-ESP* (condensate at the bottom of the ESP), are calculated on the basis of the duration of the experiment adopting the approach reported in Equation 12. The condensate obtained from the first condenser can be further divided into an aqueous liquid (*AQUEOUS*) and an oil phase after the mentioned procedure of separation into homogeneous phases (see section 3.4.1). The oil phase is added to the condensate obtained at the ESP, to gain one homogeneous bio-oil (*BIO-OIL*). The mass flow of the gas (*GAS*), which includes the nitrogen gas, is calculated following two separated procedures. The first one relies on the online measurement of the normal density of the gas and of the volumetric flow rate, which must be recalculated in normal conditions of temperature and pressure. The mass flow of the permanent gas is calculated subtracting the mass flow of the nitrogen gas from that of the gas. The approach adopted in Equation 11 for the local mass balance is also valid for the global mass balance. The first procedure makes also possible the estimation of the carbon content of the gas and the overall carbon balance, which will be discussed in section 3.3.3. A second, more sophisticated, procedure is used to take into account the leakage air (*AIR*) in Figure 25, which can be introduced into the plant, in particular downstream the filtration unit. Secondary air has negligible influence on the reactions because of the short residence time of the vapors at high temperatures downstream the filtration unit. However, it may affect the mass balance by

overestimating the yield of the permanent gas. The volumetric contents of nitrogen and of oxygen of the gas are measured at the offline-GC. Oxygen is measured online as well. The volumetric fractions can be easily converted into mass fractions for mass balance purposes. To maximize the reliability of the results, the mass flow rate of the secondary air is estimated using the balances of nitrogen and oxygen independently in Equation 14 and Equation 15.

$$\dot{m}_{N_2} + y_{N_2,AIR}\,\dot{m}_{AIR} = y_{N_2,GAS}\,\dot{m}_{GAS} \qquad \text{Equation 14}$$

$$y_{O_2,AIR}\,\dot{m}_{AIR} = y_{O_2,GAS}\,\dot{m}_{GAS} \qquad \text{Equation 15}$$

Differences in the estimations of the mass flow rate of the secondary air are an indication of oxidation reactions taking place downstream the filtration unit. The second procedure, here described, allows calculating the contents of carbon, hydrogen and oxygen of the permanent gas, which is important for performing the elemental balances. The fluctuations of the volumetric flow rate and composition of the gas are varied within the measured limits in order to minimize the mean square error of the elemental balances. The total carbon content, the heating value and the density of the gas are adopted as additional constraints in the minimization algorithm. The residual difference between the total input and output is defined as mass loss. The overall mass balance is described by Equation 16 including the nitrogen gas, the secondary air as well as the mass loss.

$$\dot{m}_{FEED} + \dot{m}_{N_2} + \dot{m}_{AIR} = \dot{m}_{CHAR} + \dot{m}_{AQUEOUS} + \dot{m}_{BIO-OIL} + \dot{m}_{GAS} + \dot{m}_{LOSS} \qquad \text{Equation 16}$$

$$\dot{m}_{FEED} = \dot{m}_{CHAR} + \dot{m}_{AQUEOUS} + \dot{m}_{BIO-OIL} + \dot{m}_{PG} + \dot{m}_{LOSS} \qquad \text{Equation 17}$$

$$y_i = \frac{\dot{m}_i}{\dot{m}_{FEED}} \qquad \text{Equation 18}$$

Equation 17 offers the mass balance on feedstock basis, i.e. considering only the mass flow rates related to the pyrolysis process. Finally, Equation 18 defines the yield of each pyrolysis product *i* as the mass fraction of the product with respect to the feedstock.

The sources of mass loss are the following:

- Filtration unit, where fine solid particles and newly formed secondary char or soot are deposited
- Condensation unit, where sticky oil can deposit at the connection between the condensers
- Gas flow meter, where organic aerosols may be impacted and captured.

The experimental experience showed that the mass loss at the condensation unit and at the gas flow meter are of negligible influence, i.e. in the range of 0.1 wt.% of the total mass of the feedstock converted in one trial. The mass loss generated by the filtration unit plays a prominent role on the overall loss. An estimation can be done using the theory of Darcy for porous materials with multiple layers.

The pressure drop of the filter candle is known for a defined volumetric flow rate of nitrogen gas ($\dot{V}_{GAS}$). The surface (S_{FILTER}), the thickness (d_{FILTER}) and the permeability (k_{FILTER}) of the filters are given by the manufacturer; therefore the pressure drop of the filter can be easily verified knowing the properties of nitrogen such as the dynamic viscosity (μ_{GAS}). The additional pressure drop of the filter cake, at a defined fixed time, is a function of its thickness and permeability (Equation 19). While the thickness of the filter cake (d_{CAKE}) increases with the duration of an experiment, the permeability (k_{CAKE}) is assumed to be constant. Suitable values for the permeability and density can be taken from the literature related to soot formation and characterization (Equation 20). Using the literature data for the permeability and own measurement of the filter cake density (ρ_{CAKE}) and porosity (ϕ_{CAKE}), the thickness of the filter cake can be estimated by fitting the pressure drop of the loaded filter from the measurements described in section 3.2.7. Finally, the mass loading of the filter cake can be estimated from its bulk density, surface (S_{CAKE}) and thickness. Although the precision of the estimation of the mass loss at the filtration unit is hampered by the large number of assumption that are required to be made, the proposed method gives reasonable results. The mass loss is in the range of 1.0 to 5.0 wt.% of the feedstock and in the range of 2.0 to 10 wt.% of the elemental carbon displaced in one experiment.

$$\dot{V}_{GAS} = \frac{S_{FILTER}}{\mu_{GAS}} \frac{\Delta p(t)}{\left(\frac{d_{FILTER}}{k_{FILTER}} + \frac{d_{CAKE}(t)}{k_{CAKE}(t)} \right)} \qquad \text{Equation 19}$$

$$m_{CAKE}(t) = \rho_{CAKE} \left[1 - \Phi_{CAKE}(t) \right] S_{CAKE} d_{CAKE}(t) \qquad \text{Equation 20}$$

3.3.3 Elemental balance

The elemental balances are performed on the basis of the elemental composition of the feedstock and of the products from the pyrolysis process. The elemental composition of the solids and liquids is measured, as reported in section 3.1. The elemental composition of the gases is calculated from the yields of each compound. The elemental balance of carbon is reported as an example in Equation 21.

The carbon flow rate of each stream is calculated by multiplying the carbon content for the respective mass flow rate.

$$y_{C,FEED}\,\dot{m}_{FEED} - \left(\begin{array}{l} y_{C,CHAR}\,\dot{m}_{CHAR} + y_{C,AQUEOUS}\,\dot{m}_{AQUEOUS} + \\ + y_{C,BIO-OIL}\,\dot{m}_{BIO-OIL} + y_{C,PG}\,\dot{m}_{PG} \end{array} \right) = \dot{m}_{C,LOSS} \qquad \text{Equation 21}$$

3.3.4 Energy balance

The energy balance of the reactor and of the whole facility are carried out to determine the energy yields distribution among the pyrolysis products and the thermal efficiency of the plant. The energy balance is expressed on the basis of the mass balance, taking into account the enthalpy flows as well as the heat input and losses. The energy balance is described by Equation 22:

$$\dot{H}_{FEED} + \dot{H}_{N_2} + \dot{H}_{AIR} + \dot{W}_{IN} = \dot{H}_{CHAR} + \dot{H}_{BIO-OIL} + \dot{H}_{AQUEOUS} + \dot{H}_{GAS} + \dot{Q}_{LOSS} + \Delta\dot{H}_{\dot{m}_{LOSS}} \qquad \text{Equation 22}$$

On the left side of Equation 22, the enthalpy flows of the feedstock ($\dot{H}_{FEED}$), of the nitrogen gas and of the secondary air are reported together with the external electrical power ($\dot{W}_{IN}$), which is required to maintain the system at the desired temperature. On the right side, the enthalpy flows of the pyrolysis products, as well as the enthalpy of the experimentally not recovered mass, are depicted. Moreover, the heat loss to the environment and the enthalpy of reaction are taken into account. Equation 23 describes the enthalpy flow of the respective stream. The chemical enthalpy is described by the lower heating value; the thermal enthalpy is obtained from the averaged specific heat capacity multiplied by the difference between the actual and the reference temperatures.

$$\dot{H}_i = \dot{m}_i \left[\bar{c}_{p,i} \left(T_i - T_{REF} \right) + LHV_i \right] \qquad \text{Equation 23}$$

$$\dot{W}_{IN} - \dot{Q}_{LOSS} = \dot{H}_{PYRO} = \dot{m}_{FEED}\, h_{PYRO} \qquad \text{Equation 24}$$

The energy requirements of the process ($\dot{H}_{PYRO}$) is the energy that must be supplied externally to perform pyrolysis at the selected conditions. It is expressed as the product of the specific enthalpy for pyrolysis (h_{PYRO}) and the mass flow rate of the feedstock in Equation 24. The specific enthalpy for pyrolysis is an important design parameter for the scale-up of a pyrolysis reactor.

The thermal losses to the environment depend on the temperature of the reactor and on the surrounding, as well as on the insulation material. The thermal losses can be measured in idle operation, with the reactor at the experimental temperature. The thermal losses of the reactor can also

be calculated on the basis of heat transfer mechanisms (Equation 25). It is assumed that the inside of the oven is at isothermal temperature, i.e. the intern side of the insulation material is at reactor temperature. The heat losses are calculated for each surface of the oven individually comparing the conduction heat losses through the insulation and the heat loss to the environment due to free convection.

$$\dot{Q}_{LOSS} = \frac{\lambda_{INSULATION}}{t_{INSULATION}} S_{EXT-SURCFACE} \left(T_{REACT} - T_{EXT-SURFACE} \right) = \\ = \alpha_{FREE-CONVECTION} S_{EXT-SURFACE} \left(T_{EXT-SURFACE} - T_{SURROUNDINGS} \right) \quad \text{Equation 25}$$

The energy balance of the condensation unit (Equation 26) is carried out on the basis of the inlet temperature of the vapors, the outlet temperature of the gas on the process side. On the cooling medium (*CM*) side, the inlet and the outlet temperatures are used as well.

$$\dot{m}_{CM} \left[\bar{c}_{p,CM} \left(T_{CM,OUT} - T_{CM,IN} \right) \right] = \dot{m}_{VAPORS} \left[\bar{c}_{p,VAPORS} \left(T_{VAPORS,IN} - T_{VAPORS,COND} \right) \right] + \\ + \dot{m}_{CONDENSATE} \overline{\Delta h}_{LV,CONDENSATE} + \dot{m}_{GAS} \left[\bar{c}_{p,GAS} \left(T_{VAPORS,COND} - T_{GAS,OUT} \right) \right] + \dot{Q}_{LOSS,COND} \quad \text{Equation 26}$$

The condensation process can be roughly described by three consecutive steps. At first, the pyrolysis vapors are cooled down from the temperature of pyrolysis to the temperature of condensation. The condensation of the organic vapors takes place on a relatively large range of temperatures. However, the contribution of the thermal enthalpy of the vapors is of about 6% to the overall energy balance. Therefore, a temperature of 100°C is assumed for their condensation. The third step is the further cooling of the non-condensable gases to the outlet temperature, i.e. 20°C. As reported in Equation 26, the specific latent enthalpy of condensation is taken into account for the condensate. It is a weighted sum of the latent enthalpy of condensation of the condensable compounds. In particular, water plays a prominent role, while the condensable organics all have comparable values that are an order of magnitude smaller than that of water. An additional term of heat loss to the environment is reported on the process side, since the cooling medium is at a lower temperature with respect to the surroundings.

The conversion efficiency of the pyrolysis process defines the ratio of the energy contained in the products with respect to the energy content of the feedstock. Since the pyrolysis condensates are recovered after a phase change, the definition of the conversion efficiency may have different interpretations. Atsonios et al. [17] defined a coefficient of chemical energy recovery (CER) based on the higher heating value (HHV), which is reported in Equation 27 as CER_{HHV}.

$$CER_{HHV} = \frac{\sum_i \dot{m}_i HHV_i}{\dot{m}_{FEED}\, HHV_{FEED}} \quad \text{Equation 27}$$

$$CER_{LHV} = \frac{\sum_i \dot{m}_i LHV_i}{\dot{m}_{FEED}\, LHV_{FEED}} \quad \text{Equation 28}$$

$$CPE = \frac{\sum_i \dot{m}_i LHV_i}{\dot{m}_{FEED}\, LHV_{FEED} + \dot{W}_{IN}} \quad \text{Equation 29}$$

$$CGE = \frac{\dot{m}_{SYNGAS}\, LHV_{SYNGAS}}{\dot{m}_{FEED}\, LHV_{FEED}} \quad \text{Equation 30}$$

However, the utilization of the HHV foresees the heat recovery from the condensation of the pyrolysis vapors. The utilization of the LHV is commonly used in flow sheet simulation and energy plant analysis and it should be preferred from an energy point of view (CER_{LHV}) in Equation 28. Additionally, the Cold Pyrolysis Efficiency is defined (Equation 29) for the direct comparison to the Cold Gas Efficiency (CGE) adopted in gasification (see Equation 30).

3.4 Measurement techniques

A range of measurement techniques were adopted for the characterization of the pyrolysis products as well as for the evaluation of the mechanical and thermal processes within the reactor.

3.4.1 Phase separation procedure

The separation procedure and duration is adjusted depending on the condensate properties. First, the condensate is strongly shaken to facilitate the filling of the decanter. Second, the condensate is left in the decanter as long as the two phases are completely separated. The operation can last up to few hours. Normally it is done overnight. Afterwards, the bottom phase is slowly removed. The removal is carried out is several steps. The transitory layer is removed separately (about 1 wt.% of the condensate for beech wood). Finally, the top phase is removed from the decanter. The aqueous condensate is sampled and stored, while the organic liquid is mixed with the mono-phase organic condensate from the second stage and finally sampled as a homogeneous product. The reproducibility of the separation procedure is below ± 5 wt.% on condensate basis for heterogeneous feedstock such as wheat straw.

3.4.2 Characterization of the pyrolysis products

The characterization of the pyrolysis products consisted in a range of standard analyses, such as the analysis of the elemental and of the proximate compositions, as well as product specific chemical and physical tests. In this paragraph, an overview of the characterization of the products is reported.

Pyrolysis char

The pyrolysis chars from the experiments at STYX were all characterized in terms of solid fuels. The water content, the proximate, the elemental and calorific analyses as well as the contents of the main minerals and of the metals were carried out following the respective DIN Standards, as reported for the feedstock in section 3.1.1.

The morphology of the char was investigated by means of SEM analysis as well as in terms of BET surface using a Quantachrome Nova 4000e.

Pyrolysis oil

The pyrolysis oils were also characterized in terms of liquid fuels. The water content, the proximate and the elemental compositions as well as the calorific values were analyzed under the respective DIN Standards for liquid fuels. The water content of the pyrolysis oils was measured in a Metrohm 870 KF Titrino Plus by means of volumetric titration, using a CombiSolvent Keto as solvent and a CombiTrant 5 Keto as corresponding titer agent; the pH-Value was measured in a Metrohm 691 pH Meter with a solution of 3M of KCl. The density was measured adopting a pycnometer after Gay-Lussac while the surface tension was measured using a customized system based on the pendant drop principle as discussed in Song and Springer [197]. The molecular weight distribution was measured adopting Gel Permeation Chromatography (GPC) and the average molecular weight was calculated. The dynamic viscosity of the pyrolysis oil was measured in a capillary viscometer Rheotest LK 2.2 at 20°C ± 0.2°C. Moreover, the rheology of the pyrolysis oils was investigated in a rotational rheometer (Physica MCR501, Anton Paar GmbH) as discussed in Jampolski et al. [109].

Solvent fractionation was carried out following the scheme described in Boscagli et al. [27], which approaches the extraction in a similar fashion to that described by Oasmaa et al. [161].

Hydrogen nuclear magnetic resonance spectroscopy (^{1}H-NMR) was also employed for a further characterization of the pyrolysis oils. With these techniques it is possible to evaluate the functionality of protons. The adopted procedure is reported in [27].

The composition of the pyrolysis condensates was investigated into details by means of gas-chromatography/mass spectrometry (GC/MS). The characterization included both low and high boiling point compounds using different devices. The preparation of the samples was as follows: the

sample were homogenized in ultrasonic bath for 10 to 15 minutes; the samples aimed at quantifying low boiling point compounds were treated with H_2SO_4 to reduce the pH value to about 1 and to ensure high vapor pressure; the samples used for high boiling point compounds were diluted with tetrahydrofuran (THF) in a 1:10 ratio. Each sample was provided with isotope marked internal standard. Two identical HP 6890 N/5963 MSD with Helium as carrier gas were adopted. The first GC/MS is equipped with 7649 E Headspace Sampler, in order to analyze quantitatively the components with low-boiling point, e.g. acetaldehyde, acetic acid and furfural from the decomposition of holocellulose. The second GC/MS is equipped with a MSD HP 5972A; it uses the direct injection of the sample and it is more suitable for substances with high boiling point, such as phenol and guaiacol from the decomposition of lignin. Moreover, benzene (C_6H_6) and naphthalene ($C_{10}H_8$) were measured to evaluate the precursors of soot from secondary gas phase reactions.

Aqueous Condensate

The aqueous condensates were analyzed in terms of liquid fuels as well. The water content, the proximate and elemental compositions as well as the calorific value were analyzed. Moreover, the water content, the pH value and the GC-MS analysis were carried out adopting the methodologies discussed for the pyrolysis oils.

Permanent Gas

The permanent gas was measured online as discussed in section 3.2.4. Moreover, GC analysis was carried out to gain a deeper insight in the composition. The GC was an HP-5890 series II, equipped with two detectors. The first was a Thermal Conductivity Detector (GC-TCD) with a packed metal column Supelco 12.392-U, matrix 60/80Carboxen-1000 support of 4.6, external diameter 1/8’ and internal diameter of 0.21 mm, for the measurement of H_2, O_2, N_2, CO, CO_2 and CH_4. The second detector was a Flame Ionization Detector (GC-FID) with a capillary column of 50 m x 0.53 mm x 10 µm. The FID was calibrated to measure CH_4, C_2H_6, C_2H_4, C_3H_8, C_3H_6, iso-C_4H_{10}, normal-C_4H_{10} and 1-C_4H_8. Both the detectors used helium as carried gas with a constant volume flow rates of 30 ml/min and 20 ml/min, respectively. The oven temperature was programmed with initial temperature of 50°C, followed by a ramp of 5°C/min up to 180°C and successively by ramp of 7.5°C/min to a final temperature of 240°C with a holding time of 4 minutes.

3.4.3 Reactor characterization

The transport mechanisms of the solids due to the rotation of the screw as well as the hydrodynamics of the gas have been investigated experimentally at the STYX reactor with the aim of validating the assumptions used for the description of the reactor.

The evaluation of the experimental results were undertaken adopting the theory of the residence time distribution [126, 79]. For more details refer to the appendix.

The *geometric residence time* of the solids $\tau_{S,GEOM}$ in a screw reactor depends only by the geometry of the screw, i.e. length (l) and pitch (p) and on the rotational speed (n), as reported in Equation 31.

The *space time* (τ_{GAS}) is the gas equivalent of the geometric residence time, which depends on the free volume of the reactor (V_{REACT}) or of the freeboard (V_{FB}) and on the volumetric flow rate of the gas ($\dot{V}_{GAS}$) (Equation 32). The volume used for the calculation of the space time at the successive segments are the cumulated volumes of the reactor or of the freeboard up to the achieved segment (see Figure 26).

$$\tau_{S,GEOM} = \frac{l}{np} \rightarrow p \equiv \left[\frac{m}{rot}\right] \qquad \text{Equation 31}$$

$$\tau_{G,ST-REACT,i} = \frac{\sum_i V_{REACT,i}}{\dot{V}_{GAS}} \qquad \text{Equation 32}$$

$$\tau_{G,ST-FB,i} = \frac{\sum_i V_{FB,i}}{\dot{V}_{GAS}}$$

The *mean residence time* of the solids $\tau_{S,MEAN}$ and of the gases $\tau_{G,MEAN}$ are the weighted average of the residence time obtained from the experimental *Residence Time Distribution* (RTD). The *normalized residence time* θ is the non-dimensional residence time based on the experimental mean residence time (see also the Appendix for more details).

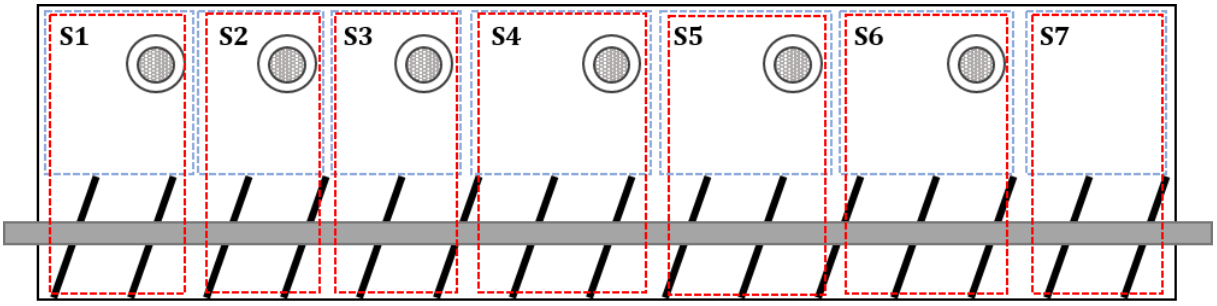

Figure 26. Volumes used for the cumulative calculation of the space time for the reactor (red) and for the freeboard (blue).

Transport of the solids

The physics of granular solids is a very complex field of research, since the behavior of such materials is different from any other state of the matter. The flow of granular solids may be associated to particles with none or negligible attractive forces. Gravitational forces dominate the behavior of granular materials through friction [108].

In the design of screw conveyor for the handling of bulk materials, the *Degree of Filling* (DoF) is the defining parameter [60]. The DoF is the volume fraction of the screw which is occupied by the material (Equation 33). For a fixed geometry, the DoF increases with an increase of the mass of the solids and a decrease of its bulk density. Moreover, the DoF is influenced by the operational parameters (Equation 31). Combining Equation 31 and Equation 33, the DoF becomes a function of the residence time of the solids and consequently of the rotational speed of the screw. For a fixed geometry, an increase of the rotational speed leads to a decrease of the DoF. The mass flow rate of the bulk solids can be increased at fixed DoF and higher rotational speed.

$$DoF \equiv \frac{V_{SOLID}}{V_{SCREW}} = \frac{\frac{m_{SOLID}}{\rho_{SOLID,BULK}}}{\pi \frac{r_{SCREW}^2 - r_{SHAFT}^2}{2} l} \qquad \text{Equation 33}$$

To gain insight into the mixing within the pitch of the screw several experiments were carried out at the transport reactor. The flow of the batch was recorded and snapshots were taken using a photocamera.

The determination of the RTD is performed experimentally, adopting suitable signal-response methods, i.e. impulse or step, with the help of tracers [49]. These can be colored dyes, radioactive compounds, magnetic particles, etc. For the purpose of this work, the impulse method was applied adopting magnetic particles of same size and weight of the wood particles used in the pyrolysis experiments as tracer. The magnetic tracers had been produced by fixing iron powder in paper tape. Afterwards, the paper tape was cut in such a way to mimic the shape and the weight of the wood particles. The material was fed continuously to the reactor until the steady state flow was achieved. Afterwards, a batch of magnetic tracers was introduced. At the outlet of the reactor, each batch corresponding to one pitch of the screw was recovered separately and weighted. The tracers were extracted using a magnet. Finally, both the tracers and the remaining particles of wood were weighted again and the mass concentration of the tracers was calculated. The residence time distribution E(t), the cumulative RTD F(t) as well as the mean residence time τ_R and the standard deviation σ were calculated adopting the respective equations. The number of continuously stirred tank reactors (N-

CSTRs) as well as the Peclet numbers were calculated as reported by Waje et al. [226, 225]. For more details about the theoretical background of the residence time distribution see the Appendix.

Hydrodynamics of the gases

An important peculiarity of the STYX reactor is the trough shape of the vessel. The design allows the insertion of horizontal filter elements in the freeboard, in contrast to typical auger pyrolysis reactors, which are characterized by a cylindrical shape (see Figure 17). The hydrodynamics of the gases flowing through the reactor shall be investigated to gain knowledge related to residence time of the vapors, and therefore the extent of the secondary reactions in the gas phase [97].

The transport of the gases was investigated experimentally with the aid of the vapors sampling unit. The reactor was held at constant temperature; therefore, isothermal, steady-state conditions were assumed. A mixture of N_2 and CO_2 was continuously fed to the reactor and the concentration of CO_2 was measured with the online instrumentation. A step variation of the composition of the gases was adopted. The methodology is known in the literature as "Step Change" [49]. The concentration of CO_2 was increased at a defined time, without altering the total volumetric flow and maintained constant until the concentration at the outlet reached steady-state. Measurements were taken at each gas sampling position upstream the respective filter candle and carried out for a range of volumetric flow rates. The mean residence time as well as the number of stirred tank reactors were subsequently calculated applying the theory of residence time distribution (see the Appendix for more details). The mean residence time (Equation 80 in the appendix) was compared with the space time (Equation 32), as described by Fogler [79]. The space time is independent from the adopted model and it is calculated as the ratio of the volume to the volumetric flow rate, as described in Equation 32.

3.4.4 Thermal processes characterization

To characterize the thermal processes, i.e. heating and drying of granular solids, specific experiments were carried out using non-reactive materials. The thermo-physical properties are reported in Table 9 in comparison to the reference feedstock beech wood.

Table 9. Physical properties of the granular materials used in the experimental validation.

Material	λ_S [W/mK]	d_P [mm]	ρ_S [kg/m^3]	c_S [kJ/kgK]	Water [%]
Glass scrap	1.05	10 - 12	370	0.75	-
Clay granulate	0.15	4 - 5	330	0.85	30
Beech wood	0.13	4 - 5	220	1.00	10

Heating of granular solids

The heating of a granular solid was investigated determining the temperature of the particles at the solid sampling positions along the screw. Glass scrap was chosen as inert and dry material because of the well-defined physical properties and of the smooth surface, which was required for applying dyes sensitive to the particle temperature. The glass scrap was washed with water to remove impurities and dried in an oven for 24 hours. The bulk density was measured following the procedure described in section 3.1.1. The other properties were taken from technical literature. Temperature sensitive dyes are liquid markers, which can be applied to the surface of solid in order to evaluate the variation of the temperature. The dyes evaporate if a defined temperature is achieved. Differently colored dyes react and evaporate at different temperature (see Figure 27). The sensitivity of each color was ±7°C. Therefore, the temperature error was in all the cases below 15°C. In such a way, it is possible to determine whether the particle has reached a defined temperature. The adopted procedure was as follows: glass scraps with a selected dye were introduced into the reactor and sampled at the first sampling port along the axis. In the case the dye was evaporated, the sequence was repeated using dyes reacting at more severe temperatures until the samples did not present traces of it on the surface of the glass particles. To confirm the results, sampling using the last reacted and the first non-reacted dyes was repeated. The temperature of the particles at the sampled position was in the range between the last reacted dye and the first non-reacted dye. The sampling continued at the following port, starting with the last evaporated temperature dye at the former sampling position.

Figure 27. Glass scrap colored with temperature sensitve markers, before and after having reached the evaporation temperature.

Drying of granular solids

The drying of porous inert material was investigated adopting clay granulates. The porous structure of clay granulates enables the uptake of a large amount of water. The purchased material was dried in an oven at 80°C for about a week, in order to ensure perfectly dried conditions. Afterwards, samples were taken, weighted and put in an oven at 105°C for 24 hours for control purpose. Finally, the material was moistened to the desired water content of 30 wt.%, and mixed to ensure a uniform water distribution. Again, for control, samples were taken and dried for 24 hours at 105°C. Moistened clay

granulate was fed continuously to the reactor. During the experiments, samples were taken along the axis of the reactor using the equipment described in Section 3.2.5. The samples were recovered at the four measuring positions along the screw and at the char hopper. The sampling position S0 (see Figure 21) was used as a further control of the actual water content. The recovered samples were immediately weighted and further dried at 105°C for 24 hours to evaluate the residual water content after the thermal treatment. Each experiment was repeated twice.

3.4.5 Pyrolysis and secondary gas phase reactions

Pyrolysis of beech wood

The pyrolysis of beech wood was investigated to evaluate the decomposition of the granular solids in the screw reactor. Samples were taken under continuous operation at the respective measurement points along the axis of the reactor (see Figure 20 and Figure 21). Each experiment was at least twice. The samples were all characterized by means of proximate analysis. The method described in section 3.3.1 was adopted for determining the mass flow rate.

Secondary gas phase reactions

The secondary gas phase reactions taking place in the screw reactor were investigated adopting beech wood as feedstock. The sampling procedure was as follows. During continuous operation, only the filter at S6 was open. In such a way, the pyrolysis vapors were forced to flow along the axis of the reactor without further mixing. Samples were taken at the measurement points along the axis before each filter. The vapors were collected adopting the equipment described in section 3.2.5. The liquid samples were weighted and analyzed as described in section 3.4.2. The permanent gas was analyzed continuously (see section 3.2.4) and sampled. Each experiment was repeated at least twice.

4. PYROLYSIS OF BIOGENIC FEEDSTOCK AT STYX

The STYX reactor was developed with the aim of producing particles and ash free pyrolysis condensates from the thermal decomposition of biomass. A large number of experimental investigations were carried out for balancing the reactor and generating sufficient pyrolysis products for a detailed characterization in terms of advanced fuels. Part of the experimental results adopting beech wood [208] and sewage sludge [209] have been already published.

In this chapter the mass, elemental and energy balances will be reported for the reference feedstock beech wood at different temperatures of the reactor. The results of the balances are also adopted in Chapter 5 for comparison with the results of the thermo-chemical model. Second, a detailed analysis of the pyrolysis products is given and compared to the typical results of other pyrolysis processes. Following, the results for three selected low-grade biogenic feedstock are reported and compared to the reference feedstock in terms of balances and products features. To conclude the chapter, the experimental results are discussed with focus on the further development of the thermo-chemical model of the STYX reactor.

4.1 Pyrolysis of beech wood at STYX

The pyrolysis of beech wood at the STYX reactor was adopted as reference for the development of the thermo-chemical model due to its invariable composition and because of the available data in the literature for direct comparison of the results. This section is structured as follows:

- Global mass, elemental and energy balances as well as yields distribution for the reference process conditions;
- Local mass balances with respect to the sequential filtration and extraction for the reference temperature;
- Effect of the offset temperature of the reactor on the global balances;
- Characterization of the pyrolysis products at different pyrolysis temperatures;
- Effect of the filtration on the composition and properties of the vapors.

4.1.1 Global balances for the reference temperature

Mass balance

The mass balance of a pyrolysis experiment was carried out for the reference process conditions, which are reported in Table 10.

Table 10. Reference process conditions adopted using beech wood as reference feedstock for the global and local balances.

Temperature of the reactor	450	°C
Geometric residence time of the solids	10	min
Mass flow of the solids	2	kg/h

The measured moisture content of the feedstock was about 10 wt.%. The evaluation of the balances was carried out using the procedure described in section 3.3. An overview of the process is depicted graphically in Figure 28.

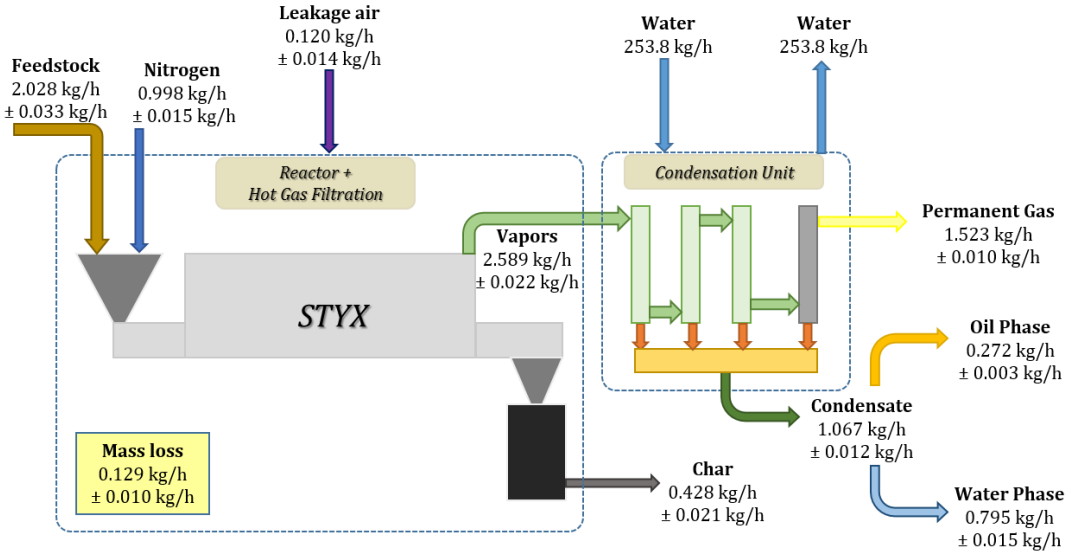

Figure 28. Mass balance of the pyrolysis process at the STYX reactor (beech wood-450°C-10min-2kg/h).

The results of the mass balances are reported in Table 11 as mass flow rates and yields of the pyrolysis products. In Figure 28, the permanent gas includes the purge gas nitrogen, whereas in Table 11 it is on N_2-free basis.

Table 11. Mass flows and yields of the pyrolysis products at the STYX reactor for the reference process conditions.

Stream	**Mass flow [kg/h]**	**Mass yield [wt.% of feed]**
Feedstock	2.028 ± 0.033	100.0
Char	0.428 ± 0.021	21.1 ± 0.7
Oil Phase	0.272 ± 0.003	13.4 ± 0.4
Water Phase	0.795 ± 0.015	39.2 ± 0.1
Permanent Gas (N_2-Air free)	0.405 ± 0.010	20.0 ± 0.2
Mass loss	0.129 ± 0.010	6.4 ± 0.6

About 6 wt.% of the feedstock on as received basis was not recovered in the pyrolysis products. The pressure drop provided by the nitrogen flow over the filtration unit was 7.6 mbar and 12.6 mbar before and after the experiment, respectively. Adopting the method discussed in section 3.3 and the analysis of the filter cake, which is reported in section 4.1.4, the total mass of filter cake retained over the filter was between 0.036 kg/h and 0.114 kg/h, i.e. between 30 wt.% and 98 wt.% of the mass loss.

Energy balance

The energy balance is depicted graphically in Figure 29 as well as reported in Table 12 for the reactor and in Table 13 for the overall pyrolysis plant including the condensation unit, for the experiment already discussed above. The enthalpy flows are calculated on the basis of the lower heating value (LHV) and on the specific heat capacity at the respective temperature.

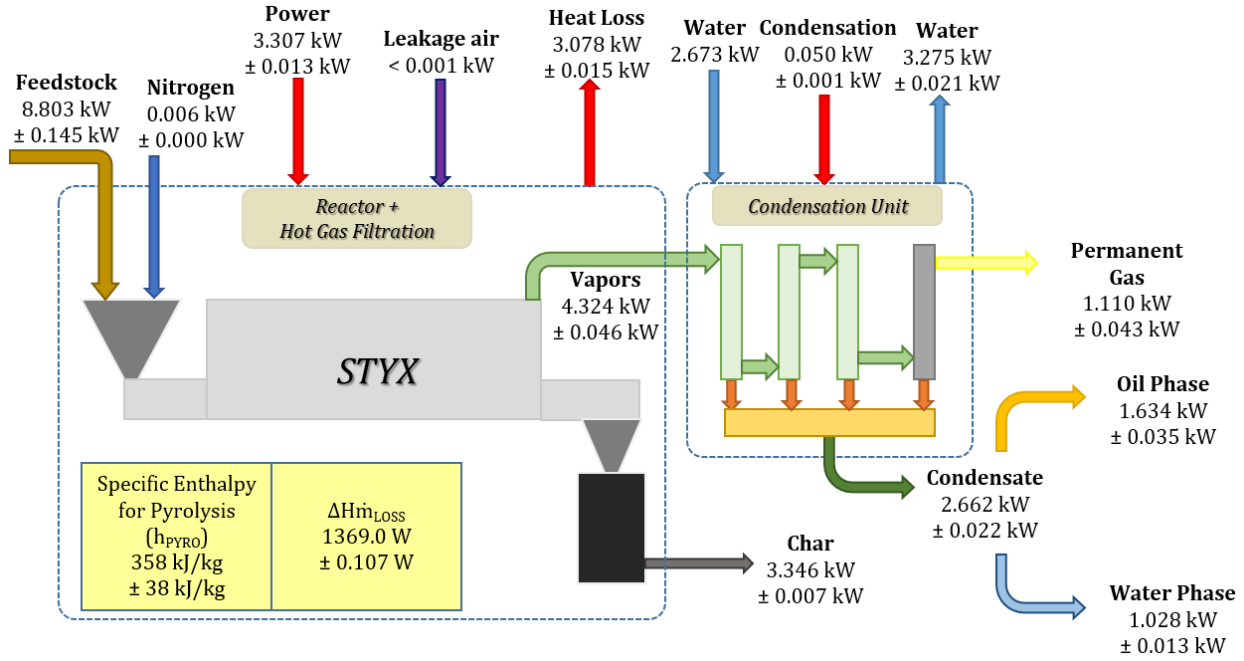

Figure 29. Energy balance of the STYX plant (beech wood-450°C-10min-2kg/h).

Table 12. Energy balance of the pyrolysis reactor (Reactor + Hot Gas Filtration).

Input Reactor			*Output Reactor*		
	kW	*% Input*		*kW*	*% Input*
Feedstock	8.803 ± 0.145	72.6 ± 0.2	**Char**	3.346 ± 0.007	27.6 ± 0.3
Nitrogen	0.006 ± 0.000	0.05 ± 0.0	**Vapors**	4.324 ± 0.046	35.7 ± 0.1
Leakage air	0.000	0.0	**Heat loss**	3.078 ± 0.015	25.4 ± 0.1
Heat supply	3.307 ± 0.013	27.3 ± 0.2	**Total Output**	10.748 ± 0.052	88.7 ± 0.7
Total input	12.117 ± 0.159	100.0	**Mass loss**	1.369 ± 0.107	11.3 ± 0.8

The input enthalpy flow of the purge gas was negligible (Table 12). At the outlet of the reactor, the enthalpy flows are divided into the char, assumed to be at room temperature, and the vapors at the

pyrolysis temperature (450°C, in the reported example). The enthalpy content of the products at the outlet of the reactor was slightly below 90% excluding the missing enthalpy due to the mass loss, indicating the high efficiency of the system. The specific enthalpy for pyrolysis accounted for 358 kJ/kg, which corresponds to about 2 % of the chemical enthalpy of the feedstock. The energy balance including the condensation unit is reported in Table 13. The thermal enthalpy of the pyrolysis vapors was removed through the condensation unit. It accounted for 0.6 kW, which corresponds to 13% of the total enthalpy of the vapors and to 6.5 % of the enthalpy of the feedstock. An effective recovery of the thermal enthalpy during the condensation of the pyrolysis vapors should be implemented at larger scale to improve the overall efficiency of the process.

Table 13. Energy balance of the pyrolysis plant (Reactor + Hot Gas Filtration + Condensation Unit).

Input pyrolysis plant			***Output pyrolysis plant***		
	kW	***% Input***		***kW***	***% Input***
Feedstock	8.803 ± 0.145	59.5 ± 0.3	**Char**	3.346 ± 0.007	22.6 ± 0.2
Nitrogen	0.006 ± 0.000	0.04 ± 0.0	**Oil phase**	1.634 ± 0.035	11.0 ± 0.1
Leakage air	0.000	0.0	**Water phase**	1.028 ± 0.013	7.0 ± 0.2
Heat Supply	3.307 ± 0.013	22.4 ± 0.1	**Permanent gas**	1.110 ± 0.043	7.5 ± 0.2
Cooling water	2.673	18.1 ± 0.2	**Cooling water**	3.276 ± 0.021	22.2 ± 0.4
Condensation	0.050 ± 0.001	0.3 ± 0.0	**Heat loss**	3.078 ± 0.015	21.0 ± 0.2
Total Input	14.840 ± 0.158	100.0	**Total Output**	13.472 ± 0.052	90.8 ± 0.5
			Mass loss	1.369 ± 0.107	9.0 ± 0.5

Elemental partitioning

The elemental balances have been carried out to evaluate the distribution of each element among the pyrolysis products. The results are depicted graphically in Figure 30.

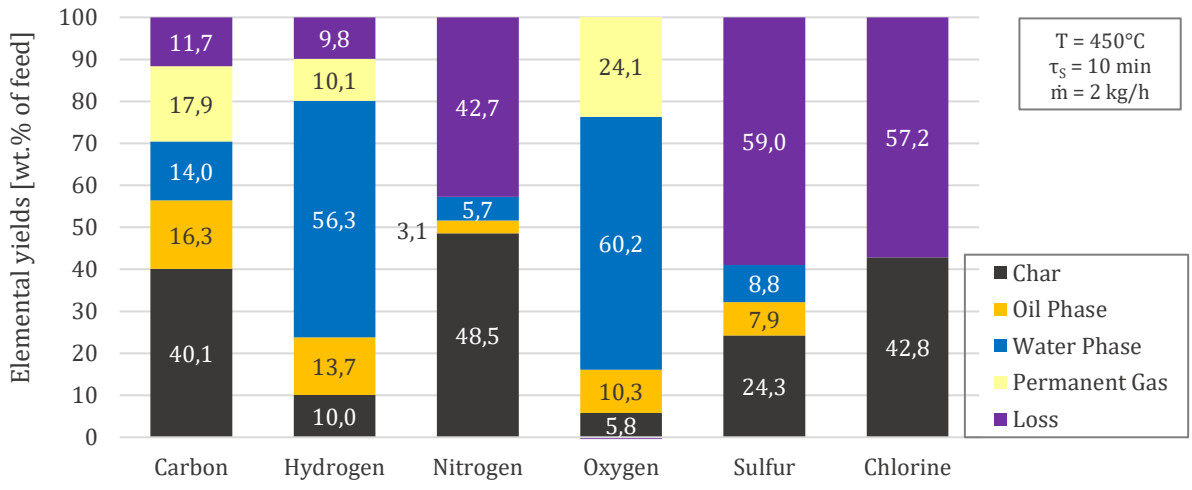

Figure 30. Elemental partitioning for the pyrolysis of beech wood at the STYX reactor, with a temperature of 450°C and a residence time of 10 minutes.

The carbon yield of the char is 40 wt.%, while the residual carbon content is equally distributed among the volatile products, i.e. the pyrolysis condensates and the permanent gas. Compared to fast pyrolysis, the yield of carbon in the pyrolysis oil is lower [84]. However, also the yield of oxygen is lower, which is beneficial in terms of oil stability [109, 73, 130]. About 12 wt.% of carbon was not found in the pyrolysis products. However, most of it could be assigned to the filter cake, whose composition consists of carbon for more than 90 wt.% (see composition and properties of the filter cake in the appendix). The hydrogen and oxygen balances present similarities in the distribution among the products. Most of these elements are concentrated in the aqueous condensate in form of water. Water is one of the main products from the pyrolysis of beech wood at the STYX reactor. Oxygen and hydrogen are readily removed from the solid matrix and only residues are still entrapped at 450°C.

The balances of nitrogen, sulfur and chlorine in Figure 30 show that only 40 wt.% to 60 wt.% of the elements were recovered in the pyrolysis products, mainly in the pyrolysis char. Nitrogen is partially fixed in the carbonaceous matrix (about 50 wt.%) and partially released to the vapor phase. However, only traces were recovered in the liquid products. Nitrogen containing compounds were not analyzed in the permanent gas. The high oxygen content of beech wood could lead to the direct production of NO_x precursors [230, 43]. The pyrolysis char obtained at 450°C retains 24 wt.% of sulfur and 42 wt.% of chlorine, while the majority of the two elements is released into the vapor phase. About 16 wt.% of sulfur was found in the pyrolysis condensate, equally distributed into the oil and the aqueous phases. Chlorine in the pyrolysis condensate led to results below the measurement limits. Therefore, only traces may be present in the liquid phase. Sulfur and chlorine were not measured in the permanent gas; however, the scientific literature reports the release of non-condensable sour gases during the pyrolysis of different biomass [180, 130]. Here, the missing sulfur and chlorine are expected to be in the permanent gas mainly as H_2S and HCl, respectively. Sour gases in moderate concentrations pose utilization issues in combustion engines (corrosion) and chemical reactors (poisoning); thus, one of the focus of the future experimental work should be related to the distribution of N-S-Cl among the pyrolysis products.

4.1.2 Local mass balances – sequential filtration and extraction

One of the main and most representative feature of the STYX reactor is the integrated hot gas filtration. This filter configuration enables the local balancing of the pyrolysis vapors, as described in section 3.3.1. The local balance for the pyrolysis of beech wood was carried out (see Table 10) and discussed in [208]. The focus of the study was to evaluate the distributions of the vapors along the reactor and to investigate the potential enrichment in one specific stream. The mass balance, which

includes N_2 in the vapors, and the N_2 balance for the reactor upstream the filtration is depicted graphically in Figure 31. The values are all expressed in g/h.

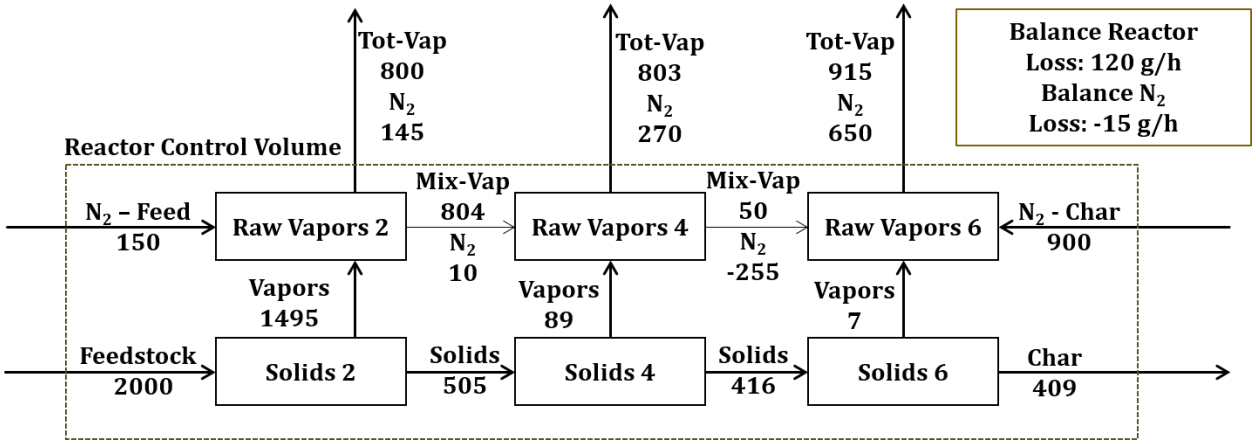

Figure 31. Local mass and nitrogen balances of the reactor before the filtration at the STYX reactor.

On the bottom of Figure 31, the mass flow rates of the solids at the three sampling positions are reported. Most of the pyrolysis vapors are released up to segment 2. Only very small amounts of vapors are released in the successive segments and have negligible effect on the mixing of the vapors. The mass flow of the char (409 g/h) was about 20 wt.% of the feedstock. From the inlet (N_2-Feed) and from the char recovery tank (N_2-Char), 2 liters per minute (150 g/h) and 12 liters per minute (900 g/h) of purge gas nitrogen are fed, respectively. At the first raw side outlet ("Raw Vapors 2" in Figure 31), 800 g/h of vapors including the purge gas, are recovered.

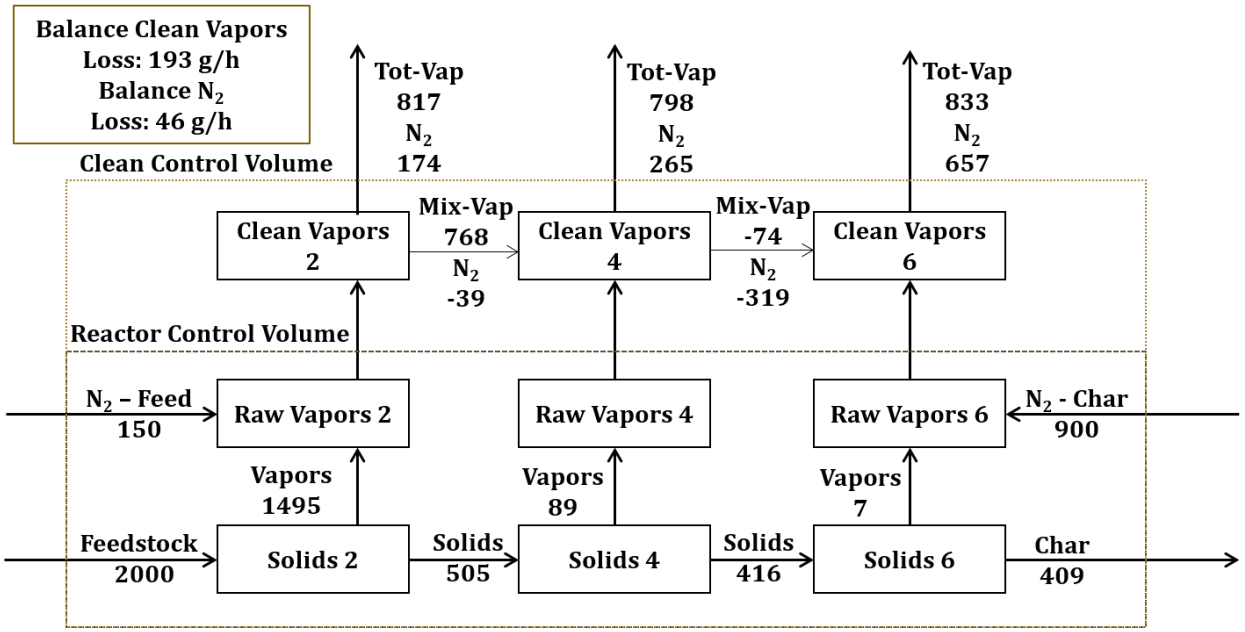

Figure 32. Local mass and nitrogen balances after filtration (clean side) for the pyrolysis of beech wood at the STYX reactor.

It corresponds to 50 wt.% of the vapors entering the segment 2 of the reactor (1495 g/h). The remaining 50 wt.% of the vapors, ie. the Mix-Vap stream between Raw Vapors 2 and Raw Vapors 4,

is forwarded to the next segment. Negligible amount of nitrogen is forwarded to the segment 4. At segment 4, most of the residual pyrolysis vapors are recovered. However, about 5 wt.% are further sent to segment 6. Overall, the mixing proceeds from segment 4 to segment 6. However, a large amount of nitrogen (255 g/h) from segment 6 goes to segment 4, indicating a high degree of mixing of the vapors between segment 4 and segment 6.

The local mass balances for the clean side of the filtration unit (Figure 32) presents similar results, i.e. a negligible mixing between segment 2 and segment 4 and an intensive mixing between segment 4 and 6.

4.1.3 Effect of the filtration

The displacement of the filters allows the investigation of the combined effect of the residence time of the vapors and of the filtration. In fact, it is possible to determine the residence time of the vapors by selecting the desired filter and closing the other ones. In order to evaluate the aforementioned effect, experiments were carried out at the reference pyrolysis temperature of 450°C. The residence time and a significantly lower mass flow rate of the solids were adjusted for the purpose (see Table 14).

The effect of the filtration was investigated comparing the mass balances as well as the CO/CO_2 molar ratios from segment 1 (S1 in Figure 20) and segment 6 (S6 in Figure 20), which corresponds to a short and a long residence time of the vapors, respectively. Online samplings were carried out both before (raw side) and after (clean side) the filters. To better evaluate the effect of the filtration, balances on the clean side were evaluated at different and increasing pressure drops to express different loads of the filters.

Table 14. Process conditions adopted using beech wood as reference feedstock for the evaluation of the effects of filtration.

Temperature of the reactor	450	°C
Geometric residence time of the solids	20	min
Mass flow of the solids	0.7	kg/h
Volumetric flow rate of the purge gas	3.5	$l_{N.}$/min

Figure 33 depicts the results of the mass balances obtained at the segment 1. It is shown that the yield of the condensate remains unaltered as long as the load of the filter cake does not reach high values, i.e. 67 mbar of pressure drop in case Clean 3. During a high filter load, the yield of the condensate is reduced by 3.5 wt.% of the feed. This variation is compensated by the increase of the yield of the permanent gas. The effect of the filtration is confirmed by the CO to CO_2 molar ratio, which increases by 25% from the raw side to the clean side with the highest filter load. An increase of the CO/CO_2

ratio indicates that the filter cake filtration favors the secondary gas phase reactions providing a large surface, which leads to an increase of CO at the expenses of the condensate [97].

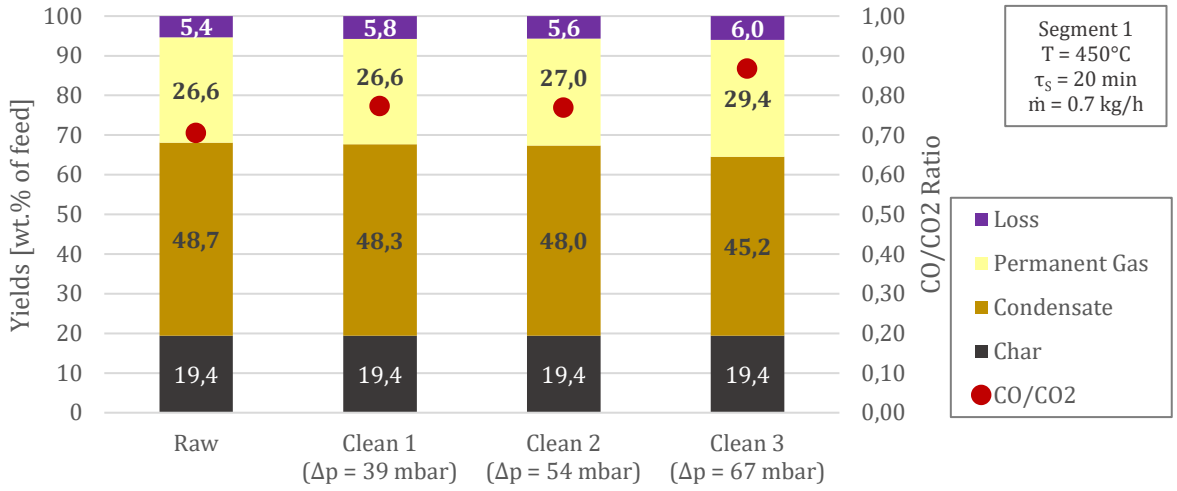

Figure 33. Mass balances and CO/CO_2 molar ratios at segment 1, before (Raw) and after (Clean) filtration with increasing pressure drop.

The results at segment 6 are depicted in Figure 34. The mass yields of the condensate and of the permanent gas remain unaltered from the raw side to the clean side, independently from the filter cake load. It has to be noted that the maximum load at segment 6 (45 mbar) did not reach the same level of segment 1 (67 mbar). That could indicate that the load of the filter might be non-uniform. However, the CO/CO_2 ratio is exactly the same obtained at high load at segment 1. Therefore, the secondary gas phase reactions proceeded under a similar regime, i.e. the filtration and secondary gas phase reactions have comparable effects.

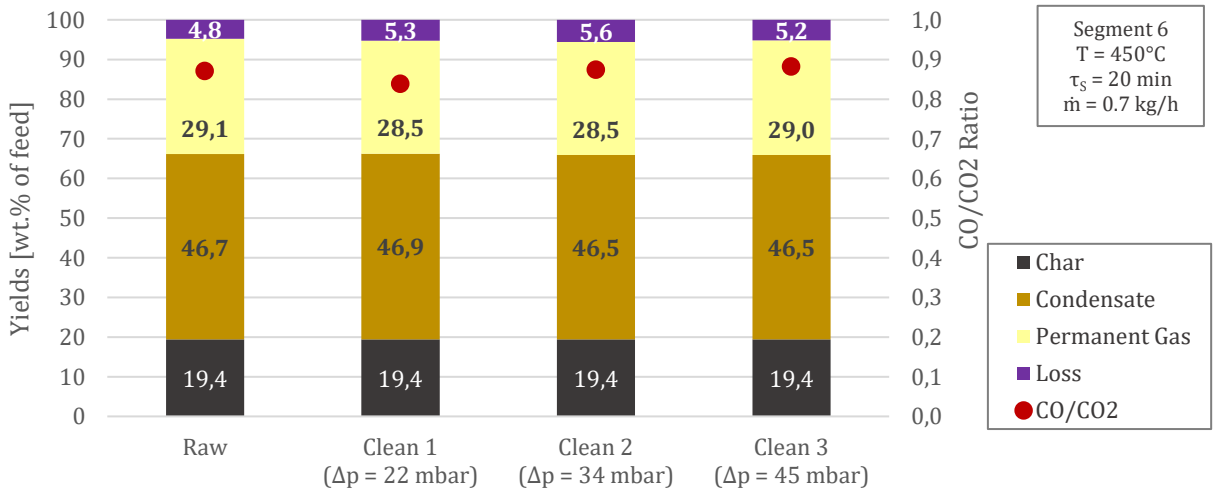

Figure 34. Mass balances and CO/CO2 molar ratios at segment 6, before (Raw) and after (Clean) filtration with increasing pressure drop.

The elemental analysis as well as the porosity of the filter cakes obtained at S1 and S6 are reported in Table 15.

Table 15. Elemental analysis of the filter cake in wt.%. Oxygen* calculated by difference. Porosity in %.

	Carbon	Hydrogen	Oxygen*	Porosity
Filter cake S1	87.2 (± 0.5)	2.45 (± 0.04)	10.4	38.0
Filter cake S6	81.1 (± 0.8)	2.33 (± 0.05)	16.7	59.2

The filter cake at S6 has a higher oxygen content and a significantly higher porosity compared to that obtained at S1, which explains the lower pressure drop.

The results underline the importance of the filters and of the filter cake. However, much more work is required to investigate the thermodynamics and the kinetics of the filtration. Additionally, the utilization of feedstock with high inert content could lead to the presence of catalytic particles on the surface of the filters, which may affect the yields and the properties of the condensates and of the permanent gas in a prominent manner.

4.1.4 Effect of the pyrolysis temperature

Yields distribution

The effect of the pyrolysis temperature on the yields distribution and properties was investigated experimentally at the STYX reactor adopting the process parameters reported in Table 16.

Table 16. Process parameters adopted in the experimental investigations using beech wood as reference feedstock

Temperature of the reactor	350-400-450-500	°C
Geometric residence time of the solids	10	min
Mass flow of the solids	2	kg/h
Volumetric flow of the purge gas (nitrogen)	10	l_N/min

The temperature is known for having the most important effect on the yields of the pyrolysis products [28]. While hemicellulose and cellulose decompose in a narrow range of temperatures, i.e. between 220°C and 350°C, lignin decomposes slowly in a wide range of temperatures, up to about 550°C.

The results of the mass balances are reported as yields of the feedstock and depicted graphically in Figure 35. The increase of the temperature leads to a decrease of the yield of the carbonized solid residue, i.e. the pyrolysis char. In fact, with increasing temperature, more volatile matter is released reducing the final yield of the solid. The yield at 500°C is higher than the sum of the fixed carbon and ash (15.8 wt.% of the feedstock on dry basis). Some volatile matter is still entrapped in the carbonized matrix. However, the results are in agreement with data from the literature. For instance, Ingram et al. obtained a yield of 17.5 wt.% to 19.9 wt.% at a pyrolysis temperature of 450°C, using

hardwood (oak) as feedstock [107]. Thangalazhy-Gopakumar obtained a yield of 20 wt.% at 500°C using pine, an important softwood [206].

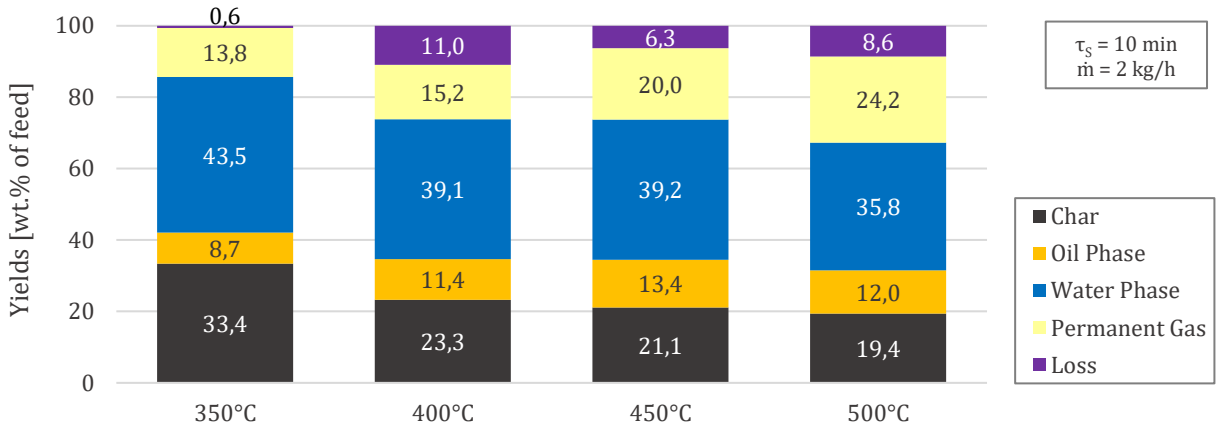

Figure 35. Yields distributions of the pyrolysis products at the STYX reactor for beech wood.

The yield of condensate, i.e. condensable organics and water, initially increased slightly to its maximum at 450°C. Due to the increasing effect of the gas phase reactions, the yield of the condensate decreased at 500°C. The overall yield of the water phase decreased with increasing temperature. The yield was in the range of 19 wt.% (±1.0 wt.%). Ingram et al. obtained a yield of reaction water of 22 wt.% at 450°C in their experiments with oak [107]. The yields of condensable organics present a maximum of 29.2 wt.% at 400°C, which remained almost constant at 450°C (28.7 wt.%).

The yield of the non-condensable gases presents an increasing trend with temperature. At higher temperatures, more gases are released from the solid, especially from the decomposition of lignin. It is known that the pyrolysis of lignin produces a higher solid residue than the cellulosic material coupled with the release of CO and CH_4 and other C_2 and C_3 hydrocarbons [38].

The closure of the balance was always above 89 wt.%. Since the reported experiments were carried out without the online recleaning of the filtration unit, some volatiles were deposited on the surface of the filters and not recovered. Moreover, some viscous oil may be accumulated in the condensation unit, in particular at the bottom of the third condenser. Inspections of the condensation unit as well as the closure of the carbon balance confirm this conclusion.

Carbon partitioning

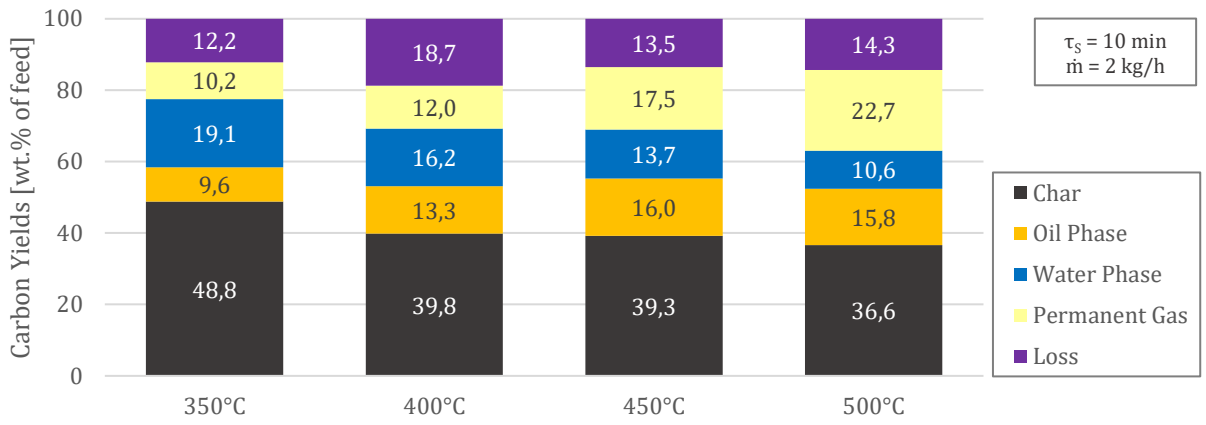

Figure 36. Carbon distribution among the pyrolysis products as function of the reactor temperature.

The carbon distribution (Figure 36) shifts increasingly from the char to the vapors with increasing temperature, reflecting the same trend shown by the distribution of the yields. In fact, increasing the offset temperature of the reactor leads to further decomposition of the biomass components. In particular, more lignin decomposes with increasing temperature. The major variation takes place between 350°C and 400°C, where the cellulose is completely decomposed. The decrease in the solid is slow at higher temperatures. In fact, lignin decomposes among a large range of temperatures. Even at 500°C, the char yield is about 37 wt.%. Some volatile matter is still unreacted and entrapped in the solid matrix. A complete decomposition of the biomass would lead to a carbon yield of 30 wt.%, which corresponds to the fraction of fixed carbon with respect to the total carbon content.

The carbon content of the condensable organics reaches a maximum between 400°C and 450°C, whereas the content of carbon is differently distributed between the bio-oil and the aqueous condensate. The highest yield of carbon in the bio-oil (oil-phase) is obtained at 450°C, mainly due to the lower solubility of the organics from water which is affected by the pH of the aqueous condensate (see also Table 22). The pH increases with increasing temperature, due to less polar compounds produced by secondary gas phase reactions influencing the distribution of the organic species between the two liquid phases. However, the mass yield of the bio-oil at 450°C is higher because of the higher contents of hydrogen and oxygen. Since the energy content of the bio-oil does not change between 450°C and 500°C due to the different carbon to hydrogen and carbon to oxygen ratios (see Table 19 in section 4.1.5), it is not straightforward to decide which pyrolysis temperature is the most suitable for the utilization of the bio-oil in fuel-related applications. For instance, if the bio-oil is to be upgraded to a defined quality through hydrodeoxygenation (HDO), the hydrogen consumption

together with economic considerations will define the optimum pyrolysis temperature. On the other hand, if the char is the most important product, lower temperatures appear to be more suitable since the carbon and the energy contents are maximized for this phase.

The aqueous condensate retains a considerably high content of carbon, with a maximum yield at 350°C. The carbon yield declines constantly with increasing temperature, since the organics lose oxygen and become less polar, which favors the separation of the bio-oil from the water-phase. Carbon in the aqueous condensate is in the form of acids, aldehydes and ketones. The main reported applications are focused on the production of hydrogen using the steam reforming route or fermentation for the production of biogas and biomethane [139, 106].

The carbon content of the permanent gases steadily increases with increasing temperature. The carbon is initially released in the organic vapors, which further react to non-condensable gases with increasing residence time and temperature. Carbon dioxide and monoxide are the main non-condensable gases. CO_2 is released both as primary product from the decomposition of the feedstock as well as a product of secondary gas phase reaction. CO, on the other hand, is a major product of the secondary cracking reactions. Besides carbon oxides, non-condensable hydrocarbons are produced during secondary gas phase reactions, such as CH_4, C_2 and C_3 compounds.

The non-condensable gases are considered a by-product of pyrolysis and they find the primary application in providing the required heat to the pyrolysis reactor.

The closure of the carbon balance was in the range of 85 to 90 wt.%. About 40 to 70 g of carbon per kilogram of beech were not recovered. The worst case was 400°C with 19 wt.% of not recovered carbon. Some carbon was measured in the non-condensable gases (FID) as hydrocarbons of at least C_{5+} but was not identified in the GC. A second source of carbon loss was the drum type volumetric flow meter. Inspections of the devices showed that the water inside the drum was heavily contaminated with organics. Sporadic measurements highlighted pH-value of 2 to 3, i.e. in the range of the aqueous condensate. Therefore, a small part of the carbon loss may be assigned to volatile organics, which are not removed by the electrostatic precipitator (ESP). Finally, as already discussed in section 4.1.1, the most important source of carbon loss was the filtration unit, which accounts for 30 wt.% to 90 wt.% of the carbon loss. The mechanisms involved in the filtration of the pyrolysis vapors still require detailed investigations.

Energy balance

The effect of the pyrolysis temperature on the energy balance was evaluated following the procedure described in section 3.3.4. The results of the balance are reported in terms of specific enthalpy for pyrolysis (Equation 24), CER_{LHV} (Equation 28) and CPE (Equation 29) in Table 17. The specific

enthalpy for pyrolysis increases from being exothermal (-0.75 MJ/kg) at 350°C to about 1.0 MJ/kg at 500°C. Pyrolysis at low temperatures is often called torrefaction or carbonization, which are considered to be an exothermal process [45]. However, external heat is still required to bring the solids to reaction temperature, where the exothermal char forming reactions will partially furnish the heat. Additionally, it has be noted that the standard deviation is large for the process at 350°C and could strongly influence the final results. The enthalpy for pyrolysis increases to 0.36 MJ/kg at 450°C, where most of the biomass is decomposed through the endothermal reaction of cellulose pyrolysis [217]. The final increase of the enthalpy of reaction is associated to the further increase of the temperature. Mei et al. [141] obtained similar values for the fast pyrolysis of pine sawdust in a fluidized bed reactor. Daugaard and Brown [55] provide the enthalpy for pyrolysis of different biomass. They found values in the range of 1.0 MJ/kg to 1.8 MJ/kg depending on the initial water content and on the biomass type. Generally, biomass with a higher ash content have lower reaction enthalpy.

Table 17. Specific enthalpy for pyrolysis and CPE of beech wood at STYX.

Pyrolysis Temperature [°C]	**Specific Enthalpy for Pyrolysis [kJ/kg]**	**CER_{LHV} [%]**	**CPE [%]**
350°C	-775 ± 805	85.3 ± 0.6	67.9 ± 0.5
400°C	167 ± 231	80.6 ± 1.8	61.8 ± 1.2
450°C	358 ± 38	80.9 ± 0.5	58.8 ± 0.2
500°C	1044 ± 220	81.1 ± 1.9	55.9 ± 0.3

The CER_{LHV} (Chemical Energy Recovery) and CPE (Cold Pyrolysis Efficiency) were evaluated for the four pyrolysis temperatures (see Table 17). The highest values are obtained at the lowest temperature. At higher temperatures, the CER_{LHV} does not show any relevant variation, indicating that the redistribution of the yields and of the energy contents among the volatile products does not offer any advantage in terms of total energy recovery. The distributions of the energy yields among the pyrolysis products at the investigated pyrolysis temperatures is depicted in Figure 37. On the other hand the CPE decreases with increasing pyrolysis temperature mainly due to increasing heat losses. The CPE at STYX is below the typical values of the CGE from gasification processes [211].

The energy yields present trends close to those shown for the elemental carbon in Figure 36, with a steadily decreasing trend for the pyrolysis char and a maximum at 450°C for the oil-phase. The energy yield of the permanent gas also increases with increasing pyrolysis temperature. The permanent gas must be necessarily converted on-site and it is the optimal choice for the task of generating the required heat for the pyrolysis process. However, the energy yield of the permanent gas alone is not sufficient to sustain the pyrolysis process and therefore an additional external heat source is always required.

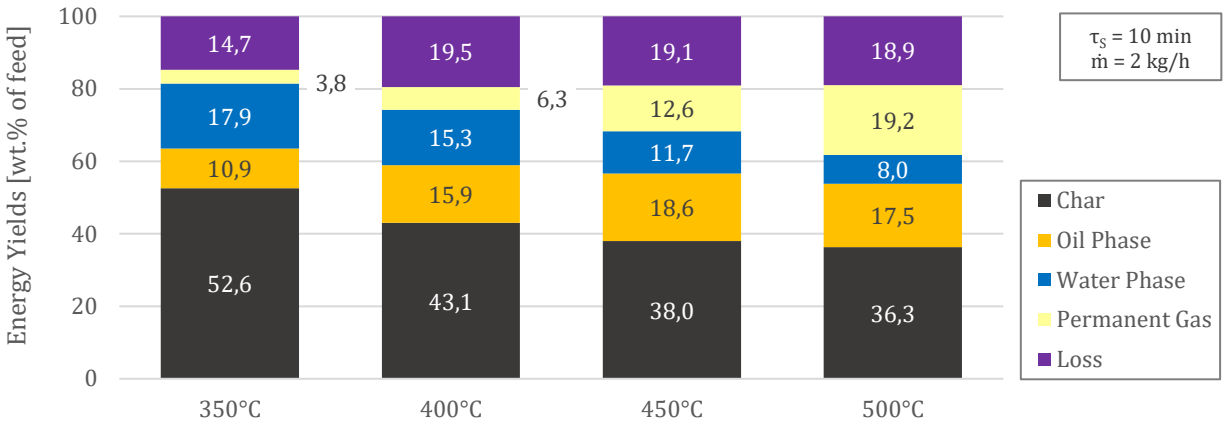

Figure 37. Energy yields distributions for the pyrolysis of beech wood at the STYX reactor.

4.1.5 Characterization of the pyrolysis products

The pyrolysis of beech wood in the STYX reactor produces four products in variable yield as function of the process parameters. In this section, the pyrolysis products from the experiments discussed in section 4.1.4 will be characterized and discussed into details.

Pyrolysis char

Qualitatively, the pyrolysis char is composed of the fixed carbon, the ash and the residual volatile matter after the pyrolysis process. The yield of the pyrolysis char always decreases with increasing temperature until the volatile matter is completely removed from the solid matrix. The higher the pyrolysis temperature, the lower is the entrapped volatile matter and the higher the carbonization degree. The proximate and the elemental analyses of the chars from the pyrolysis at the process parameters of Table 16 are reported in Table 18.

Table 18. Characterization of the pyrolysis chars from beech wood pyrolysis at the STYX reactor.

	Feedstock	**350°C**	**400°C**	**450°C**	**500°C**
Proximate analysis *(wt.% dry)*					
Volatile matter	84.2	32.7 ± 2.3	26.6 ± 0.1	20.0 ± 0.8	14.9± 0.2
Ash	1.1	3.4 ± 0.2	4.2 ±0.1	5.1 ± 0.1	5.4 ± 0.3
Fixed carbon	14.7	63.6 ± 2.3	69.3 ± 0.3	74.9± 0.8	79.7 ± 0.6
Elemental analysis *(wt.% dry)*					
Carbon (total)	49.1	72.9 ± 6.5	77.1 ± 0.1	80.5 ± 2.4	84.2 ± 0.2
Hydrogen	6.0	4.29 ± 0.49	3.85 ± 0.06	3.42 ± 0.13	3.04 ± 0.06
Nitrogen	0.1	0.24 ±0.01	0.23 ± 0.01	0.30 ± 0.01	0.31 ± 0.01
Oxygen	43.6	19.3 ± 7.6	14.6 ± 0.1	10.5 ± 2.5	6.9 ± 0.6
Sulfur	0.050	0.063 ± 0.011	0.046 ± 0.005	0.056 ± 0.002	0.040 ± 0.001
Chlorine (total)	0.017	n.b.	n.b.	0.003 ± 0.001	n.b.
Calorific properties *(dry)*					
HHV [MJ/kg]	19.7	26.9 ± 1.20	30.3 ± 0.00	30.6 ± 1.35	32.8 ± 0.05
LHV [MJ/kg]	18.4	26.1 ± 1.20	29.5 ± 0.05	29.9 ± 1.35	32.1 ± 0.05
Other properties					
BET Surface [m^2/g]	< 1.0	< 1.0	< 1.0	< 1.0	< 1.0

The increase of the pyrolysis temperature leads to a steady decrease of the volatile matter. The release of the volatile matter is accompanied by the reduction of the contents of hydrogen and oxygen. The degree of carbonization, which can be described by the ratio between the fixed carbon and the total carbon, increases from 0.87 at 350°C to 0.95 at 500°C. The ash, or mineral matter, is completely retained in the solid matrix and therefore the content increases with increasing temperature. The contents of nitrogen, sulfur and chlorine in beech wood is in traces and remain almost unaltered in the chars.

The removal of the volatile matter from the solid matrix leads to an increase of the calorific properties of the pyrolysis char with increasing temperature. Pyrolysis chars obtained at pyrolysis temperatures above 350°C can be classified as high bituminous coal of Grade C, whereas pyrolysis chars obtained at 500°C are of Grade A and have a calorific value comparable to that of anthracite [16].

The BET surface of the pyrolysis chars was measured to evaluate the potential utilization as substituent sorbent. For all the temperatures, the surface was always below the measurement limit of 1 m^2/g. From the SEM analysis in Figure 38, which depicts the side and the front of a char particle obtained at 450°C, it is clear that the macropores are obstructed by unreacted volatile matter, which reduces strongly the available surface. Similar results were reported in the literature [179]. Contrary to chars obtained in the fast pyrolysis of wood, the morphology of the particles remains unaltered. The shrinkage of the char particle is contained to few percent only.

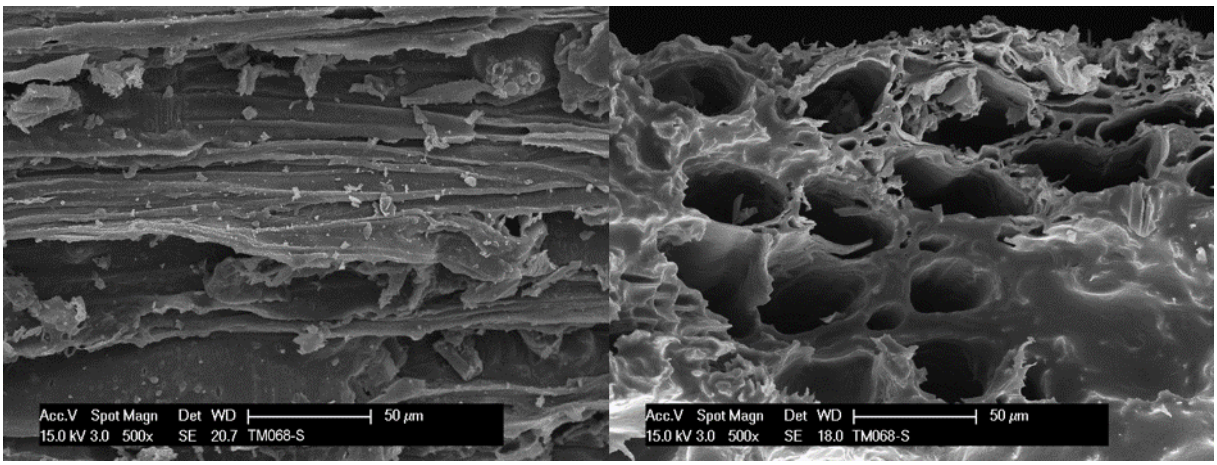

Figure 38. SEM Analysis of a pyrolysis char particle obtained at a reactor temperature of 450°C.

Pyrolysis oil

Pyrolysis of wood was extensively investigated with the main aim of producing a liquid intermediate, which could be used for energy recovery in oil furnaces or, after a secondary upgrading step, introduced in conventional refinery for the production of transportation fuels and of other more valuable chemicals [53].

The elemental compositions and the calorific properties of the pyrolysis oil are reported in Table 19. Moreover, Table 19 reports the molecular formulas, expressed as $C_6H_XO_Y$. The water content is excluded. This methods enables a direct comparison of the composition with that of the original feedstock ($C_6H_{8.8}O_4$) as well as with the composition of cellulose $(C_6H_{10}O_5)_n$. The carbon and hydrogen contents of the pyrolysis oils increase with increasing temperature, while the content of oxygen remains almost constant up to 450°C, then it slightly decreases at 500°C. The decrease of the oxygen content is strictly related to the secondary gas phase reactions, which produce mainly CO and CH_4. The effect is shown by the molecular formulas, where the hydrogen and the oxygen content decrease with increasing temperature of the reactor. Traces of nitrogen were measured, while sulfur and chlorine were below the determination limits since the original feedstock also contains only traces of the two elements.

Table 19. Characterization of the pyrolysis oils from beech wood pyrolysis at the STYX reactor.

	350°C	**400°C**	**450°C**	**500°C**
Proximate analysis *(wt.% as received)*				
Water	16.2 ± 0.5	13.5 ± 0.4	11.3± 0.5	12.6 ± 1.2
Ash	0.0 ± 0.0	0.0 ± 0.0	0.0 ± 0.0	0.0 ± 0.0
Fixed carbon (CCR)	3.7 ± 0.6	3.2 ± 0.6	7.2 ± 0.7	7.0 ± 0.7
Volatile matter*	80.1 ± 0.8	81.3 ± 0.4	81.5 ± 1.0	80.5 ± 1.6
Elemental analysis *(wt.% as received, water from proximate analysis)*				
Carbon	48.7 ± 0.4	51.2 ± 0.1	53.2 ± 0.9	56.5 ± 1.4
Hydrogen	5.6 ± 0.1	5.7 ± 0.0	5.7 ± 0.1	5.9 ± 0.1
Nitrogen	0.0 ± 0.0	0.1 ± 0.0	0.0 ± 0.0	0.2 ± 0.0
Oxygen*	29.5 ± 0.1	29.5 ± 0.4	29.8 ± 0.5	24.8 ± 0.2
Sulfur	0.0± 0.0	0.0 ± 0.0	0.0 ± 0.0	0.0 ± 0.0
Chlorine	0.0 ± 0.0	0.0 ± 0.0	0.0 ± 0.0	0.0 ± 0.0
Calorific properties *(dry)*				
HHV [MJ/kg]	21.1 ± 0.0	22.6 ± 0.1	22.6 ± 0.2	24.3 ± 0.2
LHV [MJ/kg]	19.5 ± 0.0	21.0 ± 0.1	21.6 ± 0.7	22.8 ± 0.2
Other properties				
Molecular formula	$C_6H_{8.3}O_{2.7}$	$C_6H_{8.0}O_{2.6}$	$C_6H_{7.7}O_{2.5}$	$C_6H_{7.5}O_{2.0}$
Molar mass [kg/kmol]	7.29	7.33	7.41	7.21
Density [kg/l]	1.155 ± 0.001	1.163 ± 0.003	1.179 ± 0.003	1.156 ± 0.001
Surface Tension [mN/m]	35.1 ± 0.1	35.5 ± 0.1	36.1 ± 0.1	35.6 ± 0.1
Viscosity@40°C [mPa s]	15.2	23.3	43.8	32.4

* calculated by difference

The ash content of the feedstock was about 1 wt.% (see Table 5) and normally remains entrapped in the carbonized matrix of the pyrolysis char. However, it may be transported in the vapor phase with fine particles. In comparison to the data obtained in the literature for pyrolysis of similar feedstock in a screw reactor, the content of ash in the pyrolysis oil is negligible, which confirms the superior performance of the hot gas filtration in comparison to the more classical configuration with high temperature cyclones. Water from the moisture and from dehydration reactions is one of the main products of wood pyrolysis. The liquid from condenser 1 separates into an aqueous and into an

organic phase. However, the organic phase still contains water due to the presence of polar species soluble in water. The water content decreases slightly with the increase of the pyrolysis temperature. However, small variations caused by the manual separation are to be taken into account. The water content has both positive and negative effects on the following processing of pyrolysis oil. On the one hand, the higher the water content, the lower the viscosity; on the other hand, water strongly impacts reducing its calorific properties. In fact, in Table 19 an increase of the calorific value (LHV) occurs with increasing pyrolysis temperature. Compared to other data reported in the literature for wood pyrolysis, the results present slightly higher values because of the lower oxygen and water contents [146]. However, the calorific properties are still considerably lower than those from conventional heavy oil (see Table 3).

The fixed carbon, which is the equivalent of the distillation residue in the Conradson Carbon Residue (CCR) method, was measured for the pyrolysis oils. It indicates the tendency of the oil to form deposits in combustion applications. The higher the CCR, the higher is the possibility to form deposits on the nozzle. The results obtained indicated a relatively low CCR in comparison to other studies. A maximum value of 7.2 wt.% was obtained at 450°C. The integrated filtration removes the fine particles and enhances the secondary reactions, which reduce the non-volatile carbon. Rheological characterization of the pyrolysis oils was carried out with a focus on the aging mechanisms. The results of the project are published in Jampolski et al. [109]. Both the density (1.179±0.003 kg/l) and the surface tension (36.1 mN/m) present a maximum value at a pyrolysis temperature of 450°C, as well as a similar trend with respect to the temperature. The dynamic viscosity was measured at different temperatures covering a range of shear rate between 10^{-1} and 10^{3} s^{-1}. The flow behavior of the pyrolysis oils was Newtonian for all shear rates and for all the pyrolysis temperature. For further details refer to [109].

Again, the oil obtained at 450°C presents the highest viscosity. Also the trend with respect to the temperature of pyrolysis corresponds to the ones obtained for the other physical properties. Interestingly there is no straight correlation between the chemical and the physical properties of the pyrolysis oils. A further confirmation is given by the Gel Permeation Chromatography (GPC), which was used to evaluate the molecular weight distribution of the pyrolysis oils (see Figure 39).

Four main peaks were obtained at molecular weights of 85-130-260-370 kg/kmol and a slight shoulder in the range of 900 kg/kmol. The maximum molecular weight was always below 2000 kg/kmol. The increase of the reactor temperature leads to a reduction of the peaks at low molecular weight and to an increase of the shoulder. Therefore, the average molecular weight increases with the increase of the reactor temperature (see also Table 19).

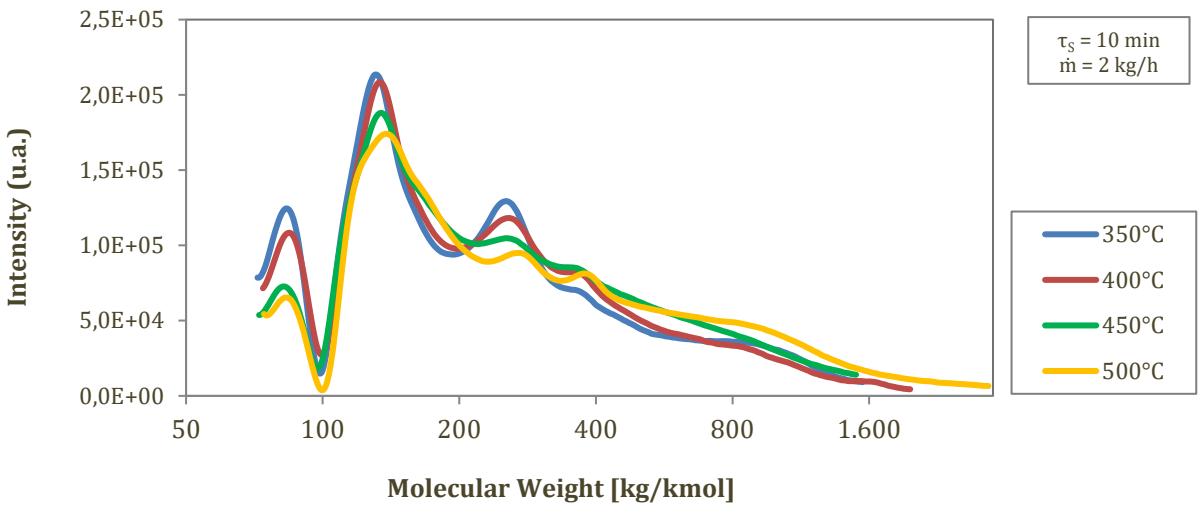

Figure 39. Molecular weight distributions of the pyrolysis oils from GPC analysis.

Solvent fractionation was carried out following the scheme described in Boscagli et al. [27]. The results are depicted graphically in Figure 40, while the fractionation is reported in Table 20.

The complete absence of solids in the oils highlights the importance of the high temperature filtration for the stabilization, i.e. reduced aging of the oil. See also [109] for aging details. Another characteristic of the pyrolysis oils is the low content of extractives, which depends essentially from the chemical composition of the feedstock (see Table 6). The largest class is represented by the low molecular weight lignin (WIS-DS), which also presents a slightly increasing trend with increasing temperature. On the other hand, high molecular weight lignin (WIS-DIS), was found in low concentrations compared to typical fast pyrolysis oils [161]. The lignin in fast pyrolysis oils is normally recovered as powder, whereas it always had the consistence of tar in pyrolysis oils from STYX. The second major class is represented by aldehydes, ketones and volatile acids (WS-DDS) with relatively unchanged content in the temperature range. The content of sugars and hydroxyacids (WS-DDIS) was much lower compared to fast pyrolysis oils.

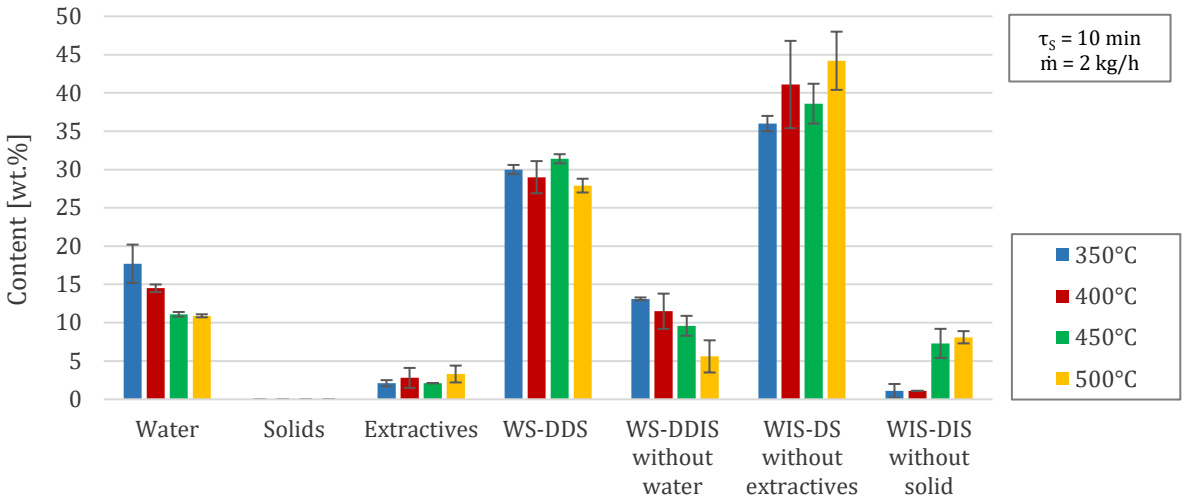

Figure 40. Solvent fractionation of pyrolysis oils.

Table 20. Fractions and contents after the solvent fractionation proposed in [27].

Fraction	**Content**
Water	water after Karl Fischer Titration
Solids	solids after methanol extraction
Extractives	extractives after n-hexane extraction
WIS-DIS *Water InSoluble & Dichloromethane InSoluble*	lignin with high molecular weight, aging products and solids
WIS-DS *Water InSoluble & Dichloromethane Soluble*	lignin with low molecular weight, aging products and extractives
WS-DDS *Water Soluble, Diethyl ether & Dichloromethane Soluble*	aldehydes, ketones, furans, lignin monomers and volatile acids
WS-DDIS *Water Soluble, Diethyl ether & Dichloromethane InSoluble*	water, sugars and hydroxyacids

Generally, the results are consistent with the reaction mechanism of wood pyrolysis. The release of the lignin-related compounds with large molecular weights mainly takes place at temperatures above 450°C. Such compounds are highly reactive and tend to decompose quickly to volatile acids and non-condensable gases with increasing temperature. Moreover, fragmentation reactions leading to WS-DDS are favored versus sugars by slower heating rates and extended residence times of the vapors at reaction temperature.

Hydrogen nuclear magnetic resonance spectroscopy (^{1}H-NMR) was also employed for a further characterization of the pyrolysis oils. With this techniques it is possible to evaluate the functionality of protons. The adopted procedure is reported in [27]. The integration range and the results of the ^{1}H-NMR analysis are reported in Table 21 and Figure 41, respectively.

The results of Figure 41 reports interesting and clear trends with respect to the pyrolysis temperature. At higher temperature the percentage of the aromatics (8.5-6.0 ppm) is increasing, supporting the

results of the solvent fractionation by the increase of the pyrolytic lignin and confirm the increase of the molecular weight with increasing temperature.

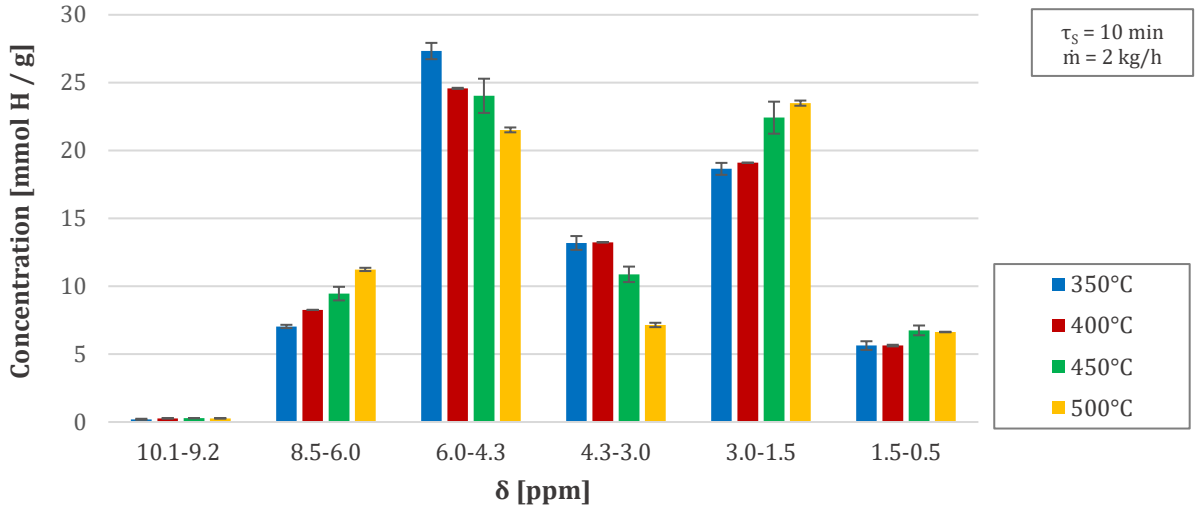

Figure 41. Results of the ^{1}H-NMR Analysis of the pyrolysis oils from beech wood.

Table 21. Analysis of the ^{1}H-NMR.

Integration range of ^{1}H-NMR spectra	**Proton assignment**
10.1-9.2 ppm	Aldehydes
8.5-6.0 ppm	(Hetero-)aromatic
6.0-4.3 ppm	Carbohydrates, water, O-H exchanging group
4.3-3.0 ppm	Alcohols, ethers, alkenes
3.0-1.5 ppm	α proton to carboxylic acid or keto-group, α proton to unsaturated groups
1.5-0.5 ppm	Alkanes

The alcohol/ether class (4.3-3.0 ppm) decreases with increasing temperature. This could be associated to the decrease of the class of sugars (6.0-4.3) and WS-DDS in Figure 40. Moreover, it could be the result of dehydration reactions, which lead to the formation of reaction water. Alpha protons to carboxyl/carbonyl/unsaturated group (3.0-1.5 ppm) are increasing with the temperature. The aliphatic fraction (1.5-0.5 ppm) shows only a negligible increase.

Finally, five selected liquid organic markers, as well as additional aromatics, were quantitatively analyzed by GC-MS. The results of the analysis are depicted in Figure 42. The most relevant organic species is acetic acid, which is present in constant concentration among the all range of pyrolysis temperatures. Acetic acid is considered to be an end product of secondary gas phase reactions from the pyrolysis of lignocellulosic feedstock. Moreover, it is the main responsible for the acid and corrosive behavior of the overall pyrolysis oil. Furfural and acetaldehyde are markers for the conversion of cellulose and hemicellulose. The first decreases steadily with increasing temperature

due to the reactive aldehyde group. On the other hand, acetaldehyde increases by a factor 2 with increasing pyrolysis temperature. It is considered to be the main product from the fragmentation reactions of cellulose. In the literature, it is reported that the increase of acetaldehyde is associated with the decrease of the sugars, which is confirmed by NMR analysis in Figure 41.

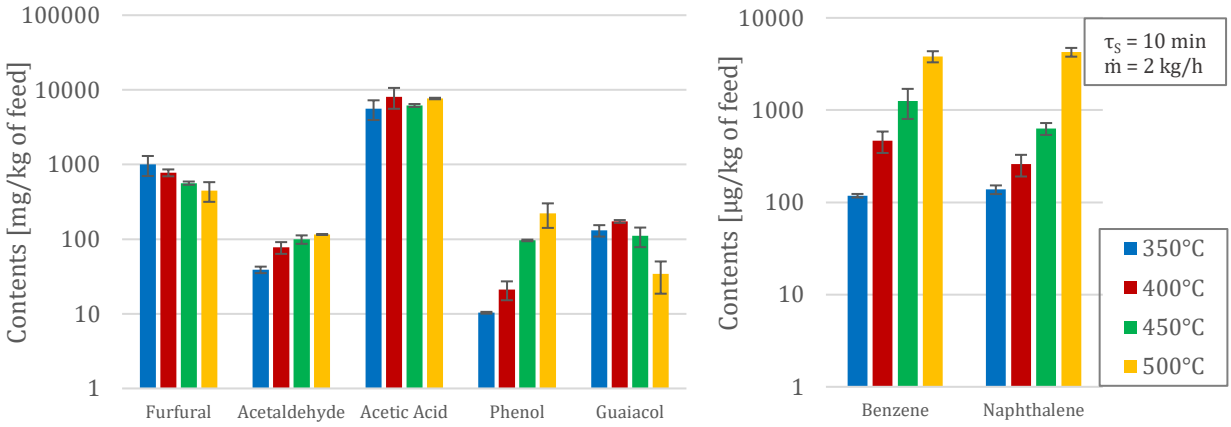

Figure 42. Contribution of the pyrolysis oil to the yields of selected liquid organic markers from the pyrolysis of beech wood.

Guaiacol and phenol are the most important primary and secondary products from the pyrolysis of lignin. They present inverse trends. The decrease of guaiacol is strictly related to the increase of phenol, which is the main product from the gas phase secondary reactions of lignin-derived species and thus of guaiacol.

To evaluate the further decomposition of the pyrolysis vapors, benzene and naphthalene were analyzed quantitatively. Although the contents of these aromatics are three orders of magnitude lower than those of the main markers, they present an increase by a factor 500 with increasing temperature. The results are in agreement with the NMR analysis of Figure 41 and evidence the effect of secondary gas phase reactions influencing the chemical composition of the pyrolysis oil with varying process conditions.

In conclusion, the analysis of the pyrolysis oil, i.e. of oil phase, highlights the prominent influence of the offset temperature of the reactor on its chemical and physical properties. In future work, specific analysis should be carried out depending on the foreseen application.

Aqueous condensate

The second liquid phase is the aqueous condensate, which is a mixture of water and water-soluble organic species. Water is released from the moisture content and produced during pyrolysis by dehydration reactions [191]. As discussed in section 3.2.7, the aqueous condensate is separated from the oil phase by decantation.

On as received basis, the water phase accounts for 35 wt.% to 40 wt.% of the feedstock. Pyrolysis vapors contain high oxygenated compounds, which further react releasing water. In fact, the water phase separates naturally from the organic phase after the condensation of the pyrolysis vapors. The characterization of the water phase was mainly carried out for balance purposes. The elemental compositions, as well as few other properties, of the aqueous condensates are reported in Table 22.

Table 22. Characterizaiton of the aqueous condensate from the pyrolysis of beech wood at the STYX reactor.

	350°C	**400°C**	**450°C**	**500°C**
Proximate analysis *(wt.% as received)*				
Water	59.7 ± 1.0	60.5 ± 3.1	65.9 ± 1.1	74.6 ± 0.9
Ash	0.177 ± 0.012	0.097 ± 0.012	0.000 ± 0.000	0.063 ± 0.010
Volatile matter	40.1 ± 1.0	39.5 ± 3.0	34.1 ± 1.1	25.3 ± 0.9
Elemental analysis *(wt.% dry)*				
Carbon	49.1 ± 2.1	45.6 ± 2.7	44.8 ± 2.0	50.7 ± 2.7
Hydrogen	6.2 ± 0.1	6.1 ± 0.3	6.3 ± 0.3	5.4 ± 0.2
Nitrogen	0.050 ± 0.000	0.050 ± 0.002	0.050 ± 0.001	0.050 ± 0.000
Oxygen	44.1 ± 2.1	48.0 ± 2.4	48.8 ± 1.7	43.6 ± 2.5
Sulfur	0.015 ± 0.007	-	0.020 ± 0.010	-
Chlorine	0.020 ± 0.010	-	0.020 ± 0.010	-
Calorific properties *(as received)*				
HHV [MJ/kg]	8.7 ± 0.0	8.5 ± 0.2	8.1 ± 0.2	7.4 ± 0.1
LHV [MJ/kg]	6.7 ± 0.0	6.1 ± 0.2	4.6 ± 0.2	3.6 ± 0.1
Other properties				
pH-value	2.4	2.5	2.8	3.1

With increasing pyrolysis temperature, the content of organics in the water phase decreases while the content of water increases from 60 wt.% at lower reactor temperatures, where the composition is relatively stable due to the minor relevance of the secondary gas phase reactions, to about 75 wt.% at 500°C. The secondary reactions decompose the high oxygenated species into gas and less oxygenated compounds. A decrease of the oxygen content is also correlated to the increase of the content of water. Since the polarity of the organics decreases, i.e. the pH-value increases, the separation of the water phase from the organic phase becomes more effective. A quantitative GC-MS analysis was carried out to determine the content of the main organic compounds. Acetic acid was the most relevant organic, yielding 7.7 wt.% of the aqueous condensate at 350°C and decreasing with increasing temperature of the reactor. Of the overall organic content, about 15% to 20% was made of acetic acid, whose content was at least an order of magnitude higher than those of the other compounds. The contents of the other measured species are reported in the Appendix (see Table 52).

Permanent gas

The permanent gas is a relatively complex mixture made of carbon monoxide and dioxide as well as of non-condensable hydrocarbons. The composition of the permanent gas from the pyrolysis of beech wood at the STYX reactor is reported in Figure 43. Carbon dioxide is mainly a product of the

decomposition of the biomass [169]. On a feedstock basis the yield of CO_2 increases with increasing temperature, but its concentration in the permanent gas reaches a maximum value at 400°C, then decreases constantly at higher temperatures. On the other hand CO and the hydrocarbons, such as CH_4 and compounds up to C_4, are products of the secondary gas phase reactions. In particular the so-called thermal tar cracking leads to the production of C_2 and C_3 alkanes and alkenes, i.e. C_2H_6 and C_2H_4 as well as C_3H_8 and C_3H_6 (see Figure 91 in the Appendix). Overall, the content of the hydrocarbons increases by a factor of 10 from 350°C to 500°C. Figure 43 reports the volumetric concentration of H_2 on the right axis. With increasing temperature, also the content of H_2 drastically increases from 400°C to 500°C from < 0.8 vol.% to about 7.5 vol.% of the permanent gas. The increase of the temperature of the reactor leads to an increase of the yield and of the energy content of the permanent gases. In comparison to the permanent gas from fast pyrolysis and to other pyrolysis processes without hot gas filtration, the yields of combustible gases and consequently the calorific content of the permanent gas obtained at the STYX reactor are higher due to the combined effects of longer residence times and hot gas filtration [88, 17, 141]. The LHV of the permanent gas increases by a factor 3, up to values comparable to biogas from anaerobic digestion [68], which makes the permanent gas suitable for the direct utilization in micro gas turbines and gas motors for heat and power generation.

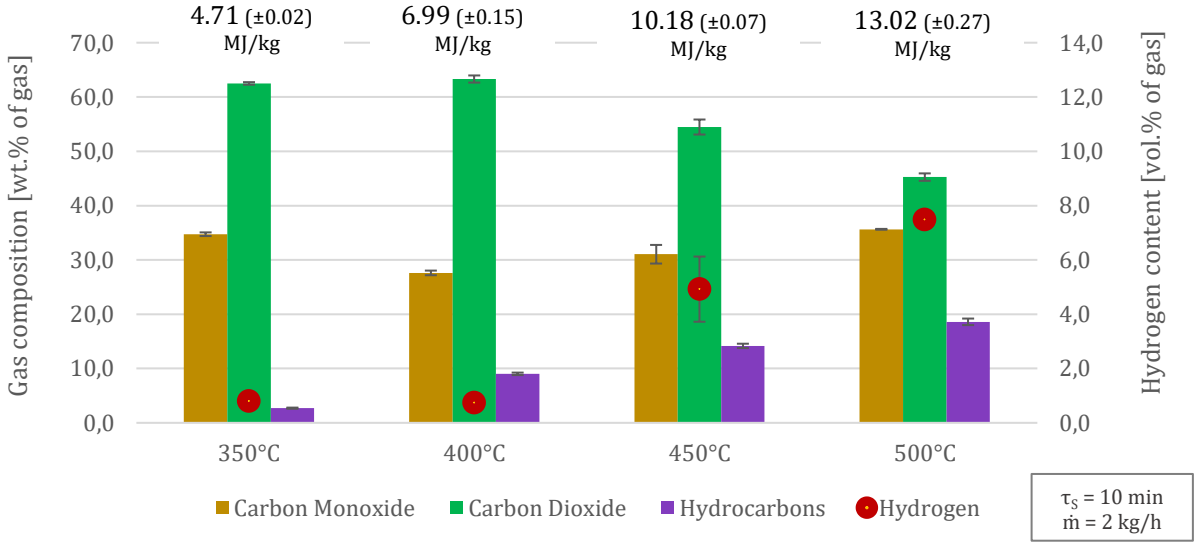

Figure 43. Composition of the permanent gas on N_2-free and dry basis for the pyrolysis of beech wood at the STYX reactor.

4.2 Pyrolysis of low-grade biogenic feedstock at STYX

This section aims at evaluating the pyrolysis process at the STYX reactor using low grade biogenic residues from different origin, which are characterized by inhomogeneous composition, considerably high contents of nitrogen, sulfur and chlorine as well as by high minerals and metals contents (see

also Figure 14 and Table 5 for detailed analysis). The feedstock is compared by means of mass, elements and energy yields distributions as well as in terms of pyrolysis products properties.

4.2.1 Mass balance and elemental partitioning

The mass balance was carried out for the low-grade biogenic feedstock at the reference process conditions (see Table 23) in order to investigate the yields distribution of the pyrolysis products in comparison to beech wood. The mass flow rates were adjusted for each feedstock with the aim of obtaining similar residence times of the vapors. The results are depicted graphically in Figure 44.

Table 23. Selected process parameters adopted for the pyrolysis of low-grade biogenic feedstock.

Feedstock	Temperature	Residence time solids	Mass flow feedstock
Beech wood	450°C	10 min	2 kg/h
Wheat straw	450°C	10 min	3 kg/h
Chicken manure	450°C	10 min	4 kg/h
Sewage sludge	450°C	10 min	4 kg/h

Figure 44. Yields distribution for the pyrolysis of low-grade biogenic feedstock with a pyrolysis temperature of 450°C and a residence time of the solids of 10 minutes.

As expected, the yield of the pyrolysis solids increases with increasing mineral content of the feedstock because the ash remains quantitatively in the char. An inverse trend is reported for the permanent gas, which is reduced for feedstock with high ash contents as chicken manure and sewage sludge. On the other hand, the yields of the oil phase are all very similar, where the lowest one is obtained using wheat straw. Identical values are obtained for chicken manure and sewage sludge. Their low content of fixed carbon in comparison to the lignocellulosic feedstock and the higher content of volatile carbon causes the relatively high oil yields (see Table 5). Moreover, the water phase is also reduced with increasing ash content. This fact is strongly correlated to the oxygen

content of the feedstock. The deficit in oxygen in the vapors from non-lignocellulosic biomass slows the secondary cracking reactions. Less vapors will be converted into non-condensable gases, and particularly less carbon monoxide and dioxide as well as reaction water will be produced. Moreover, the high content of heteroatoms, such as nitrogen, leads to the formation of an ammonia solution and heteroaromatic compounds in the oil phase. The elemental balances for the pyrolysis of low-grade feedstock at the STYX reactor with an offset reactor temperature of 450°C are reported in Table 24. The distributions of the elements among the pyrolysis products are similar for all the adopted feedstock. However, the carbon yield of the char increases with the increase of ash content in the feedstock. A similar trend is also given for the carbon yield of the oil phase. Whereas the pyrolysis oil from beech wood retains only 16.3 wt.%, those from chicken manure and sewage sludge retain 21.9 wt.% and 30.7 wt.%, respectively. The trend is strongly correlated with the oxygen content of the feedstock. The lower the oxygen content, the lower the secondary gas phase reactions. The yield of the permanent gas increases through CO formation at the expense of the yields of the pyrolysis oil. About 50 wt.% of the elemental hydrogen is recovered in the aqueous condensate as water, with a decreasing trend for an increasing ash content. The oxygen is also mainly present in the water phase as water. However, there is no systematic trend with respect to the original feedstock. About 10 wt.% of the oxygen is present in the oil phase and less than 6 wt.% in the pyrolysis char. The residual oxygen is mainly present in the permanent gas as CO and CO_2.

The distribution of nitrogen among the pyrolysis products for the different feedstock shows similarities with respect to the retention in the char. Beech wood, wheat straw and sewage sludge retain 48.5 wt.%, 47.2 wt.% and 43.6 wt.%. On the other hand chicken manure char contains only 34.4 wt.% of the total nitrogen. It is known from literature that proteins and amino acids are promptly decomposed into amides and NO_x precursors [151]. As a consequence, about 50 wt.% of the nitrogen from the pyrolysis of chicken manure is recovered in the liquid products. Similar results are also obtained for sewage sludge and slightly lower for wheat straw. That is not the case for beech wood, where less of 60 wt.% of nitrogen was recovered. The content of nitrogen in beech wood is in traces, which hinders the quality of the overall balance. The residual nitrogen, for all the feedstock is expected to be present in the permanent gas, as NH_3, HCN (hydrogen cyanide), HCNO (isocyanic acid) or other NO_x precursors. The fate of nitrogen during pyrolysis needs to be addressed in future works, both experimentally as well as from a modelling point of view also with respect to emission reduction [43]. The sulfur distribution among the pyrolysis products present close results for wheat straw, chicken manure and sewage sludge. About 60 wt.% to 70 wt.% was recovered in the solids and liquid products, with 45 wt.% in the char and the rest equally distributed among the condensates. The missing sulfur is expected to be in the permanent gas, probably as H_2S (hydrogen sulfide). In this

work, sulfur was not measured in the permanent gas, but literature related to the pyrolysis of sewage sludge confirms the assumption [130].

Table 24. Elemental balances (in wt.% of the feedstock on as received basis) from low-grade biogenic feedstock obtained at the STYX reactor with an offset temperature of 450°C and a residence time of the solids of 10 minutes.

	Beech wood	Wheat straw	Chicken manure	Sewage sludge
Carbon partitioning *(in wt.% as received)*				
Char	39.3	44.5	43.4	48.6
Oil phase	16.0	16.0	21.9	30.7
Water phase	13.7	9.1	8.5	6.6
Permanent gas	17.5	16.2	12.6	8.5
Loss	13.5	14.2	13.6	5.6
Hydrogen partitioning *(in wt.% as received)*				
Char	10.0	15.4	14.4	18.7
Oil phase	13.7	15.6	20.4	24.5
Water phase	56.3	51.0	47.2	43.9
Permanent gas	10.1	8.9	4.5	5.7
Loss	9.8	9.1	13.5	7.2
Oxygen partitioning *(in wt.% as received)*				
Char	5.8	5.9	5.1	2.5
Oil phase	10.3	10.7	9.4	9.7
Water phase	60.2	56.6	66.9	67.8
Permanent gas	24.1	24.4	29.9	15.7
Loss	-0.4	2.4	-11.3	4.3
Nitrogen partitioning *(in wt.% as received)*				
Char	48.5	47.2	34.4	43.6
Oil phase	3.1	19.0	17.9	22.3
Water phase	5.7	13.0	31.3	23.7
Permanent gas	nb	nb	nb	nb
Loss	42.7	20.7	16.4	10.5
Sulfur partitioning *(in wt.% as received)*				
Char	24.3	46.5	44.9	43.5
Oil phase	7.9	10.1	13.4	13.6
Water phase	8.8	9.1	11.6	6.7
Permanent gas	nb	nb	nb	nb
Loss	59.0	34.3	30.1	36.2
Chlorine partitioning *(in wt.% as received)*				
Char	42.8	46.2	66.8	71.3
Oil phase	nb	2.0	1.0	1.2
Water phase	nb	3.1	2.1	2.6
Permanent gas	nb	nb	nb	nb
Loss	57.2	48.8	30.1	24.9

Finally, the distribution of chlorine is also of relevance for emissions control and potential corrosion. Taking into account that the content of chlorine in beech wood is in traces, the experimental results show an increasing retention of chlorine in the char with increasing total content in the original feedstock. While the char from beech wood retains 43 wt.% of chlorine, more than 70 wt.% is recovered in the char from sewage sludge due to the high calcium and magnesium contents, which form chlorides. Very low amounts of chlorine were found in the condensates; however, it is an indication that not only HCl (hydrogen chloride) but also methyl-chloride (CH_3Cl) is released during the pyrolysis of low-grade biogenic feedstock [180].

4.2.2 Energy balance

The energy balance for the pyrolysis of low-grade biogenic feedstock was carried out for a pyrolysis temperature of 450°C and a residence time of 10 minutes. The energy yields distributions among the products is depicted in Figure 45.

Figure 45. Energy yields of the pyrolysis products from the pyrolysis of low-grade biogenic feedstock at the STYX reactor.

The energy yields of the chars ranged between 38.0% for beech wood and 47.0% for wheat straw. For lignocellulosic feedstock an increase of the ash content leads to an increase of the carbon content due to charring reactions. The energy yield of the char increases as a direct consequence. For high ash contents, the increase of ash content in the solids affects negatively the energy yield although more carbon is retained. Moreover, the energy yields of the oil phase increases and the yields of the water phase and of the permanent gas decrease with an increasing ash content of the original feedstock. The result has to be related to the oxygen content of the feedstock. The oil phase from beech wood is composed by highly oxygenated compounds, which reduce the calorific properties in comparison to hydrocarbon-like oils from chicken manure and sewage sludge. A further consequence of the oxygen content is the reduction of the yields of the water phase, both in terms of mass and of energy. Less water leads to less dissolved organics in the water phase and thus to a higher recovery of energy in the pyrolysis oil. From an engineering point of view, the production of pyrolysis oil for heat and power generation from low-grade biogenic feedstock should be preferred to that from high quality wood. However, considerations related to the economic feasibility of more severe emissions control equipment should not be neglected.

Adopting the methodology discussed in chapter 3.3.4 and used in chapter 4.1.4 for beech wood, the specific enthalpy for pyrolysis, the CER_{LHV} and the CPE were derived and reported in Table 25. The external heat required for pyrolysis increases from 0.36 MJ/kg for beech wood to 0.9 MJ/kg for wheat

straw. The variation of the specific heat for pyrolysis has at least two explanations, which are related to the content of oxygen and to the content and physical properties of the ash.

Table 25. Enthalpy for pyrolysis and CPE for the pyrolysis of low-grade biogenic feedstock at the STYX reactor with a pyrolysis temperature of 450°C and a residence time of 10 minutes.

	Specific Enthalpy for pyrolysis [kJ/kg]	CER_{LHV} [%]	CPE [%]
Beech wood	358	81.1	58.9
Wheat straw	870	82.8	63.4
Chicken manure	780	77.7	72.3
Sewage sludge	687	88.7	66.6

On the one hand, less oxygen is present in low grade biogenic feedstock, which is expected to reduce the reactivity. Secondly, the minerals in low grade biogenic feedstock, even considering the eventual catalytic effect, do not contribute substantially to the conversion of the feedstock into its products. A dedicated work on the specific enthalpy for pyrolysis, as well as on the reactions enthalpy, is mandatory to clarify the single contributions to these results. However, Table 25 highlights that the energy yield of the permanent gas is not sufficient for the sustainment of the pyrolysis process independently from the feedstock. The complete utilization of the pyrolysis vapors or another external source is always required.

4.2.3 Characterization of the pyrolysis products

The pyrolysis products obtained at a pyrolysis temperature of 450°C have been characterized adopting the methodologies described in chapter 3.4.2. The bio-oil and the aqueous condensate were characterized by means of elemental analysis, heating values as well as GC-MS. Moreover, the pyrolysis oils were characterized in terms of physical properties. The pyrolysis chars were analyzed for elemental and proximate compositions, ash and metal contents and heating values. The permanent gases by means of composition and heating value.

Pyrolysis char

The pyrolysis chars obtained from the pyrolysis of low-grade feedstock at the STYX reactor with a pyrolysis temperature of 450°C and a residence time of 10 minutes were analyzed with respect to their fuel properties (Table 26). From the proximate analysis it is shown that the ash remains quantitatively (> 95 wt.%) in the solid matrix. Therefore, the composition of the ash from the pyrolysis char is almost identical to that of the respective feedstock. The volatile matter is reduced to values of 19 wt.% to 28 wt.% for wheat straw and chicken manure, respectively. The higher residual volatile matter of chicken manure is given by the unreacted carbonates which is also the cause of the

lower carbonization degree of chicken manure and sewage sludge in comparison to the lignocellulosic feedstock.

Table 26. Characterization of the pyrolysis chars from low-grade biogenic feedstock obtained at the STYX reactor.

		Beech wood	Wheat straw	Chicken manure	Sewage sludge
Proximate analysis *(wt.% as received basis)*					
Moisture		2.0	0.8	0.1	< 0.1
Ash		5.1	22.8	49.3	68.6
Volatile matter		20.0	19.0	28.8	22.4
Fixed carbon		74.9	58.2	21.9	9.0
Elemental analysis *(wt.% dry)*					
Carbon (total)		80.5	63.7	39.4	24.1
Hydrogen		3.42	3.28	2.00	1.70
Nitrogen		0.30	1.28	4.49	3.45
Oxygen*		10.5	8.4	3.8	1.1
Sulfur		0.056	0.21	0.44	0.85
Halogens *(mg/kg dry)*					
Chlorine (total)		297	3380	5140	1710
Fluorine		< 50	< 50	< 50	266
Calorific properties *(dry)*					
HHV [MJ/kg]		30.9	25.8	14.5	9.3
LHV [MJ/kg]		30.2	25.1	14.1	9.0
Minerals in ash *(mg/kg dry feed)*					
Silicon	Si	370	55540	20475	96360
Aluminum	Al	1170	845	3915	39950
Calcium	Ca	10010	16775	121140	64190
Magnesium	Mg	2220	2750	13675	8270
Phosphorus	P	430	2985	27985	47025
Sodium	Na	2005	170	5490	2035
Potassium	K	5300	26490	45410	7970
Sulfur	S	490	1550	4735	8230
Metals in ash *(mg/kg dry feed)*					
Antimony	Sb	< 1	< 1	< 1	10
Arsenic	As	< 0.8	< 0.8	< 0.8	6
Lead	Pb	5	< 2	4	86
Cadmium	Cd	< 0.2	< 0.2	< 0.2	2.1
Chromium	Cr	96	15	4	340
Cobalt	Co	< 1	< 1	2	14
Copper	Cu	6	4	140	610
Iron	Fe	-	-	2910	69900
Manganese	Mn	470	74	960	1250
Nickel	Ni	53	8	17	180
Mercury	Hg	< 0.07	< 0.07	< 0.07	< 0.07
Thallium	Tl	< 0.2	< 0.2	< 0.2	0.3
Tin	Sn	< 3	< 3	< 3	39
Vanadium	V	2	< 1	9	53
Zinc	Zn	-	-	-	2080

* calculated by difference

The calorific values of the chars from lignocellulosic biomass are doubled compared to the original feedstock (Table 5 in chapter 3.1.1). However, the high chlorine content of wheat straw poses an issue for the utilization of the pyrolysis char as solid fuels in combustion furnaces. Corrosion and slagging given by the condensation of potassium chloride (KCl) on the heat exchangers are of major concern

and could ultimately compromise the plant operation [152, 155]. On the other hand, the pyrolysis char from chicken manure and sewage sludge present similar or worse calorific properties with respect to the original materials due to the high ash content. Nevertheless, the pyrolysis chars from chicken manure and sewage sludge appear promising in non-energy fields due to the high contents of nutrients, in particular of phosphorus [52, 86, 112].

Pyrolysis Oil

Pyrolysis oils from the four different feedstock obtained at a pyrolysis temperature of 450°C were analyzed by means of proximate and elemental composition, calorific properties and selected physical properties. The results are reported on as received basis in Table 27.

Table 27. Characterization of the pyrolysis oils from low grade biogenic feedstock obtained at the STYX reactor.

	Beech Wood	**Wheat Straw**	**Chicken Manure**	**Sewage Sludge**
Proximate analysis *(wt.% as received)*				
Water	11.3	19.1	15.3	13.2
Ash	< 0.05	< 0.05	< 0.05	< 0.05
Fixed carbon	6.7	7.2	4.8	1.3
Volatile matter	82.0	73.7	79.9	85.5
Elemental analysis *(wt.% dry)*				
Carbon	60.0	65.5	72.5	73.8
Hydrogen	6.4	7.1	8.4	9.1
Nitrogen	0.025	1.470	8.490	8.550
Oxygen	33.6	25.8	10.2	7.2
Sulfur	0.030	0.130	0.480	1.290
Chlorine	0.000	0.041	0.029	0.014
Calorific properties *(dry)*				
HHV [kJ/kg]	23.8	23.9	29.8	31.3
LHV [kJ/kg]	22.3	22.2	27.9	29.3
Other properties *(as received)*				
Density [kg/l]	1.179 ± 0.003	1.108 ± 0.003	1.044 ± 0.006	0.998 ± 0.001
Surface tension [N/m]	36.1 ± 0.1	25.7 ± 0.8	32.4 ± 0.1	28.4 ± 0.1
Viscosity [mPa s @ 40°C]	44	Non-Newtonian	161	40

The pyrolysis oils obtained from low-grade biogenic feedstock present important differences in comparison to those from lignocellulosic materials. The separation of the bio-oils was extremely simple for sewage sludge, more difficult for chicken manure, while for wheat straw it was long and complex. During decantation of the pyrolysis oil from wheat straw, two organic phases were formed, with different densities. The water phase was found between the organic phases. After decantation, the two organic phases were mixed without showing separation tendencies. The increasing complexity of the separation is highlighted by the final water content, which is higher by a factor 2 for oil from wheat straw. Bio-oils from chicken manure and sewage sludge are characterized by a higher degree of deoxygenation compared to lignocellulosic materials. An oxygen content below 15 wt.% is required in order to avoid preliminary treatments of deoxygenation before being dropped in

refineries' streams [85]. On the other hand, bio-oils from beech wood and wheat straw have contents of 34 wt.% and 26 wt.% on dry basis. That implies a pretreatment with the consequent increase of the production costs. The degree of deoxygenation can be well correlated with the mineral content of the feedstock. The minerals in the solid matrix of the feedstock act like a catalyst favoring the reactions of decarboxylation at the expenses of decarbonylation, i.e. the release of CO_2 versus that of CO, for a more efficient deoxygenation of the pyrolysis oil. The carbon and hydrogen contents were higher for chicken manure and sewage sludge. On the other hand, also the contents of nitrogen and of sulfur were high. Nitrogen was in the range of 8.5 wt.%, while sulfur was higher (> 1.0 wt.%) for sewage sludge. That is a cause of concerns related to the utilization of such bio-oils for heat and power production, since an extensive gas-treatment unit will be required to avoid NO_X and SO_2 emissions. In the case such bio-oils are used as drop-in fuels in refineries, hydrodenitrogenation and hydrodesulfurization will be required. The content of sulfur in the bio-oil from wheat straw is also of concern, if hydrodeoxygenation is the expected downstream treatment for upgrading to drop-in fuel. In fact, the catalysts for hydrodeoxygenation are readily poisoned by sulfur [150]. The calorific values of the bio-oils reflects the composition and specifically the degree of deoxygenation and water content. The bio-oil from sewage sludge exhibits the highest LHV (29.3 MJ/kg), while that from wheat straw was 22.2 MJ/kg, close to that from beech wood. Generally speaking, the bio-oils obtained at STYX have a higher degree of deoxygenation compared to those obtained in fast pyrolysis processes, reflecting the longer residence time of the vapors at the temperature of the reactor as well as the effect of the high temperature filtration. Moreover, the fixed carbon is low, i.e. 7.2 wt.% for wheat straw and only 1.3 wt.% for sewage sludge, which diminishes the complications caused by the carbonization and plugging of nozzles during the application of the bio-oils as fuels in motors [123]. Some relevant physical properties of the bio-oils are also reported in Table 27. The bio-oils showed a decreasing density with increasing ash content in the origin biomass due to the lower content of oxygen atoms. Whereas the bio-oil from beech wood had a density of 1.18 kg/l, that of the bio-oil from sewage sludge was 0.998 kg/l. The bio-oil from sewage also presented the lowest surface tension and the lowest viscosity. On the other hand, chicken manure had a viscosity higher by a factor 4 compared to the other oils. Only the bio-oil from wheat straw presented a non-Newtonian behavior. As discussed by Jampolski et al. [109], the behavior may be caused by the high content of lignin-derived species, which melt at about 50°C forming a sample-spanning network of small crystals. At temperatures higher than 50°C, the pyrolysis oil from wheat straw presents a Newtonian flow behavior.

In conclusion, pyrolysis oil from a low-grade biogenic feedstock is a challenging intermediate product. Its valorization is of fundamental relevance for the economics of the pyrolysis process.

However, a series of upgrading steps to suitable fuel quality is required hindering till nowadays its sustainable utilization.

Aqueous Condensate

The aqueous condensate is the other liquid intermediate from the pyrolysis of low-grade biogenic feedstock. During the years, it has always been considered a by-product. Investigations and analysis focuses on the bio-oil, while the aqueous condensate was overseen even if it yields about 75 wt.% of the whole liquid. Few research aimed at using the aqueous condensate in reforming processes to obtain syngas [139, 163, 163, 12]. The obtained hydrogen could be used for hydrodeoxygenation of the pyrolysis oil [165]. The aqueous condensates obtained at the STYX reactor were characterized by means of elemental analysis, water content, calorific value and pH value. The results are reported in Table 28.

Table 28. Characterization of the aqueous condensates from the pyrolysis of low grade biogenic feedstock obtained at the STYX reactor.

	Beech Wood	**Wheat Straw**	**Chicken Manure**	**Sewage Sludge**
Proximate analysis *(wt.% as received)*				
Water	67.1	77.0	66.2	78.7
Ash	< 0.05	0.1	< 0.05	< 0.05
Volatile matter	32.9	22.9	33.8	21.3
Elemental analysis *(wt.% dry)*				
Carbon	44.7	50.9	32.9	39.2
Hydrogen	6.3	6.0	6.0	6.4
Nitrogen	0.05	1.4	17.3	22.5
Oxygen	48.9	41.2	43.3	30.4
Sulfur	0.03	0.16	0.48	1.57
Chlorine	0.000	0.088	0.068	0.074
Calorific properties *(as received)*				
HHV [MJ/kg]	6.5	5.3	3.5	4.7
LHV [MJ/kg]	4.4	3.1	1.5	2.5
Other properties				
pH-Value	2.4	3.1	8.9	9.1

The water content was in the range of 66 wt.% to 79 wt.% for chicken manure and sewage sludge, respectively. The carbon contents of the liquids were very low and always below 16 wt.% on as received basis). Whereas the aqueous condensates from lignocellulosic feedstock were essentially a mixture of oxygenated hydrocarbons with negligible contents of nitrogen, sulfur and chlorine, the condensates from chicken manure and sewage sludge had high nitrogen contents. The pH-Value was in the range of 9.5 to 10, indicating the co-existence of ammonium ions and dissolved ammonia gas. The sulfur contents were 0.16 wt.% and 0.33 wt.% on as received basis, while the content of chlorine was an order of magnitude lower. The pH value of the lignocellulosic aqueous condensates were in the range of 2.4 to 3, consistent with the results from former literature related to fast pyrolysis of

lignocellulosic feedstock [162]. On a received basis, the lower heating values of the aqueous condensates were very low, i.e. 4.4 MJ/kg for beech wood and 1.5 MJ/kg for chicken manure. It is obvious that the energy valorization of the aqueous condensate is not feasible. GC-MS screening was carried out for all the aqueous condensates (see Appendix for the qualitative compositions). While the aqueous condensates from lignocellulosic feedstock mainly contains acids, aldehydes and ketones, those from chicken manure and sewage sludge are characterized by high contents of amines In conclusion, the aqueous condensate is also a challenging intermediate liquid. Two valorization routes appear to be feasible. One option for small-scale facilities is that the pyrolysis vapors, without condensation, could be thermally destroyed to generate process heat for the pyrolysis reactor. A second option for larger facilities could be directed to the recovery of chemicals. Aqueous condensates from manure and sludge could be adopted to generate ammonia and other basic chemicals for fertilization.

Permanent Gas

The permanent gas from the pyrolysis of low-grade biogenic feedstock presents different compositions (see Figure 46). The main difference is given by the ratio between CO and CO_2. With increasing ash content, the CO/CO_2 ratio decreases. Decarboxylation reactions are favored against decarbonylation reactions [156, 128]. Moreover, the content of CO_2 is particularly high for chicken manure, i.e. about 80 wt.%, due to the release of CO_2 from dolomite, which is used as a drying and hygienization medium in livestock husbandry [112]. The content of hydrocarbons also decreases with increasing ash content, with the exception of sewage sludge, which has the highest content of hydrocarbons as well as the highest content of H_2, probably due to the high content of iron in the solid matrix, which favors reforming reactions. The lower heating value of the permanent gas is in the range of 9 MJ/kg to 10.25 MJ/kg for wheat straw and sewage sludge, respectively. Due to the high content of CO_2 and low contents of CO and hydrocarbons, the permanent gas from chicken manure present an LHV of only 5 MJ/kg. While the permanent gas from the other feedstock may be combusted in established combustion systems for low caloric fuel gas, that from chicken manure is not suitable; therefore, a secondary fuel or fuel and air pre-heating may be required for stable combustion. Moreover, taking into account the sulfur and chlorine balance, sour gases such as H_2S and HCl might be present in the permanent gas, further hindering the utilization in combustion applications. A better understanding of the content of the mentioned gases should be prosecuted with the aim of developing strategies for a profitable removal of these pollutants.

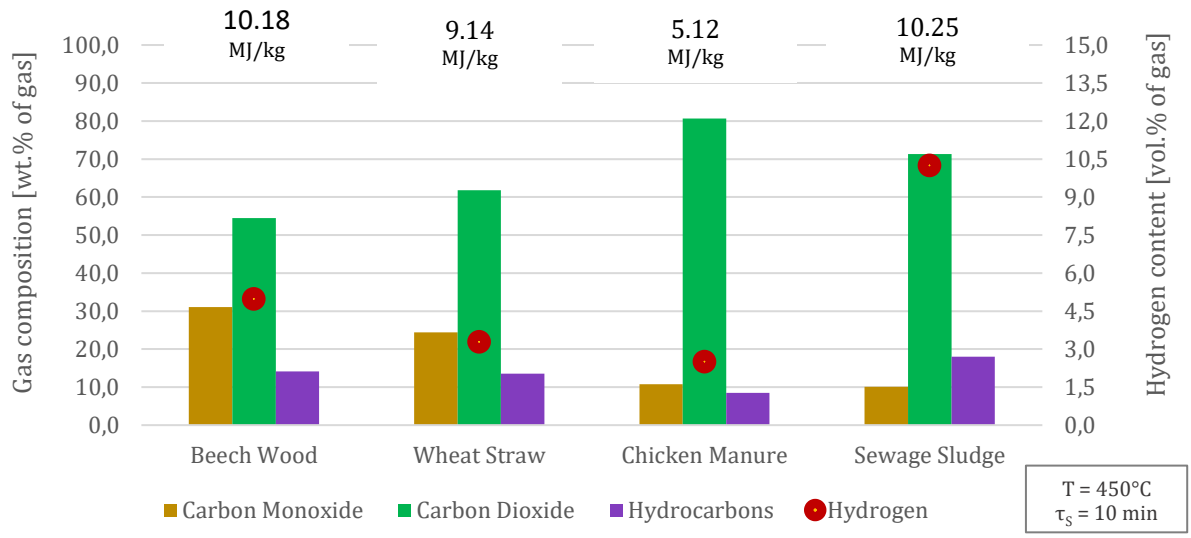

Figure 46. Composition of the permanent gas from the pyrolysis of low-grade biogenic feedstock with a temperature of the reactor of 450°C and a residence time of the solids of 10 minutes.

5. MODELING THE SCREW PYROLYSIS REACTOR STYX

In this chapter, a thermochemical model for the pyrolysis of biogenic feedstock in the screw reactor STYX will be discussed. The implementation of a numerical tool for the simulation of pyrolysis in a screw reactor may help to gain deeper understanding of the mechanisms involved during the process as well as to reduce the experimental effort, the development costs and time during the optimization and the scale-up of the reactor. The simulation of the pyrolysis process was implemented both with one-dimensional (1D) and CFD models for a range of reactors [120, 25, 129, 21, 233, 10]. CFD models were mainly adopted to investigate the hydrodynamics of the reactor; 1D models are more suitable for the optimization of the process parameters and of the reactor's geometry. Moreover, 1D models may be adopted for scale-up purposes. Simplified 1D models for the pyrolysis of biogenic feedstock have been developed for fluidized beds and rotary kiln (see chapter 2.2.2); however, no literature was found for screw reactors.

5.1 Approach to the model

5.1.1 Compartment module

The STYX reactor, and screw reactors in general, is a transport system, where a number of unit operations takes place at a defined position along the screw axis. The principle approach to the processes is depicted graphically in Figure 47.

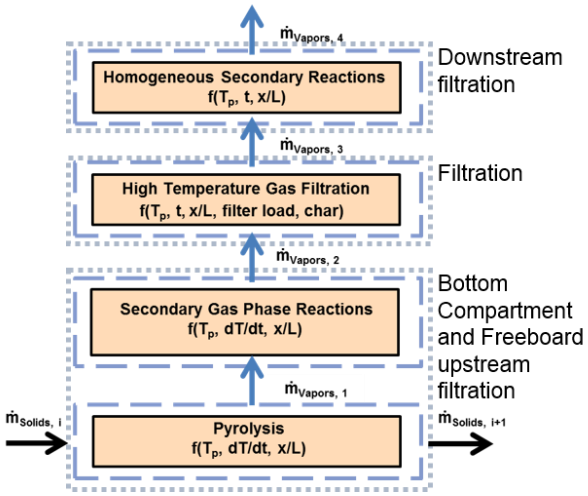

Figure 47. Processes taking place in a compartment of the screw reactor STYX.

The processes related to the solids all take place in the compartment at the bottom. The bulk solid is transported and mixed; the temperature of the solids is a function of the position along the screw. Heat transfer from the vessel to the bulk is responsible for the increase of the bulk temperature and for the following physical and chemical reactions. At first, the temperature of bulk solids increases

up to 100°C, where the main drying process takes place. When the drying is completed, the temperature increases further up to the final offset point. In this range of temperatures, *pyrolysis*, i.e. the thermal decomposition of the organic matter takes place and the organic vapors are released, without further interactions with the solid matrix. Fine char particles can be entrapped in the vapors, which are released vertically from the bulk solid. In the second step, the vapors undergo *secondary gas phase reactions*. The involved reactions take place at a defined position along the screw reactor. They depend on their current temperature; heterogeneous reactions can take place in the case fine char particles are transported by the flow of the vapors. The vapors are filtered during the *high temperature gas filtration*, where the fine particles are removed from the vapor stream. Reactions can take place on the surface of the filter, depending on the local temperature, as well as a function of the filter load and of the composition of the char particles. Downstream the filter, and before condensation, *homogeneous secondary reactions* can be foreseen depending again on the temperature and on the residence time at elevated temperatures.

5.1.2 Cascade reactor model

The previous paragraph described the processes, which take place within a compartment module. The reactor model is generated by a cascade of modules, as depicted in Figure 48.

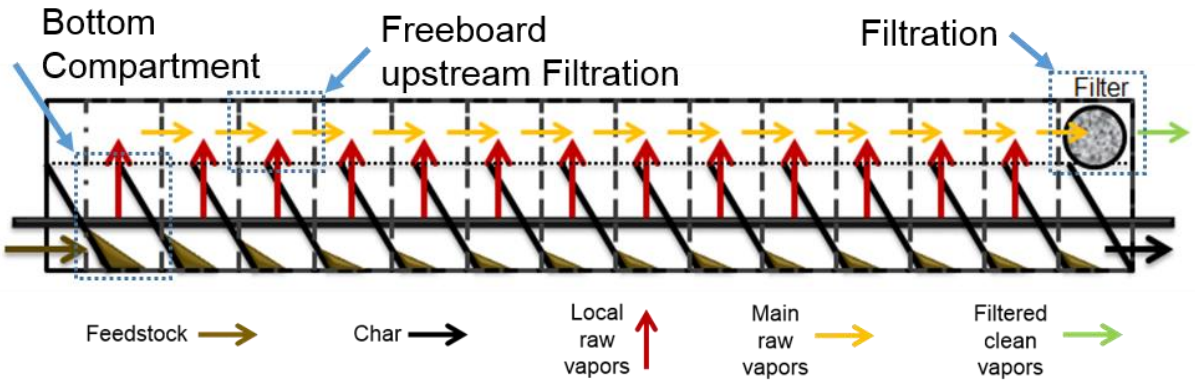

Figure 48. Cascade reactor model of the screw pyrolysis reactor STYX.

Each bottom compartment is evaluated independently as described in paragraph 5.1.1. The solids are transported from one compartment to the next one, while the vapors are released vertically to reach the freeboard. The vapors are released locally without mixing among the compartments. At the cross section between the bottom compartment and the freeboard, the locally released vapors (red arrows in Figure 48) and the main vapors stream (yellow arrows in Figure 48) are mixed and flow horizontally to the next freeboard compartment. The filtration module can be optionally implemented, depending on the position along the screw. The effects of the filtration were discussed in section

4.1.3. The implementation of a filtration module requires further examination of the mechanisms involved in the high temperature filtration of pyrolysis vapors.

5.2 Mathematical model

5.2.1 General assumption

The reactor model is considered a 1D (axial direction) +1D (vertical direction) system, as shown in Figure 48. The continuous solids with effective properties, i.e. the weighted sum of the properties of the components of the continuum, proceed along the axis of the reactor. The vapors are released locally and move vertically form the bottom to the freeboard. It is assumed that no mass exchange between the vapors released at a defined position and those released at the following position takes place. The vapors are summed in the freeboard, where they are assumed to be instantly perfectly mixed. The composition, the temperature and the other properties of the new mixture are calculated on the basis of the weighted sum. The stream of vapors flows along the axis of the reactor covering only the volume occupied by the freeboard. The presence of the filters along the freeboard is neglected. Finally, the vapors are removed from the reactor at its end, i.e. no sequential extraction and filtration is considered. It is assumed that the condensation of the vapors is immediate and no further reactions take place between the outlet of the reactor at process temperature and the liquid recovery flasks at ambient temperature. In reality, after filtration, the vapors need about 2 seconds to leave the hot reactor and enter the condensation unit. Therefore, deviations between the experimental results and the simulations can be expected.

5.2.2 Substances properties

A continuum model was adopted for the bulk solids. The physical properties of the continuum are evaluated adopting the effective coefficients based on the mass fractions of the components of the solids, i.e. feedstock, on dry ash free basis (*FEED,DAF*), water content as well as carbonized char fraction, which includes also the ash fraction of the feedstock. This assumption is used for the bulk density, the thermal conductivity of the particles and the specific heat capacity, which is used in Equation 34 to clarify the adopted approach.

$$c_{SOLIDS} = \frac{m_{FEED,DAF} c_{FEED,DAF} + m_{MOISTURE} c_{WATER} + m_{CHAR} c_{CHAR}}{m_{FEED,DAF} + m_{MOISTURE} + m_{CHAR}} \qquad \text{Equation 34}$$

The thermal conductivity of the bulk, which includes the interstitial gas, is calculated adopting the method described by Tsotsas [213]. The methods take into account the size and the roughness of the

particles as well as the void volume. The properties of the gases are calculated adopting the instructions given for gas mixtures [220].

5.2.3 Solids transport and mixing properties

The mechanical motion of the solids along the screw axis is modeled as an N-series of CSTRs, assuming a local perfect mixing. As a consequence, no exchange of solids between the pitches of the screw is considered. Moreover, the overall residence time of the solids is expressed by the geometric residence time as discussed in section 3.4.3.

The flow of the solids depends on the physical properties of the bulk, such as the angle of repose (α_0) and the friction, which depends on the particle size and shape. The angle of repose defines the displacement of the bulk material within the pitch and consequently the contact area between the first layer of solid particles and the reactor (Figure 49). The constraints of Figure 49 a, i.e. flow without bridge building, should be always satisfied. The procedure for the evaluation of the maximum permitted mass flow rate and for the description of the geometry of the bulk are reported in detail in the Appendix.

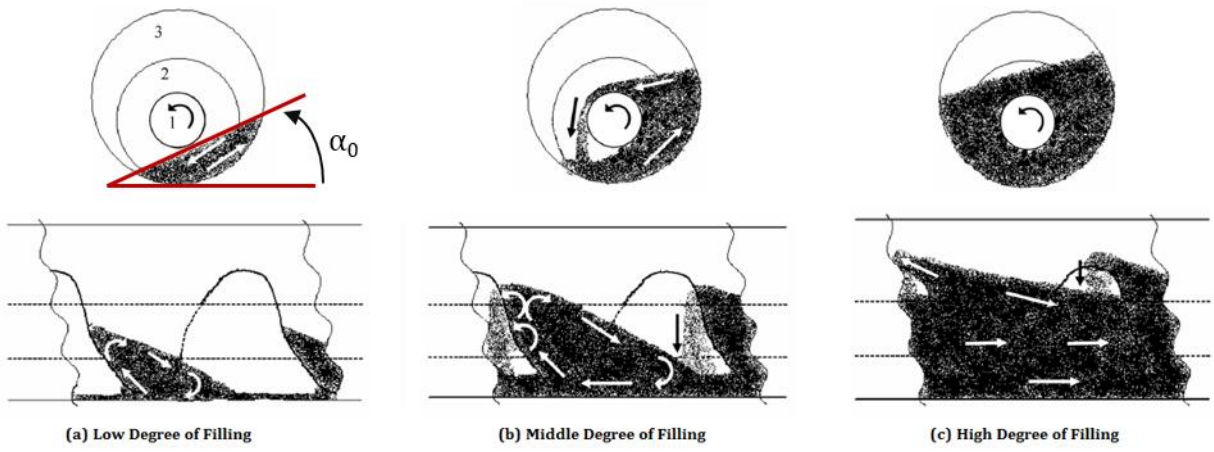

Figure 49. Flow patterns in a screw conveyor at different Degree of Filling. Front view (top); side view (bottom). Source: [226].

As already mentioned, the solid is modeled as a continuum with effective properties. One of the most important properties is the mixing quality of the material within the single pitch of the screw, which has important repercussions on the heat transfer. In this work, the heat transfer within the granular solids is modeled using the theory of the penetration model developed by Schlünder and Mollekopf [184] and will be discussed in Section 5.2.4. To this theory, considerations are made in relation to the so-called time of contact or stagnant period t_R, which describes the time required for perfect mixing of the bulk and thus defines the mixing quality of the solids (Equation 35).

The stagnant time is a function of the mixing time t_{MIX} and of the mixing number N_{MIX}. The mixing time is the inverse of the rotational frequency n (Equation 36). The mixing number (Equation 37) is an empirical correlation related to the Froude number for rotating machines (D is the diameter of the screw in Equation 38). The Mixing number depends on the mechanical properties of the system such as the apparatus, the stirrer and the particles. In Equation 37, the coefficients C and x depend on the geometry of the reactor and need to be estimated empirically. In this work, the correlation for rotary drums was adopted [213]. Additionally, in Equation 37 a multiplicative factor (f_{MIX}) is included to evaluate the effect of an improved mixing quality of the bulk solid. In the standard case, $f_{MIX} = 1$.

$$t_R = t_{MIX} N_{MIX} = \frac{N_{MIX}}{n} \quad \text{Equation 35}$$

$$t_{MIX} = \frac{1}{n} \quad \text{Equation 36}$$

$$N_{MIX} = \frac{1}{f_{MIX}} C Fr^x \quad \text{Equation 37}$$

$$Fr = \frac{(2\pi n)^2 D}{2g} \quad \text{Equation 38}$$

5.2.4 Heat transfer model

The modeling of a thermochemical reactor consists in the coupling of the heat transfer mechanisms and of the chemical reactions taking place in the reactor. The heat transfer model describes the heat exchange among the components of the reactor and the reacting media. The components of the screw reactor are the vessel, the shaft and the flights. In the case of pyrolysis, the reacting media are solid and gaseous, both undergoing chemical reactions as well as exchanging mass from one phase to another.

Heat transfer in the compartment

The mechanisms of heat transfer in a compartment of the reactors involve the interactions between the reactor and the reacting media, which are subjected to external energy transfer in form of heat from the reactor surface. The system is described by three enthalpy balances. The first is related to the solids, while the second and the third are related to the vertically released vapors and to the main vapors stream in the freeboard, respectively. On the basis of the reactor model described in Figure 48, the overall mechanisms of heat exchange and the respective heat transfer surfaces are depicted graphically in Figure 50 for a compartment of the trough screw reactor STYX.

Enthalpy balance of the solid

$$\frac{dH_S}{dt} = \dot{Q}_{WS,eff} + \dot{Q}_{WS,\varepsilon} + \dot{Q}_{ShS,eff} + \dot{Q}_{ShS,\varepsilon} - \dot{Q}_{S\Delta m,\alpha} - \dot{Q}_{S\Delta m,\varepsilon} - \dot{Q}_{LAT} - \dot{H}_{S\Delta m}$$

Equation 39

Enthalpy of the locally released vapors

$$\frac{dH_{\Delta m}}{dt} = \dot{Q}_{Sh\Delta m,\alpha} + \dot{Q}_{Sh\Delta m,\varepsilon} + \dot{Q}_{W\Delta m,\alpha} + \dot{Q}_{W\Delta m,\varepsilon} + \dot{Q}_{S\Delta m,\alpha} + \dot{Q}_{S\Delta m,\varepsilon} + \dot{H}_{S\Delta m} - \dot{H}_{\Delta mG}$$

Equation 40

Enthalpy of the main stream of vapors (freeboard)

$$\frac{dH_G}{dt} = \dot{Q}_{WG,\alpha} + \dot{Q}_{WG,\varepsilon} - \dot{H}_G + \dot{H}_{\Delta mG}$$

Equation 41

The enthalpy balance of the solids (Equation 39) considers the conductive (*WS,eff*) and the radiative (*WS,ε*) heat exchange to the solids from the wall including the flights, which are assumed to be at the same temperature of the vessel. In addition, the radiative (*ShS,ε*) and eventually effective (*ShS,eff*) heat exchange from the shaft are taken into account. The shaft is considered at the same temperature of the vessel, as a first approach. Secondly, the convective (*SΔm,α*) and the radiative (*SΔm,ε*) heat exchanges with the released vapors are considered as well as the enthalpy flow (*SΔm*) given by the mass released during drying and pyrolysis. In the model, the shaft and the flights are assumed to have the temperature of the external vessel at each position along the axis of the reactor, which implies no heat exchange along the longitudinal axis of the shaft. The assumption is valid in steady state operations, the thermal inertia of the shaft is relatively large in comparison to the energy absorbed by the feedstock. Therefore, it is fair assuming a constant temperature of the shaft as it would be actively heated. This assumption may not be fulfilled for larger scale systems and steady state operation for a non- actively heated shaft. The shaft will reach a temperature of equilibrium at each location along the reactor; therefore an additional energy balance for the shaft should be included in such a case.

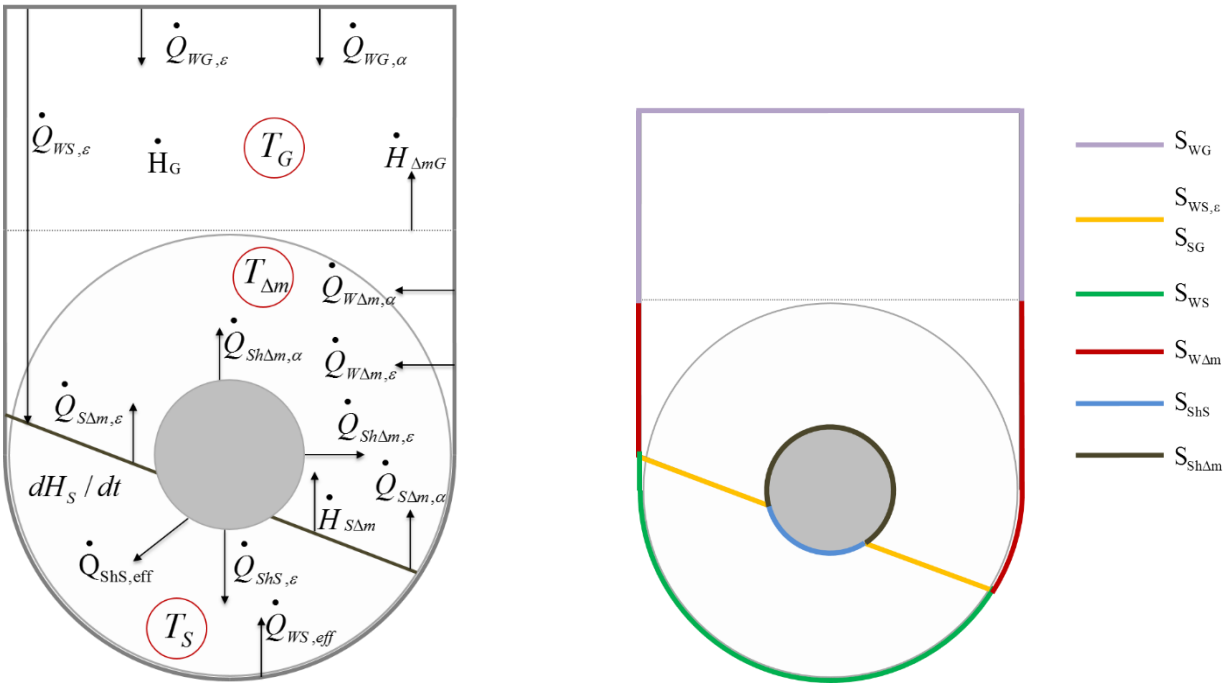

Figure 50. Heat transfer model (left) and respective heat transfer surfaces (right) of the trough screw reactor STYX.

Equation 40 considers the vertical flow of the locally released vapors (Δm). The energy balance includes the heat exchange (convective and radiative) with the wall ($W\Delta m$) and the shaft ($Sh\Delta m$); it is coupled with the energy balance of the solids ($S\Delta m$) and with the main gas stream (ΔmG) through the enthalpy flow contained in the gases. Finally, the energy balance of the main gas stream (Equation 41) is coupled with the vertical gases and exchanges convective and radiative heat with the wall. The mechanisms of heat transfer involving the gases are modeled adopting the appropriate correlations to evaluate the Nusselt number for forced convection at the respective hydrodynamic regime, as well as taking into account the radiative effect of the wall for adsorbing gases such as water vapor and CO_2. It is worth noting that the solids and the main vapors stream on the freeboard are not directly coupled, but they exchange mass as well as enthalpy through the vertical stream of vapors.

To understand the working principle of the model, the whole system may be described as a 1D + 1D, with a multiple riding observer. From the point of view of the solids, at a defined residence time of the solids t_S, the vapors are released vertically, taking a $\Delta t_{\Delta m}$ to reach the freeboard. During this time, the temperature of the vertical vapors increases and secondary homogeneous and heterogeneous reactions take place with the respective reaction rate. Entering the freeboard, the vertical vapors are mixed perfectly with the main vapors stream, which enters the compartment at a defined residence time of the gas t_G and requires a Δt_G to cross the section. As a result, the new temperature and mass flow rate of the main vapors stream at the outlet of the compartment are the weighted sum of the vertical vapors and of the main gas stream. Each vapor stream released at a defined time t_S and

position of the solids x_S will have a different composition and a different total residence time of the reactor. Therefore, the overall final composition of the vapors is the superposition of the compositions of the single vapor streams.

The components of the enthalpy balance of the solids are described into details by the following equations. Equation 42 describes the overall enthalpy balance as the variation of the temperature of the solids dT_S. From Equation 43 to Equation 48, the individual heat exchanges are reported. The latent heat exchange due to the evaporation of the water content is described in the section devoted to the drying process. In Equation 49, the enthalpy flow caused by the chemical conversion is described by the variation of the mass of the solids multiplied by the specific enthalpy of pyrolysis reaction. The unknowns are the temperature of the solids T_S and the temperature of the locally released gas $T_{\Delta m}$. The shaft is assumed to be at the same temperature of the wall, therefore $T_{Sh} = T_W$.

$$\frac{dH_S}{dt} = \dot{m}_S c_S \frac{dT_S}{dt} = \dot{Q}_{WS,eff} + \dot{Q}_{WS,\varepsilon} + \dot{Q}_{ShS,eff} + \dot{Q}_{ShS,\varepsilon} - \dot{Q}_{S\Delta m,\alpha} - \dot{Q}_{S\Delta m,\varepsilon} - \dot{Q}_{LAT} - \dot{H}_{S\Delta m} \quad \text{Equation 42}$$

$$\dot{Q}_{WS,eff} = \alpha_{eff} S_{WS} \left(T_W - T_S \right) \quad \text{Equation 43}$$

$$\dot{Q}_{WS,\varepsilon} = \varepsilon_{WS} \sigma S_{WS} \left(T_W^4 - T_S^4 \right) \quad \text{Equation 44}$$

$$\dot{Q}_{ShS,eff} = \alpha_{eff} S_{ShS} \left(T_{Sh} - T_S \right) \quad \text{Equation 45}$$

$$\dot{Q}_{ShS,\varepsilon} = \varepsilon_{ShS} \sigma S_{ShS} \left(T_{Sh}^4 - T_S^4 \right) \quad \text{Equation 46}$$

$$\dot{Q}_{S\Delta m,\alpha} = \alpha_{S\Delta m} S_{S\Delta m} \left(T_S - T_{\Delta m} \right) \quad \text{Equation 47}$$

$$\dot{Q}_{S\Delta m,\varepsilon} = \varepsilon_{S\Delta m} \sigma S_{S\Delta m} \left(T_S^4 - T_{\Delta m}^4 \right) \quad \text{Equation 48}$$

$$\dot{H}_{S\Delta m} = \frac{dm_S}{dt} \Delta h_{react} \quad \text{Equation 49}$$

The enthalpy balance of the locally released gas (*Δm*) describes the energy flows of the locally released gas at a fixed time along the screw axis (Equation 50). The locally released gas flows from the bottom of the screw to the freeboard, exchanging heat with the shaft of the screw (Equation 51 and Equation 52) and with the wall of the reactor (Equation 53 and Equation 54), taking into account the respective surfaces. Moreover, the enthalpy balance is coupled with the enthalpy balance of the solids through Equation 48 and it influences the main gas stream flowing on the freeboard. Furthermore, the locally released gas undergoes secondary gas phase reactions with its own enthalpy of reaction (Equation 55).

$$\frac{dH_{\Delta m}}{dt_{\Delta m}} = \dot{m}_{\Delta m}\, c_{p,\Delta m} \frac{dT_{\Delta m}}{dt} = \dot{Q}_{Sh\Delta m,\alpha} + \dot{Q}_{Sh\Delta m,\varepsilon} + \dot{Q}_{W\Delta m,\alpha} + \\ + \dot{Q}_{W\Delta m,\varepsilon} + \dot{Q}_{S\Delta m,\alpha} + \dot{Q}_{S\Delta m,\varepsilon} + \dot{H}_{S\Delta m} - \dot{H}_{\Delta mG}$$ Equation 50

$$\dot{Q}_{Sh\Delta m,\alpha} = \alpha_{Sh\Delta m} S_{Sh\Delta m} \left(T_{Sh} - T_{\Delta m} \right)$$ Equation 51

$$\dot{Q}_{Sh\Delta m,\varepsilon} = \varepsilon_{Sh\Delta m} \sigma S_{Sh\Delta m} \left(T_{Sh}^4 - T_{\Delta m}^4 \right)$$ Equation 52

$$\dot{Q}_{W\Delta m,\alpha} = \alpha_{W\Delta m} S_{W\Delta m} \left(T_W - T_{\Delta m} \right)$$ Equation 53

$$\dot{Q}_{W\Delta m,\varepsilon} = \varepsilon_{W\Delta m} \sigma S_{W\Delta m} \left(T_W^4 - T_{\Delta m}^4 \right)$$ Equation 54

$$\dot{H}_{\Delta mG} = \frac{dm_S}{dt_{\Delta m}} \Delta h_{sec}$$ Equation 55

The main gas stream, i.e. the stream of gas and vapors flowing along the freeboard of the reactor, is described by the enthalpy balance reported in Equation 41 and in Equation 56. The variation of the enthalpy of the main vapor stream is caused by convective (Equation 57) and radiative (Equation 58) heat exchange with the wall surface as well as by the enthalpy of reaction of the secondary gas phase reactions taking place in the freeboard (Equation 59) and by the additional enthalpy introduced into the stream by the locally released vapors (Equation 55).

$$\frac{dH_G}{dt} = \dot{m}_G\, c_{p,G} \frac{dT_G}{dt} = \dot{Q}_{WG,\alpha} + \dot{Q}_{WG,\varepsilon} - \dot{H}_G + \dot{H}_{\Delta mG}$$ Equation 56

$$\dot{Q}_{WG,\alpha} = \alpha_{WG} S_{WG} \left(T_W - T_G \right)$$ Equation 57

$$\dot{Q}_{WG,\varepsilon} = \varepsilon_{WG} \sigma S_{WG} \left(T_W^4 - T_G^4 \right)$$ Equation 58

$$\dot{H}_G = \frac{dm_G}{dt_G} \Delta h_{sec}$$ Equation 59

The convective heat transfer coefficients used in the model rely on the theory of the convective heat transfer adjusted for the fluid flow regime and geometry. The radiative heat transfer coefficients are also derived from the Stefan-Boltzmann law. The details are reported in the Appendix.

Heat transfer in the bulk solids

The heat transfer within the bulk solids defines the increase of the temperature, i.e. the heating rate, as well as the pyrolysis reaction rate. It is a complex mechanism involving conductive heat exchange

from the wall of the vessel to the first layer of solid particles, convective and contact heat exchange within the bulk itself and radiative heat exchange from the wall, as well as heat transfer in the gas voids. The approach adopted consists in the utilization of the so-called penetration model, which was introduced by Schlünder and Mollekopf to describe the indirect contact heating of a granular solid with a hot surface [184]. The model was further extended to evaluate the vacuum drying process in stagnant and agitated granular beds. Figure 51 describes the approach used by the penetration model adopting the variation of the moisture content X in the granular solid. At the starting condition (a), the granular solid has homogeneous conditions of temperature ($T_S = T_{bed,0}$) and moisture X_0. Heat is applied at the contact surface for a defined time t_R. The first layers of particles (the drying or temperature front $Z_{T,1}$) close to the heated wall are dried (X = 0) and a temperature profile is built from the wall (b). The remaining layers still have the initial temperature $T_{bed,0}$ and moisture content X_0. For the penetration model, which converts the granular system into a continuous system, an instantaneous mixing takes place (c). Therefore, a new homogeneous system is built with new average values for the bed temperature $T_{bed,1}$ and moisture X_1. The same procedure is repeated for the next step. Heat is applied and additional layers of the solid are dried, i.e. the drying front moves from the bottom of the bulk solid to the top ($Z_{T,2}$ in Figure 51 d). Then, the instantaneous mixing takes place (e) and the new homogeneous conditions $T_{bed,2}$ and X_2 are obtained. The utilization of the penetration model was found in the literature, in particular for the modeling of batch dryers [235] and to a minor extent of continuous units, such as rotary dryers and pyrolysis kilns [182, 21]. As highlighted by Tsotsas [212], the main advantage of the penetration model is its universality and versatility of application, while the main drawback is its reliance on the concept of the stagnant period, i.e. the conversion of granular mechanics and statistics into a continuous system.

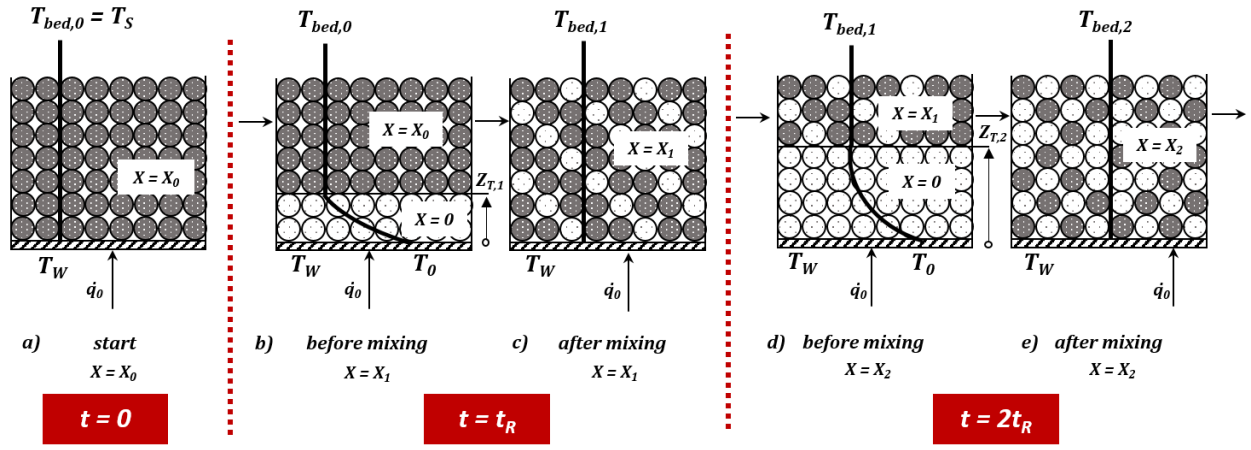

Figure 51. Scheme of the penetration model extended to the vacuum drying. Elaboration from [213].

One of the most recent application of the penetration model was presented by Vega [221] and dealt with the simulation of the indirect drying of copper concentrate in an industrial scale rotating-coil dryer. In its work, Vega fitted the Mixing number experimentally.

The penetration model describes an effective heat transfer coefficient α_{EFF} between a hot surface and a packed bed (Equation 60). The effective coefficient is a combination of conductive (Equation 63) and radiative (Equation 64) heat transfer between the wall and the first layer of particles (α_{WS} in Equation 62) and a penetration heat transfer (α_{BED}) within the granular bed. The first term is a function of the conductivity and of the geometry of the gap, which itself depends on the particle size and on the gas mean free pathway *l*. In Equation 62, Φ is the surface coverage factor, which is 0.8 for mono-dispersed bed of spheres. The second one takes into account the resistance within the packed bed and depends on its properties, such as the specific heat capacity *c*, the conductivity λ and the density ρ. The properties are also intended to be evaluated as a mixture made of the granular solid and the interstitial gases. The heat transfer of the bed depends on the stagnant period t_R (Equation 35). Moreover, for a wet bed and for chemically reacting material, a front penetrating from the wall into the bed is considered. The dimensionless position of the front is expressed by ξ (see Equation 68). In Equation 61, erf ξ is the error function, which varies from zero to one, for perfectly dried or reacted solid.

$$\frac{1}{\alpha_{eff}} = \frac{1}{\alpha_{WS}} + \frac{1}{\alpha_{bed}} \qquad \text{Equation 60}$$

$$\alpha_{bed} = \frac{2}{\sqrt{\pi}} \frac{\sqrt{(c\lambda\rho)_{bed,eff}}}{\sqrt{t_R}} \frac{1}{\operatorname{erf}(\xi)} \qquad \text{Equation 61}$$

$$\alpha_{WS} = \phi\alpha_{WP} + \alpha_{rad} \qquad \text{Equation 62}$$

$$\alpha_{WP} = 4\frac{\lambda_{GAS}}{d}\left[\left(1+\frac{2(1+\delta)}{d}\right)\ln\left(1+\frac{d}{2(1+\delta)}\right)-1\right] \qquad \text{Equation 63}$$

$$\alpha_{rad} = 4C_{W,bed}T^3 \qquad \text{Equation 64}$$

$$C_{W,bed} = \frac{\sigma}{\frac{1}{\varepsilon_W}+\frac{1}{\varepsilon_{bed}}-1} \qquad \text{Equation 65}$$

Drying

The drying was modeled assuming that the water is always available at the surface of the particles, i.e. the drying rate is limited by the heat transfer but not by the mass transfer from the inner pores of

the particles to the surface. For the implementation of the drying, the extension of the penetration model to the vacuum drying of a granular solid medium is adopted.

The penetration heat transfer (α_{BED}) in Equation 61 depends on the error function of the dimensionless position of the front, which may be expressed as a function of the Phase Change number Ph (Equation 66), which itself is defined as the ratio of the latent heat Δh_{LV}, where X is the moisture, to the sensible heat during a phase transition and denotes the strength of the latent heat sink. The relationship between the Phase Change number and the dimensionless front position (Equation 67) is solved implicitly as reported in the VDI Heat Atlas [213]. Physically, the dimensionless position of the front is the ratio between the position of the front Z_T and the thermal diffusivity of the bed $\kappa_{bed,dry}$ (Equation 68).

$$Ph = \frac{X\Delta h_{LV}}{c_{bed,eff}\left(T_W - T_S\right)} \qquad \text{Equation 66}$$

$$\xi\sqrt{\pi}\exp\left(\xi^2\right)\left[1+\left(\frac{\alpha_{WS}}{\alpha_{eff}}-1\right)\mathrm{erf}\left(\xi\right)\right] = \left(\frac{\alpha_{WS}}{\alpha_{eff}}-1\right)\frac{1}{Ph} \qquad \text{Equation 67}$$

$$\xi = \frac{Z_T}{2\sqrt{\kappa_{bed,dry}t}} \rightarrow \kappa_{bed,dry} = \frac{\lambda_{bed,dry}}{\left(\rho c\right)_{bed,dry}} \qquad \text{Equation 68}$$

Approaching dry conditions, the Phase Change number tends to zero; therefore, the dimensionless front position approaches infinity and the error function converges to 1 and the effective coefficients (from Equation 60 to Equation 64) for “wet” bed approach those for “dry” materials.

During the drying of the material, mass from the bulk of the granular solid is transferred to the environment. The heat introduced through the wall of the reactor is used for the evaporation of the water. The mass transfer can be described by the one-side diffusion kinetics for convective drying, with the partial pressure of water steam in the bulk and the saturation pressure at the surface of the bed (Equation 69).

$$\dot{m}_{H_2O(g)} = \rho_{H_2O(g)}\dot{n}_{H_2O(g)} = \rho_{H_2O(g)}n_{GAS}\beta_{GAS}\ln\frac{p - p_{H_2O(g)}}{p - p_{SAT,H_2O(g)}\left(T_{SOLID}\right)} \qquad \text{Equation 69}$$

$$\dot{Q}_{LAT} = \dot{m}_{H_2O(g)}\Delta h_{LV} \qquad \text{Equation 70}$$

Adopting the analogy for heat and mass transfer, $\beta_{H_2O(g)}$ can be calculated from the heat transfer coefficient solid-to-gas (α_{SG}) for a combination of water and nitrogen and a Lewis Number of 1.

Finally, $\dot{n}_{H_2O(g)}$ can be converted into the mass flow of evaporating water steam and the latent heat of evaporation can be calculated (Equation 70). Because of the dependence on the temperature, the coupling between the heat and mass transfer must be calculated iteratively.

5.2.5 Pyrolysis model

Pyrolysis of wood has been studied extensively in the literature, with the main target of describing the decomposition of the biomass and the secondary gas phase reactions as well. Several models and approaches were developed in the last 40 years. Biomass was assumed to be one single component or the weighted sum of its main model compounds, i.e. cellulose, hemicellulose and lignin [177, 234, 145, 6]. The utilization of the model compounds make the models more flexible, since the model can be transferred to materials with different contents of the three model compounds. The models are limited to mineral-free materials. In fact, the content of minerals influences catalytically the decomposition reactions. Some authors attempted to take into account the effect of the minerals adopting correlations from the experimental data. However, the considerations related to the ash content go beyond the scope of this work and therefore the effect of the minerals will be neglected. The scope of this work is the description of the decomposition of the reference biomass, i.e. beech wood. The pyrolysis model relies on a five step global kinetic mechanism attempting to close the elemental (carbon, hydrogen, oxygen) balances. A similar approach, although more detailed, was adopted by Ranzi and coworkers, which implemented a sophisticated lumping process [175]. For this work, the markers adopted in the experimental sections, with the addition of furan, were used to describe the composition of the produced primary and secondary condensable organics. The set of kinetic parameters are taken from Mätzing et al. [137], who also developed the fundamental structure of the model, as depicted in Figure 52. Pre-exponential factors k_0, activation energies E_a and the reaction enthalpies Δh are reported in Table 29.

Table 29. Kinetic parameters of the five step pyrolysis model [137].

Equation	**Abbreviation**	**k_0 [sec^{-1}]**	**E_a [kJ/mol]**	**Δh_{react} [kJ/kg]**
Cellulose, fast	CELL,FAST	$3.0 \cdot 10^{13}$	195	0
Cellulose, slow	CELL,SLOW	$2.0 \cdot 10^{8}$	132	0
Hemicellulose	HEMI	$1.0 \cdot 10^{7}$	105	0
Lignin	LIGN	$1.5 \cdot 10^{14}$	192	0
Secondary reactions	SEC	$2.0 \cdot 10^{7}$	122	0

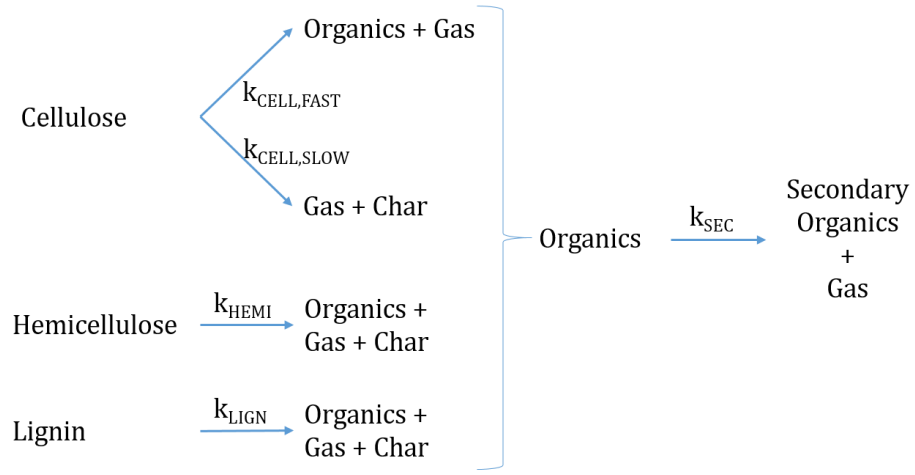

Figure 52. Schematic representation of the pyrolysis model [137].

The literature reports both exothermal and endothermal reaction enthalpies [217, 64]. Therefore, they are all set to neutral (zero) as first approach.

Pyrolysis

The primary decomposition of the biomass is described by four reactions, of which two are for cellulose, the remaining two are for hemicellulose and lignin. Cellulose is described by competitive fast and slow regimes. It is known from the literature that the fast pyrolysis of cellulose does not generate any solid residue or char, while the carbonization (slow pyrolysis) produces water and a carbonaceous residue [78]. The stoichiometry of the four reactions is reported in Table 30.

Table 30. Primary decomposition reactions of the model compounds of wood

$$C_6H_{10}O_5 \xrightarrow{k_{CELL,FAST}} 0,417C_5H_4O_2 + 1,071C_2H_4O + 0,621C_2H_4O_2 + 0,783H_2O(g) + 0,536CO_2$$

$$C_6H_{10}O_5 \xrightarrow{k_{CELL,SLOW}} 5H_2O(g) + 6C$$

$$C_5H_8O_4 \xrightarrow{k_{HEMI}} 1,239C_2H_4O + 1,525H_2O(g) + 0,618CO_2 + 1,903C$$

$$C_{10}H_{10,5}O_3 \xrightarrow{k_{LIGN}} 0,295C_7H_8O_2 + 1,226CO + 0,592CO_2 + 2,036CH_4 + 4,083C$$

The elemental compositions of cellulose and hemicellulose are taken from the literature, while that of lignin was derived from the elemental analysis of the reference feedstock beech wood.
The fast pyrolysis of cellulose produces a mixture of condensable organics such as furfural ($C_5H_4O_2$), acetaldehyde (C_2H_4O) and acetic acid ($C_2H_4O_2$) as well as water and carbon dioxide. No solid carbon is produced. On the other hand, the slow pyrolysis of cellulose generates only water steam and carbon. The pyrolysis of hemicellulose also generates acetaldehyde, water and CO_2. Additionally, it produces a solid carbonaceous residue, which accounts for 17.3 wt.% of hemicellulose. The calculated yield of

carbon is lower than the typical values reported in the literature of thermogravimetric analysis of hemicellulose [177, 193]. The pyrolysis of lignin produces guaiacol ($C_7H_8O_2$) as only condensable organic compound. Moreover, it produces carbon monoxide and dioxide as well as methane. Finally, the carbonaceous residue accounts for 27.5 wt.% of the model compound. Also for the lignin, the carbonaceous residue is lower than those from experimental literature [234, 177].

Secondary gas phase reactions

The secondary homogeneous gas phase reactions were modelled with a single set of kinetic parameters but the composition of the products of each reaction was maintained independent from one another. For each reaction, a combination of up to five species was used. The composition was obtained by maximizing the yield of the selected condensable organics. The stoichiometry of each reaction is reported in Table 31. The products of furfural were furan (C_4H_4O) and carbon monoxide; those of acetaldehyde were acetic acid, water, carbon oxides and ethylene (C_2H_4) as representative non-condensable hydrocarbons with the exclusion of methane. Guaiacol produced phenol (C_6H_6O), carbon monoxide and methane.

Table 31. Secondary Gas-phase reactions.

$$C_5H_4O_2 \xrightarrow{k_{SEC}} C_4H_4O + CO$$

$$C_2H_4O \xrightarrow{k_{SEC}} 0,155C_2H_4O_2 + 0,209CO + 0,301H_2O(g) + 0,090CO_2 + 0,695C_2H_4$$

$$C_7H_8O_2 \xrightarrow{k_{SEC}} 0,857C_6H_6O + 1,143CO + 0,713CH_4$$

5.3 Sensitivity analysis of the model

In order to evaluate and to rank the influence of the parameters of the model, an extended sensitivity analysis was carried out. During the simulations, the variables were investigated independently from one to another. The sensitivity analysis is structured as follows:

1. Physical properties of the feedstock on the heating of a dry and inert feedstock
2. Process conditions and reactor design on the heating of a dry and inert feedstock
3. Process conditions and feedstock composition on the pyrolysis of biomass

The physical properties of the material adopted for the sensitivity analysis are reported in Table 32:

Table 32. Basis physical properties of the feedstock adopted in the sensitivity analysis.

Thermal Conductivity	λ_S	0.13	W/mK
Specific Heat Capacity	c_S	1.00	kJ/kgK
Particle Size	d_p	4.0	mm
Bulk Density	$\rho_{S,BULK}$	220	kg/m^3
Material Density	$\rho_{S,MAT}$	700	kg/m^3

The basis process conditions as well as the reactor geometry parameters are reported in Table 33:

Table 33. Basis process conditions adopted in the sensitivity analysis for the evaluation of the effects of the physical properties and of the process conditions on the heating of a dry and inert feedstock.

Process Conditions		
Temperature of the reactor	450	°C
Geometric residence of the solids	5	min
Mass flow of the solids	10	kg/h
Volumetric flow of the purge gas (nitrogen)	10	l_N/min
Initial temperature of the solids	20	°C
Initial temperature of the purge gas	20	°C
Reactor Geometry		
Length	2	m
Diameter Screw	150	mm
Diameter Shaft	76	mm
Pitch	80	mm
Thickness Flight	4	mm
Height Freeboard	165	mm
Rotational Speed	5	rpm

The effects of the examined parameters are evaluated systematically at 0.5 m from the inlet. The position was chosen from preliminary simulations. The temperature of the solids is close to the starting temperature of pyrolysis, i.e. about 300 °C. The starting temperature of pyrolysis is also relevant to determine the heating rate of the solids.

5.3.1 Physical properties of the feedstock

The physical properties of the feedstock were investigated assuming an inert and perfectly dry material. The parametric analysis is summarized in Table 34. The effects of the specific heat capacity and of the particle size were considered. Moreover, the conditioning of the feedstock was evaluated in terms of combined effect of the particle size and of the bulk density. For more details related to minor parameters refer to the Appendix.

Table 34. Parameters variations of the physical properties of the feedstock.

Parameter	Symbol	Range of variation	Unit
Specific Heat Capacity	c_S	0.85 – 1.00 – 1.15	kJ/kgK
Particle Size	d_P	0.5 – 4 – 10 – 20 – 40	mm

Specific heat capacity

The variation range of the specific heat capacity covers a wide spectrum of materials from typical ash minerals (0.85 kJ/kgK) to carbonized wood at high temperature (1.15 kJ/kgK). The results are shown in Figure 53. A decrease of 15% of the specific heat capacity leads to an increase of the temperature of 24.6 °C. A corresponding increase of 15% leads to a decrease of the temperature of the solids by 20.5 °C. Taking into account the narrow variation of the parameter, the influence of the specific heat capacity is the most relevant physical property of the solids.

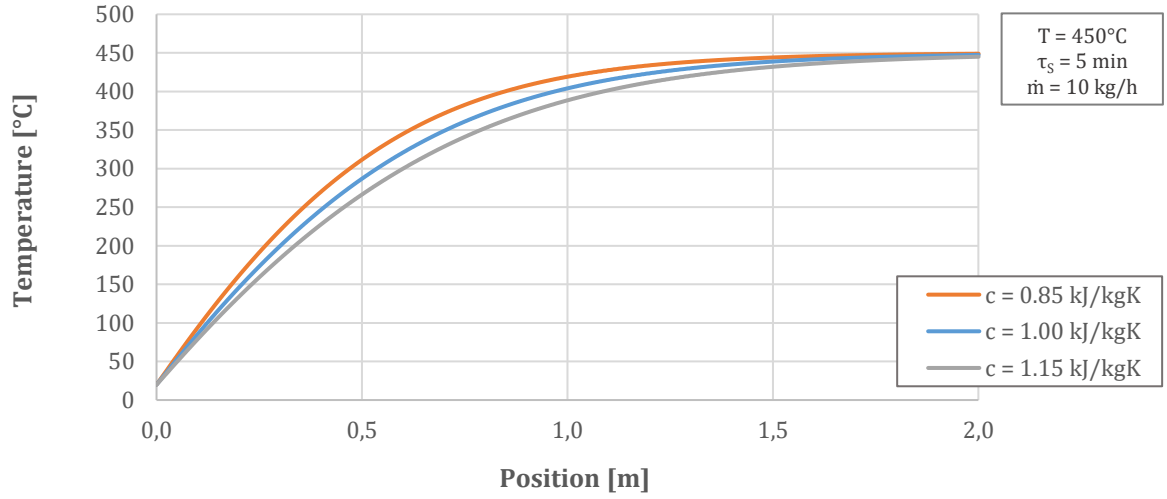

Figure 53. Variation of the specific heat capacity of the solids.

Particle size

The particle size of the solids was investigated in the range of 0.5 mm to 40 mm, corresponding to typical values of wood powder to pellets (Figure 54). An increase of the particle size leads to a slight improvement of the heat transfer coefficient in the bulk (α_{BED} in Equation 61). However, the deterioration of the heat transfer from the wall to the solids (α_{WS} in Equation 62) is higher by a

magnitude of 10^3. With a particle size of 40 mm, the wall-to-particle heat transfer (α_{WP} in Equation 63) becomes the limiting factor. Overall, the influence of the particle size is less significant than that of the specific heat capacity but more relevant than the effects of the thermal conductivity and of the bulk density of the solids. Additionally, it has to be reminded that the heat transfer inside the single particles is not taken into account by the model, which might have a dominant effect with increasing particle size.

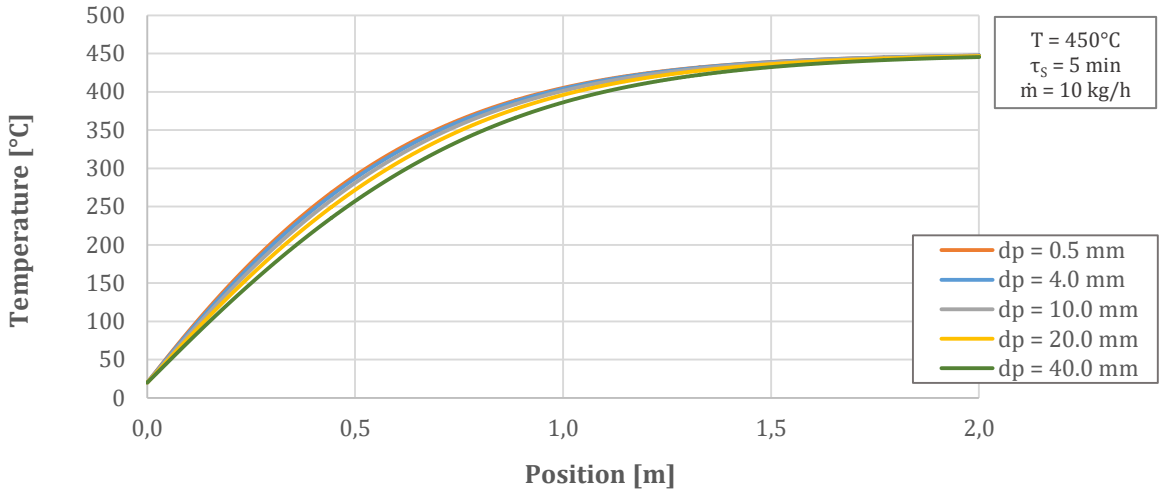

Figure 54. Variation of the particle size of the solid particles.

Conditioning of the feedstock

Finally, the mechanical conditioning of the feedstock was evaluated by the combined variation of the particle size and of the bulk density. In such a way it is possible to directly compare powder and pellets, typical feedstock for fast and intermediate pyrolysis, respectively. The parameters adopted in the following simulations are reported in Table 35. The bulk density of the pellets is similar to the material density of wood from Table 32. Due to the fine milling of wood and the following compaction process for pellets production, the inner pores can be destroyed and therefore the material density is higher than that of the powder.

Table 35. Conditioning properties (particle size and bulk density) of the feedstock.

Conditioning	Particle Size	Bulk Density
Powder	0.5 mm	220 kg/m^3
Pellets	40 mm	660 kg/m^3

The temperature profiles of the solids for the simulations are reported in Figure 55. At 0.5 m, the temperature of the powder is 45°C higher than that of the pellets. The heating rates are both close to 150°C/min at 0.5 m. However, the heating rate of the powder at lower temperatures, i.e. up to a solids temperature of about 200°C, is higher than that of the pellets by 25%. In fact, the Degree of Filling

(DoF in Equation 33) and thus the contact surface between the powder and the vessel of the reactor is higher, due to the lower bulk density at fixed mass flow rate. The heat transfer is limited by the internal heat transfer (α_{BED} in Equation 61) of the granular bed for the powder and by the wall-to-particle (α_{WP} Equation 63) heat transfer for the pellets. However, the effective heat transfer coefficients (α_{EFF} in Equation 60) are in a close range, i.e. 18.8 W/m^{2}K for the powder and 17.4 W/m^{2}K for the pellets, respectively.

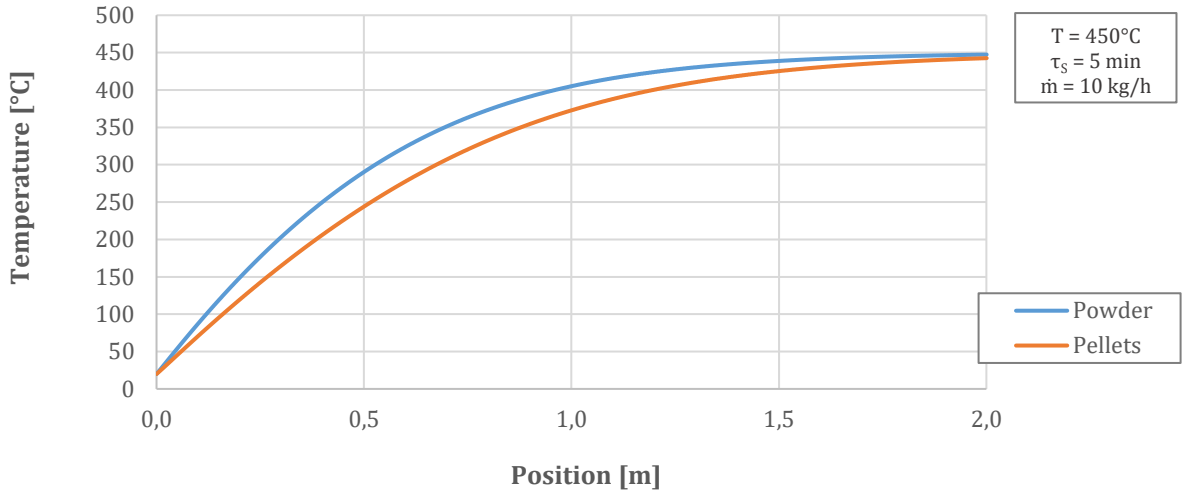

Figure 55. Comparison between different conditioning of the feedstock (powder vs. pellets).

The main consequence of this result is that, in a screw reactor with indirect heating, the milling of biomass to small particle sizes for the achievement of high heat transfer rates does not provide a direct advantage in terms of overall heating rates. Consequently the yield of the condensable organics of the pellets will be close to that of the powder. In contrast to the classical fast pyrolysis processes, where fine particles size is mandatory to achieve high heating rates and short intra-particle residence time, pyrolysis in indirect heated screw reactors can be carried out adopting larger particles size or pellets due to the intrinsically limited effective heat transfer [61, 89].

5.3.2 Process conditions and reactor design on the heating of a dry inert feedstock

The effect of the process conditions, i.e. offset temperature of the reactor and the combined effects of residence time and mass flow of the feedstock (capacity optimization) for a constant DoF were simulated for an inert and dry material adopting the basic physical properties described in Table 32. Further analyses were carried out to evaluate the effects of the design of the screw, i.e. pitch and mixing quality. The variation of the pitch and constant residence time implies a variation of the rotational speed. The mixing quality is intended as a multiplicative factor with respect to the Mixing Number in Equation 37. The mixing quality may be technically improved by implementing pins on the core and on the flights of the screw.

Temperature of the reactor

The temperature of the reactor was varied among the range of the pyrolysis process (Table 36). Isothermal conditions were adopted for the reactor, to reproduce an external electrical heating. The temperature profiles are plotted against the position along the reactor in Figure 56.

Table 36. Temperature range and process conditions.

	Parameter variation	
Temperature of the reactor	350-400-450-500	°C
Residence time of the solids	5	min
Mass flow rate the solids	10	kg/h

The final temperature of the solids reaches the offset temperature for all the simulations. However, evaluating the temperature at 0.5 m, the heating rates are 180°C/min and 120°C/min for an offset temperature of 500°C and 350°C, respectively. At 0.5 m with an offset temperature of 500°C, the solids are at a temperature of 345°C, which corresponds to the final temperature of the solids for an offset temperature of 350°C. Obviously, the higher the offset temperature of the reactor, the faster the heating of the solids. As a direct consequence, an increase of the offset temperature enables higher mass flow rates and shorter residence times, i.e. increasing the overall capacity of the system, assuming an unaltered availability of heat supply.

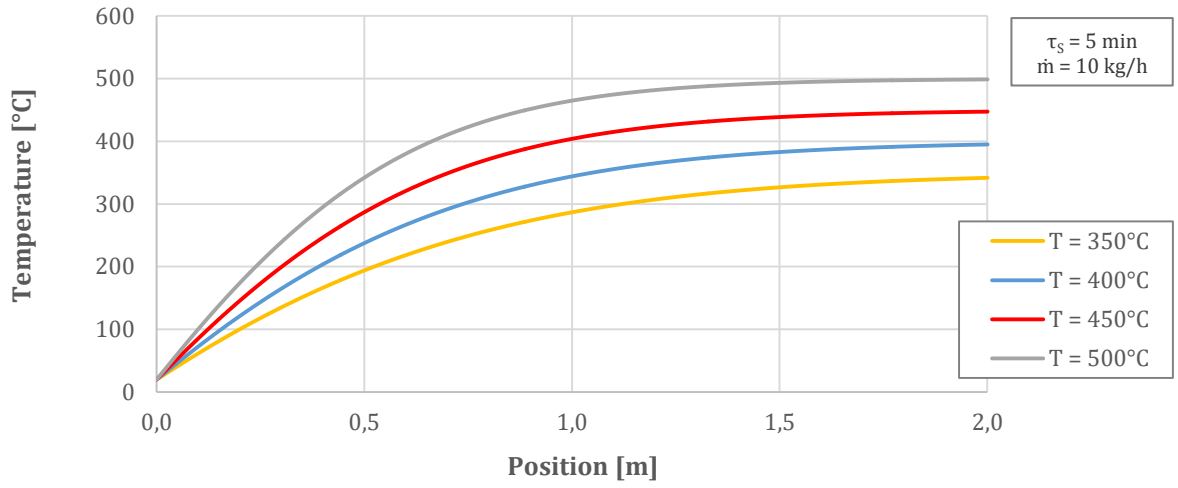

Figure 56. Variation of the offset temperature of the reactor.

Capacity optimization

The effects of the residence time and of the mass flow rate of the solids were evaluated in combination, since the relevant parameter is the Degree of Filling (DoF), which defines the amount of granular solid in the compartment (see the Appendix for more details). The intent was to find the combination of parameters, which maximizes the capacity of the reactor at an offset temperature of

the reactor (see Table 37). The discrimination parameter was the final temperature difference between the offset and the solid temperatures, which should be below 5°C. The DoF was held constant at 14.4%, corresponding to the basis case reported in Table 33.

Table 37. Parameters adopted for the capacity optimization at 450°C.

	Residence time [min]	Mass flow rate [kg/h]
1	1.25	40
2	2.5	20
3 (basis)	5	10
4	7.5	7.5
5	10	5

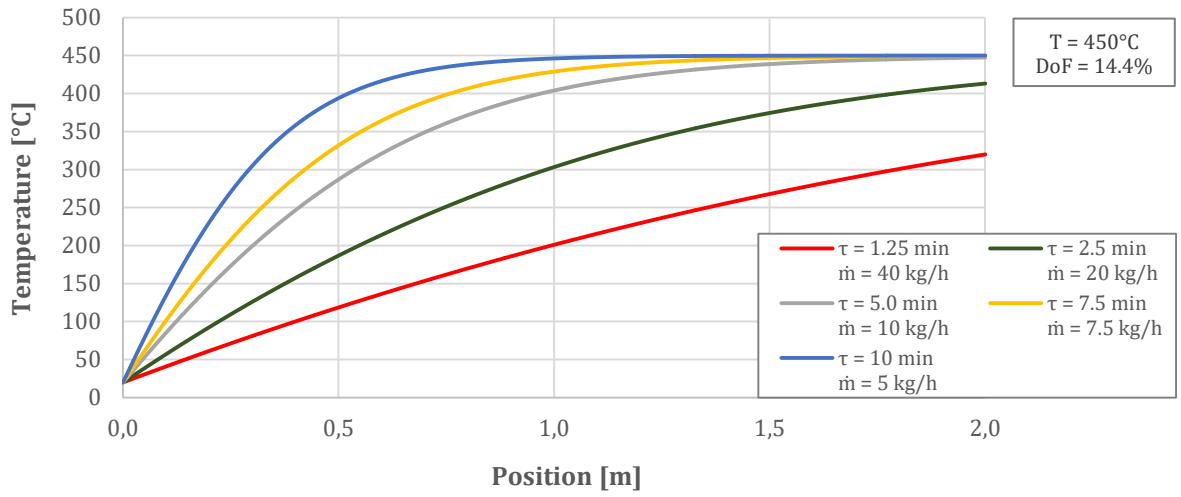

Figure 57. Combined variation of the residence time and of the mass flow of the solids at 450°C and DoF of 14.4%.

Figure 57 reports the results of the simulations, plotting the temperature of the solids against the position along the reactor. In the basis case, the final temperature is 3°C below the offset temperature of the reactor. As expected, an increase of the residence time of the solids leads to a less effective utilization of the length of the reactor, i.e. the offset temperature is reached at 1.5 m. The final temperature of the solids is below the set limit of 5°C for mass flow rates of 20 and 40 kg/h and residence time of the solids of 2.5 and 1.25 minutes, respectively. Higher mass flow rates would lead to larger difference. The optimal operation parameters for a final temperature of 445°C are obtained using a mass flow rate of 11.5 kg/h with a residence time of 5 minutes, corresponding to a DoF of 16.6%.

Design of the screw

The length of the pitch (see Figure 19) was varied in order to consider the effect of the speed of rotation of the screw for a given residence time of the solids, without influencing the capacity of the reactor. The parameters are reported in Table 38.

Table 38. Screw design variation and process conditions.

	Parameter variation	
Pitch	40-60-80	mm
Rotational speed of the screw	10-7.5-5	rpm
Temperature of the reactor	450	°C
Residence time of the solids	5	min
Mass flow rate the solids	10	kg/h

The reduction of the pitch corresponds to the increase of the speed of rotation and consequently the Froude number (Equation 38).

The results of the simulations are depicted in Figure 58, which shows negligible effect on the temperature profile of the solids. At 0.5 m, the temperature of the solids is 300°C and 287°C for a pitch of the screw of 40 mm and of 80 mm, respectively. The minimal improvement in the heat transfer by reducing the pitch length appears to be not worth considering the additional limitations in terms of particle size and the increased investment due to the doubling of the number of flights.

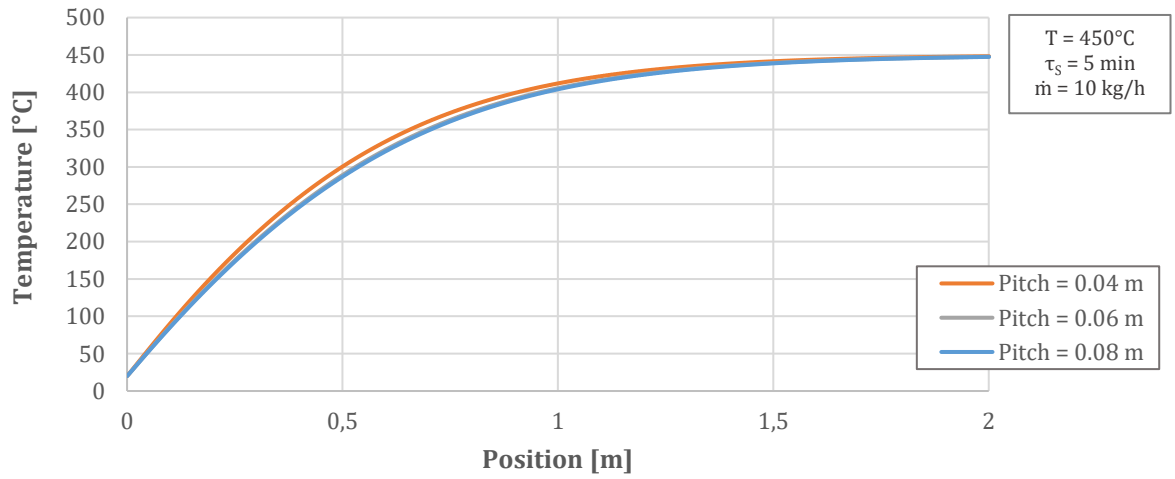

Figure 58. Variation of the pitch of the screw.

Mixing quality

Another option to increase the mixing quality is offered by the possibility of introducing mixing elements on the flights or on the core of the screw, which will come into contact with the bulk and agitate it. The mixing quality is described qualitatively by the stagnant time t_R in Equation 35. The lower t_R, the higher the effective heat transfer coefficient in Equation 61. The model offers the option of directly influence the stagnant time t_R by dividing the mixing number (N_{MIX}) by a mixing factor

(f_{MIX} in Equation 37), which correlates empirically to the addition of mixing elements on the screw. The mixing factor was increased from 1, which represents the screw without mixing elements to 2 and 4, corresponding to the addition of one or more mixing elements.

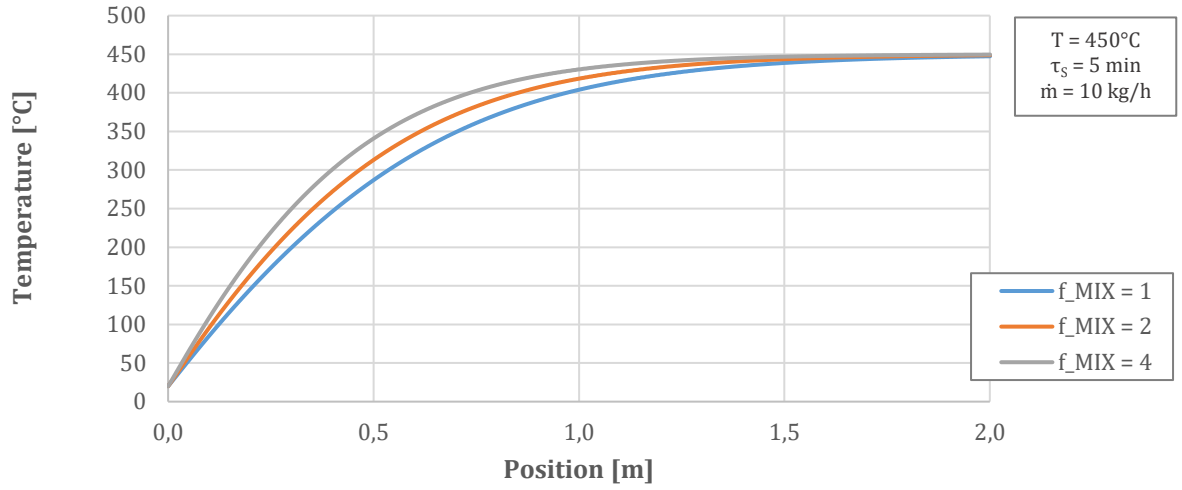

Figure 59. Variation of the mixing quality.

Figure 59 reports the results of the simulations for the three selected conditions. At 0.5 m, the temperature of the solids is higher by 26°C and 55°C, respectively. The effective heat transfer coefficient increases by a factor 1.5 and 2 for the two cases. The addition of mixing pins appears to be a worthy option for the improvement of the heat transfer within the bulk of granular solids.

This section investigated numerically the effect of the process parameters on the heating of a dry inert granular solid. Future extension of the model should take into account the additional heat resistance of the vessel of the reactor as well as the fouling of the surface, which would lead to a worsening of the overall heat transfer to the solids with repercussions on the maximum capacity of the reactor. Moreover, the temperature of the reactor was considered isothermal, due to the electrical heating of the system. Considerations related to the scale-up of the reactor should deal with the replacement of the electrical heating by a hot gas stream. Therefore, they should consider the heat transfer from the gas to the reactor vessel, which may become the limiting factor in terms of capacity.

5.3.3 Process conditions and feedstock composition on the pyrolysis of biomass

In this sections, the results of the simulations of the pyrolysis process are reported for a selected range of process conditions, i.e. temperature of the reactor, mass flow rate and residence time of the solids, as well as for different compositions of the biomass, i.e. water and ash contents as well as the contents of the model compounds cellulose, hemicellulose and lignin. For the chemical composition of the reference biomass beech wood see Table 6 in section 3.1.1. The physical properties and the process

conditions are reported in Table 32 and Table 33, respectively. On the contrary to Table 33, the reference mass flow rate of the solids was set to 5 kg/h for the simulation of this section. The overall parameter variations are reported in Table 39.

Table 39. Parameters variations for the analysis of the effects of the process conditions and feedstock properties on the yields distributions of the pyrolysis products.

	Parameter Variation	
Temperature of the reactor	350;400;450;500	°C
Residence time of the solids	2.5;5;7.5;10	min
Mass flow rate of the feedstock	1.25;2.5;5;10	kg/h
Enthalpy of reaction	-250;-100;0;100	kJ/kg
Moisture content of the feedstock	0;5;10;20	wt.%

Moreover, the effects of the chemical composition of the feedstock on the yields distribution of the pyrolysis products were considered. The parametrization is reported in the respective paragraph.
The effect of other parameters, such as the conditioning of the feedstock, were of negligible relevance and therefore were not further discussed (see the Appendix for more details).
The results are reported in the form of yields of the pyrolysis products, as mass fraction in % of the feedstock on as received basis.

Temperature of the reactor

The results of the simulations for the evaluation of the effect of the temperature of the reactor are reported in Figure 60.

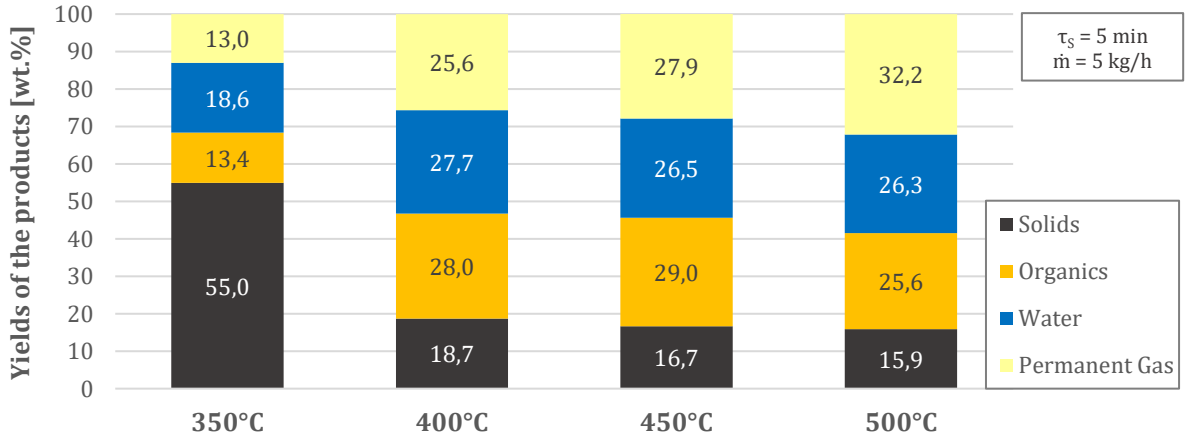

Figure 60. Effect of the reactor temperature on the yields of the pyrolysis products.

The simulations indicates that, under the selected process conditions, the yield of the solids slightly decreases from 400°C to 500°C. At 350°C, the yield of the solids is 55.0 wt.% of the original feedstock, due to non-reacted feedstock. The offset temperature of the reactor was not achieved. In

fact, at low reactor temperatures, the heating rate of the solids is lower in comparison to that achieved at higher offset temperatures (see Figure 56). Thus, the reaction rate is lower. Moreover, the pyrolysis rate of reaction contributes to the production of more solid carbon, since the carbonization reaction of cellulose is favored at lower temperatures. The yields of the permanent gas increases steadily with increasing temperatures, as widely reported in experimental literature related to the pyrolysis of wood biomass, independently from the reactor type and configuration [232, 98]. The yield of the condensate, i.e. the sum of water and organics in Figure 60, reaches a maximum of 55.7 wt.% at 400°C. At higher temperatures, it slightly decreases to 51.9 wt.% at 500°C. However, the yields of the organics, which are to be intended as the condensable oxygenated hydrocarbons, reaches its maximum at 450°C increasing from 13.4 wt.% at 350°C and then decreasing to 25.6 wt.% at 500°C due to the incremented reaction rate of the secondary gas phase reactions, which compensates the decreased overall residence time of the vapors. On the other hand, the water content of the condensate decreases starting from an offset temperature of 400°C. In fact, at increasing temperature, the heating rate increases favoring the fast reaction of cellulose to more condensable organics and less char and reaction water. Therefore, with the aim of maximizing the yield of the organics, an offset temperature of 450°C is suggested for the pyrolysis of beech wood at the STYX reactor.

Residence time of the solids

The second parameter investigated is the residence time of the solids. It showed relevant effects on the heating of dry and inert granular material only in combination with the mass flow rate (see section 5.3.2 for further details).

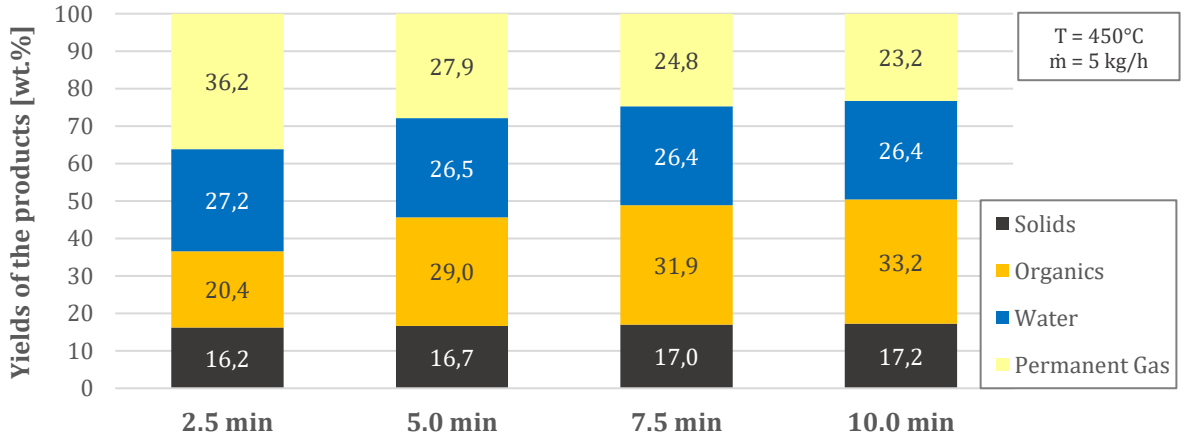

Figure 61. Effect of the residence time of the solids on the yields of the pyrolysis products.

The results of the simulations, reported in Figure 61, show a steady increase of the char yield with increasing residence time. As already mentioned, the residence time influences the DoF of the screw

pitch, i.e. more material is displaced within the single compartment, which leads to a slight reduction of the heating rate at low temperatures favoring the carbonization reaction of the cellulose. Nevertheless, the yield of the condensate increases strongly from 47.6 wt.% to 59.6 wt.% with a residence time of 2.5 minutes and 10.0 minutes, respectively. A similar trend is shown by the yield of the organics, which increases by a factor of 1.5 from short to long residence time. The yield of water is relatively constant. The described effect, as well as the additional decrease of the permanent gas with increasing residence time, is caused by the hydrodynamic behavior of the pyrolysis vapors. At short overall residence times, the solids move fast and the release of the vapors is evenly distributed along the reactor (for more details see Figure 105 in the Appendix). As a direct consequence, the vapors released in a single compartment present a lower volumetric flow rate, which causes longer residence times and faster heating from the bottom of the screw to the freeboard (see Figure 48). Both the effects favor the secondary gas phase reactions, which lead to the increase of the permanent gas yields and reduction of the organics yields.

Mass flow of the feedstock

The effect of the mass flow of the solids was evaluated at an offset temperature of the reactor of 450°C and a residence time of the solids of 5 minutes (Figure 62). The increase of the mass flow of the feedstock present a similar effect as the reduction of the residence time. Increasing the mass flow increases the DoF and therefore lowers the heating of the solids for a higher yield of char at high mass flow rates. The increase of the mass flow rate of the feedstock from 5 kg/h to 10 kg/h corresponds to an increase of the residence time from 5 minutes to 10 minutes. As already discussed for the optimization of the capacity for heating of dry and inert materials (section 5.3.2), the optimal process conditions appear to be 10 kg/h mass flow and 5 minutes of residence time of the solids also for the maximization of the yields of the condensable organics.

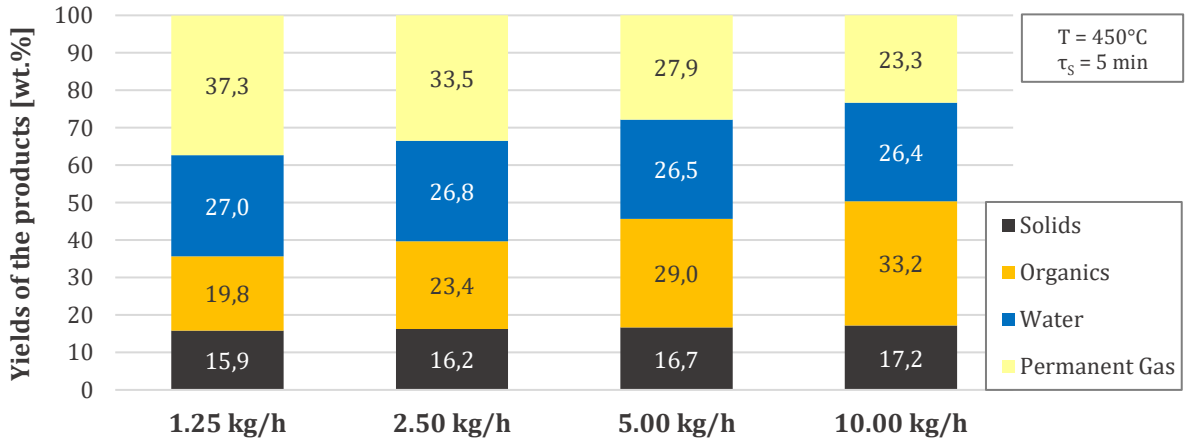

Figure 62. Effect of the mass flow of the feedstock on the yields of the pyrolysis products.

Moisture content of the feedstock

The variation of the water content in the feedstock was evaluated in the simulation model to account for the effect of the drying on the yields of the pyrolysis products. Biogenic feedstock, such as wood, present a seasonal variable water content, which may influence the overall performance of the pyrolysis system and particularly the heat requirements. The simulations were carried out with a reactor temperature of 450°C, a residence time of the solids of 5 minutes and a constant mass flow rate of 5 kg/h on as received basis. The results of the yields distribution are depicted in Figure 63 on as received basis. As expected, the yield of the char decreases with increasing water content on as received basis, due to the lower effective organic feedstock. However, the yield of the char is constant on a dry basis, indicating a negligible effect of the water content on the chemistry of the process. On the other hand, the pyrolysis vapors are strongly influenced by the water content. The increase of the water content leads to an overall increase of the condensate, but to a reduction of the condensable organics. However, higher water contents increase the volumetric flow rate of the vapors reducing their overall residence time decreasing the effect of the secondary gas phase reactions, which lead to the further conversion of the organics into permanent gas (see the carbon balance in the Appendix). Therefore, the yields of the permanent gas are reduced by increasing the moisture content of the feedstock. Finally, the heat requirements of the reactor increase by 35% from a water content of 10 wt.% to 20 wt.%. These considerations should be taken into account during the design and thermal integration of a pyrolysis-based facility.

The ash content has the opposite effect on the yields of the pyrolysis products (see the Appendix).

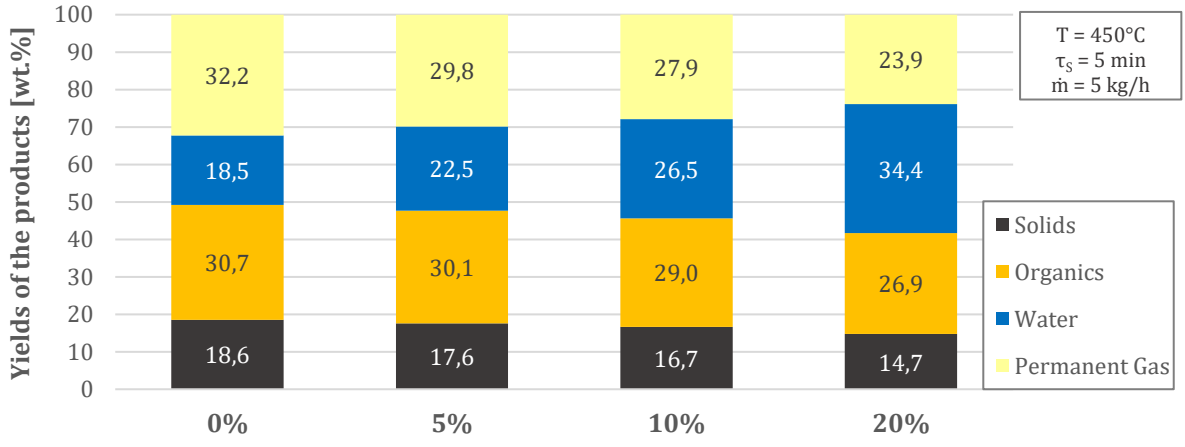

Figure 63. Effect of the water content of the feedstock on the yields of the pyrolysis products on wt.% as received basis.

Different biomass

A set of simulations were carried out varying the composition of the feedstock in terms of ash content and share of the model compounds cellulose, hemicellulose and lignin. No differentiation in the

assumptions were taken with respect to the water content (10 wt.% of the feedstock) as well as to the physical properties of the solid particles.

The compositions of the different feedstock (Table 40), excluding the own values for beech wood, were taken from the available data in the scientific literature [218, 219].

Table 40. Ash contents (wt.% on dry basis) and chemical compositions (wt.% on daf) of the selected feedstock.

	Ash [218]	**Cellulose** [219]	**Hemicellulose** [219]	**Lignin** [219]
Beech Wood	**1.0**	43.1	**35.7**	**21.2**
Wood bark	**7.8**	**25.2**	30.3	**44.5**
Wheat Straw	6.4	**44.5**	33.2	22.3
Coconuts Shells	3.2	40.3	**27.8**	31.9

The results of the simulations are depicted in Figure 64. The feedstock with lower ash contents are characterized by lower yields of the solids, which contain quantitatively the mineral matter. Moreover, a higher share of lignin leads to higher yields of solids and lower yields of water. For example, wood bark presents notably lower yields of the condensable organics and water, which have to be related to the highest share of lignin and the lowest share of cellulose. It is worth noting that beech wood and wheat straw present very close yields of the products due to the almost identical chemical composition (Table 40). From the literature it is known that the mineral matter influences the decomposition of the feedstock, increasing the reaction rate that leads to higher yields of the solids, due to the formation of secondary char [231, 228, 176]. Catalytic activity of the mineral matter is not implemented in the model yet, but it should be one of the topics for its further extension.

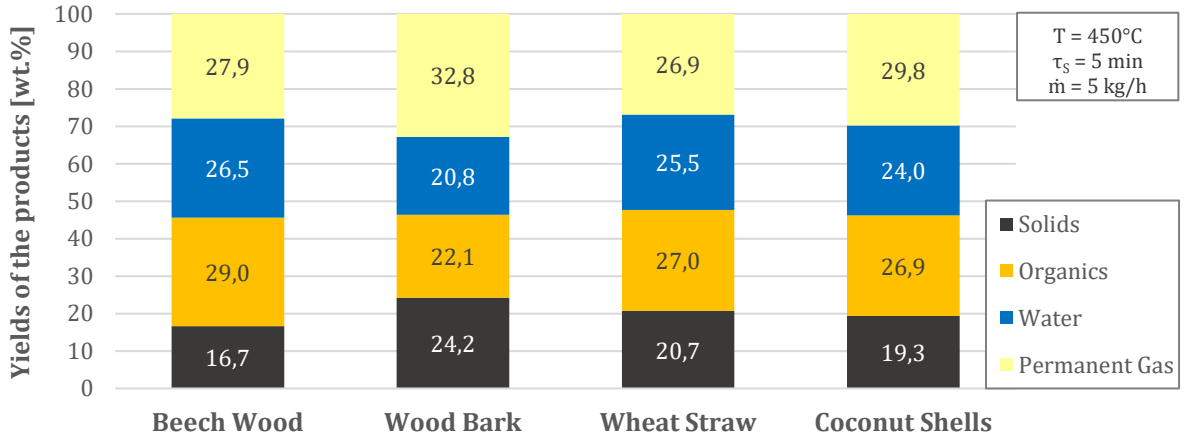

Figure 64. Yields on as received basis of the pyrolysis products from different biomass.

Enthalpy of reaction

Finally, the effect of the enthalpy of reaction was taken into consideration.

The enthalpy of reaction, also reported in the literature as heat of pyrolysis, was studied extensively in the literature for cellulose, hemicellulose and lignin. The estimation of the heat of pyrolysis has been controversial. Both endothermal as well as exothermal heat of pyrolysis have been reported [217, 64].

To avoid controversies, the enthalpy of reaction was firstly assumed to be neutral (h = 0 kJ/kg). In the following it was varied in the range of +100 kJ/kg to -250 kJ/kg, where plus indicates exothermal and minus endothermal reactions, respectively. Different from the other simulations, for the analysis of the effect of the enthalpy of reaction, the mass flow rate of the feedstock was set to 10 kg/h in order to better highlight the importance of this parameter.

The results of the simulations are depicted in Figure 65. Compared to the reference case the exothermal process leads to a lower yield of the solids and to a higher yield of the organics.

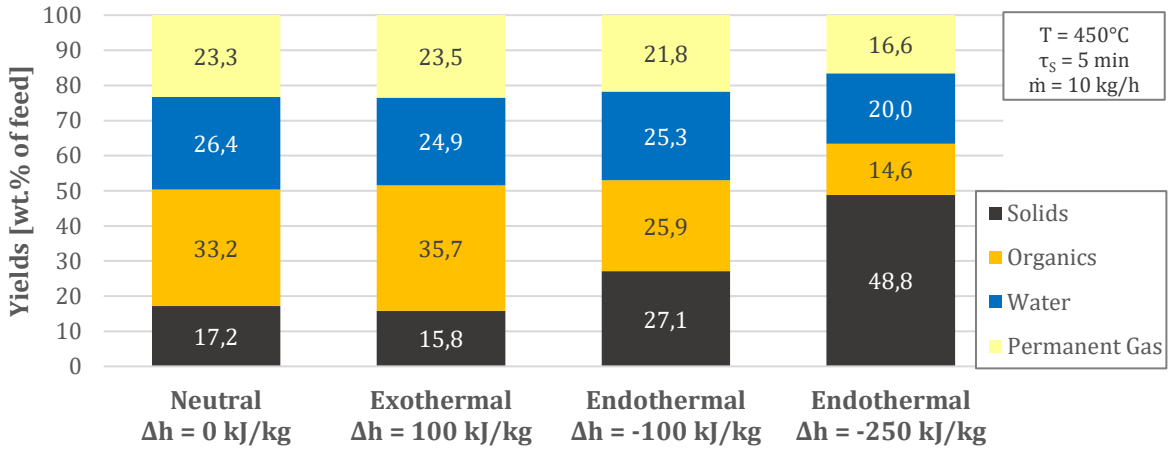

Figure 65. Effect of the enthalpy of reaction on the yields of the pyrolysis products.

The release of heat leads to a faster heating of the solids, which favors the reaction of fast pyrolysis of cellulose at the expenses of the carbonization reaction. However, the effects of an endothermal process are more pronounced. In fact, for an endothermal heat of pyrolysis of 100 kJ/kg, the variation of the yields of the solids and or of the organics is considerably higher than that for an exothermal process. The further increase of the enthalpy of reaction (h = -250 kJ/kg) would result in a further increase of the solids at the expenses of the vapors. A large amount of feedstock would be unconverted into the pyrolysis products, as depicted in Figure 66. The evident consequence is that the capacity of the reactor must be considerably reduced in order to obtain an exhaustive conversion of the feed.

It appears evident that the enthalpy of reaction is a fundamental parameter for a correct estimation of the yields of the products and of the total energy requirements of the pyrolysis reactor. In conclusion, precise evaluation of the enthalpy of reaction is mandatory for a successful process design.

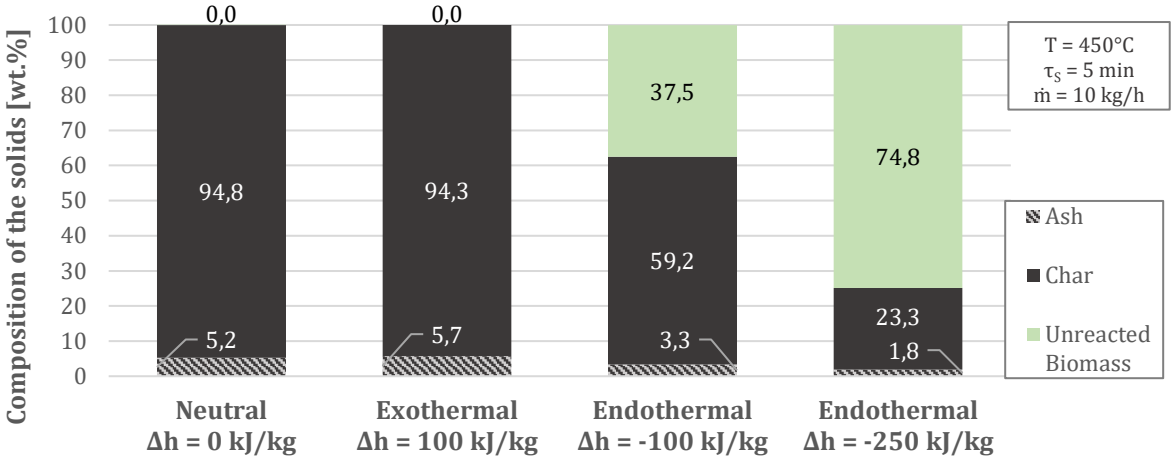

Figure 66. Effect of the heat of reaction on the final composition of the solids.

A comprehensive sensitivity study was provided in this section including the effects of the biomass physical parameters and of the process condition on the thermochemical processes taking place in a screw pyrolysis reactor.

It was shown that the physical properties of the biomass are the limiting factor for the heat transfer in a screw pyrolysis reactor. Increasing the offset reactor temperature is a suitable approach to increase the throughput for thermal processes but not for thermochemical processes, in which the temperature influences the yields and composition of the products. Mass flow rate and residence time of the solids should be considered in combination because of their strong influence on the vapors yields and composition. The composition of the feedstock is an important factor for the engineering of the reactor.

5.4 Experimental validation

In order to validate the model, a number of experiments were carried out at the STYX reactor and at the cold transport reactor (see section 3.2). The approach to the verification of the model can be distinguished into two phases. In the first phase, experiments were carried out to validate the assumptions adopted for the reactor model, i.e. transport of the solids and of the vapors. In the second phase, targeted experiments were carried out at the STYX reactor to validate the main components of the heat and pyrolysis models. This section will follow a similar approach. First, the experimental results related to the transport of the solids and vapors will be discussed to ensure the plausibility of the adopted assumption. Secondly, the mechanisms of the heat transfer, the drying and the pyrolysis of the solids will be investigated along the axis of the screw for a selected number of parameters. Following, the homogeneous secondary gas phase reactions will be investigated adopting a similar approach, i.e. evaluating the evolution of the vapors along the axis of the reactor. In the final step, a comparison between the experimental results and the simulations will be carried out in terms of global mass balances as well as of compositions of the pyrolysis products.

5.4.1 Reactor model

The reactor model was evaluated in terms of the transport of the solids and of the gases along the axis of the reactor. Experiments were carried out to evaluate the residence time distribution as discussed in section 3.4.3 for the gases and for the solids, respectively.

Transport of the gases

The transport of the gases, i.e. the hydrodynamics of the gas phase, was investigated experimentally at the STYX reactor under inert conditions adopting a mixture of N_2 and CO_2 with different volumetric flow rates and a constant composition. The reactor was held at a constant temperature of 450°C; therefore, isothermal, steady-state conditions were assumed. Adopting the methodology of "step input", the concentration of CO_2 was increased without altering the total volumetric flow rate. The concentration of CO_2 was constantly monitored until the composition reached steady-state conditions. The mean residence time as well as the number of stirred tank reactors were subsequently calculated.

The results of the experimental evaluation for the six positions along the axis of the screw are reported in Figure 67 in comparison to the ideal models for a nominal flow rate of 40 l_N./min. The residence time has been normalized with respect to the mean residence time. See the Appendix for further details.

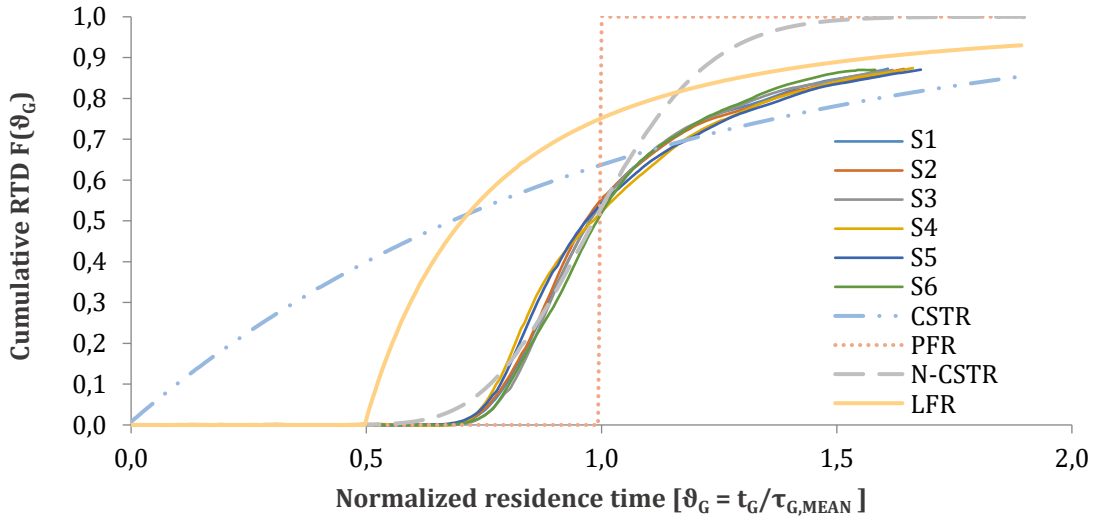

Figure 67. Cumulative residence time distribution of the gases for the six outlets in comparison to ideal models.

Figure 67 highlights that the experimental curves all have an identical behavior. About 50% of the cumulative residence time distribution is achieved at the average residence time, i.e. ϑ=1. A perfect steady state is never reached. Moreover, it is possible to see that the N-Series CSTR fits very well the experimental curves up to the average residence time. On the other hand, above 50% of the total conversion, the experimental curves lay between the CSTR and the LFR. This is an indication of the relatively large axial dispersion. According to Coker [49], the curves show the behavior of a system with dead space. For a further evaluation, the measured mean residence times at the six sampling positions are compared with the calculated space time considering only the freeboard and the total volume of the reactor. The calculated residence time has to be considered as the increment of the volume from the beginning of the reactor to the current position (see Equation 32 and Figure 26 in section 3.4.3). The results depicted in Figure 68 show that, for lower volumetric flow rates and for the first three sampling positions, the total volume of the reactor better approaches the measured values.

The gases are fed to the reactor at the inlet and must flow throughout the screw flights, possibly following the spiral shape. Along the axis of the reactor, moving closer to the outlet, the gases move upwards to the freeboard to minimize the pressure resistance. Therefore, the measured values for higher flow rates and closer to the reactor's tail are lower than the expected ones, if the total volume of the reactor is taken into account. On the other hand, the measured mean residence times become closer to the space time values for the volume of the freeboard. The difference between the calculated freeboard space time and the measured mean residence time is lower with increasing flow rates. See the Appendix for additional validation related to the Reynolds and Bodenstein numbers.

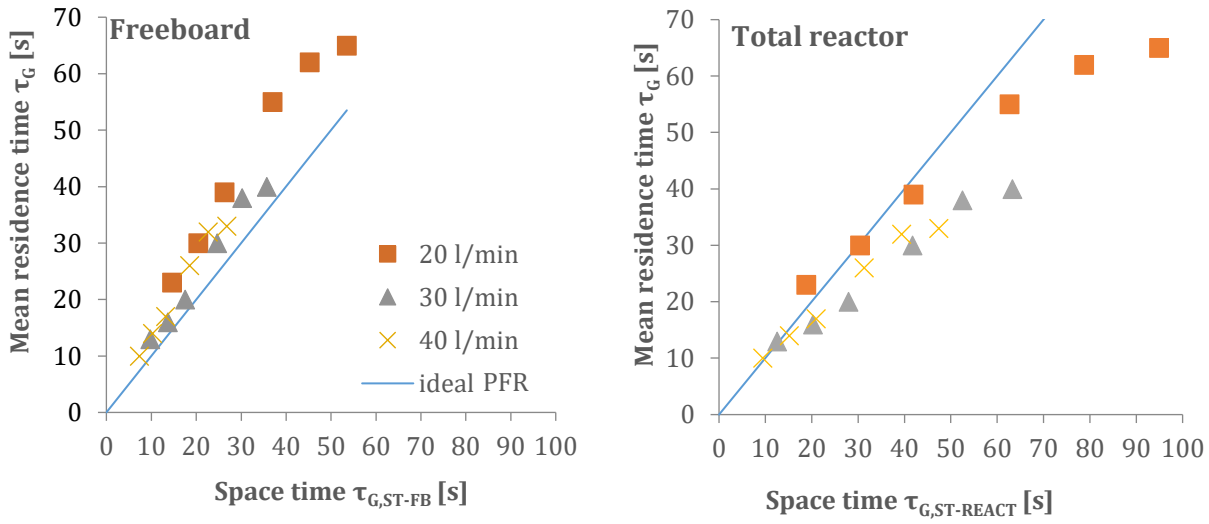

Figure 68. Comparison of the measured mean residence time and the calculated space time considering only the freeboard volume (left) and the total reactor volume (right). See also Equation 32 in section 3.4.3.

Therefore, the application of the axial dispersion model or the N-series CSTR appears to be the most suitable approach to describe the flow of the gases at the STYX reactor.

Transport of the solids

The transport of the solids was investigated experimentally in order to determine the appropriate reactor model for the screw reactor STYX. Preliminary experiments were carried out at the transport reactor to evaluate the following conditions:

- Qualitative visualization of the involved mechanisms and of the mixing of the particles in the single compartment;
- Mechanical limits in terms of maximum flow rate.

The transport mechanisms involved during the moving of bulk solids in a screw are visualized in Figure 69 and Figure 70 for lower and higher DoF, respectively.

At low DoF (Figure 69) and depending on the particle size, the main mechanism of backflow was the "slip". In such situation, the particles flow back passing through the clearance between the flight of the screw and the wall of the reactor. At constant speed of revolutions, the effect decreases with increasing mass flow rate. The ratio between the free surface and the total surface occupied by the material decreases. Therefore, a lower fraction of the total material can flow back. Consequently, at fixed mass flow rate, the increase of the speed of revolution increases the ratio of the free surface to the total surface. With further increase of the mass flow rate (middle DoF in Figure 49 b), the second effect becomes prominent. The flowback increases due to the bridge-building, as visualized in Figure 70. The granular material flows back passing above the core of the screw. It falls down on the other side of the flight and accumulates in the next pitch.

Figure 69. Granular material transport without bridge-building.

Figure 70. Granular material transport with bridge-building.

The overflow starts affecting the flow behavior once the bridge is formed and stabilized, and increases with increasing volumetric flow rate. This effect limits the maximum allowed flow rate. In fact, once the limit is reached, the screw starts acting as a feeder and regulated itself, as it is depicted in Figure 71. For a system made of a screw conveyor as the main reactor and a dosing unit, the mass flow limit provided by the self-regulation should not be exceeded in order to avoid accumulation of bulk material in the connecting pipe and consequently a blockage of the feeding (Figure 72). The maximum capacity has to be determined and expressed in terms of DoF.

Figure 71. Transitory to feeder modus of the screw.

Figure 72. Excessive load of the screw.

For this purpose, some trials were carried out at the transport reactor adopting beech wood granulates, slowly increasing the DoF, i.e. the dosed mass flow, from 9% (Figure 69) to 87% (Figure 72). However, for the selected speed of rotation of the screw, the mass flow stabilized to a fixed value corresponding to a DoF of 68%. Such DoF represents the value, which is established in the feeder modus and it is much higher than the suggested maximum DoF of 30% for screw conveyors with pure transport purposes [60].

The qualitative mixing of the particles in a single compartment was observed introducing colored particles in the bulk and its behavior constantly visualized with a camera until the colored particles completely disappeared in the bulk. An example is provided in the Appendix. The internal mixing is positively influenced by increasing the rotational speed, while the effect of the mass flow was of

minor importance. Therefore, the utilization of the Froude number (Equation 38 in section 5.2.3) for stirred tanks appears a suitable approximation in order to account for the mixing in a screw compartment.

In order to characterize the residence time distribution (RTD) of the STYX reactor, a set of experiments was carried out. Table 41 reports the results. The theoretical background of the RTD evaluation is reported in the Appendix.

Table 41. Results of the transport of the solids.

Experiment	Mass Flow [kg/h]	Rotational speed [rpm]	Geometric residence time oven [min]	Geometric residence time screw [min]	DoF [%]
1	2	5.00	5	5.65	2.25
2	2	2.50	10	11.25	4.50
3	2	1.25	20	22.50	9.00
4	4	2.50	10	11.25	9.00
5	8	2.50	10	11.25	18.00
6	4	5.00	5	5.65	4.50
7	8	5.00	5	5.65	9.00

Experiment	Time Step [s]	$\tau_{S,MEAN}$ [s]	$\tau_{S,MEAN}$ [min]	N-CSTR [-]	Peclet [-]
1	1.475	412	6.9	279	558
2	1.517	760	12.7	501	1002
3	3.578	1351	22.5	378	756
4	1.683	746	12.4	443	886
5	1.783	748	12.5	419	838
6	1.285	398	6.6	310	620
7	0.932	390	6.5	418	836

The cumulative RTD for all the experimental conditions is depicted in Figure 73 as a function of the normalized mean residence time, as defined in section 3.4.3. It is shown that for every experimental condition, the cumulative RTD lays in a range of ±10% of the normalized mean residence time. The results highlight that the transport behavior of the STYX reactor closely resembles that of a plug flow reactor. That is confirmed by the number of CSTRs (see Table 41).

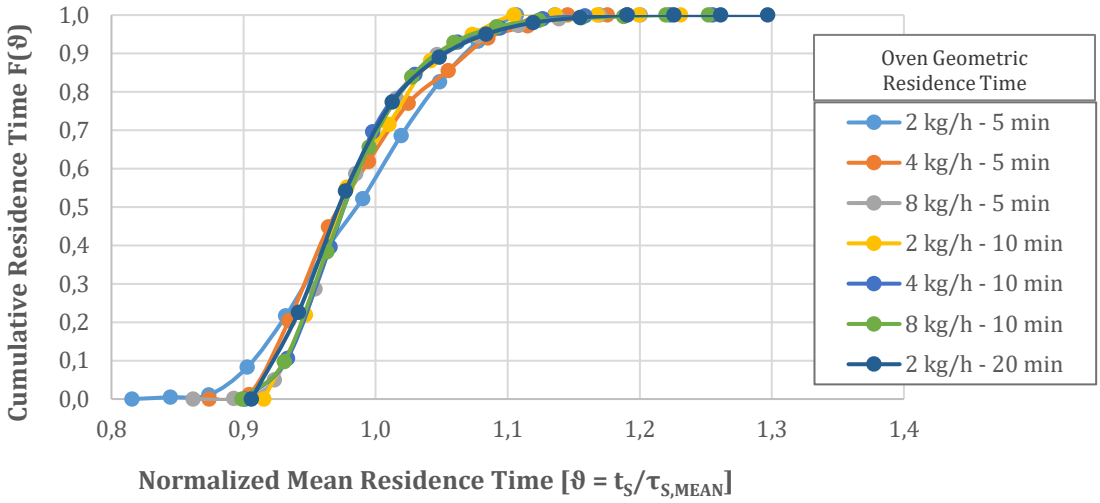

Figure 73. Cumulative residence time distributions of the bulk material under the selected operational conditions at STYX .

The time step in Table 41, i.e. the mean residence time divided by the number of CSTRs, is proportional to the inverse of the mixing quality. Using it as a reference, the increase of the mass flow rate has an interesting effect, which depends on the speed of revolution. At a low speed of revolution, the time step increases with the increase of the mass flow. At constant DoF or constant mass flow rate, an increase of the speed of rotation always leads to a decrease of time step. To resume, the mean residence time approximates at best the geometrical residence time for degree of fillings between 9% and 18%.

In conclusion, the adoption of an N-series of CSTRs as reactor model for the solids is confirmed by the extensive experimental investigations.

5.4.2 Thermo-physical processes of the solids

The validation of the thermo-physical processes involving the solids, i.e. heat transfer to the bulk and drying, was conducted for adopting inert feedstock, whose properties are reported in Table 9 in section 3.4.4 and compared to beech wood, as reference feedstock for the validation of the pyrolysis model.

Experiments were carried out at the STYX reactor and the selected process parameters were then introduced into the model for its validation.

Heat transfer in the granular solid

The heat transfer model was validated by means of heating granular inert and dry material. The adopted process parameters are reported in Table 42. The parameters allow maintaining the Degree of Filling (DoF) in a close range. The only major difference was the rotational speed, which is

expected to affect the mixing within the granular material, according to the Froude Number (see Equation 38).

Table 42. Parameters adopted for the experimental validation of the heat transfer model.

	Temperature [°C]	Residence Time [min]	Mass Flow Rate [kg/h]	Rotational Speed [rpm]	DoF [%]
1	450	5	16	5	13.6
2	450	10	10	2.5	17.0

Figure 74 depicts the results of the simulations in comparison with the experimental results. An average heating rate of about 200 K/min was achieved for both process conditions, corresponding to the range of the typical heating rate for intermediate pyrolysis [102]. The effective heat transfer coefficient (α_{EFF} in Equation 60) was below 30 W/m^{2}K, indicating a low heat transfer within the granular bed. The measured temperatures at 0.55 m were slightly higher than the simulated ones. The colored dyes are applied to the surface of the particles, where the temperature is higher than that at the core. Therefore, a slight overestimation of the measured temperature cannot be completely excluded. At the second sampling position, the measured temperatures already reached the offset temperature. Measurements and simulation converged at the last sampling position. The differences between the measured and the simulated temperatures can be assigned to both experimental issues, i.e. measuring the temperature of a bulk solid, as well as to the model. The coefficients C and x in Equation 37 adopted for the simulations were taken for rotary drums, thus deviations in the mixing number and stagnant period may be expected. The flights and the shaft may influence the internal mixing and the heat exchange within the granular bed.

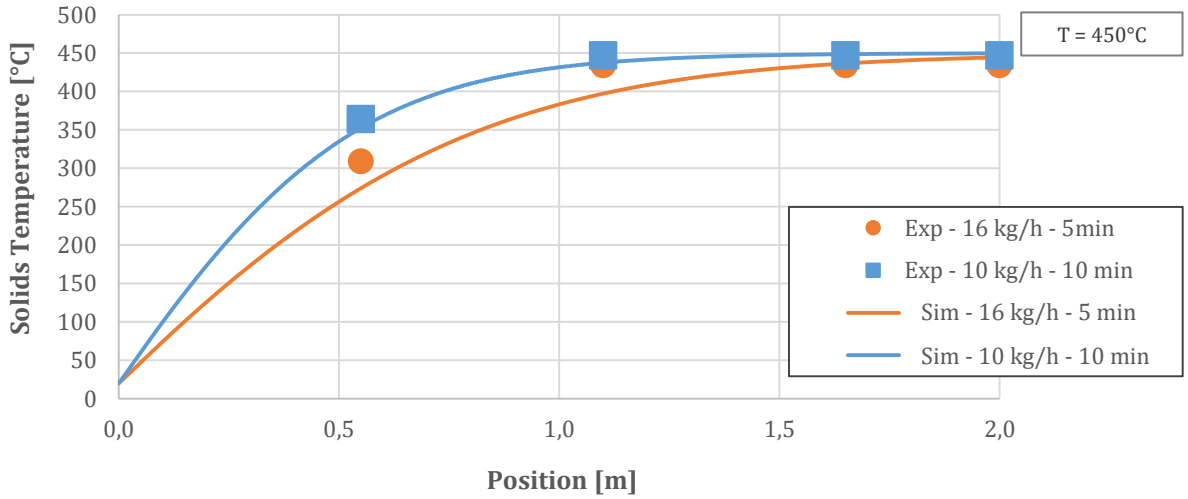

Figure 74. Comparison of the simulated temperature profiles and the experimental results at STYX.

Drying of the granular solids

The drying of porous inert material was investigated adopting clay granulates. The material was dried at 80°C for a week as reported in chapter 3.4.4 before further being moistened to the desired content of 30 wt.%. The process parameters are reported in Table 43.

Table 43. Parameters adopted for the experimental validation of the drying model.

	Temperature [°C]	Residence Time [min]	Mass Flow Rate [kg/h]	Initial Moisture [wt.%]
1	400	2.5	3	30
2	400	2.5	6	30
3	400	2.5	9	30

Experiments were carried out varying the mass flow rate from 3 kg/h to 9 kg/h in order to stretch the drying process along the full length of the reactor. Samples were taken along the reactor axis at four positions. The first position (S0 in Figure 16) was just before the insulation layer of the oven and used to control the initial water content of the bulk bed. Simulation were carried out setting the initial water content equal to the one measured at the first sampling position. The comparison between the simulations and the experimental results is depicted in Figure 75. At 0.55 m, for a mass flow rate of 3 kg/h, the measured water content was 3.4 wt.%, while the simulation predicted a completely dried solid. The simulations overestimated the water content for all the other measured points. In accordance to the results related to the heating of a dry inert material, the simulated process is slower. Again, the deviation may be assigned to the mixing quality of the material. The stagnant period t_R of Equation 35 is overestimated and the experimental mixing is better than the simulated one. However, the measured water content may be slightly underestimated because the recovery of hot drying granular material in continuous operation would require an active quench to freeze the water content of the sample. Taking into consideration the mentioned issues, the results of the simulations are very satisfactory.

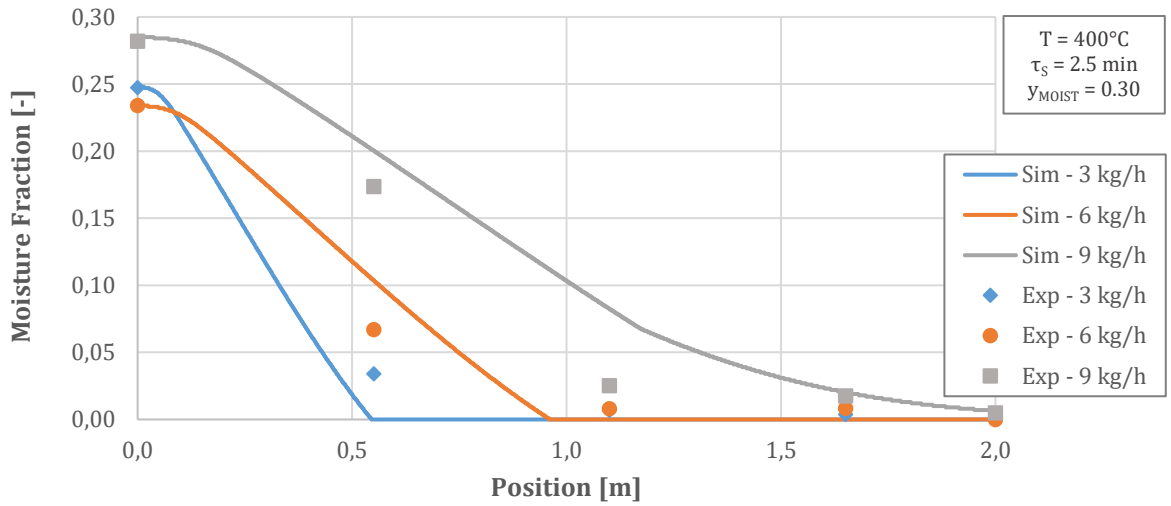

Figure 75. Simulated water fraction profiles of the solids along the reactor in comparison to the experimental results.

5.4.3 Conversion of the solids

The pyrolysis of beech wood was investigated along the axis of the reactor in order to verify the capability of the model in describing the evolution of the primary decomposition of the solids under a range of process conditions. The chemical composition of the feedstock was modelled as weighted sum of the main model compounds of biomass as reported in Table 6 in chapter 3.1.1. The water content was 10 wt.%.

The following parameters have been considered:

- Offset temperature of the reactor;
- Residence time and mass flow of the solids;
- Particle size of the solids.

The results are reported in terms of yield of the solids in wt.% of the feedstock on as received basis as a function of the position along the reactor, adopting the procedure described in section 3.3.1. Beech wood KL 1-4 was adopted for the experimental investigations where not otherwise stated.

Offset temperature of the reactor

The effect of the offset temperature of the reactor was investigated experimentally at the STYX reactor (see Figure 16) in the range of typical pyrolysis temperatures at constant residence time and mass flow rate of the solids (Table 44).

Table 44. Parameters adopted for the variation of the offset temperature.

	Temperature [°C]	Residence Time [min]	Mass Flow Rate [kg/h]
1	400	10	2
2	450	10	2
3	500	10	2

The simulated results from Figure 76 show that the decomposition of the solid at 500°C is almost instantaneous, taking less than 0.2 m to be completed. At the first sampling point, the experimental decomposition of the feedstock was already completed; in fact, the yield of the solids do not present further decrease from the sampling point at 0.55 m to those at 1.1 m, 1.65 m and 2.0 m. A similar trend is highlighted also for the results at 450°C. The simulation (55.0 wt.%) and the experimental yields (55.9 wt.% ± 8.2 wt.%) at 400°C correlate very well at the first sampling point (S2). The conversion of the solids is also completed at the second sampling position for both the simulation and the experiments. The final yield of the solids is generally underestimated by the model. In fact, the chars obtained experimentally contain volatile matter, which reacts at more elevated temperatures. On the other hand, the pyrolysis model describes the solid as pure carbon.

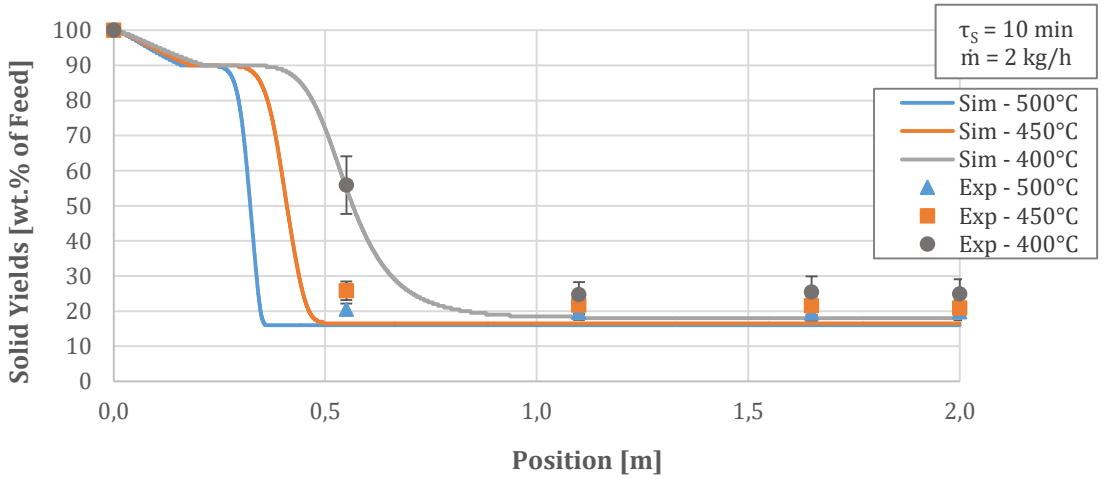

Figure 76. Comparison of the simulated profiles and the experimental yields of the solids as function of the temperature of the reactor.

Residence time and mass flow of the solids

The profiles of the solid yields along the axis of the reactor were investigated for a set of mass flow rates and residence times of the solids at 450°C.

Table 45. Parameters adopted for the combined variation of residence time and mass flow rate.

	Residence Time [min]	Mass Flow Rate [kg/h]	Temperature [°C]
1	5	2	450
2	5	4	450
3	10	2	450
4	10	4	450

The results are shown in Figure 77. Since the pyrolysis process is completed in all the simulations and experiments before reaching the sampling point at 1.1 m, only the results at the first sampling point (0.55 m) will be discussed. The model is generally able to predict the yields of the solids. The deviations were below 5 wt.% in all the cases.

Only experiment 1 (5 minutes and 2 kg/h) presented a large difference at the sampling point at 0.55 m. On the one hand, the samples recovered under these process conditions may be not representative, i.e. due to the relative small amount of material in the screw large deviations in the compositions can be expected. On the other hand, the reaction rate is strongly influenced by the particle size and by the reaction enthalpy Δh_{pyro} in Equation 49, which is assumed neutral as first reference in this model. On the one hand, the reaction rate of the simulated pyrolysis process would be slowed down under the assumption of endothermal reactions. Moreover, the estimation of the kinetic parameters was carried out under TGA conditions and mass transport effects within the particles pores may be neglected although also heating rates as high as 1000 K/min were adopted. The transport resistance within the particle is known from the literature to reduce the reaction rate at heating rates typical of intermediate and fast pyrolysis [61]. The profile of the solid yields along the reactor in comparison to the experimental yields further confirms that the chemical reactions model, i.e. the chemical equation and kinetics, still requires improvements.

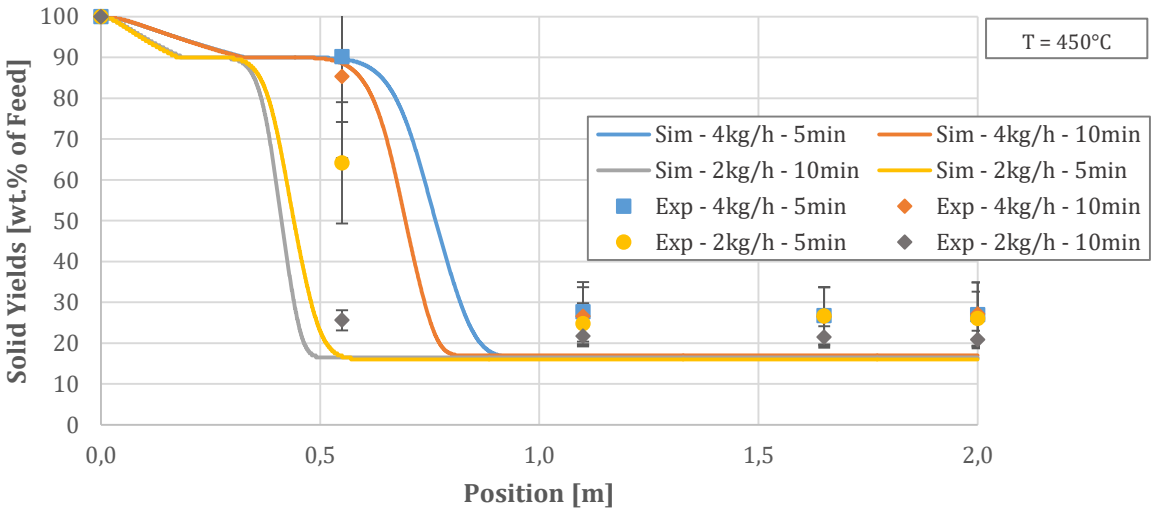

Figure 77. Comparison of the simulated profiles and the experimental yields of the solids for varying mass flow rate and residence time at 450°C

Particle size of the solids

The effect of the particle size of the solids was investigated using beech wood of three different particle sizes, i.e. 0.5 mm, 1.5 mm and 1.9 mm. The size of the particles is referred to the smallest of the dimensions, which is the critical one in terms of heat transfer. The set parameters are reported in

Table 46. The results are depicted in Figure 78 and are compared with the simulated solid yields profiles.

Table 46. Parameters adopted for the variation of the particle size of the feedstock..

	Particle Size [mm]	Temperature [°C]	Residence Time [min]	Mass Flow Rate [kg/h]
1	0.5	450	2.5	3
2	1.5	450	2.5	3
3	1.9	450	2.5	3

Generally, the simulations fit well the experimental results. However, the measured solid yield at 0.55 m for a particle size of 0.5 mm is not reliable due to issues related to the recovery of the sample. As described in section 3.2.5, the solid samples are recovered at the bottom of the sampling position. The samples are expected to fall down into the sealed recovery flask. However, the method is not suitable for such small particles before conversion into more flowable carbonized solid.

Moreover, the model was not able to predict correctly the conversion of the largest particle size. In fact, the conversion was incomplete at 1.1 m. The experimental results confirm the analysis based on the Biot and Pyrolysis numbers, which indicated a thermally thick regime for all the particle sizes. See Figure 12 for the regimes and the appendix for details related to the analysis of the dimensionless numbers.

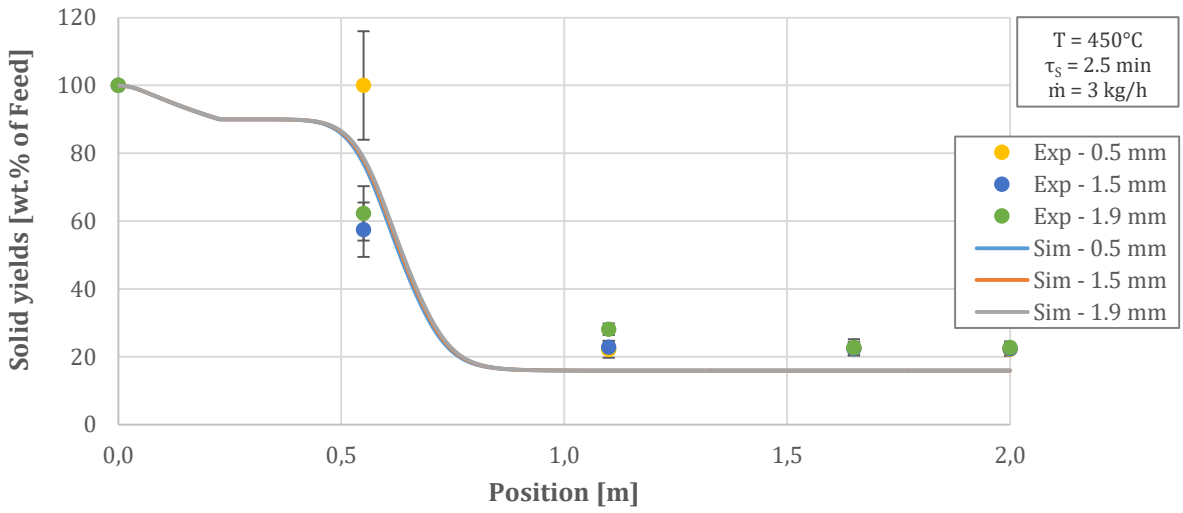

Figure 78. Comparison of the simulated profiles and the experimental yields of the solids for different particle sizes of the feedstock.

5.4.4 Secondary gas phase reactions

On the contrary to the previous section, the target of this one is to assess the secondary gas phase reactions along the main axis of the reactor. The secondary gas phase reactions have been investigated experimentally at the STYX reactor at 450°C and 500°C. For the experiments, the process parameters residence time and mass flow rate of the solids were set with the aim of completing the decomposition of the feedstock into char and vapors just before the first sampling point of the vapors. See the Appendix A.4.6 for further details.

The yields of the condensable organics and of the water and reaction water at 450°C are depicted in Figure 79 and Figure 80, respectively. At the first sampling position, i.e. at 0.15 m from the inlet, the simulation fails to reproduce the experimental results. In fact, only the moisture water was already released into the vapor phase, while the experiments show a complete decomposition of the feedstock for a yield of the condensate, which is given by the sum of the condensable organics and water. The simulation is able to reproduce the decreasing trend of the condensable organics but the yield is continuously overestimated by the model. On the contrary to previous literature, the experimental results obtained at the STYX reactor show that the secondary gas phase reactions are not completed even after more than 30 seconds [97]. The reaction rate of the secondary gas phase reactions, i.e. the variation of the yields between two successive sampling positions, is also overestimated by the model. The yield of the reaction water (Figure 80) increases with increasing residence time of the vapors with close reaction rates for the simulation and the experiments. The yield is slightly underestimated by the model.

The yields of the main permanent gases are reported from Figure 81 to Figure 83. It is shown that the carbon dioxide is well reproduced by the model in terms of yields and of yield variation along the screw. Carbon monoxide is generally underestimated by the model but the CO yield increases faster in the simulation. On the other hand, the yield of CH_4 obtained in the simulation is higher by a factor 3 in comparison to that from the experimental investigations. The overestimation of the yields of the non-condensable hydrocarbon is a major issue of the pyrolysis model. However, since the measured and the simulated yields trends are comparable, the issue of the model is mainly related to the selectivity of the hydrocarbons, which appears to be higher than the experimental one. The mass and the carbon balances from the experimental investigations (see chapter 4.1.1) show that a consistent amount of carbon is converted into secondary char, or soot, and recovered on the surface of the filters. Therefore, future work should focus on the improvement of the chemical equation related to the secondary gas phase reactions, taking into account the formation of secondary char.

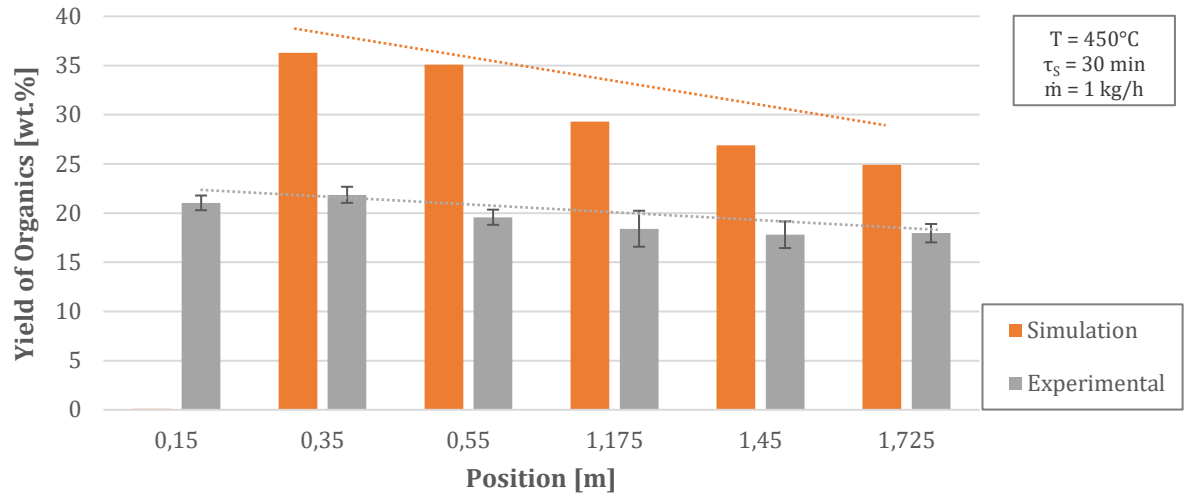

Figure 79. Validation of the yields of the condensable organics along the axis of the reactor.

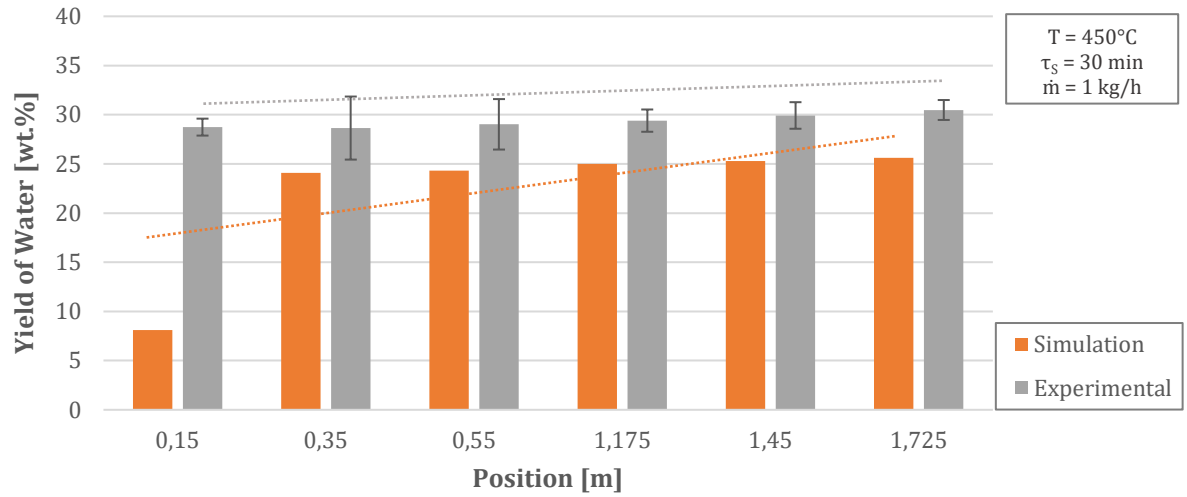

Figure 80. Validation of the yields of moisture and reaction water along the axis of the reactor.

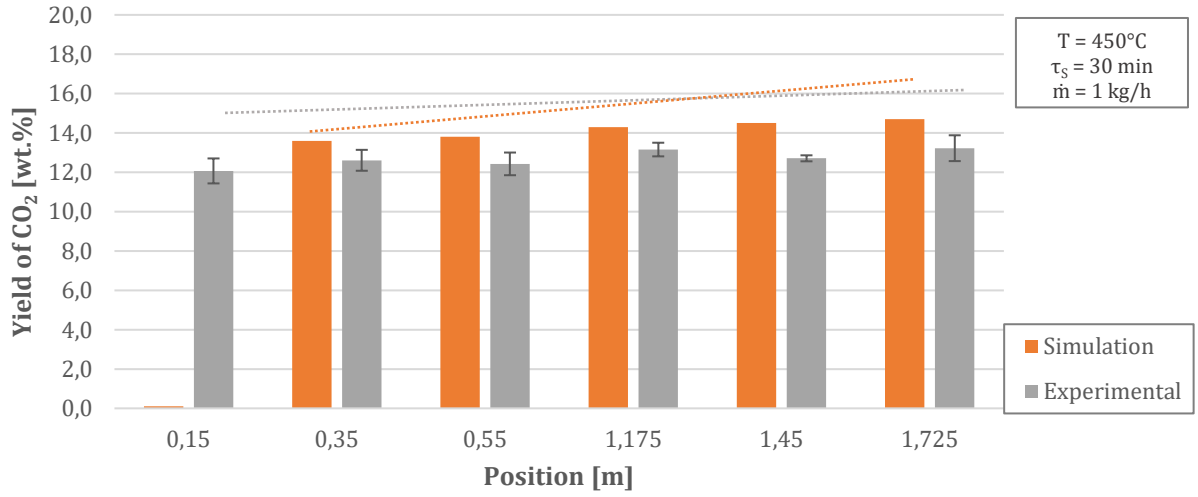

Figure 81. Validation of the yields of CO_2 along the axis of the reactor.

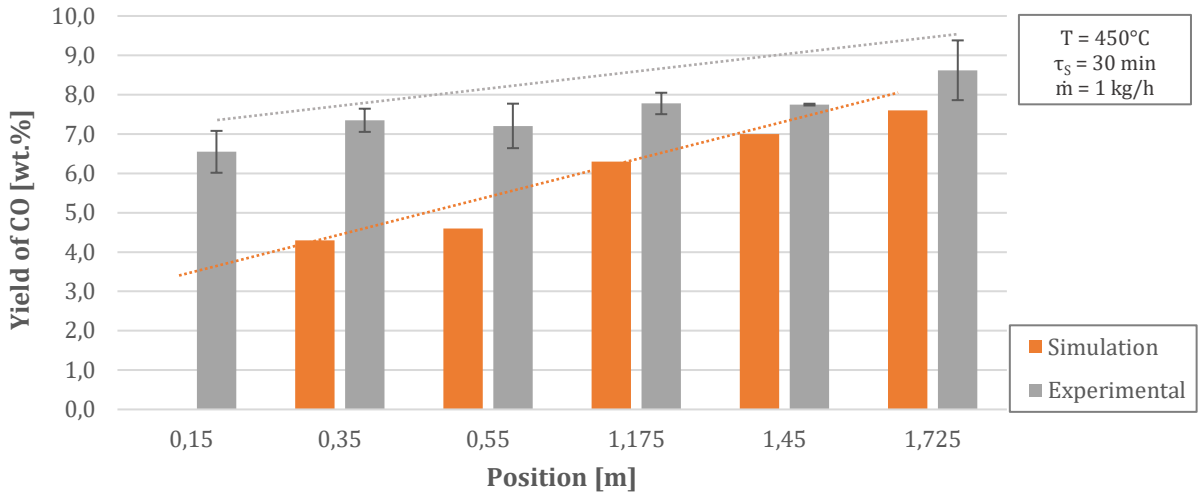

Figure 82. Validation of the yields of CO along the axis of the reactor.

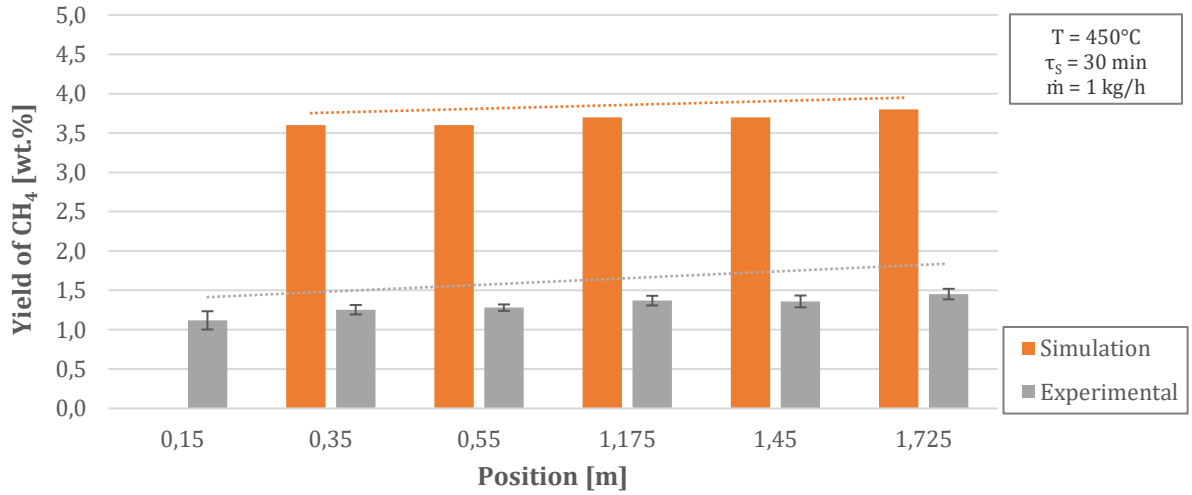

Figure 83. Validation of the yields of CH_4 along the axis of the reactor.

The comparison of the experimental results with the simulation at 500°C leads to results close to the ones just discussed for the secondary reactions at 450°C with the exception of water.

The results are reported in Figure 84.

The simulated trend shows an increasing yield, while the experimental trend presents a decreasing yield of water. Although the experimental standard error is quite high at 0.15 m, the experiments give evidence that water is reduced along the reactor with increasing residence time. At 500°C, reactions such as the water gas shift under atmospheric pressure and steam reforming of oxygenated hydrocarbons may play a role during the pyrolysis of wood. The evaluation of CO and CO_2 gives contradicting results; thus, it is not possible to report conclusive considerations. Morf et al. report similar observations for temperatures of 600°C and higher [148]. However, the yields of water

increased at 500°C after homogeneous secondary reactions. Similar results were presented in a previous work by Boroson et al. [26]. The implementation of the gasification reactions would be an interesting extension of the model in the case a broader range of temperatures is to be taken into account.

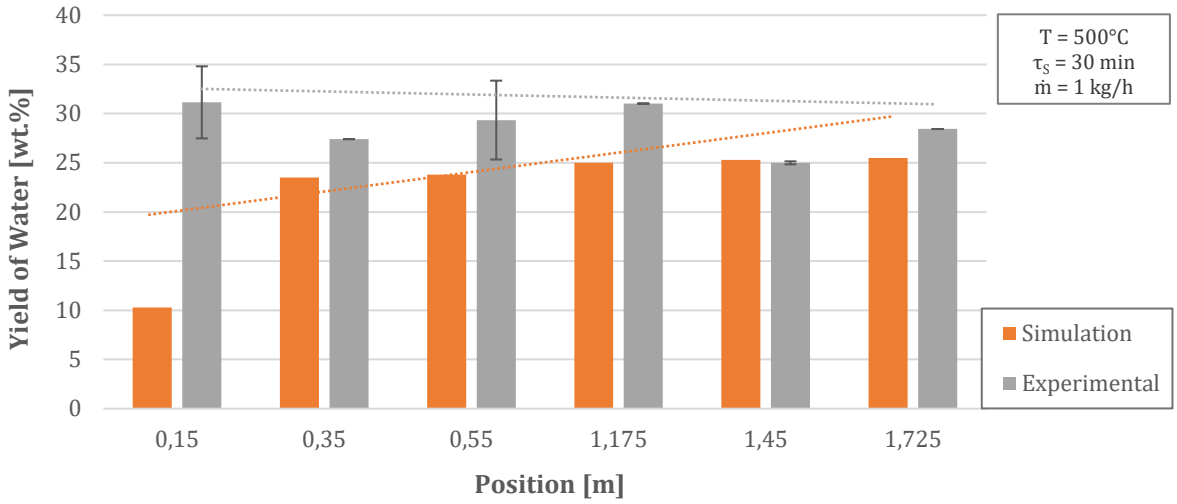

Figure 84. Validation of the yields of moisture and reaction water along the axis of the reactor at 500°C.

The secondary homogeneous gas phase reactions were modeled as reported in section 5.2.5 and validated for selected process conditions. The selected kinetics appear to fit well the experimental results in most of the cases; however, the yields of the hydrocarbons are not represented well in the model. Therefore, the chemical equations require further improvements. In particular, the formation of soot should be taken into account as a by-product of hydrocarbon formation, whose yields would be reduced by such adjustment and better represent the real mechanisms involved in secondary gas phase reactions.

5.4.5 Global mass balance and products compositions

In this final section of the chapter, the target is to evaluate the overall pyrolysis process of beech wood at the STYX reactor. An example for the reference process conditions will be discussed and followed by the analysis of the mass balances and of the products compositions for the all range of pyrolysis temperatures.

Reference Conditions

Table 47 reports the process parameters adopted for the reference conditions. Beech wood (see Table 6 for the composition) was used as reference feedstock.

Table 47. Reference process parameters adopted for the validation of the overall pyrolysis at STYX reactor.

Offset Temperature	450	°C
Residence time of the solids	5	min
Mass flow rate of the solids	4	kg/h
Volumetric flow rate of the purge gas	10	l_N/min
Inlet temperature of the solids	20	°C
Inlet temperature of the purge gas	20	°C

The results of the simulation are reported in Figure 85 as a function of the position along the reactor. The yields of the pyrolysis products on a received basis, as well as the temperatures of the solids (T_S in Figure 50) and of the main gas stream (T_G in Figure 50) are depicted in Figure 85. After the drying step, the temperature of the solids increased with a heating rate of about 250 K/min up to the offset temperature of the reactor, confirming the intermediate pyrolysis conditions [102]. The temperature of the purge gas increased quickly to about 400°C but the temperature of the reactor was achieved only at the tail. The mass flow of the solids decreased in the first 0.35 m of the reactor, where the drying took place. The pyrolysis process, i.e. the decomposition of the feedstock, was completed within the first section of the reactor leaving unexploited a considerably large potential.

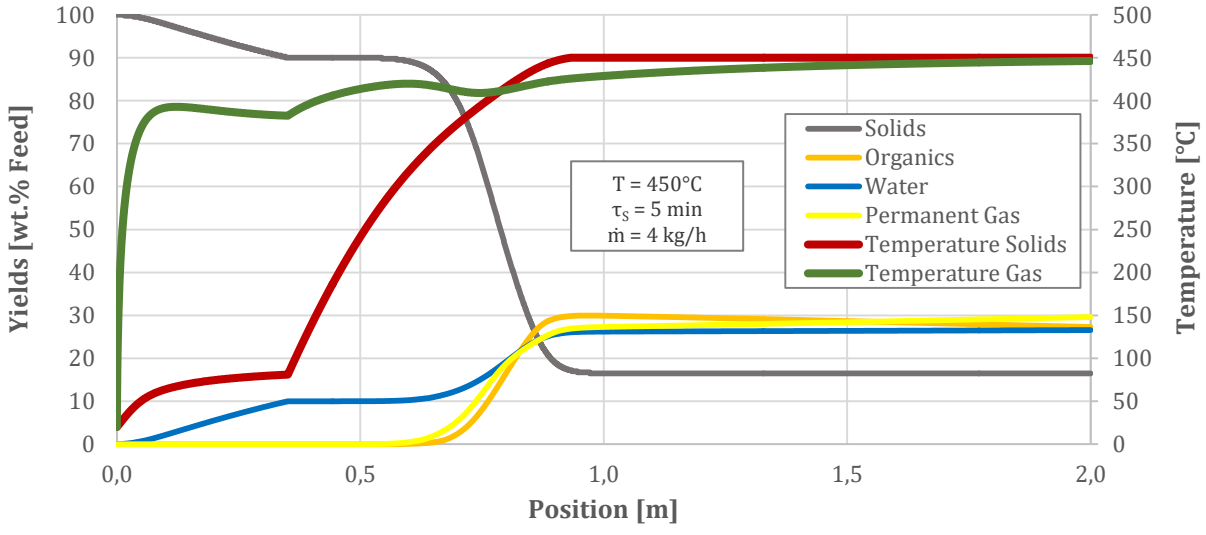

Figure 85. Simulation of the pyrolysis of beech wood at the STYX reactor.

The yield of water increased first during the drying and afterwards during pyrolysis, while secondary reactions contributed to a minor extent to the further increase of the yield of water. On the other hand, the condensable organics showed a maximum yield of 30 wt.% at 1 m, followed by a steady decrease. The total yield of the condensate was 53.9 wt.%. Finally, the non-condensable gases, or permanent gas, increased quickly during the primary decomposition and slightly increased because of the secondary reactions. Gas-phase reactions involving water steam, such as water-gas shift and steam reforming, were not taken into account in the model and therefore cannot contribute to the final distribution of the yields of the vapors. The final yields of the simulated process are reported in Table 48 and compared with the experimental results at the STYX reactor. For the execution of the experiment, only the filters at the tail of the reactor were used in order to obtain identical configuration and avoid the mixing of the vapors caused by the displacement of the filters. The yields of the condensable organics and of the water fit very well the experimental results. However, as already discussed in the previous sections 5.4.3 and 5.4.4, the yield of the char is underestimated, where the yields of the permanent gases are overestimated.

Table 48. Comparison of the simulated yields and the experimental results for the pyrolysis of beech wood at STYX

	Experimental (TM036)	**Simulation**
Char (solids)	20.4	16.5
Organics	26.8	27.3
Water	27.4	26.6
CO_2	9.0	14.3
CO	5.7	6.7
CH_4	0.8	3.6
C_{2+}	1.2	5.0
Loss	8.7	-

The compositions of the simulated products condensable organics and char are reported in Table 49 and Table 50, respectively. Additionally, the compositions of the products obtained experimentally are reported for a direct comparison of the products.

Table 49. Comparison of the simulated and the measured compositions of the condensable organics (wt.% dry).

	Experimental (TM036)	**Simulation**
C	53.0	54.4
H	5.8	7.1
O	41.2	38.5

While the composition of the simulated condensable organics fits exceptionally well that of the selected experiment, the composition of the simulated solid, i.e. of the char, does not well replicate

that obtained experimentally. In fact, the kinetic model does not take into account the residual volatiles, which may be entrapped in the solid matrix or being released at higher temperatures. The total carbon of the simulated char (15.6 wt.% of the feedstock) is in good agreement with the fixed carbon of the experimental char (15.2 wt.% of the feedstock). About 23 wt.% of the recovered solids consist of volatile matter, which would react only at higher temperatures.

Table 50. Comparison of the simulated and the measured compositions of the char (wt.% dry).

	Experimental	Simulation
C	81.3	94.5
H	3.6	0.0
O	12.3	0.0
Ash	2.8	5.5
C_{FIX}	74.6	94.5
VM	22.6	0.0

Moreover, the model was developed to evaluate the global kinetics of pyrolysis and therefore does not take into account the secondary reactions occurring within the particle matrix, but uses the competitive reactions (cellulose fast and slow) to address the effect of the heating rate. In order to improve the prediction capability of the model, a particle model would be required to improve the coupling of the heat transfer to the reaction kinetics. In such a way, it would be possible to consider the reactions taking place within the pores of the biomass particle, which further alter the structure of the solids. Taking into account the mentioned issues of a continuous model, the accordance between the experimental results and the simulations is acceptable for a first estimation of the yields and elemental compositions of the pyrolysis products.

Effect of the temperature on the pyrolysis of beech wood

The effect of the offset temperature of the reactor was investigated experimentally for validation of the model. The process parameters are reported in Table 51. Yields and compositions of the pyrolysis products were compared.

Table 51. Parameters adopted for the variation of the offset temperature.

	Temperature [°C]	Residence Time [min]	Mass Flow Rate [kg/h]
1	350	10	2
2	400	10	2
3	450	10	2
4	500	10	2

The experimental results have been already discussed in detail in chapter 4. The comparisons are depicted in Figure 86. The simulations are able to reproduce the trend of decreasing yield of the solids;

however, they always underestimate the yield for the reasons discussed in the previous section. The experimental yield of the organics present a maximum value at 400°C and then decreases. The simulations reproduce the trend very well with absolute differences below 1 wt.%. The largest difference between the experimental and the simulated yields of the organics was obtained at 350°C, where the carbonization reaction of cellulose leads to no release of organics underestimating the yield. The model is able to well predict the effect of the secondary gas phase reactions (see Table 31), which become predominant in the range of temperatures between 450°C and 500°C [97].

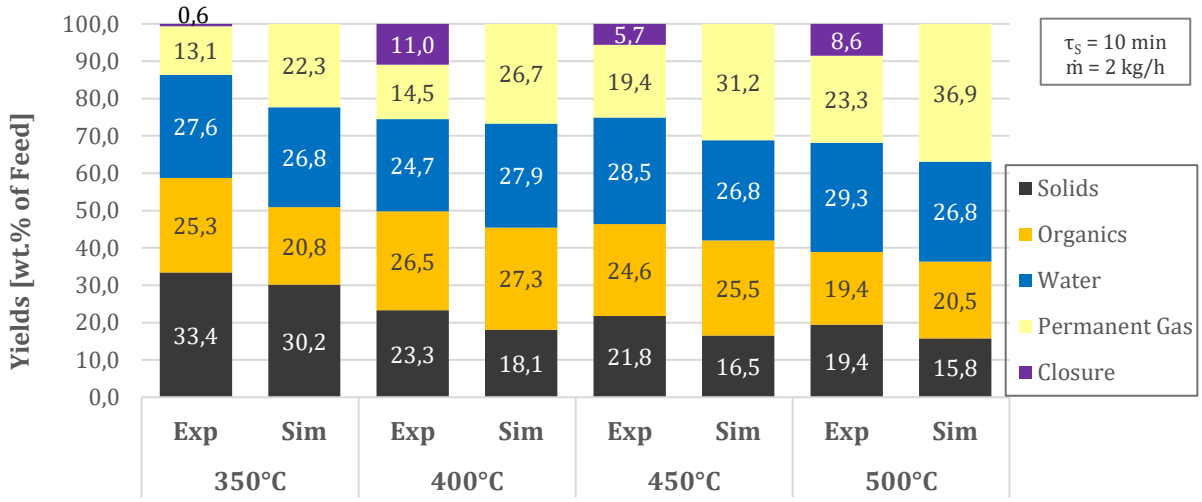

Figure 86. Comparison between the simulations and the experimental results at STYX. Yields of the products as function of the temperature of the reactor, on as received basis.

The yield of water presents a peak at 400°C in the simulations, but it remains overall stable along the all range of temperatures. The largest deviation from the experimental results was obtained at 400°C. The comparison for the gases was not as good as for the condensate. The model overestimates the yields of the permanent gas. However, the increasing trend from low to high temperature is correctly predicted. In order to provide a more detailed evaluation of the permanent gases, the yields of the non-condensable compounds are reported graphically in Figure 87. All the simulated yields are overestimated in comparison to the experimental results. The deviations for CO and CO_2 are about 4 wt.% maximum. The model greatly overestimates the yields of methane and of C_{2+} hydrocarbons. The selectivity to hydrocarbons is one important issue of the pyrolysis model (see Table 30 and Table 31). Another important issue is given by the formation of the filter cake. The literature reports the formation of polyaromatic hydrocarbons and of soot as a side reaction from the decomposition of the primary products from lignin, which leads to the formation of hydrocarbons and carbon oxides [13]. The yield of the filter cake is in the range of 2-4 wt.% of the feedstock, which roughly corresponds to the overestimation of the hydrocarbons. The reactions involving the soot formation were not implemented into the model and should be the focus of more fundamental work.

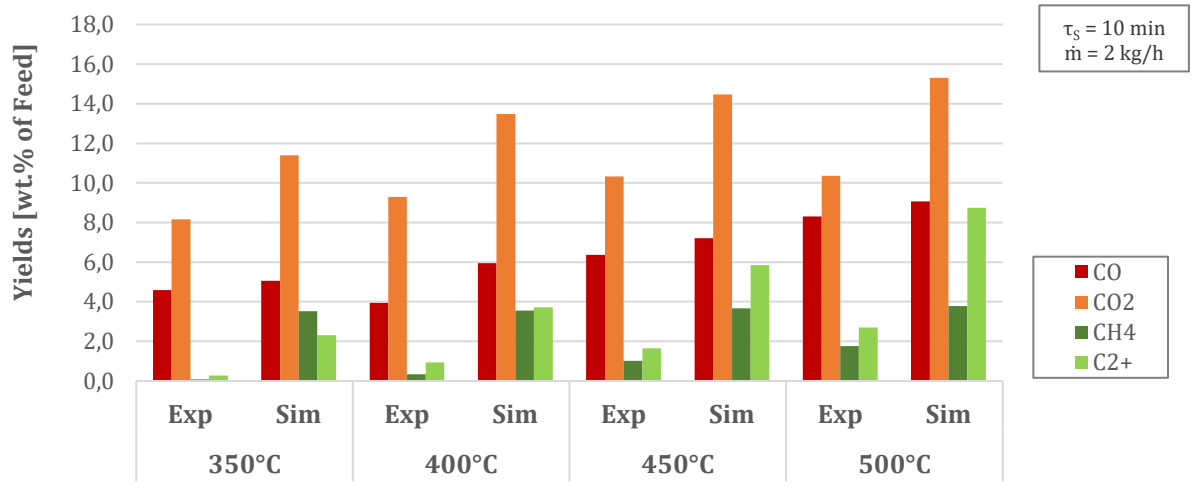

Figure 87. Comparison of the yields of the permanent gas as function of the temperature of the reactor.

Finally, the elemental composition of the condensate will be considered. Again, the comparison between the simulated and the experimental compositions is depicted graphically in Figure 88 as a function of the reactor temperature. The composition at the reference temperature of 450°C was very well predicted by the model. However, the trends were not correctly predicted by the model, which showed a decrease of the carbon content and an increase of the oxygen content with increasing temperature. Again, the reason lays in the selectivity of the secondary gas phase reactions.

In conclusion, the chemical reactions still require adjustment efforts in order to provide a more adequate elemental composition and species yields for the pyrolysis of beech wood.

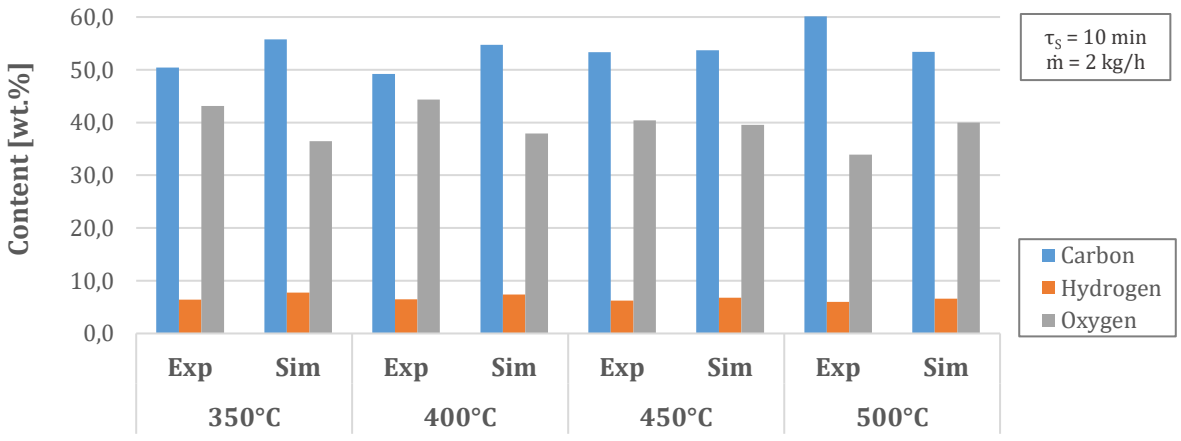

Figure 88. Elemental composition of the simulated and experimental condensates, on water-free basis.

6. CONCLUSION AND OUTLOOK

This dissertation focused on the development of a novel screw pyrolysis reactor with integrated hot gas filtration for the production of particle-free organic vapors, condensate and gas as well as solid char.

The application of the pyrolysis process in the screw reactor STYX to low-grade biogenic feedstock resulted successful for the generation of pyrolysis products with reproducible properties. It was shown that the yields and the properties of the products can be adjusted by process control for a reference feedstock, i.e. beech wood. The optimal process conditions depend on the targeted product. In order to obtain the highest oil phase yield, the optimal process temperature was found to be 450°C, which is lower than the typical fast pyrolysis temperature.

Pyrolysis products were characterized mainly in terms of fuel properties, such as the elemental composition and the heating value. An increase of the process temperature leads to an increase of the calorific properties of the char, due to the decrease of hydrogen and oxygen contents as well as to the increase of the fixed carbon content. The content of combustible gases in the permanent gas increased with the increase of the pyrolysis temperature. Carbon dioxide is the dominant species at low temperatures whereas carbon monoxide and non-condensable hydrocarbons became more relevant at temperatures above 450°C. The aqueous condensate showed a decrease of organic content with increasing temperature, due to a decrease of the oxygen content as well as to an increase of the pH value.

The oil phase was investigated into more details to also evaluate its potential for the production of chemicals. On the one hand, the heating value increased with increasing pyrolysis temperature due to the increase of the carbon to hydrogen and carbon to oxygen ratios as well as a slight decrease of the water content. On other hand, the increase of the pyrolysis temperature led to an increase of the aromatics and alkanes contents as well as to a reduction of the sugars contents, as confirmed by a number of measurement techniques. Due to the absence of solid particles, the pyrolysis oils produced at the STYX reactor are exceptionally suitable for downstream upgrading.

Low-grade biogenic feedstock from different origin were also successfully converted at the STYX pyrolysis reactor. The yields distribution was strongly influenced by the composition of the feedstock. However, the yield of the oil phase was always in a relatively narrow range indicating the robustness of the STYX technology. The char produced from non-lignocellulosic materials such as chicken manure and sewage sludge may find interesting applications outside the energy field due to the content of nutrients like phosphorus and nitrogen, as well as due to the content of metals such as iron

and zinc. However, the presence of relevant contents of nitrogen sulfur and chlorine is an important drawback of such feedstock because the implementation of gas treatment units has to be addressed.
Within the framework of this dissertation a thermochemical model for the STYX reactor was developed and experimentally validated. The model aimed at the description of the mechanisms involved during the pyrolysis of wood in the screw reactor STYX, using models taken from the literature in the field of transport, heat transfer and pyrolysis reactions for solids and gases.
The model relied on the following assumptions:

- Reactor distinguished between a bottom compartment for the transport of the solids and the local release of the pyrolysis vapors and a freeboard on the top for the transport of the vapors;
- Transport of the solids based on a cascade of perfectly mixed reactors;
- No mixing of the locally released pyrolysis vapors on the bottom of the reactor;
- Heat transfer model for the granular solids based on the penetration model, which considers the granular solid as a continuum with averaged thermo-physical and chemical properties;
- Intra and extra particle mass and heat transfer mechanisms negligible;
- Heat transfer model of the gas, which includes forced convection and radiative heat transfer, based on the non-dimensional numbers;
- Pyrolysis kinetic model based on a 5 steps multi component system adopting the main model compounds of wood;
- Formal chemical reactions based on solid, gaseous and liquid model compounds as intermediate and final products for the closure of the carbon, hydrogen and oxygen balance.

A comprehensive sensitivity analysis of the dominant parameters was given in order to deepen the understanding of the pyrolysis process in the screw pyrolysis reactor STYX from the engineering point of view. It was shown that the thermo-physical properties of wood, like the specific heat capacity, are a limiting factor for the effective heat transfer in screw reactors. The particle size plays a less prominent role in comparison to that played in fast pyrolysis systems with direct heat transfer media. Moreover, the variation of the process parameters, such as temperature, residence time of the solids and mass flow rate is able to influence the yields of the pyrolysis products. However, the properties of the products may differ although similar yields can be obtained by multiple sets of process parameters. Such considerations should be taken into account during the design of a screw pyrolysis reactor.
The thermochemical model was systematically validated experimentally at the STYX reactor.
First, the transport mechanism of the solids and the hydrodynamics of the gas were investigated implementing the theory of the residence time distribution. It was confirmed that the solids globally

behave like a plug flow; thus, the utilization of an n-series of perfectly mixed reactor is the most suitable to model the transport of the granular material. It was also shown that the gas tends to flow from the bottom compartment, where the screw is displaced, to the freeboard on top of the reactor to minimize the pressure loss.

Experimental methods were developed to measure the temperature and other properties of the granular solids along the main axis of the reactor. With these methods, the temperature and the moisture profiles of the solids were validated at the STYX reactor for selected process conditions. The model reproduces accurately the heat transfer and the drying process.

The pyrolysis model was also validated experimentally. It was shown that the experimental decomposition of the solids was slower compared to simulations. Additionally, the final yield of the solids was always underestimated by the model. The yields and the compositions of the pyrolysis vapors were in fair agreement with the experimental results obtained at the STYX reactor only at the tail of the reactor. The yield of carbon dioxide was very well reproduced by the model, whereas the yield of carbon monoxide was always underestimated. The yields of the non-condensable hydrocarbons were always overestimated by the model. The differences between the simulation and the experiments are caused by the adopted formal chemical reactions, which underestimate the yield of carbon and oxygen and overestimate the hydrogen yield of the permanent gas, i.e. the CO yield and the non-condensable hydrocarbons yields, respectively.

The overall capability of the model to predict the yields of the main products was reported. The trends of the products yields are very well reproduced. On other hand, it was shown that the compositions of the condensable organics estimated by the model did not follow the trend reported from the experiments.

Future experimental works should address the following relevant topics:

- Role of the hot gas filtration on the kinetics of the secondary gas phase reactions. In this way it was highlighted that the hot gas filtration affects the yield and composition of the vapors. However, the mechanisms involved need to be investigated with tailored experiments at the STYX reactor as well as on a lab scale test rig;
- Application driven analysis and upgrading of the pyrolysis products. The analyses are required to provide a feedback for process optimization. Moreover, it is suggested to evaluate the opportunity of upgrading the pyrolysis products to market ready products, e.g. liquid fuels or chemicals from both liquid phases;

- Emissions relevant investigations as well as integration of a vapors or gas cleaning unit mainly due to the presence of nitrogen, sulfur and chlorine in low-grade biogenic feedstock.

Although the thermochemical model is able to predict correctly the relevant mechanisms taking place during the pyrolysis of wood in the screw reactor STYX, some improvements are required to refine the prediction abilities of the model.

The following modifications are suggested for future works:

- Inclusion of a particle model to enable the shift from a global kinetic approach to intrinsic kinetics. A particle model will also enable a more suitable coupling between the heat and mass transfer within the single particle and the reaction kinetics including the heterogeneous reaction taking place in the pore system. More work should be carried out in relation to the change pore structure of the particle, which is expected to be the main factor for the differences in the yields of the solids;
- Extension of the kinetic model to non-lignocellulosic feedstock to implement the behavior of model compounds containing nitrogen, sulfur and chlorine as well as the fundamental catalytic effect of the mineral matter;
- Different or additional model components should be implemented to describe the composition of the pyrolysis products. For instance, a solid model compound containing hydrogen for the char and different model compounds for the condensate should be considered;
- Overall implementation of a filtration model including the mechanism of soot formation should be carefully addressed due to the relevance of the filter cake for the production of valuable liquid products and for the reliable operation of the pyrolysis reactor;
- Extension of the heat transfer model to address the fouling on the bottom of the reactor, which creates an additional layer of carbonized solid between the reactor vessel and the fresh material. Fouling acts as an insulation layer and it is expected to severely affect the overall heat transfer on long term operations.

BIBLIOGRAPHY

[1] Adrados, A., Marco, I. de, and López-Urionabarrenechea, A., et al. Materials, vol. 9, p. 3, 2016.

[2] Agirre, I., Griessacher, T., and Rösler, G., et al. Fuel Processing Technology, vol. 106, pp. 114–121, 2013.

[3] Alén, R., Kuoppala, E., and Oesch, P. Journal of Analytical and Applied Pyrolysis, vol. 36, pp. 137–148, 1996.

[4] Anca-Couce, A., Berger, A., and Zobel, N. Fuel, vol. 123, pp. 230–240, 2014.

[5] Anca-Couce, A., Mehrabian, R., and Scharler, R., et al. Energy Conversion and Management, vol. 87, pp. 687–696, 2014.

[6] Anca-Couce, A. Progress in Energy and Combustion Science, vol. 53, pp. 41–79, 2016.

[7] Antal, M.J., JR. Ind. Eng. Chem. Res. Dev., vol. 22, pp. 366–375, 1983.

[8] Antal, M.J., JR. Ind. Eng. Chem. Res., vol. 34, pp. 708–717, 1995.

[9] Antal, M.J., JR. and Grønli, M. Ind. Eng. Chem. Res., vol. 42, pp. 1619–1640, 2003.

[10] Aramideh, S., Xiong, Q., and Kong, S.-C., et al. Fuel, vol. 156, pp. 234–242, 2015.

[11] Argyle, M. and Bartholomew, C. Catalysts, vol. 5, pp. 145–269, 2015.

[12] Arregi, A., Lopez, G., and Amutio, M., et al. RSC Adv, vol. 6, pp. 25975–25985, 2016.

[13] Asmadi, M., Kawamoto, H., and Saka, S. Journal of Analytical and Applied Pyrolysis, vol. 92, pp. 88–98, 2011.

[14] ASTM Committee D18, D7481-09 Standard Test Methods for Determining Loose and Tapped Bulk Densities of Powder using a Graduated Cylinder. West Conshohocken, PA, 2009.

[15] ASTM Committee D18, D6393-14 Standard Test Method for Bulk Solids Characterization by Carr Indices. West Conshohocken, PA, 2014.

[16] ASTM Standard D388 - 18, Standard Classification of Coals by Rank. West Conshohocken, PA, 2018.

[17] Atsonios, K., Panopoulos, K.D., and Bridgwater, A.V., et al. Int. J. Thermo, vol. 18, p. 267, 2015.

[18] AVA-CO2, AVA-CO2 Schweiz AG, http://www.ava-co2.com/web/pages/en/home.php, 2016.

[19] Azargohar, R., Nanda, S., and Kozinski, J.A., et al. Fuel, vol. 125, pp. 90–100, 2014.

[20] Banyasz, J.L., Li, S., and Lyons-Hart Jim L., et al. Journal of Analytical and Applied Pyrolysis, vol. 57, pp. 223–248, 2001.

[21] Beckmann, M., Fontana, A., and Gehrmann, H.-J., Beckmann, Michael; Fontana, A.; Gehrmann, H.-J. in Waste Thermal Treatment Technologies, 2005.

[22] Biogreen, Biogreen: Think sustainable, http://www.biogreen-energy.com/, 2017.

[23] Biomasseverordnung vom 21. Juni 2001 (BGBl. I S. 1234), die zuletzt durch Artikel 12 des Gesetzes vom 21. Juli 2014 (BGBl. I S. 1066) geändert worden ist. Verordnung über die Erzeugung von Strom aus Biomasse (Biomasseverordnung - BiomasseV), 2001.

[24] Blomberg, M., Large-Scale Biomass Gasification Plant integrated to a Coal-Fired Boiler, Nov, 2014.

[25] Boateng, A.A. and Barr, P.V. Int. J. Heat Mass Transfer, vol. 39, pp. 2131–2147, 1996.

[26] Boroson, M.L., Howard, J.B., and Longwell, J.P., et al. AIChE J., vol. 35, pp. 120–128, 1989.

[27] Boscagli, C., Raffelt, K., and Zevaco, T.A., et al. Biomass and Bioenergy, vol. 83, pp. 525–538, 2015.

[28] Bridgwater, A.V. Biomass and Bioenergy, vol. 38, pp. 68–94, 2012.

[29] Briens, C., Piskorz, J., and Berruti, F. International Journal of Chemical Reactor Engineering, vol. 6, 2008.

[30] R. C. Brown, Ed., Thermochemical Processing of Biomass. Conversion into Fuels, Chemicals and Power. West Sussex, PO19 8SQ, United Kingdom. John Wiley & Sons, Ltd, 2011.

[31] Brown, R.A., Kercher, A.K., and Nguyen, T.H., et al. Organic Geochemistry, vol. 37, pp. 321–333, 2006.

[32] Bryden, K.M., Ragland, K.W., and Rutland, C.J. Biomass and Bioenergy, vol. 22, pp. 41–53, 2002.

[33] Buekens, A. G.; Schoeters, J. G. in Thermal Conversion of Solid Wastes and Biomass. J. L. Jones, S. B. Radding, Eds., 1980, pp. 397–421.

[34] Bulushev, D.A. and Ross, J.R. Catalysis Today, vol. 171, pp. 1–13, 2011.

[35] Bundes-Immissionsschutzgesetz in der Fassung der Bekanntmachung vom 17. Mai 2013 (BGBl. I S. 1274), das durch Artikel 3 des Gesetzes vom 26. Juli 2016 (BGBl. I S. 1839) geändert worden ist, 1974.

[36] Bundesministerium für Umwelt, Naturschutz, Bau und Reaktorsicherheit (BMUB), www.bmub.bund.de, Entwurf zur Anpassung der Ersten Allgemeinen Verwaltungsvorschrift zum Bundes–Immissionsschutzgesetz. Entwurf zur Anpassung der TA Luft, 2016.

[37] Bundesumweltministerium (BMU), Technische Anleitung zur Reinhaltung der Luft - TA Luft. TA Luft, 2002.

[38] Caballero, J.A., Font, R., and Marcilla, A. Journal of Analytical and Applied Pyrolysis, vol. 36, pp. 159–178, 1996.

[39] Cai, J., Wu, W., and Liu, R., et al. Green Chem., vol. 15, p. 1331, 2013.

[40] Calabria, R., Chiariello, F., and Massoli, P. Experimental Thermal and Fluid Science, vol. 31, pp. 413–420, 2007.

[41] Camp, D.W., Mild Coal Gasification - Screw Pyrolyzer Development and Design, 1990.

[42] Cantrell, K.B., Hunt, P.G., and Uchimiya, M., et al. Bioresource technology, vol. 107, pp. 419–428, 2012.

[43] Cao, J.-P., Li, L.-Y., and Morishita, K., et al. Fuel, vol. 104, pp. 1–6, 2013.

[44] Cao, Y. and Pawłowski, A. Renewable and Sustainable Energy Reviews, vol. 16, pp. 1657–1665, 2012.

[45] Cavagnol, S., Roesler, J.F., and Sanz, E., et al. Can. J. Chem. Eng., vol. 93, pp. 331–339, 2015.

[46] Chen, D., Zhou, J., and Zhang, Q. Bioresource technology, vol. 169, pp. 313–319, 2014.

[47] Chiaramonti, D., Oasmaa, A., and Solantausta, Y. Renewable and Sustainable Energy Reviews, vol. 11, pp. 1056–1086, 2007.

[48] J. H. Clark and F. E. I. Deswarte, Eds., Introduction to Chemicals from Biomass. Wiley, 2011.

[49] Coker, A.K., Modeling of Chemical Kinetics and reactor Design. Gulf Professional Publishing, 2001.

[50] Couhert, C., Commandre, J.-M., and Salvador, S. Fuel, vol. 88, pp. 408–417, 2009.

[51] Council Directive 86/278/EEC of 12 June 1986 on the protection of the environment, and in particular of the soil, when sewage sludge is used in agriculture, 1986.

[52] Cross, A. and Sohi, S.P. Soil Biology and Biochemistry, vol. 43, pp. 2127–2134, 2011.

[53] Czernik, S. and Bridgwater, A.V. Energy Fuels, vol. 18, pp. 590–598, 2004.

[54] Dahmen, N., Dinjus, E., and Kolb, T., et al. Environ. Prog. Sustainable Energy, vol. 31, pp. 176–181, 2012.

[55] Daugaard, D.E. and Brown, R.C. Energy Fuels, vol. 17, pp. 934–939, 2003.

[56] Deguchi, S., Tsujii, K., and Horikoshi, K. Chemical communications (Cambridge, England), pp. 3293–3295, 2006.

[57] Demirbaş, A. Energy Conversion and Management, vol. 42, pp. 1357–1378, 2001.

[58] Demirbaş, A. Energy Sources, vol. 27, pp. 1269–1276, 2005.

[59] Demirbaş, A. Journal of Analytical and Applied Pyrolysis, vol. 73, pp. 39–43, 2005.

[60] Deutsches Institut für Normung e.V., DIN 15262 Schneckenförderer für Schüttgut, Jan, 1983.

[61] Di Blasi, C. AIChE J., vol. 48, pp. 2386–2397, 2002.

[62] Di Blasi, C. Progress in Energy and Combustion Science, vol. 34, pp. 47–90, 2008.

[63] Di Blasi, C. Progress in Energy and Combustion Science, vol. 35, pp. 121–140, 2009.

[64] Di Blasi, C., Branca, C., and Galgano, A. Energy Technol., vol. 5, pp. 19–29, 2017.

[65] Dickerson, T. and Soria, J. Energies, vol. 6, pp. 514–538, 2013.

[66] J. P. Diebold, Ed., Specialists' Workshop on Fast Pyrolysis of Biomass Proceedings, 1980.

[67] Diebold, J.P. and Czernik, S. Energy Fuels, vol. 11, pp. 1081–1091, 1997.

[68] Dinuccio, E., Balsari, P., and Gioelli, F., et al. Bioresource technology, vol. 101, pp. 3780–3783, 2010.

[69] Directive 2009/28/EC of the European Parliament and of the Council of 23 April 2009 on the promotion of the use of energy from renewable sources and amending and subsequently repealing Directives 2001/77/EC and 2003/30/EC, 2009.

[70] DWA - Deutsche Vereinigung für Wasserwirtschaft, Abwasser und Abfall, Info zur neuen AbfKlaerV 02 06 2017, 2018.

[71] Ebringerová, A.; Hromádková, Z.; Heinze, T. in Polysaccharides I. T. Heinze, Ed. Berlin, Heidelberg: Springer-Verlag GmbH, 2005.

[72] Efika, C.E., Wu, C., and Williams, P.T. Journal of Analytical and Applied Pyrolysis, vol. 95, pp. 87–94, 2012.

[73] Elliott, D.C., Oasmaa, A., and Meier, D., et al. Energy Fuels, vol. 26, pp. 7362–7366, 2012.

[74] Empyro, Empyro: energy & materials from pyrolysis, http://www.empyroproject.eu/index.php?id=1, 2015.

[75] Erneuerbare-Energien-Gesetz vom 21. Juli 2014 (BGBl. I S. 1066), das durch Artikel 9 des Gesetzes vom 26. Juli 2016 (BGBl. I S. 1786) geändert worden ist, 2014.

[76] European Biochar Foundation, European Biochar Certificate, http://www.european-biochar.org/en, 2013.

[77] FAO, 2014 Global Forest Products Facts and Figures, 2016.

[78] Faravelli, T., Frassoldati, A., and Migliavacca, G., et al. Biomass and Bioenergy, vol. 34, pp. 290–301, 2010.

[79] Fogler, H.S., Elements of Chemical Reaction Engineering. Upper Saddle River, New Jersey 07458, 1999.

[80] Fonts, I., Gea, G., and Azuara, M., et al. Renewable and Sustainable Energy Reviews, vol. 16, pp. 2781–2805, 2012.

[81] French, R. and Czernik, S. Fuel Processing Technology, vol. 91, pp. 25–32, 2010.

[82] Funke, A. and Ziegler, F. Biofuels, Bioprod., Bioref, vol. 4, pp. 160–177, 2010.

[83] Funke, A., Niebel, A., and Richter, D., et al. Bioresource technology, vol. 200, pp. 905–913, 2016.

[84] Funke, A., Tomasi Morgano, M., and Dahmen, N., et al. Journal of Analytical and Applied Pyrolysis, vol. 124, pp. 504–514, 2017.

[85] Furimsky, E. Applied Catalysis A: General, vol. 199, pp. 147–190, 2000.

[86] Galinato, S.P., Yoder, J.K., and Granatstein, D. Energy Policy, vol. 39, pp. 6344–6350, 2011.

[87] Garcia-Perez, M., Chaala, A., and Pakdel, H., et al. Biomass and Bioenergy, vol. 31, pp. 222–242, 2007.

[88] Garcia-Perez, M., Wang, X.S., and Shen, J., et al. Ind. Eng. Chem. Res., vol. 47, pp. 1846–1854, 2008.

[89] Gaston, K.R., Jarvis, M.W., and Pepiot, P., et al. Energy Fuels, vol. 25, pp. 3747–3757, 2011.

[90] Grønli, M.G., A Theoretical and Experimental Study of the Thermal Degradation of Biomass. Trondheim, Norway, 1996.

[91] Hart, H., Craine, L.E., and Hart, D.J., Organic Chemistry: A Short Course, 10th edition. Boston, MA. Houghton Mifflin, 1999.

[92] Hasan Khan Tushar, Mohammad Shahed, Mahinpey, N., and Khan, A., et al. Biomass and Bioenergy, vol. 37, pp. 97–105, 2012.

[93] Haydary, J., Susa, D., and Dudas, J. Waste management (New York, N.Y.), vol. 33, pp. 1136–1141, 2013.

[94] Hendriks, W.H., Butts, C.A., and Thomas, D.V., et al. Asian Australas. J. Anim. Sci, vol. 15, pp. 1507–1516, 2002.

[95] Henrich, E., Dahmen, N., and Weirich, F., et al. Fuel Processing Technology, vol. 143, pp. 151–161, 2016.

[96] Himmel, M.E., Ding, S.-Y., and Johnson, D.K., et al. Science (New York, N.Y.), vol. 315, pp. 804–807, 2007.

[97] Hoekstra, E., Westerhof, R.J.M., and Brilman, W., et al. AIChE J., vol. 58, pp. 2830–2842, 2012.

[98] Horne, P.A. and Williams, P.T. Fuel, vol. 75, pp. 1051–1059, 1996.

[99] Hornung, A., Apfelbacher, A., and Lenzi, F., et al. Chemie Ingenieur Technik, vol. 77, p. 1154, 2005.

[100] Hornung, A., Apfelbacher, A., and Sagi, S. Journal of Scientific & industrial Research, vol. 70, pp. 664–667, 2011.

[101] Hornung, A., Intermediate Pyrolysis as an Alternative to Fast Pyrolysis, 2013.

[102] A. Hornung, Ed., Transformation of Biomass: Theory to Practice. John Wiley & Sons, Ltd, 2014.

[103] Hornung, U., Schneider, D., and Hornung, A., et al. Journal of Analytical and Applied Pyrolysis, vol. 85, pp. 145–150, 2009.

[104] Hosoya, T., Kawamoto, H., and Saka, S. Journal of Analytical and Applied Pyrolysis, vol. 85, pp. 237–246, 2009.

[105] Huber, G.W., Iborra, S., and Corma, A. Chemical reviews, vol. 106, pp. 4044–4098, 2006.

[106] Hübner, T. and Mumme, J. Bioresource technology, vol. 183, pp. 86–92, 2015.

[107] Ingram, L., Mohan, D., and Bricka, M., et al. Energy Fuels, vol. 22, pp. 614–625, 2008.

[108] Jaeger, H.M., Nagel, S.R., and Behringer, R.P. Physics Today, vol. 49, pp. 32–38, 1996.

[109] Jampolski, L., Tomasi Morgano, M., and Seifert, H., et al. Energy Fuels, vol. 31, pp. 5165–5173, 2017.

[110] Jenkins, B., Baxter, L., and Miles, T. Fuel Processing Technology, vol. 54, pp. 17–46, 1998.

[111] Jindo, K., Mizumoto, H., and Sawada, Y., et al. Biogeosciences, vol. 11, pp. 6613–6621, 2014.

[112] Kahiluoto, H., Kuisma, M., and Ketoja, E., et al. Environmental science & technology, vol. 49, pp. 2115–2122, 2015.

[113] Kelessidis, A. and Stasinakis, A.S. Waste management (New York, N.Y.), vol. 32, pp. 1186–1195, 2012.

[114] Kelkar, S., Saffron, C.M., and Chai, L., et al. Fuel Processing Technology, vol. 137, pp. 170–178, 2015.

[115] Kim, P., Weaver, S., and Noh, K., et al. Energy Fuels, vol. 28, pp. 6966–6973, 2014.

[116] Kistler, R.C., Widmer, F., and Brunner, P.H. Environmental science & technology, vol. 21, pp. 704–708, 1987.

[117] Klein, M.T. and Virk, P.S. Energy Fuels, vol. 22, pp. 2175–2182, 2008.

[118] Kyoto Protocol to the United Nations Framework Convention on Climate Change, 1998.

[119] Lakshmanan, C.M., Gal-or, B., and Hoelscher, H.E. Ind. Eng. Chem. Prod. Res. Dev., vol. 8, pp. 261–267, 1969.

[120] Lamarche, P., Tazerout, M., and Gelix, F., et al. Fuel, vol. 106, pp. 118–128, 2013.

[121] Le Manquais, K., Snape, C., and McRobbie, I., et al. Energy Fuels, vol. 23, pp. 4269–4277, 2009.

[122] Lee, C.S., Robinson, J., and Chong, M.F. Process Safety and Environmental Protection, vol. 92, pp. 489–508, 2014.

[123] Lehto, J., Oasmaa, A., and Solantausta, Y., et al., Fuel oil quality and combustion of fast pyrolysis bio-oils. Espoo, Finland, 2013.

[124] Lerch, R.N., Barbarick, K.A., and Azari, P., et al. Journal of Environmental Quality, vol. 22, pp. 620–624, 1993.

[125] Lestari, S., Mäki-Arvela, P., and Beltramini, J., et al. ChemSusChem, vol. 2, pp. 1109–1119, 2009.

[126] Levenspiel, O., Chemical Reaction Engineering. John Wiley & Sons, Ltd, 1999.

[127] Liaw, S.-S., Zhou, S., and Wu, H., et al. Fuel, vol. 103, pp. 672–682, 2013.

[128] Lin, Y., Zhang, C., and Zhang, M., et al. Energy Fuels, vol. 24, pp. 5686–5695, 2010.

[129] Li, S.-Q., Ma, L.-B., and Wan, W., et al. Chem. Eng. Technol., vol. 28, pp. 1480–1489, 2005.

[130] Liu, S., Wei, M., and Qiao, Y., et al. Proceedings of the Combustion Institute, vol. 35, pp. 2767–2775, 2015.

[131] Lu, Q., Li, W.-Z., and Zhu, X.-F. Energy Conversion and Management, vol. 50, pp. 1376–1383, 2009.

[132] Lu, Y., Wei, X.-Y., and Cao, J.-P., et al. Bioresource technology, vol. 116, pp. 114–119, 2012.

[133] Maher, K.D. and Bressler, D.C. Bioresource technology, vol. 98, pp. 2351–2368, 2007.

[134] Mahmood, A.S., Brammer, J.G., and Hornung, A., et al. Journal of Analytical and Applied Pyrolysis, vol. 103, pp. 328–342, 2013.

[135] Mai, R., Leibold, H., and Seifert, H., et al. Chem. Eng. Technol., vol. 26, pp. 577–579, 2003.

[136] Martinez, J.D., Murillo, R., and Garcia, T., et al. Journal of hazardous materials, vol. 261, pp. 637–645, 2013.

[137] Mätzing, H., Gehrmann, H.-J., and Merz, D., et al., Mätzing, H.; Gehrmann, H.-J.; Merz, D.; Kolb, T.; Seifert, H. in Proceedings of the 19th European Biomass Conference and Exhibition. From Research to Industry and Markets. ETA-Florence Renewable Energies, Ed., 2010.

[138] McKendry, P. Bioresource technology, vol. 83, pp. 37–46, 2002.

[139] Medrano, J.A., Oliva, M., and Ruiz, J., et al. Energy, vol. 36, pp. 2215–2224, 2011.

[140] Meier, D. and Faix, O. Bioresource technology, vol. 68, pp. 71–77, 1999.

[141] Mei, Y., Liu, R., and Wu, W., et al. Energy Fuels, vol. 30, pp. 10458–10469, 2016.

[142] Metso Group, Metso to supply a bio oil production plant to Fortum power plant in Joensuu, Finland, http://www.metso.com/news/2012/3/metso-to-supply-a-bio-oil-production-plant-to-fortum-power-plant-in-joensuu-finland/, 2012.

[143] Metso Group, Metso-supplied world's largest biomass gasification plant inaugurated in Finland, http://www.metso.com/news/2013/3/metso-supplied-worlds-largest-biomass-gasification-plant-inaugurated-in-finland/, 2013.

[144] Mierzwa-Hersztek, M., Gondek, K., and Klimkowicz-Pawlas, A., et al. International Agrophysics, vol. 31, p. 7, 2017.

[145] Miller, R.S. and Bellan, J. Combustion Science and Technology, vol. 126, pp. 97–137, 2010.

[146] Mohan, D., Pittman,, Charles U., and Steele, P.H. Energy Fuels, vol. 20, pp. 848–889, 2006.

[147] Monlau, F., Sambusiti, C., and Antoniou, N., et al. Applied Energy, vol. 148, pp. 32–38, 2015.

[148] Morf, P., Hasler, P., and Nussbaumer, T. Fuel, vol. 81, pp. 843–853, 2002.

[149] Mortensen, P.M., Grunwaldt, J.-D., and Jensen, P.A., et al. Applied Catalysis A: General, vol. 407, pp. 1–19, 2011.

[150] Mortensen, P.M., Gardini, D., and de Carvalho, Hudson W. P., et al. Catal. Sci. Technol., vol. 4, pp. 3672–3686, 2014.

[151] Mura, E., Debono, O., and Villot, A., et al. Biomass and Bioenergy, vol. 59, pp. 187–194, 2013.

[152] Näzelius, I.-L., Fagerström, J., and Boman, C., et al. Energy Fuels, vol. 29, pp. 894–908, 2015.

[153] Nelles, M., Grünes, J., and Morscheck, G. Procedia Environmental Sciences, vol. 35, pp. 6–14, 2016.

[154] Neumann, J., Binder, S., and Apfelbacher, A., et al. Journal of Analytical and Applied Pyrolysis, vol. 113, pp. 137–142, 2015.

[155] Nielsen, H.P., Frandsen, F.J., and Dam-Johansen, K., et al. Progress in Energy and Combustion Science, vol. 26, pp. 283–298, 2000.

[156] Nik-Azar, M., Hajaligol, M.R., and Sohrabi, M., et al. Fuel Processing Technology, vol. 51, pp. 7–17, 1997.

[157] Nolte, M.W. and Liberatore, M.W. Energy Fuels, vol. 24, pp. 6601–6608, 2010.

[158] Oasmaa, A., Leppämäki, E., and Koponen, P., et al., Physical characterisation of biomass-based pyrolysis liquids: Application of standard fuel oil analyses. Espoo, Finland, 1997.

[159] Oasmaa, A. and Peacoke, C., A guide to physical property characterization of biomass-derived fast pyrolysis liquids. Espoo, Finland, 2001.

[160] Oasmaa, A., Peacocke, C., and Gust, S., et al. Energy Fuels, vol. 19, pp. 2155–2163, 2005.

[161] Oasmaa, A. and Kuoppala, E. Energy Fuels, vol. 22, pp. 4245–4248, 2008.

[162] Oasmaa, A., Elliott, D.C., and Korhonen, J. Energy Fuels, vol. 24, pp. 6548–6554, 2010.

[163] Ortiz-toral, P.J., Steam reforming of water-soluble fast pyrolysis bio-oil: Studies on bio-oil composition effect, carbon deposition, and catalyst modifications, 2011.

[164] Ouadi, M., Brammer, J.G., and Yang, Y., et al. Journal of Analytical and Applied Pyrolysis, vol. 102, pp. 24–32, 2013.

[165] Paasikallio, V., Kihlman, J., and Sánchez, C.A.S., et al. International Journal of Hydrogen Energy, vol. 40, pp. 3149–3157, 2015.

[166] Park, S.-W. and Jang, C.-H. Energy, vol. 39, pp. 187–195, 2012.

[167] Pathak, A., Dastidar, M.G., and Sreekrishnan, T.R. Journal of environmental management, vol. 90, pp. 2343–2353, 2009.

[168] Patwardhan, P.R., Satrio, J.A., and Brown, R.C., et al. Bioresource technology, vol. 101, pp. 4646–4655, 2010.

[169] Patwardhan, P.R., Dalluge, D.L., and Shanks, B.H., et al. Bioresource technology, vol. 102, pp. 5265–5269, 2011.

[170] Peters, B. and Bruch, C. Journal of Analytical and Applied Pyrolysis, vol. 70, pp. 233–250, 2003.

[171] Piskorz, J., Radlein, D.S., and Scott, D.S., et al. Journal of Analytical and Applied Pyrolysis, vol. 16, pp. 127–142, 1989.

[172] Pyle, D.L. and Zaror, C.A. Chemical Engineering Science, vol. 39, pp. 147–158, 1984.

[173] PYREG GmbH, PYREG, http://www.pyreg.de/home.html, 2017.

[174] Qian, T., Zhang, X., and Hu, J., et al. Chemosphere, vol. 93, pp. 2069–2075, 2013.

[175] Ranzi, E., Cuoci, A., and Faravelli, T., et al. Energy Fuels, vol. 22, pp. 4292–4300, 2008.

[176] Raveendran, K., Ganesh, A., and Khilar, K.C. Fuel, vol. 74, pp. 1812–1822, 1995.

[177] Raveendran, K., Ganesh, A., and Khilar, K.C. Fuel, vol. 75, pp. 987–998, 1996.

[178] Regenis, REW Regenis Regenerative Energie Wirtschaftssysteme GmbH, http://www.regenis.de/, 2017.

[179] Ronsse, F., van Hecke, S., and Dickinson, D., et al. GCB Bioenergy, vol. 5, pp. 104–115, 2013.

[180] Saleh, S.B., Flensborg, J.P., and Shoulaifar, T.K., et al. Energy Fuels, vol. 28, pp. 3738–3746, 2014.

[181] Samanya, J., Hornung, A., and Apfelbacher, A., et al. Journal of Analytical and Applied Pyrolysis, vol. 94, pp. 120–125, 2012.

[182] Schene, C. and Bravo, S. Drying Technology, vol. 16, pp. 1567–1583, 1998.

[183] Schinkel, A.-P., Zur Bildung und Degradation von Teeren aus der Pyrolyse nachwachsender Rohstoffe. Kassel. Kassel Univ. Press, May, 2008.

[184] Schlünder, E.-U. Chemie Ingenieur Technik, vol. 53, pp. 925–941, 1981.

[185] Scholz, M., Melin, T., and Wessling, M. Renewable and Sustainable Energy Reviews, vol. 17, pp. 199–212, 2013.

[186] Schröder, Elisabeth; Thomauske, Klaus; Oeksler, Benjamin; Herberger, Sabrina; Baur, Sabine; Hornung, Andreas in Progress in Biomass and Bioenergy Production. S. Shaukat, Ed.: InTech, 2011.

[187] Schuurman, Y. Catalysis Today, vol. 138, pp. 15–20, 2008.

[188] Scott, S.S., Dennis, J.S., and Davidson, J.F., et al. Fuel, vol. 85, pp. 1248–1253, 2006.

[189] Seifert, H., Vorlesung in Hoch Temperatur Verfahrenstechnik, 2014.

[190] Sewry, J.D. and Brown, M.E. Thermochimica Acta, vol. 390, pp. 217–225, 2002.

[191] Shafidazeh, F. Journal of Analytical and Applied Pyrolysis, vol. 78, pp. 283–305, 1982.

[192] Shao, J., Yan, R., and Chen, H., et al. Fuel Processing Technology, vol. 91, pp. 1113–1118, 2010.

[193] Shen, D.K., Gu, S., and Bridgwater, A.V. Carbohydrate Polymers, vol. 82, pp. 39–45, 2010.

[194] Siebzehnte Verordnung zur Durchführung des Bundes Immissionsschutzgesetzes (Verordnung über die Verbrennung und die Mitverbrennung von Abfällen - 17. BImSchV), 2013.

[195] Singh, S., Wu, C., and Williams, P.T. Journal of Analytical and Applied Pyrolysis, vol. 94, pp. 99–107, 2012.

[196] Smith, K.M., Fowler, G.D., and Pullket, S., et al. Water research, vol. 43, pp. 2569–2594, 2009.

[197] Song, B. and Springer, J. Journal of Colloid and Interface Science, vol. 184, pp. 64–76, 1996.

[198] Sonobe, T. and Worasuwannarak, N. Fuel, vol. 87, pp. 414–421, 2008.

[199] Specht, E., Wärme- und Stoffübertragung in der Thermoprozesstechnik: Grundlagen | Berechnungen | Prozesse. Vulkan, 2014.

[200] Starr, K., Gabarrell, X., and Villalba, G., et al. Waste management (New York, N.Y.), vol. 32, pp. 991–999, 2012.

[201] Strassberger, Z., Tanase, S., and Rothenberg, G. RSC Adv., vol. 4, p. 25310, 2014.

[202] V. Strezov and T. J. Evans, Eds., Biomass Processing Technologies. Taylor & Francis Group, LCC, 2015.

[203] Sukiran, M.A., Kheang, L.S., and Bakar, N.A., et al. American Journal of Applied Sciences, vol. 8, pp. 984–988, 2011.

[204] Susteen Technologies GmbH, Susteen Technologies GmbH: sustainable efficient energy, http://www.susteen-tech.com/, 2017.

[205] Takaoka, M., Domoto, S., and Oshita, K., et al. J Mater Cycles Waste Manag, vol. 14, pp. 113–119, 2012.

[206] Thangalazhy-Gopakumar, S., Adhikari, S., and Ravindran, H., et al. Bioresource technology, vol. 101, pp. 8389–8395, 2010.

[207] Tomasi Morgano, Marco; Leibold, Hans; Richter, Frank; Seifert, Helmut in Energie aus Abfall. Band 12. K. J. Thomé-Kozmienski, M. Beckmann, Eds. Neuruppin: TK Verlag Karl Thomé-Kozmienski, 2015, pp. 507–526.

[208] Tomasi Morgano, M., Leibold, H., and Richter, F., et al. Journal of Analytical and Applied Pyrolysis, vol. 113, pp. 216–224, 2015.

[209] Tomasi Morgano, M., Leibold, H., and Richter, F., et al. Waste management (New York, N.Y.), vol. 73, pp. 487–495, 2018.

[210] Trinh, T.N., Jensen, P.A., and Dam-Johansen, K., et al. Biomass and Bioenergy, vol. 61, pp. 227–235, 2014.

[211] Trippe, F., Fröhling, M., and Schultmann, F., et al. Fuel Processing Technology, vol. 92, pp. 2169–2184, 2011.

[212] Tsotsas, E., Kwapinska, M., and Saage, G. Drying Technology, vol. 25, pp. 1377–1391, 2007.

[213] Tsotsas, E., Tsotsas, Evangelos in VDI Heat Atlas. VDI-Gesellschaft, Ed. Berlin, Heidelberg: Springer-Verlag GmbH, 2010, pp. 1311–1326.

[214] Umweltbundesamt (UBA), Sewage sludge management in Germany. Dessau, Germany, 2013.

[215] US EPA, Wastewater Technology Fact Sheet: Chlorine Disinfection, 1999.

[216] van de Beld, B., Holle, E., and Florijn, J. Applied Energy, vol. 102, pp. 190–197, 2013.

[217] van de Velden, M., Baeyens, J., and Brems, A., et al. Renewable Energy, vol. 35, pp. 232–242, 2010.

[218] Vassilev, S.V., Baxter, D., and Andersen, L.K., et al. Fuel, vol. 89, pp. 913–933, 2010.

[219] Vassilev, S.V., Baxter, D., and Andersen, L.K., et al. Fuel, vol. 94, pp. 1–33, 2012.

[220] VDI-Gesellschaft, Ed., VDI Heat Atlas. Berlin, Heidelberg. Springer-Verlag GmbH, 2010.

[221] Vega, R.E., Zúñiga, P., and Thibault, J., et al. JFFHMT, 2016.

[222] Verordnung über die Verwertung von Klärschlamm, Klärschlammgemisch und Klärschlammkompost (Klärschlammverordnung - AbfKlärV). AbfKlärV, 2017.

[223] Veses, A., Aznar, M., and Martinez, I., et al. Bioresource technology, vol. 162, pp. 250–258, 2014.

[224] Vyazovkin, S., Burnham, A.K., and Criado, J.M., et al. Thermochimica Acta, vol. 520, pp. 1–19, 2011.

[225] Waje, S.S., Thorat, B.N., and Mujumdar, A.S. Drying Technology, vol. 25, pp. 609–616, 2007.

[226] Waje, S.S., Patel, A.K., and Thorat, B.N., et al. Drying Technology, vol. 25, pp. 249–259, 2007.

[227] Wang, L., Weller, C.L., and Jones, D.D., et al. Biomass and Bioenergy, vol. 32, pp. 573–581, 2008.

[228] Wang, S., Guo, X., and Wang, K., et al. Journal of Analytical and Applied Pyrolysis, vol. 91, pp. 183–189, 2011.

[229] Wang, S., Ru, B., and Lin, H., et al. Bioresource technology, vol. 143, pp. 378–383, 2013.

[230] Wang, X., Si, J., and Tan, H., et al. Energy Fuels, vol. 24, pp. 5215–5221, 2010.

[231] Williams, P.T. and Horne, P.A. Renewable Energy, vol. 4, pp. 1–13, 1994.

[232] Williams, P.T. and Besler, S. Renewable Energy, vol. 7, pp. 223–250, 1996.

[233] Xue, Q., Dalluge, D., and Heindel, T.J., et al. Fuel, vol. 97, pp. 757–769, 2012.

[234] Yang, H., Yan, R., and Chen, H., et al. Fuel, vol. 86, pp. 1781–1788, 2007.

[235] Yan, J.-H., Deng, W.-Y., and Li, X.-D., et al. Drying Technology, vol. 27, pp. 787–796, 2009.

[236] Yildiz, G., Pronk, M., and Djokic, M., et al. Journal of Analytical and Applied Pyrolysis, vol. 103, pp. 343–351, 2013.

[237] Yildiz, G., Ronsse, F., and van Duren, R., et al. Renewable and Sustainable Energy Reviews, vol. 57, pp. 1596–1610, 2016.

[238] Zhao, B., Zhang, X., and Chen, L., et al. Bioresource technology, vol. 156, pp. 78–83, 2014.

APPENDIX

A.1 Feedstock characterization

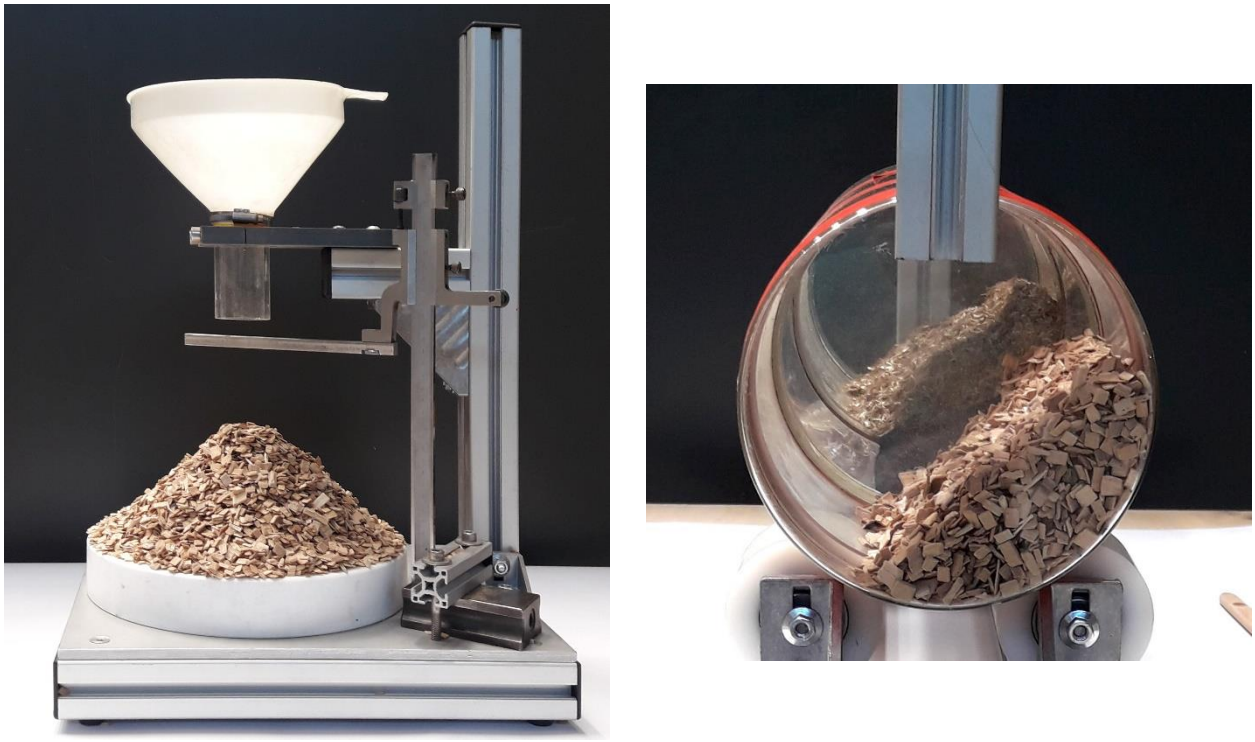

(a) (b)

Figure 89. (a) Static angle of repose equipment
(b) Dynamic Angle of repose equipment

A.2 Fundamentals of reactor design

A.2.1 Transport mechanism in the screw reactor

The principal mechanisms involved in the transport of granular solids in a screw reactor depend on:

- Physical properties of the particles, such as the particle shape, size and size distribution as well as the coefficient of friction among the particles, which define the angle of repose of the bulk;
- Geometry of the reactor, specifically the diameter and the pitch of the screw;
- Operational conditions such as the mass flow rate and rotational speed of the screw, which are responsible for the assessment of the DoF in combination with the geometry.

In a screw reactor, the first layer of particles covering the flight is pushed forward against the following layer. The friction between particles and with the wall of the screw is responsible for the movement of the bulk solids and of the relative displacement of the particles. Once the angle of repose

is achieved, the top layer of particles starts flowing along the surface of the bulk material inducing a continuous renewal of the layer on the top of the bulk and consequently a mixing of the whole granular solid. The mechanisms affecting the RTD can be distinguished depending on the DoF (see Figure 49 in chapter 5.4.1).

As already mentioned, during the transport in an auger, the bulk material is pushed forward by the flight of the screw and assumes the shape of a half conus with an inclination defined by the angle of repose. However, in real systems, the transport of bulk materials is affected by constructive limitations, which lead to back flow of the material.

At low DoF (Figure 49 a) and depending on the particle size, the main mechanism of back flow is the "slip". In such situation, the particles flow back passing through the clearance between the flight of the screw and the wall of the reactor. At constant speed of revolutions, the effect decreases with increasing mass flow rate and particle size. The second effect is visualized at middle DoF (Figure 49 b). The granular material flows back passing above the core of the screw. It falls on the other side of the flight and accumulates in the following pitch. The slip mechanism is still present but to a minor degree. Finally, the third condition takes place at high DoF (Figure 49 c). The granular material produce the so-called "bridges" between the wall and the shaft; the angle of repose is lower or even not recognizable. The pushing side of the flight is completely covered by the granular solid. The mechanisms of slip and of the back flow over the core are still present but their influence is reduced. The main mechanisms is the over flow through the free space between the flight and the auger.

A.2.2 Theory of residence time distribution

The transport mechanisms of gases and solids in a chemical flow reactor are investigated experimentally in order to evaluate the most suitable ideal reactor model to be implemented the simulation tool. The aim of the ideal reactor models is to provide information with respect to the residence time distribution (RTD), which is defined as the probability distribution function that describe the amount of time that the material spends in the reactor (Equation 71). The integral of the RTD function is shown in Equation 72. It describes the response function to a change in the input. In other words, it describes the time necessary to completely recover the desired product. Moreover, the RTD function allows to define a mean residence time inside the reactor, i.e. the statistical average residence time (Equation 73).

$$E(t) = \frac{C_i}{\int_0^\infty C dt}$$ Equation 71

$$F(t) = \int_0^t E(t) dt$$ Equation 72

$$\overline{\tau}_R = \int_0^\infty t E(t) dt$$ Equation 73

The transport of a homogeneous material in a reactor can be described by four different ideal flow reactor models, i.e. the plug flow reactor (PFR in Equation 74), the laminar flow reactor (LFR in Equation 75), the continuously stirred tank reactor (CSTR in Equation 76) and the N-Series CSTR (N-CSTR in Equation 77). Each model provides a different RTD function, which can be compared with the experimental ones. In the presented equation, *E(t)* represents the residence time function, τ_R is the mean residence time, *t* is the actual residence time and *n* is the number of reactors. While the PFR and the CSTR models are applicable to both fluids and bulk solids, the LFR is suitable only for fluids.

PFR $$E(t) = \frac{\tau_R^2}{2t^3}$$ Equation 74

LFR $$\begin{cases} E(t) = 0, t \le \frac{\tau_R}{2} \\ E(t) = \frac{\tau_R^2}{2t^3}, t \ge \frac{\tau_R}{2} \end{cases}$$ Equation 75

CSTR $$E(t) = \frac{1}{\tau_R} e^{\frac{-t}{\tau_R}}$$ Equation 76

N-CSTR $$E(t) = \frac{t^{n-1}}{(n-1)!\tau_{R,i}^n} e^{\frac{-t}{\tau_{R,i}}}, \tau_{R,i} = \frac{\tau_R}{n}$$ Equation 77

The RTD function can be reconstructed from the experimental investigations, replacing the integral form of Equation 71 with the discretized results, as described in Equation 78. The same procedure can be applied to the response function (Equation 79) and to the mean residence time (Equation 80). With the aid of the mean residence time and of the response function, the standard deviation expressed in time (Equation 81) and in dimensionless form (Equation 82) can be calculated. Finally, the equivalent number of CSTR reactors (Equation 83) and the related Peclet number (Equation 84) assess the dispersion of the residence time as well as maximal time step (Equation 85) to be adopted in the simulations. The herein discussed methodology provides the theoretical background during the evaluation and the discussion of the transport mechanisms for both the gases and the solids.

$$E(t) \cong \frac{C_i}{\sum_0^\infty C_i \Delta t_i}$$ Equation 78

$$F(t) \cong \frac{\sum_0^t C_i \Delta t_i}{\sum_0^\infty C_i \Delta t_i}$$ Equation 79

$$\tau_R \cong \frac{\sum_0^t t_i C_i \Delta t_i}{\sum_0^\infty C_i \Delta t_i}$$ Equation 80

$$\sigma^2 = \int_0^1 (t - \tau_R)^2 \, dF$$ Equation 81

$$\sigma_D^2 = \left(\frac{\sigma}{\tau_R} \right)^2$$ Equation 82

$$N = \frac{1}{\sigma_D^2}$$ Equation 83

$$Pe = \frac{2}{\sigma_D^2}$$ Equation 84

$$\Delta\tau = \frac{\tau_R}{N}$$ Equation 85

A.3 Additional experimental details

Flow Sheet Heat Loss

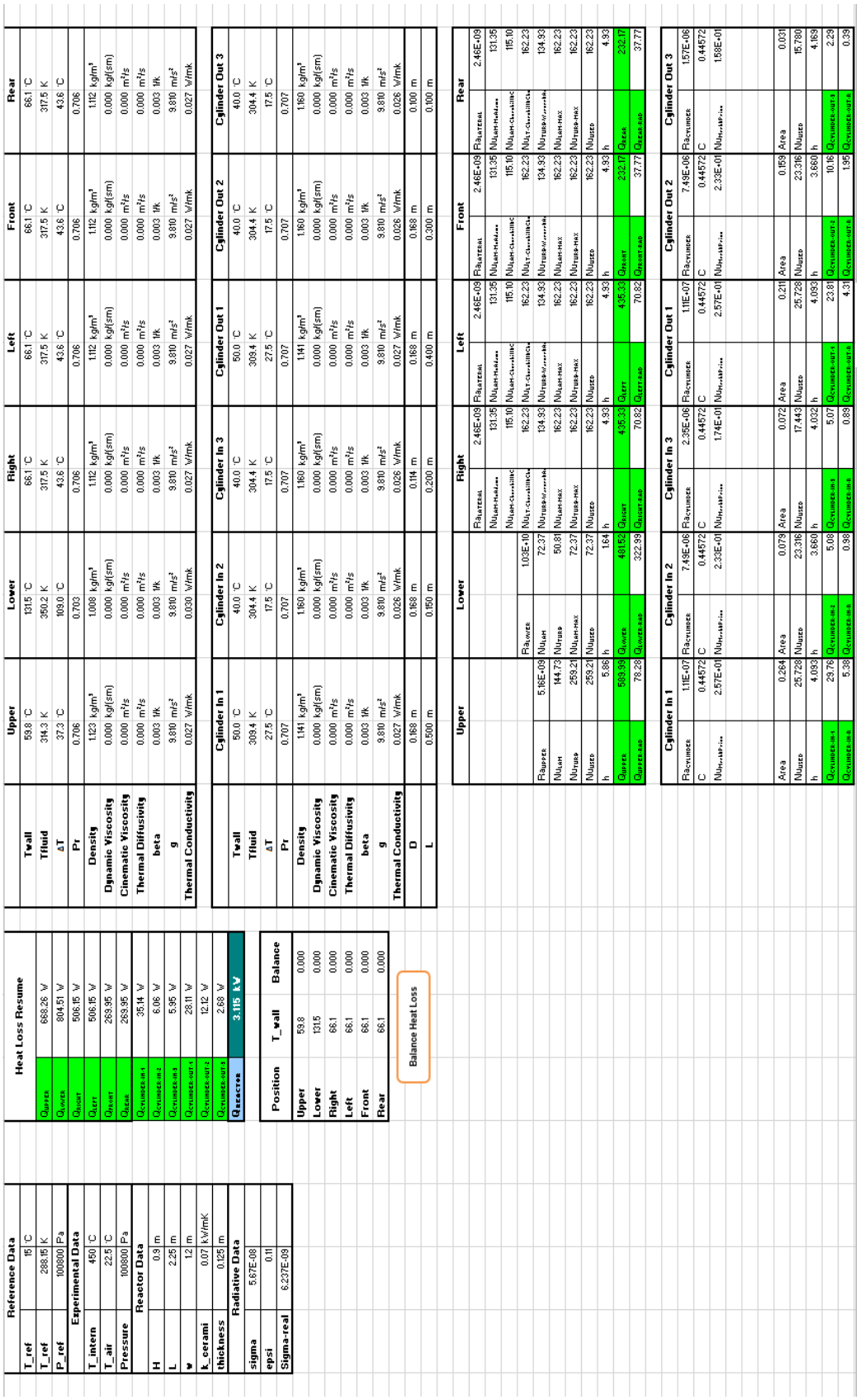

Figure 90. Flow sheet of the heat loss calculation procedure.

Organic yields in the aqueous condensate from beech wood pyrolysis

Table 52. Contents of the organic markers in the water phase products from the pyrolysis of beech wood.

		350°C	400°C	450°C	500°C
Furfural	mg/g	4.86	3.79	2.88	2.63
Acetaldehyde	mg/g	1.08	1.66	2.08	2.45
Acetic Acid	mg/g	77.32	60.57	62.85	54.72
Phenol	mg/g	0.13	0.22	0.43	0.86
Guaiacol	mg/g	1.58	1.36	0.42	0.10
Benzene	µg/g	0.84	2.00	4.10	6.85
Naphthalene	µg/g	0.16	0.40	0.62	1.07

Hydrocarbons contents for the pyrolysis of beech wood

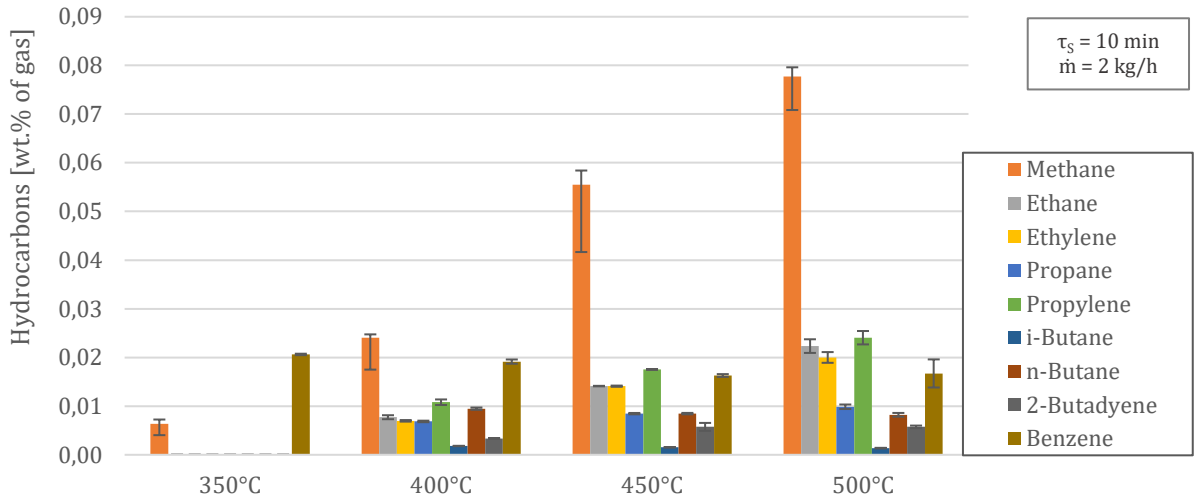

Figure 91. Contents of the hydrocarbons from the pyrolysis of beech wood at the STYX reactor.

Hydrocarbons from the pyrolysis of low-grade biogenic feedstock at 450°C

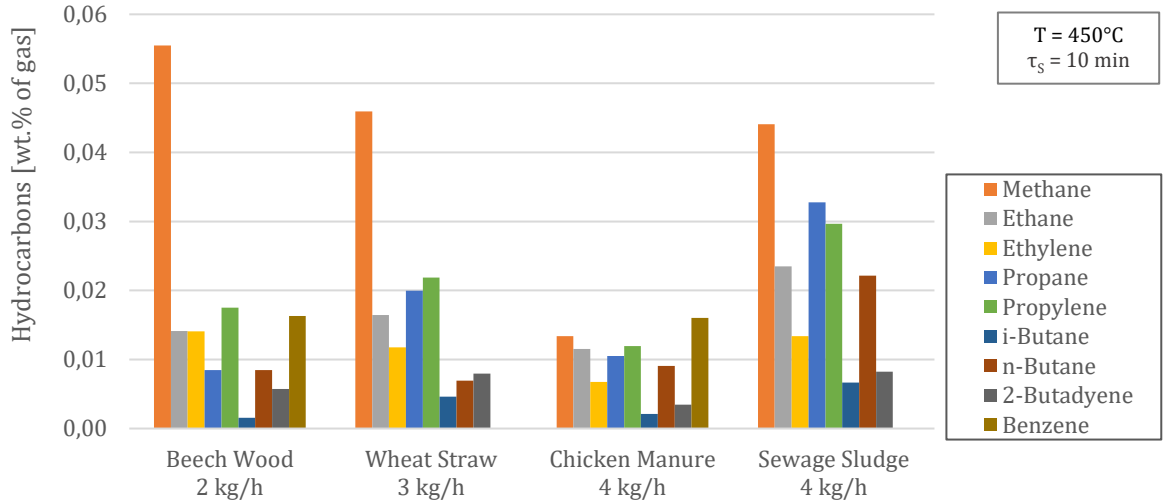

Figure 92. Contents of the hydrocarbons from the pyrolysis of low-grade biogenic feedstock at 450°C at the STYX reactor.

GC-MS Screening of Pyrolysis Oils

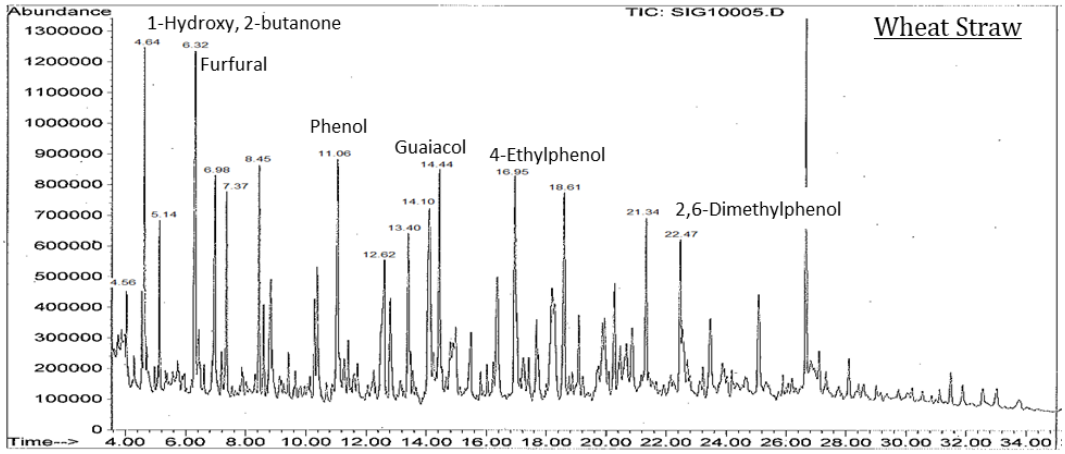

Figure 93. GC-MS spectrum of the pyrolysis oil from wheat straw.

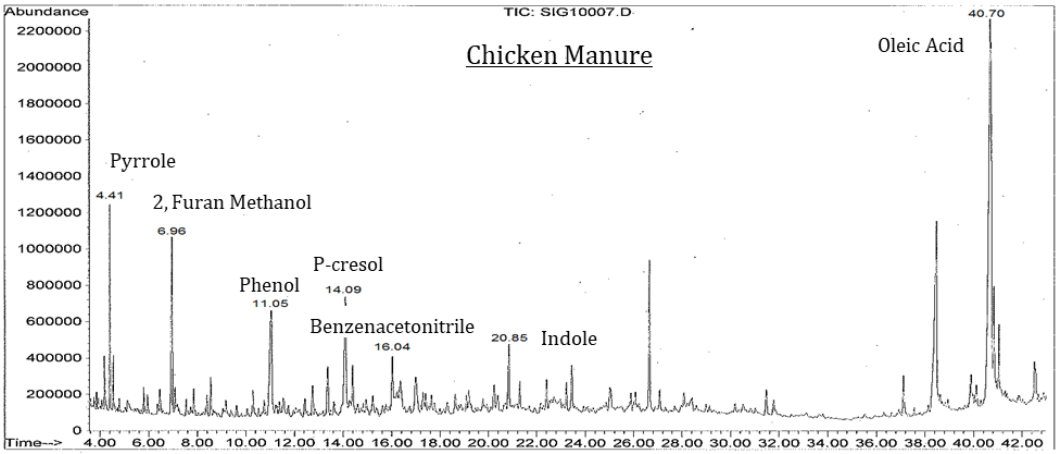

Figure 94. GC-MS spectrum of the pyrolysis oil from chicken manure.

GC-MS Screening of Aqueous Condensates

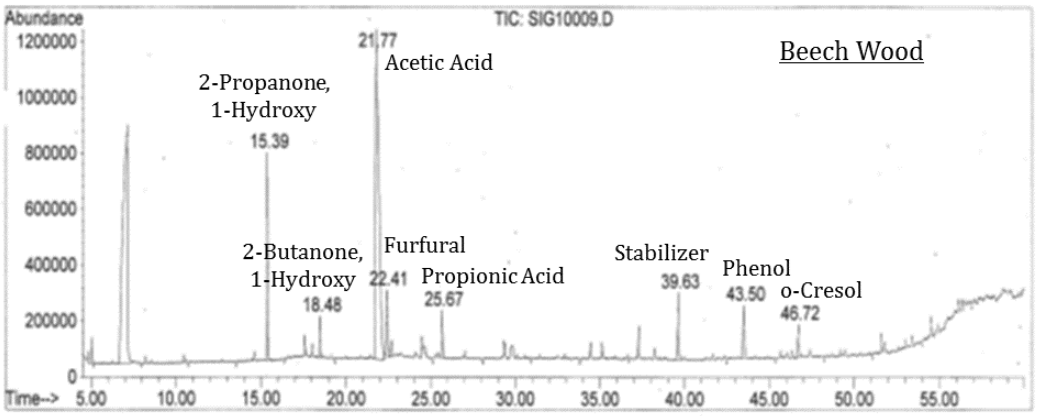

Figure 95. GC-MS spectrum of the water phase from beech wood.

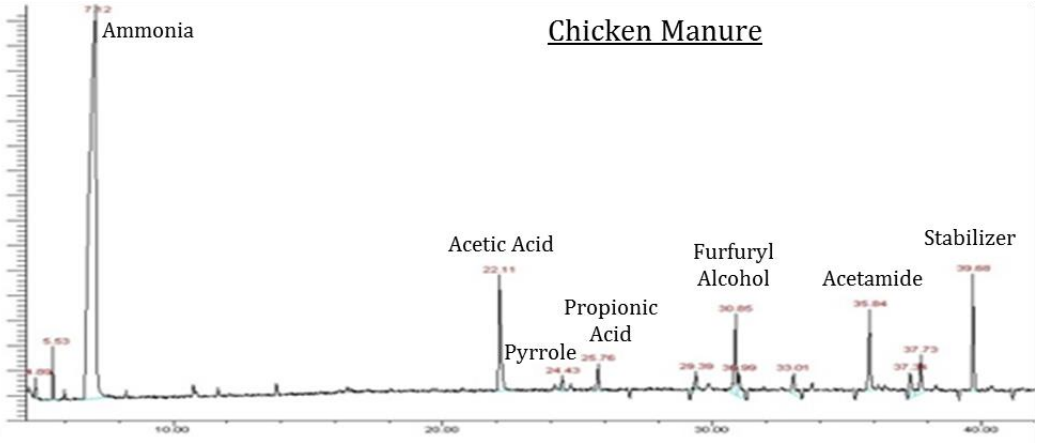

Figure 96. GC-MS spectrum of the water phase from chicken manure.

Yields of the organics on DAF basis.

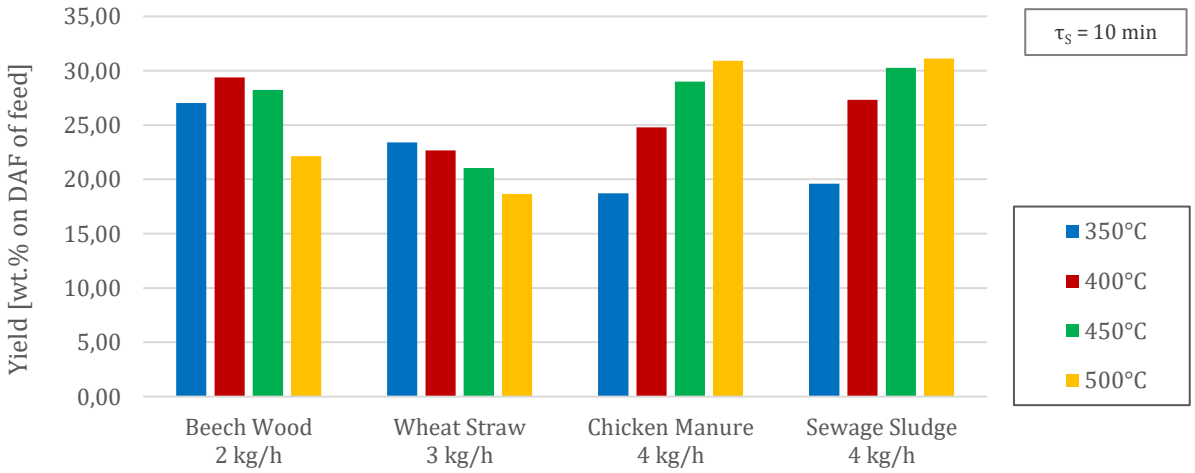

Figure 97. Yields of the condensable organics on dry ash free basis for the selected feedstock.

A.4 Details of the mathematical model

A.4.1 Details of the transport model

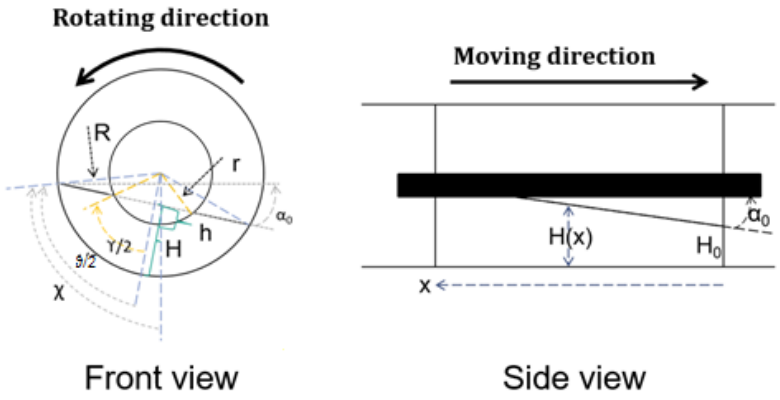

Figure 98. Transport of the solids. Geometry of the bulk and relevant dimensions.

Table 53. Equations and sketch for the calculation of the frontal geometry of the bulk.

$$\vartheta = 2\arccos\left(\frac{R-H}{R}\right)$$

$$\gamma = 2\arccos\left(\frac{r-h}{r}\right)$$

$$\text{if} \rightarrow H > (R-r) \rightarrow h = H-(R-r)$$

$$\text{else} \rightarrow h = 0$$

$$S_{SHAFT} = \frac{r^2}{2}(\gamma - \sin(\gamma))$$

$$S_{SOLID} = \frac{R^2}{2}(\vartheta - \sin\vartheta) - S_{SHAFT}$$

$$\chi = \frac{\vartheta}{2} + \alpha_0$$

Table 54. Equations and sketch for the calculation of the lateral geometry of the bulk.

$$H(x) = \left(\int_0^{x_f} dx - \int_0^{x} dx\right)\tan(\alpha_0) + H_0$$

H(x) is the height of filling at the x position along the single pitch
x_f is the total length along the pitch taken by the solid ≤ p
H_0 is the height of filling on the backside of the previous flight
α_0 is the angle of repose of the material
θ is the angle of the external wall in contact with the solids
γ is the angle of the shaft in contact with the solids
χ is the angle of the external vessel from the vertical in contact with the solids
H is the height of filling at the flight
h is the fraction of the shaft radius in contact with the solids

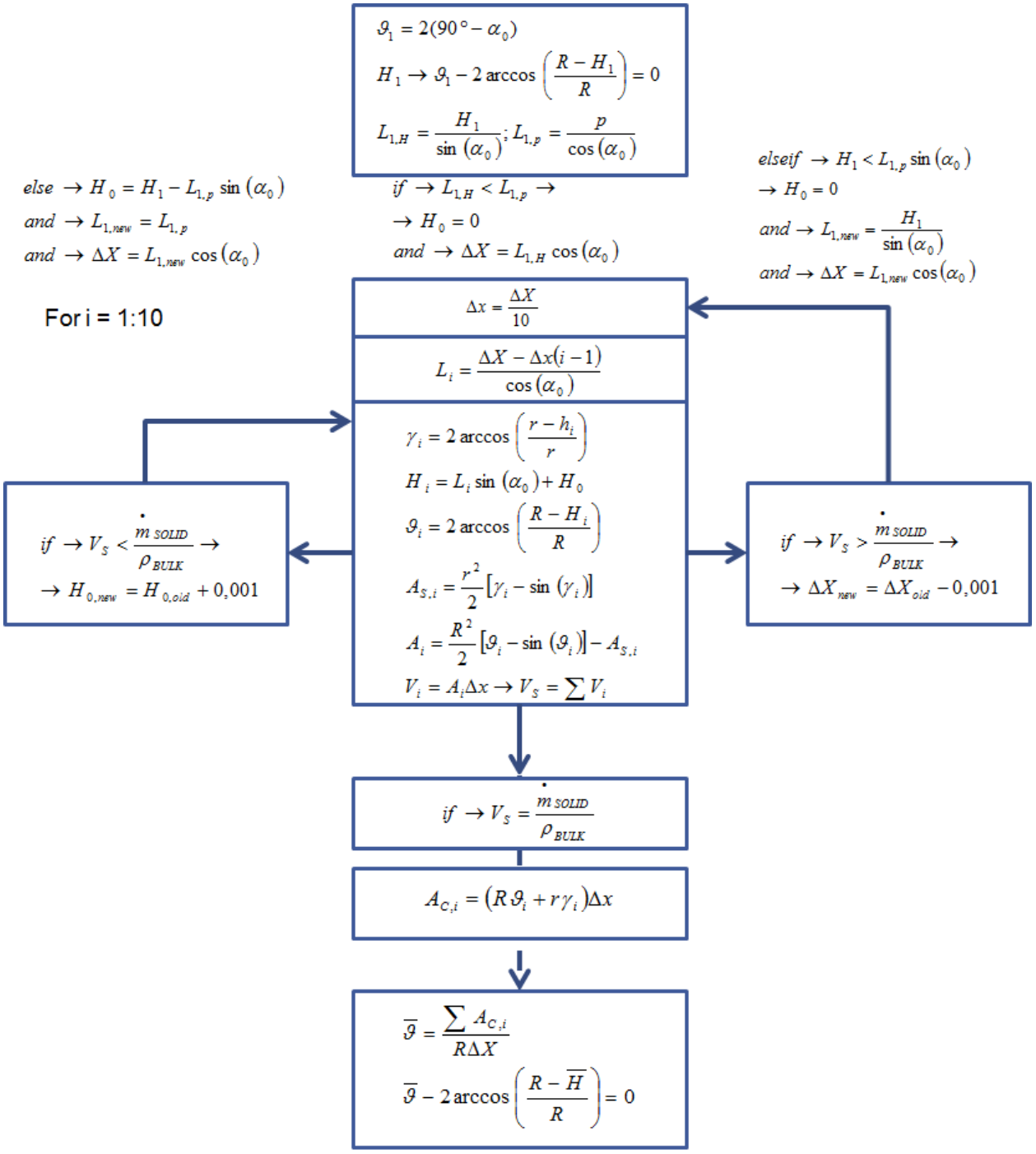

Figure 99. Procedure for the detemination of the maximum mass flow rate of the solids.

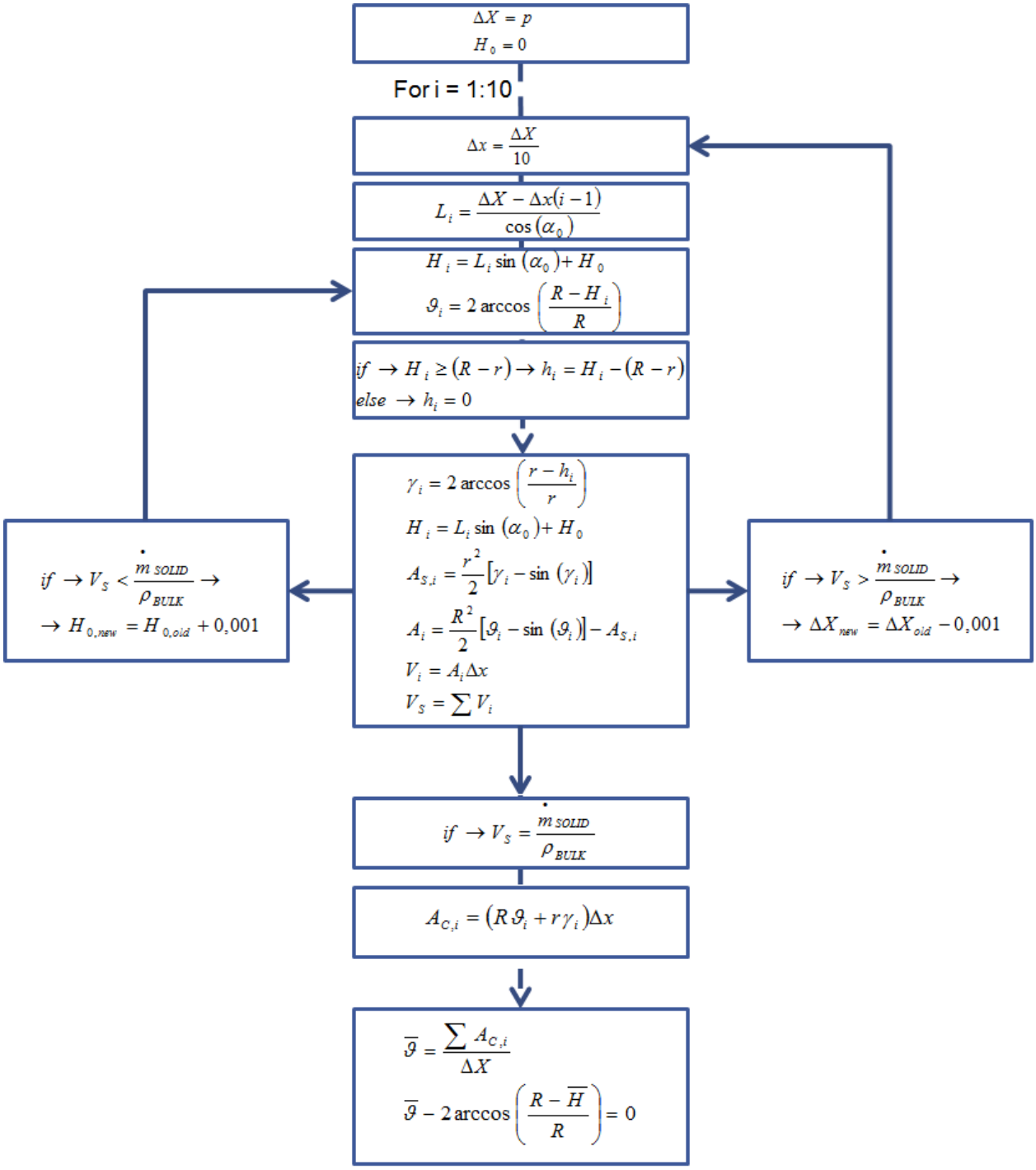

Figure 100. Procedure for the calculation of the geometry of the bulk.

A.4.2 Details of the heat transfer model

Heat exchange surfaces

The respective surfaces for the heat exchange calculations are reported in Table 55.

Table 55. Relevant surfaces for heat exchange.

$$S_{TOT} = \left[\pi R + 2\left(\pi r + R + l\right)\right]\Delta x$$

$$S_{WS} = R\vartheta\Delta x$$

$$S_{W\Delta m} = \left[\left(2 + \pi - \vartheta\right)R\right]\Delta x$$

$$S_{ShS} = r\gamma\Delta x$$

$$S_{Sh\Delta m} = \left[\left(2\pi - \gamma\right)r\right]\Delta x$$

$$S_{WG} = \left[2R + 2\left(l - R\right)\right]\Delta x = 2l\Delta x$$

$$S_{SG} \equiv S_{WS,\varepsilon} = R\sin\vartheta\Delta x$$

Convective heat transfer coefficient

The convective heat transfer coefficients are calculated following the procedure here described.

The same procedure is adopted for calculation of the convective heat transfer between the wall and the locally released vapors as well as between the shaft and the locally released vapors. The geometries are adjusted as required.

Table 56. Convective heat transfer wall-to-gas for laminar flow conditions. Re < 2300 [220].

$$\dot{Q}_{WG,\alpha} = \alpha_{WG} S_{WG}\left(T_W - T_G\right)$$

$$\alpha_{WG} = \frac{Nu}{d_i}\lambda_G$$

$$Nu = \left\{Nu^3{}_{x,T,1} + 0,7^3 + \left[Nu_{x,T,2} - 0,7\right]^3 + Nu^3_{x,T,3}\right\}^{\frac{1}{3}}$$

$$Nu_{x,T,1} = 3,66$$

$$Nu_{x,T,2} = 1,077\sqrt[3]{Re\,Pr\left(\frac{d_i}{x}\right)}$$

$$Nu_{x,T,3} = \frac{1}{2}\left(\frac{2}{1 + 22\,Pr}\right)^{\frac{1}{6}}\left[Re\,Pr\left(\frac{d_i}{x}\right)\right]^{\frac{1}{2}}$$

$$Re = \frac{Qd_i}{\nu_G A} = \frac{\rho_G v d_i}{\mu_G} = \frac{\dot{m}_G d_i}{\mu_G S_{F,WG}}$$

$$Pr = \frac{cp_G \mu_G}{\lambda_G}$$

$$S_{F,WG} = hD - \frac{1}{2}D^2$$

$$d_i = 4\frac{S_{F,WG}}{2h} = 2\frac{S_{F,WG}}{h}$$

α_{WG} is the wall-gas convective coefficient
S_{WG} is the wall to gas surface
T are the temperature of the wall and of the gas
λ_G is the thermal conductivity of the gas
di is the reference dimension, depends on the geometry
x is the actual position
Nu is the Nusselt number
Re is the Reynolds number
Pr is the Prandtl number
ρ_G is the density of the gas
v is the velocity of the gas
$\dot{m}_G$ is the mass flow of the gas
μ_G is the dynamic viscosity of the gas
ν_G is the kinematic viscosity of the gas
$S_{F,WG}$ is the frontal surface wall-gas

Table 57. Convective heat transfer wall-to-gas for turbolent flow conditions. Re > 10^4 [220].

$$Nu_x = \frac{\left(\frac{\xi}{8}\right) Re\, Pr}{1 + 12,7\sqrt{\frac{\xi}{8}}\left(Pr^{\frac{2}{3}} - 1\right)}\left[1 + \frac{1}{3}\left(\frac{d_i}{x}\right)^{\frac{2}{3}}\right]$$

$$\xi = \left(1,8\log_{10} Re - 1,5\right)^{-2}$$

Table 58. Convective heat transfer wall-to-gas for transition flow conditions. $2300 < Re < 10^4$ [220].

$$Nu = (1-\gamma)\,Nu_{lam,2300} + \gamma Nu_{turb,10^4}$$

$$\gamma = \frac{Re - 2300}{10^4 - 2300}$$

$$Nu_{turb,10^4} = \frac{\left(\frac{0,0308}{8}\right)10^4\,Pr}{1+12,7\sqrt{\frac{0,0308}{8}}\left(Pr^{\frac{2}{3}}-1\right)}\left[1+\left(\frac{d_i}{L}\right)^{\frac{2}{3}}\right]$$

$$Nu_{lam,2300} = \left\{49,371+\left(Nu_{T,2,2300}-0,7\right)^3 + Nu_{T,3,2300}^3\right\}^{\frac{1}{3}}$$

$$Nu_{T,2,2300} = 1,615\left(2300\,Pr\frac{d}{L}\right)^{\frac{1}{3}}$$

$$Nu_{T,3,2300} = \left(\frac{2}{1+22\,Pr}\right)^{\frac{1}{6}}\left(2300\,Pr\frac{d}{L}\right)^{0,5}$$

Table 59. Correction of the Nusselt Number due to the effect of the temperature [220].

$$Nu = Nu_0\left(\frac{Pr}{Pr_W}\right)^{0,11}$$

The Nusselt number must be adjusted for the effect of the temperature.
Pr is the Prandtl Number at the mean averaged temperature (fluid-wall) Tm
Pr_W is that the wall temperature

Radiative heat transfer

Table 60. Radiative heat transfer coefficient for wall-to-solid heat exchange [220].

$$\dot{Q}_{WS} = \varepsilon_{WS} S_{WS} \sigma\left(T_W^4 - T_S^4\right)$$

$$\phi_S = \frac{S_{SG}}{S_{WG}}$$

$$U = (1-\varepsilon_W)(1-A_W)\left[\phi_S(1-\varepsilon_G)(1-A_S)+(1-\phi_S)\right]$$

$$\varepsilon_{WS} = \frac{A_W A_S (1-\varepsilon_G)}{1-U}$$

ε_{WS} is the emission factor wall to solid
ε_W is the emissivity of the wall
ϕ_S is the area-ratio o view factor
σ is the Boltzmann constant
S_{SG} surface solid-to-gas
S_{WG} surface wall-to-gas
A_W Absorption degree of wall
A_S Absorption degree of solid

Table 61. Radiative heat transfer coefficient for wall-to-gas heat exchange [220].

$\dot{Q}_{WG} = S_{WG}\sigma\varepsilon_{WG}\left(T_W^4 - T_G^4\right)$
$\varepsilon_{WG} = \frac{A_W\varepsilon_G\left[1+\phi_S\left(1-\varepsilon_G\right)\left(1-A_S\right)\right]}{1-U}$
ε_{WG} is the emission factor wall to gas ε_G is the emissivity of the gas ε_W is the emissivity of the wall σ is the Boltzmann constant A_W Absorption degree of wall A_S Absorption degree of wall

Table 62. Radiative heat transfer coefficient for solid-to-gas heat exchange [220].

$\dot{Q}_{SG} = S_{SG}\sigma\varepsilon_{SG}\left(T_S^4 - T_G^4\right)$
$\varepsilon_{SG} = \frac{A_S\varepsilon_G\left[1+\phi_S\left(1-\varepsilon_G\right)\left(1-A_W\right)\right]}{1-U}$
ε_{SG} is the emission factor wall to gas ε_G is the emissivity of the gas σ is the Boltzmann constant A_W Absorption degree of wall A_S Absorption degree of wall

Table 63. Emission coefficient of gas after [199].

$\varepsilon_G = \varepsilon_{CO_2} + \varepsilon_{H_2O} - \varepsilon_{CO_2}\varepsilon_{H_2O}$

A.4.3 Matlab tool

In this work, a model has been developed using MATLAB® aiming at creating a user-friendly tool, where a large number of simulations parameters can be taken into account with short computational time. The tool enables the variation of a wide spectrum of parameters, including the geometry of the reactor, the physical and chemical properties of the feedstock as well as the process conditions, such as the temperature of the reactor, the residence time of the solids and the composition of the purge gas. A screenshot of the mask is depicted in Figure 101. On the left hand side, the properties of the feedstock is reported. Moisture water and ash contents as well as the elemental composition and the physical properties can be adjusted. On the bottom left, the geometric parameters of the screw, such as length and diameter can be modified. In the middle of the mask, it is possible to define the process parameters such as the mass flow rate, the residence time and the initial temperatures of the feedstock and of the purge gas. Moreover, a mask enables defining some options for the temperature of the wall. The options are isothermal, linear increase or decrease of the temperature to reproduce the heat exchange of co-current and counter-current gas, with and without an isothermal section. Finally, a stepwise variation of the temperature option is given. It may be helpful for a more detailed control of the temperature in a real heat exchanger, where a specific flow of the heating gases is foreseen to improve the indirect heat transfer. Below the operation parameter mask, the section of kinetics is reported. The model is made for lignocellulosic feedstock, therefore the kinetic parameters for three components are given. It is distinguished between pyrolysis (fast) kinetics and carbonization kinetics. Moreover, the secondary reactions are considered. On the center-bottom, the volumetric composition of the purge gas in input and that of the vapors in output are reported. The right side of the mask is dedicated to the results of the model. The final temperatures, the required external heat and the yields are reported together with a graphical plot of the evolution of the temperatures of the solids and of the gases.

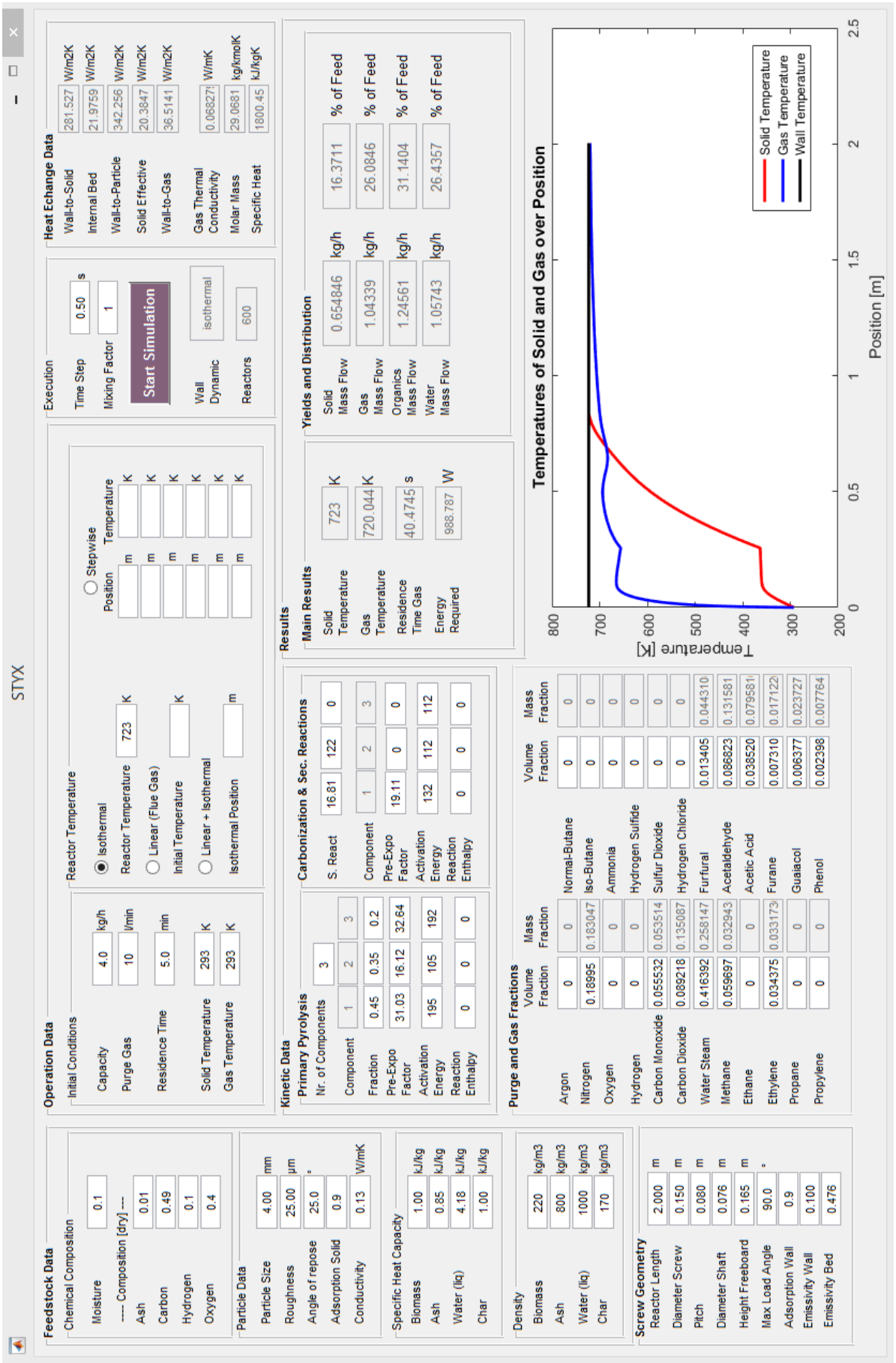

Figure 101. Screenshot of the mask of the Matlab tool

A.4.5 Details of Sensitivity Analysis

Thermal conductivity

The variation of the thermal conductivity of the solids was evaluated at 0.5 m from the inlet, where the temperature is in the range of 300°C and thus close to the initial pyrolysis temperature of wood. The results are depicted in Figure 102. An increase of λ_S from 0.13 W/mK to 0.26 W/mK led to an increase of the bulk temperature by 4.4°C. An increase to λ_S = 50 W/mK led to an increase by 45.6°C. At the standard particle size of 4 mm, the heat transfer within the bulk is the limiting factor. An increase of the thermal conductivity by a factor by 100 corresponds to an increase of the heat transfer coefficient α_{BED} of about 50%. The heat transfer from the wall to the solids remains an order of magnitude higher than that inside the bulk. The results indicate that the thermal conductivity of the solids has a low influence on the process.

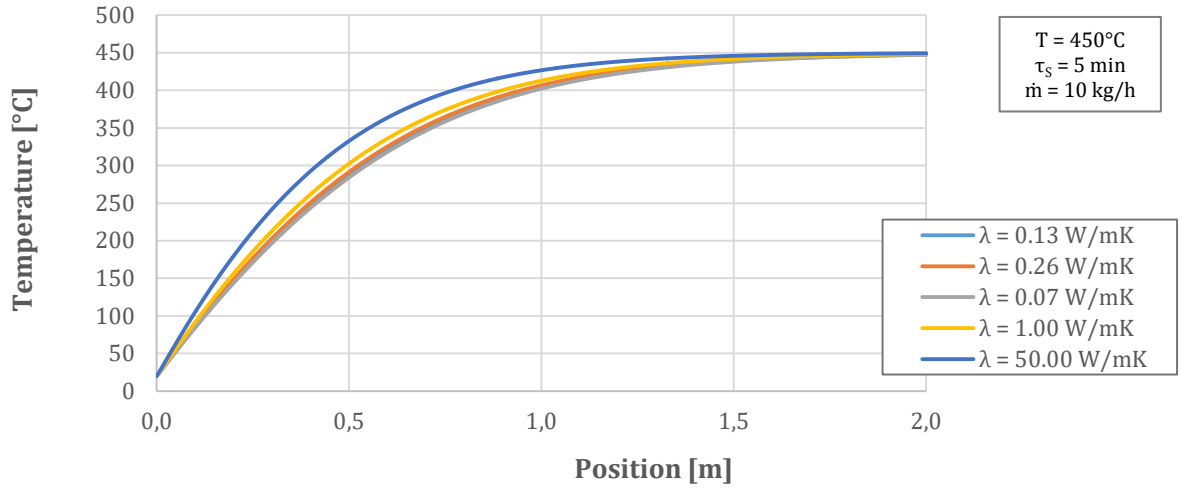

Figure 102. Variation of the thermal conductivity of the solid particles.

Bulk density

The variation of the bulk density was simulated in the range of 220 kg/m^3 to 660 kg/m^3 at a constant real density of 700 kg/m^3, which corresponds to a reduction of the void volume from 69% to 5% and to a reduction of the DoF from 14.4% to 4.8%. The results of the simulations are depicted in Figure 103. The increase of the bulk density leads to an increase of the temperature by 15°C at 0.5 m. The effect caused by the increase of the heat transfer coefficient within the bed by a factor of 2. The reduction of the contact surface between the wall and the particles does not influence the overall heat transfer, which remains limited by α_{BED} in all the simulation.

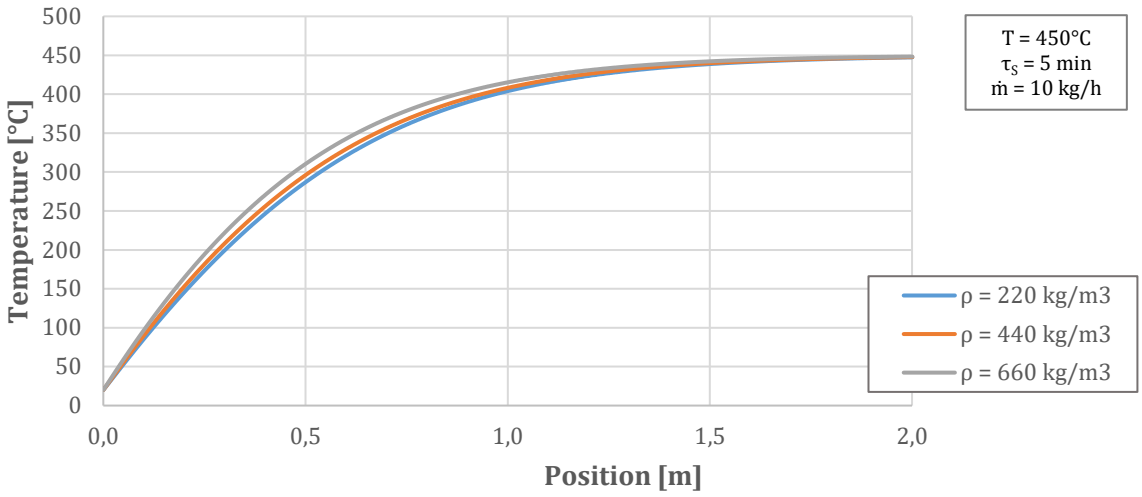

Figure 103. Variation of the bulk density of the solid particles.

Residence Time

The effect of the residence time of the solids was simulated at 450°C for a mass flow of 10 kg/h. The residence time was evaluated at 1.25-2.5-5 minutes, which corresponds to DoF of 3.6-7.2-14.4%, respectively. Longer residence times would lead to solids back flow and thus are not allowed by the model. For instance, a residence time of 7.5 minutes would give a DoF of 21.6%, which would lead to back flow, or overflow, of beech wood. Figure 104 reports the results of the simulations showing a minor variation of the temperature profiles for the selected parameters. The temperature difference between τ_S = 5 min and τ_S = 1.25 min is 12°C at 0.5 m. A reduction of the residence time, at constant mass flow rate of the solids, leads to a decrease of the mass of the solids in the screw compartment, which causes a faster heating. As a direct consequence, the limitation is given by the mechanical stability of the screw, whom rotational speed can be increased, i.e. the residence time of the solids can be reduced, to the desired value.

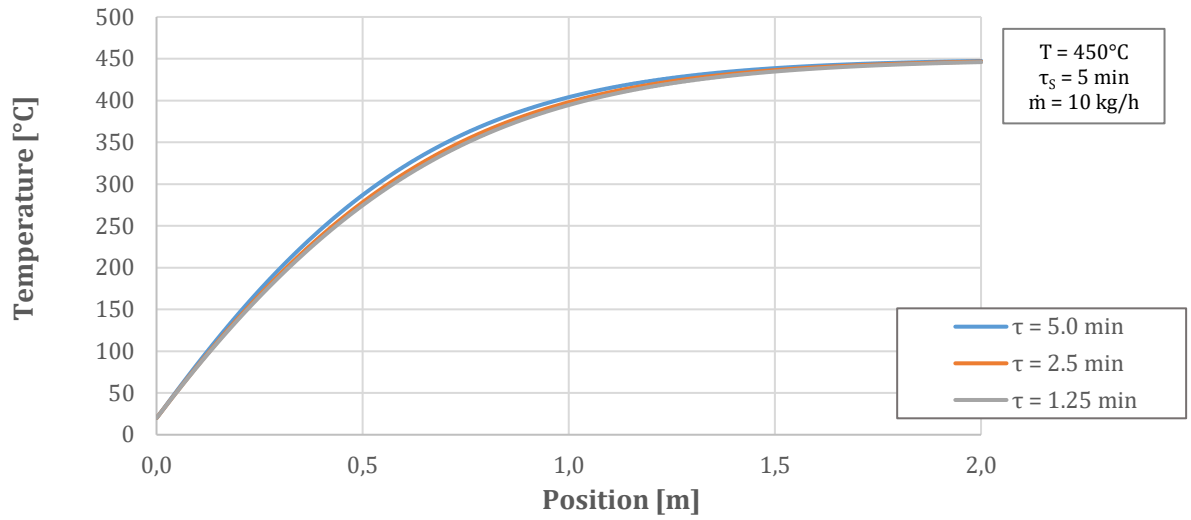

Figure 104. Variation of the residence time of the solids.

Release of the vapors along the reactor with different residence time of the solids.

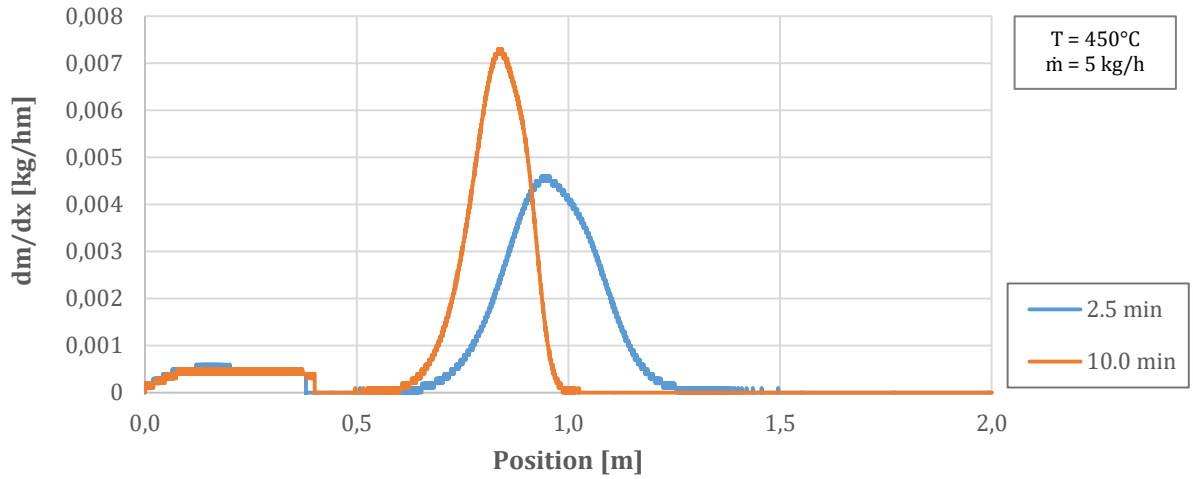

Figure 105. Release fo the vapors along the reactor for the pyrolysis of beech wood at 450°C with residece time of 2.5 and 10 minutes and mass flow rate of 5 kg/h.

Mass flow of the solids

From the previous paragraph it is clear that the effect of the residence time and of the mass flow rate are dependent from one to another. The consequence is that for a defined residence time, the mass flow rate, i.e. the mass in a compartment will have a similar effect, i.e. an increase or a reduction of the heating rate. To verify this consideration, simulations were carried out varying the mass flow rate of the solids in the range of 2.5-5-10 kg/h at 450°C and 5 minutes of residence time. The results are depicted graphically in Figure 106. As expected, the heating rate, i.e. the slope of the temperature profile, increased by a factor 2 and by a factor 4 for the simulations with 5 kg/h and 2.5 kg/h,

respectively. Therefore, the obvious conclusion is that the maximum capacity of the reactor should consider the residence time and the mass flow rate in combination.

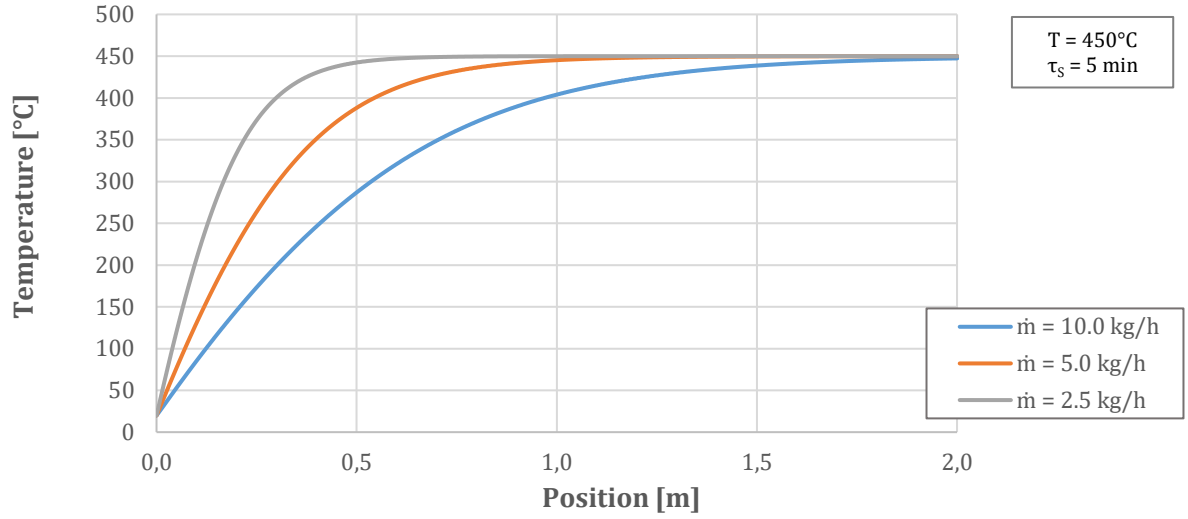

Figure 106. Variation of the mass flow of the solids.

Ash content of the feedstock

The ash content of the feedstock, i.e. the mineral content, is known for having strong influence on the yield and composition of the pyrolysis oil [176, 168, 146]. To evaluate its effect, simulation were carried out increasing the ash content of the feedstock from 1 wt.% to 10 wt.%. The results of the yields of the pyrolysis products are reported on as received basis in Figure 107.

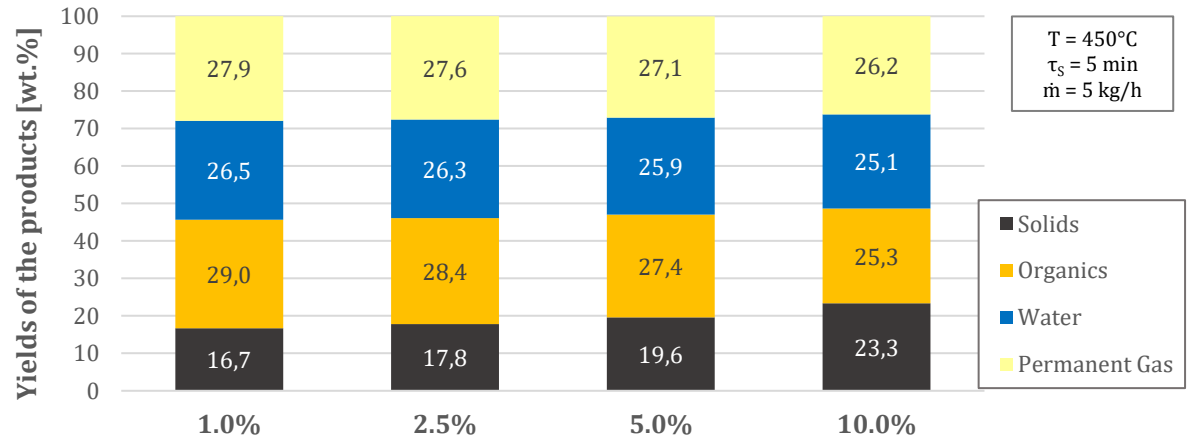

Figure 107. Effect of the ash content of the feedstock on the yields of the pyrolysis products on as received basis.

The results of Figure 107 show an increase of the yield of the solids with increasing ash content, as it should be expected since the ash remains quantitatively in the solid matrix. On the other hand, the yield of the condensable organics decreases with a slightly higher trend. In fact, the residence time of the vapors also increases with the increase of the ash content due to the reduced mass and volumetric

flow rates of the vapors. As for the water content, the cause is again the indirect effect of the residence time of the vapors, i.e. lower for higher water contents and higher for higher ash contents.

Conditioning of the feedstock

The feedstock can undergo different conditioning treatment before pyrolysis (Table 64). For instance, milling to powder with particle size of about 500 µm or lower is common praxis in fast pyrolysis; on the other hand, wood is often delivered as pellets of different sizes and bulk density. Therefore, simulations were carried out varying particle size (Equation 63) and bulk density (Equation 61) of the feedstock in order to account for different conditioning processes.

Table 64. Relevant properties of the different conditioning of the feedstock.

	Shape	Particle Size [mm]	Bulk Density [kg/m^3]
1 (Base case)	Granulates	4	220
2	Powder	0.5	220
3	Pellets	20	440
4	Pellets	40	660

The results of the simulation for the selected conditioned feedstock is depicted in Figure 108.

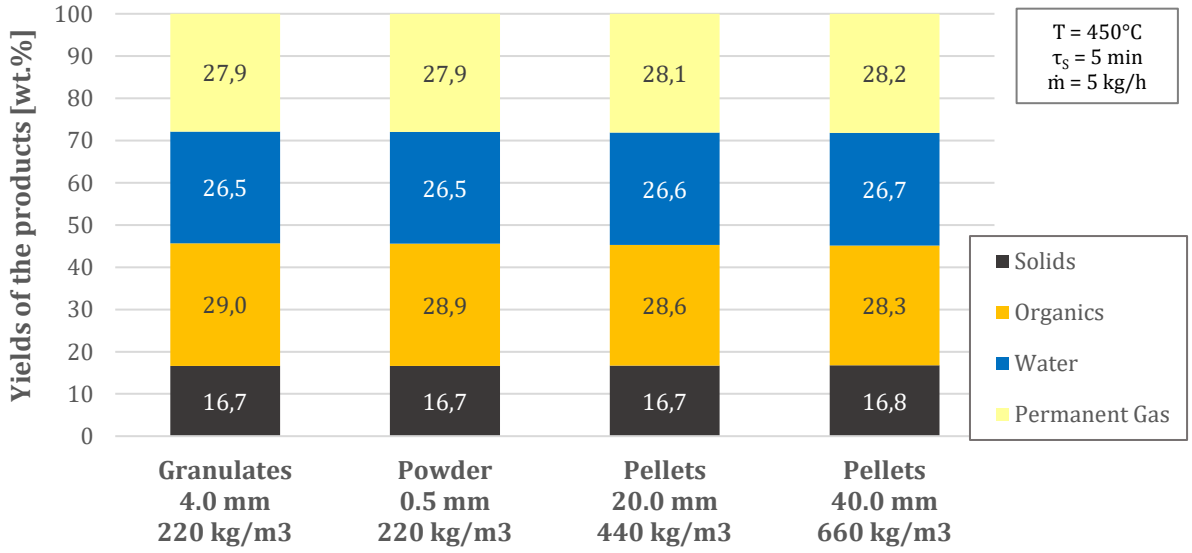

Figure 108. Effect of the conditioning treatment on the yields of the pyrolysis products.

Minimal variations of the yields have been obtained. In particular, the yield of the solids is constant for all the selected cases, indicating that the overall reaction rate of the primary decomposition process is not influenced by the conditioning of the biomass. The only relevant difference was found for the yield of the organics, which decreases slightly from the reference case using granulates to large and more compressed pellets. Such results indicate that the overall heat transfer to bulk lays in a narrow

range. For this reason as well as because the mass transfer within the single particle is not implemented in the model no notable differences in the yields of the solids are obtained. However, the slight variation of the yield of the organics is caused by the overall residence time of the vapors, which is longer by 5 seconds for large pellets favoring secondary gas phase reactions.

The profiles of the solids mass flow along the screw for the different biomass conditioning (Figure 109) confirms that the release of the vapors from the larger pellets takes place slower than the other ones, leading to longer residence times of the vapors.

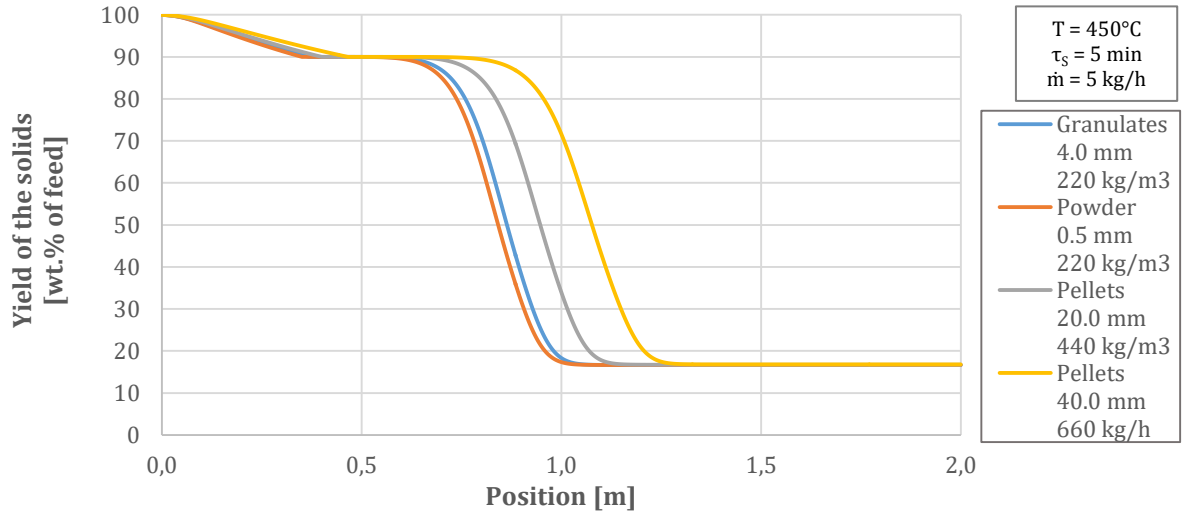

Figure 109. Profile of the yields of the solids along the screw for the variation of the conditioning process.

A.4.6. Details of the validation

Qualitative mixing of the solids

To gain an insight on the mixing within the pitch of the screw several experiments were carried out at the transport reactor. The procedure described to evaluate the RTD was used; some colored wood particles (10 wt.%) were co-fed in a single batch once the steady state was achieved. Using a camera, the flow of the batch was recorded, in order to understand the mechanism of mixing. The colored particles were introduced at the top of the bulk and observed until they completely disappeared. The time required by the colored particles to disappear was assumed to be the internal mixing time or stagnant period, which is the time required for a complete mixing and depends on the Froude number. Qualitative mixing of the particles in a compartment for a rotational speed of the screw of 2.5 rpm, corresponding to a residence time of the solids of 10 minutes at STYX.

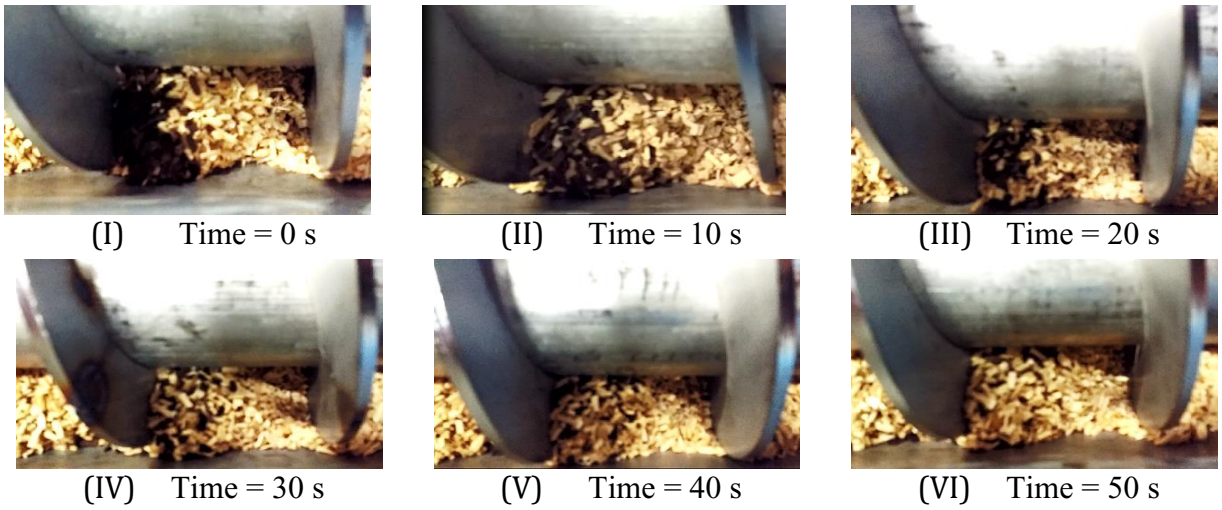

Figure 110. Internal mixing of beech wood in the model screw. Mass flow rate: 4 kg/h / Speed of rotation: 2.5 rpm.

Transport of the Gas

Finally, the Bodenstein number describes the flow regime and it is a measurement of the contribution of the molecular diffusion to the flow.

It is calculated from the Reynolds and Schmidt numbers (Bo = Re * Sc) and compared with the flow regimes table from Levenspiel [126].

The Reynolds number was in the range of 200, thus in pure laminar flow. For the evaluated cases, the flow regime is at the limit between the axial dispersion model and the intermediate regime, which separates the axial dispersion regime and the pure convection regime (see Figure 111).

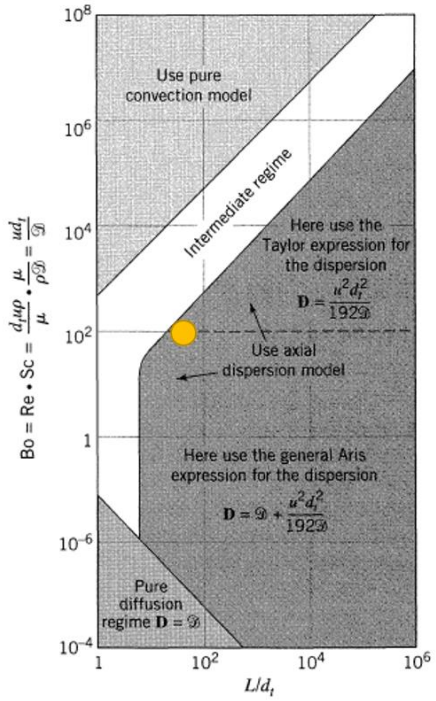

Figure 15.2 Map showing which flow models should be used in any situation.

Figure 111. Flow models after Levenspiel and relevant condition at STYX [126].

Dimensionless Analysis

The analysis based on the dimensionless Biot and Pyrolysis numbers was carried out to assess the validity of the kinetic model. The Biot and the Pyrolysis numbers were evaluated in a range of temperatures from 25°C to 450°C and for temperature differences of 20°C and 100°C. The results are reported in Table 65. In all the conditions, the particles are in Regime III (thermally thick), i.e. Bi > 0.1.

Table 65. Biot numbers for the different particle sizes at the selected pyrolysis conditions.

ΔT [K]		**20**							**100**				
T [K]		**298**	**300**	**400**	**500**	**600**	**700**	**723**	**400**	**500**	**600**	**700**	**723**
Bi [-]	**0.5 mm**	0.24	0.24	0.26	0.29	0.32	0.36	0.36	0.26	0.29	0.31	0.35	0.35
	1.5 mm	0.26	0.26	0.28	0.32	0.36	0.43	0.44	0.28	0.31	0.35	0.40	0.42
	1.9 mm	0.26	0.26	0.29	0.32	0.38	0.45	0.47	0.28	0.31	0.36	0.42	0.44

Validation of the secondary gas phase reactions

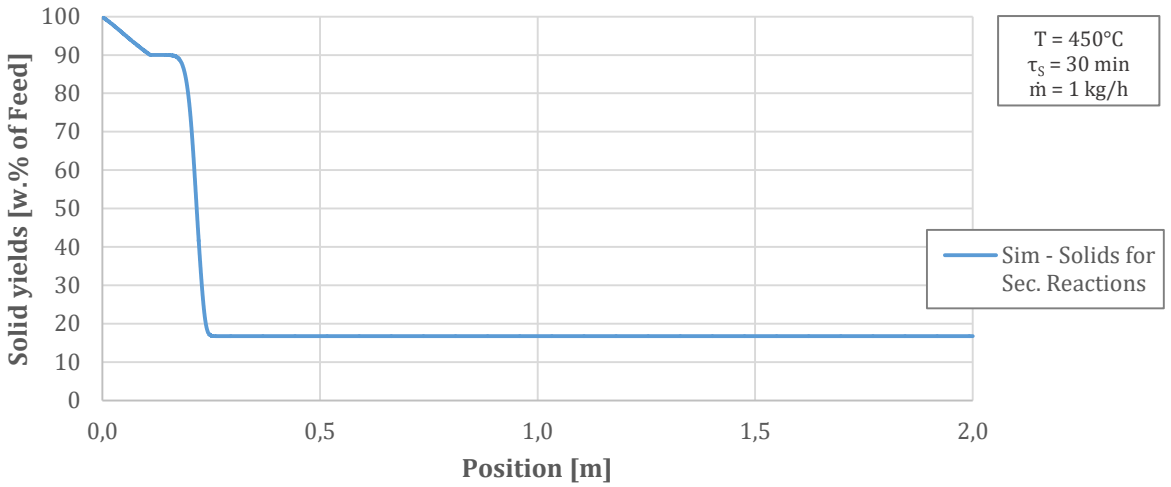

Figure 112. Simulation of the solid yield evolution for the validation of the secondary gas phase reactions.

Figure 112 reports the evolution of the solid yield along the reactor for the selected process conditions. It is shown that the drying process is completed before the sampling point. On the other hand, the decomposition of the solids takes place exactly at the sampling position 0.15 m, i.e. S1 on the gas side. Considering the geometry of the screw and the back mixing of the gas, the assumption appears to be fulfilled for the comparison of the simulations with the experimental setup.